Universidade de Lisboa

Faculdade de Farmácia

Sphingosine-induced alterations in membrane biophysical properties: biological relevance in the pathophysiology of human disease

Ana Cláudia Nunes Carreira

Orientadores:
Doutora Liana Casquinha da Silva
Doutor Rodrigo de Almeida
Doutor Emyr Lloyd-Evans

Tese especialmente elaborada para a obtenção do grau de Doutor em Farmácia, especialidade em Tecnologia Farmacêutica.

2019

Universidade de Lisboa

Faculdade de Farmácia

Sphingosine-induced alterations in membrane biophysical properties: biological relevance in the pathophysiology of human disease

Ana Cláudia Nunes Carreira

Orientadores: Doutora Liana Casquinha da Silva
Doutor Rodrigo de Almeida
Doutor Emyr Lloyd-Evans

Tese especialmente elaborada para a obtenção do grau de Doutor em Farmácia, especialidade em Tecnologia Farmacêutica

Júri:
Presidente:
Doutor António José Leitão das Neves Almeida, Professor Catedrático da Faculdade de Farmácia da Universidade de Lisboa
Vogais:
Doutora Maria João Martins Sarmento, *Posdoctoral Researcher*
J. Heyrovský Institute of Physical Chemistry - CAS, Czech Republic;
Doutora Otília Vitoriana Vieira, Investigadora principal
Faculdade de Ciências Médicas da Universidade Nova de Lisboa
Doutor Nuno Fernando Duarte Cordeiro Correia dos Santos, Professor Associado com Agregação
Faculdade de Medicina da Universidade de Lisboa
Doutora Helena Maria Cabral Marques, Professora Associada com Agregação
Faculdade de Farmácia da Universidade de Lisboa
Doutora Maria Luísa Teixeira de Azevedo Rodrigues Corvo, Investigadora Aixiliar
Faculdade de Farmácia da Universidade de Lisboa
Doutora Liana Casquinha da Silva, Investigadora FCT nível inicial com Agregação, Faculdade de Farmácia da Universidade de Lisboa, Orientadora

Trabalho financiado pela Fundação para a Ciência e a Tecnologia através da bolsa de doutoramento SFRH/BD/88194/2012

2019

Dedicated to my family.

For all their love and support.

ACKNOWLEGMENTS

In the beginning of this project it was an adventure to enter and explore the complex world of membrane biophysics. These last couple of years were full of new challenges and discoveries, and at this point I feel it is necessary to acknowledge to all the entities that in a way or another helped me to put this PhD project in practice.

I will start to direct my first thanks to the institutions that supported the realization of this doctoral project: to Fundação para a Ciência e Tecnologia (FCT) for believing in the potential of the project and giving financial support to its progress (PhD Scholarship - SFRH/BD/88194/2012), to Faculdade de Farmácia (FFUL) and Faculdade de Ciências (FCUL) from Universidade de Lisboa (UL) and School of Biosciences from Cardiff University, for facilities and equipment provided.

I would also like to thank Dr. Helena Florindo, for allowing me to perform this project in the BioNanoSciences – Drug Delivery and Immunotherapy group (iMed.ULisboa, FFUL).

A special acknowledgment to my advisors, Dr. Liana Silva, Dr. Rodrigo de Almeida and Dr. Emyr Lloyd-Evans, for having provided all necessary conditions for the realization of this work. For the sharing knowledge, incentive and constructive opinions that have been fundamental for the progress of my performance and my scientific training. I also thank all the friendship and availability to support me in this scientific journey.

To my FFUL colleagues, Ester, Tânia, Carina, Vanessa, Nuno, João, Joana, Raquel, Eva, Andreia, Ana Matos and Melissa for the friendship and all shared experiences. A special thanks to Eva, Raquel and Andreia for the valuable tips and availability to help in the first steps of this work.

I would like to express a special acknowledgment to my colleagues at the School of Biosciences (Cardiff University): Mat, Kim, Helen, Luke, Emily C., Emily M., Chris, Laura, Jule and Naomi for the friendliness and the good work environment that provided an easy adaption to the laboratory.

Most of the experimental work was performed in the Molecular Biophysics laboratory, FCUL. Thus, I would like to express my gratitude to the colleagues and friends that I met there. The excellent working environment and the team spirit would not be possible if you did not

exist. Therefore, Filipa, Catarina, Joaquim, André, Telmo, Andreia Sousa, António, Telma, Hugo and Carla thank you for all shared moments. A special acknowledgment to Filipa, Carla and Joaquim, whose support was fundamental for the conclusion of this journey.

Last, but not least I want to thank to my wonderful family. To my parents, grandparents, sister and brother and you Fábio for the unconditional support, encouragement and patience at all times. A special thanks to my baby daughter Maria Luísa that despite consuming much of my energy (day and night), was able to encourage me in the final steps of this journey with her sweet and magnificent smiles. Love you all!

THIS WORK WAS DEVELOPED UNDER THE SUPERVISION OF:

- Dr. Liana C. Silva (Supervisor)

  Assistant Researcher

  Research Institute for Medicines (iMed.ULisboa), Faculdade de Farmácia, Universidade de Lisboa, Portugal

- Dr. Rodrigo de Almeida (Co-supervisor)

  Principal Investigator

  Centro de Química e Bioquímica, Faculdade de Ciências, Universidade de Lisboa, Portugal

- Dr. Emyr Lloyd-Evans (Co-supervisor)

  Research Group Leader, Senior Lecturer

  School of Biosciences, Cardiff University

THIS WORK WAS DEVELOPED AT:

iMed.ULisboa – Research Institute for Medicines (grupo BioNanoSciences), Faculdade de Farmácia, Universidade de Lisboa, Av. Professor Gama Pinto, 1649-003 Lisboa, Portugal

Centro de Química e Bioquímica (grupo de Biofísica molecular), Faculdade de Ciências, Universidade de Lisboa, Campo Grande, 1749-016 Lisboa, Portugal

School of Biosciencies (Neuroscience division), Cardiff University, Sir Martin Evans Building, Museum Avenue, Cardiff, CF10 3AX

Ana Cláudia Nunes Carreira was financially supported by Fundação para a Ciência e a Tecnologia (FCT) with a PhD grant SFRH/BD/88194/2012. The work in this thesis was supported by FCT grants PTDC/BBB-BQB/0506/2012, UID/DTP/04138/2013, UID/00612/2013, PTDC/BBB-BQB/3710/2014.

LIST OF PUBLICATIONS

My contribution to the articles/chapters included in the thesis:

1. Carreira A.C., Santos T.C., Lone M.A., Zupančič E., Lloyd-Evans E., de Almeida R.F.M., Hornemann T., Silva L.C. Mammalian sphingoind bases: biophysical, physiological and phatological properties. Progress in Lipid Research. 2019 (submitted)

Took an active part in the writing and revision of the review.

2. Ana C. Carreira, Rodrigo F. M. de Almeida and Liana C. Silva. Development of lysosome-mimicking vesicles to study the effect of sphingosine abnormal accumulation on membrane properties. Scientific Reports. 2017. 7: 3949

Took an active part in the planning of the work and performed all the experiments. Took an active part in the writing of the paper.

3. Ana E. Ventura, Tânia Santos, Ana C. Carreira, Nuno M. Martinho, J. Conniot, Ana R. Varela, Rogério Gaspar, Helena F. Florindo, Liana C. Silva. 2016. Drugs, delivery systems and membrane organization in model and cell membranes. In: Angel Catala (Eds) "Membrane organization and lipid rafts in the cell and artificial membranes", Nova Science Publishers Inc, New York.

Took an active part in the writing of the two first sections of the chapter and gave a contribution in the revision of the other sections.

4. Ana C. Carreira, Ana E. Ventura, Ana R. P. Varela and Liana C. Silva. Tackling the biophysical properties of sphingolipids to decipher their biological roles. Biological Chemistry. 2015. 396: 597–609

Took an active part in the planning and writing of the paper.

5. Eva Zupančič, Ana C. Carreira, Rodrigo de Almeida, Liana Silva. Biophysical Implications of Sphingosine Accumulation in Membrane Properties at Neutral and Acidic pH. Journal of Physical Chemistry B. 2014. 118: 4858–4866

Took an active part in the planning of the work and performed the majority of the experiments. Wrote the paper.

Papers to which I have contributed that are not included in the thesis:

Ana R.P. Varela, Ana E. Ventura, **Ana C. Carreira**, Alexander Fedorov, Anthony H. Futerman, Manuel Prieto, Liana C. Silva. Pathological levels of glucosylceramide change the biophysical properties of artificial and cell membranes. Phys Chem Chem Phys. 2017. 19: 340-346

A. G. dos Santos, J. T. Marquês, **A. C. Carreira**, I. R. Castro, A. S. Viana, M.-P. Mingeot-Leclercq, R. F. M. de Almeida and L. C. Silva. The molecular mechanism of Nystatin action is dependent on the membrane biophysical properties and lipid composition. Phys Chem Chem Phys. 2017. 19: 30078-30088

ABSTRACT

The study of biological and model membrane systems currently represents an important area of scientific research. Lipids are involved in the regulation of multiple cellular processes, being fundamental for the mantainance of cell homeostasis. Sphingosine (Sph) belongs to this group of biologically active lipids and is an important signaling molecule. When abnormally accumulated in the lysosomes and late endosomes (LE), Sph is associated to one of the most complex lysosomal storage diseases (LSD), Niemann-Pick type C (NPC). Despite this, little is known about its role in the lysosome, in particular with respect to the biophysical effects of its accumulation. By understanding the interactions of Sph with other lipids and their effect on the physical state of model and cell membranes, new insights into its mode of action may arise. Using complementary established techniques (fluorescence spectroscopy, dynamic (DLS) and electrophoretic (ELS) light scattering), a thorough biophysical characterization of membranes containing Sph was performed. This study revealed that Sph is able to decrease membrane fluidity both in fluid 1-palmitoyl-2-oleoyl-*sn*-glycero-3-phosphocholine (POPC) and lipid raft-mimicking (POPC/SM/Chol) membrane models in a concentration dependent way. Sph-induced changes on membrane fluidity are highly dependent on pH and membrane lipid composition. It was observed that Sph has a more dramatic impact on membrane organization and permeability in vesicles with a pH gradient resembling the lysosome - the lysosome mimicking vesicles - LMVs (pH $5.0_{in}/7.4_{out}$) - particularly in those with a lipid composition mimicking NPC1 conditions (i.e. higher Chol, SM and Sph content), compared to physiological-like situations. In the biological context, it was shown that cells displaying the NPC phenotype have an altered membrane fluidity when compared with the wild-type (WT) cells and that these changes are complex and cell type dependent. Moreover, it was observed that Sph has the ability to decrease the fluidity of biological membranes in accordance with model membrane data.

Overall the results suggest that Sph abnormal accumulation in cells is associated with alterations in membrane biophysical properties, likely affecting different membrane associated cellular processes. These changes could urderly some Sph biological actions. In particular, Sph-induced biophysical alterations might affect the endocytic trafficking and consequently the normal cell function in NPC disease.

KEYWORDS

- ✓ Lipid domains
- ✓ Membrane biophysics
- ✓ Membrane models
- ✓ Niemann-Pick disease
- ✓ Sphingosine

RESUMO

As membranas biológicas são responsáveis em primeira instância pela separação física entre o interior e o exterior das células e dos organelos celulares, no caso de células eucariotas. Para além desta função de compartimentalização, as membranas são essenciais para a manutenção da homeostasia celular, estando envolvidas em diversos processos celulares tais como: produção de energia, controlo de entrada e saída de iões e outras moléculas da célula/organelos, comunicação celular, entre outros. Em termos de composição estrutural, as membranas biológicas são compostas por uma grande diversidade de lípidos, proteínas e hidratos de carbono, todos eles com funções específicas. Diferentes composições destes componentes permitem diferentes morfologias membranares, que por sua vez, estão associadas a funções especializadas na célula (p.e. junções apertadas). Cada membrana apresenta, portanto, uma composição estrutural única que está na base da sua função específica na célula. Diferentes interações entre os componentes membranares, lípido-lípido, proteína-proteína, lípido-proteína conferem à membrana uma organização complexa constituída por diversos domínios cujas propriedades biofísicas diferem entre si. Esta noção de compartimentalização da membrana, só se conseguiu devido aos avanços tecnológicos que permitiram uma caracterização mais detalhada da membrana a nível microscópico e sub-microscópico. Hoje em dia, o modelo do mosaico fluído, inicialmente proposto em 1972, é ainda considerado o conceito principal de biomembrana abrangendo, no entanto, novos aspectos, como é o caso da formação de domínios especializados na membrana. Um exemplo destes domínios são as jangadas lipídicas, regiões enriquecidas em colesterol e esfingolípidos saturados que conferem à membrana uma natureza menos fluída. Estas são plataformas transientes e funcionais, as quais estão presumivelmente envolvidas no recrutamento de moléculas sinalizadoras e na criação de condições para a activação de eventos de sinalização celular. Atualmente, um dos campos mais ativos de estudo entre as comunidades biofísica e biológica, é precisamente a organização lateral das biomembranas em domínios e as suas implicações em diversos processos celulares.

A complexidade das membranas biológicas implica que se tenha de recorrer a sistemas modelo de membrana mais simples e mais adequados à análise biofísica molecular. Os

lipossomas, são exemplos comuns de sistemas modelo utilizados na caracterização das propriedades dos lípidos e respetivas funções na estrutura da bicamada lipídica. Com o acumular de evidências de que os lípidos são mais do que meros componentes estruturais da célula, surge a necessidade de se explorarem os mecanismos subjacentes ao papel ativo que estas moléculas desempenham na manutenção do equilíbrio celular. Dentro do grupo de lípidos biologicamente ativos, encontra-se a esfingosina, um dos lípidos mais simples e simultaneamente mais potente em termos de sinalização celular. Apesar de estar envolvida na regulação de vários processos biológicos, quando anormalmente acumulada nos lisossomas e endossomas tardios, a esfingosina pode ser responsável por alterações na homeostasia do cálcio, conduzindo ao desenvolvimento de uma das mais complexas doenças de acumulação lisossomal, a doença de Niemann Pick do tipo C (NPC). Esta é uma doença hereditária rara transmitida de forma autossómica recessiva. O desenvolvimento desta patologia está associado maioritariamente a mutações no gene NPC1 (cerca de 95% dos casos), enquanto alguns casos estão também associados a mutações no gene NPC2. As proteínas NPC1 e NPC2 desempenham, concomitantemente, um papel no transporte intracelular de colesterol e podem também estar envolvidas no transporte de outras moléculas (possivelmente também facilitam o transporte das moléculas de esfingosina positivamente carregadas) através do sistema endo-lisossomal. O quadro clínico pode ser muito heterogéneo, sendo que a doença se pode manifestar no período perinatal mas também já em idade adulta. O funcionamento de vários órgãos pode ser afetado, sendo o prognóstico da doença mais complicado quando as manifestações neurológicas são precoces. Atualmente, não existe um tratamento eficaz para a doença e é importante que sejam desenvolvidos estudos, na tentativa de melhor compreender os mecanismos moleculares que estão na base do desenvolvimento da mesma. Existem evidências de que a esfingosina é o primeiro metabolito a desencadear a doença, no entanto, pouco se sabe acerca do seu papel no lisossoma, em particular no que diz respeito às implicações biofísicas que a sua acumulação representa para a membrana lisossomal. Com a compreensão das interações da esfingosina com outros lípidos das membranas biológicas e do seu efeito no estado físico de membranas modelo, poderão surgir novas pistas sobre os mecanismos que estão na base do seu papel biológico. Existem na literatura alguns estudos referentes ao impacto da esfingosína nas

propriedades biofísicas de membranas (na grande maioria dos casos membranas artificiais) e foi inclusive sugerido que alterações biofísicas induzidas pela esfingosina e outros lípidos poderão explicar, em parte, o seu mecanismo de ação nas células.

No presente trabalho de dissertação, as propriedades biofísicas da esfingosina foram exploradas no contexto de membranas modelo com complexidade crescente e também em membranas de células vivas. Pretende-se com este estudo responder às seguintes questões: i) Quais os efeitos da esfingosina em membranas fluídas constituídas por POPC?; ii) Como é que a esfingosina afeta as propriedades de membranas com composição típica de jangada lipídica?; iii) Diferenças de pH como as observadas em diferentes localizações celulares podem afetar o papel da esfingosina nas células?; iv) Qual a importância do desenvolvimento de novos sistemas modelo de membrana que mais se assemelham às situações fisiológicas ocorridas na célula?; v) Qual o impacto da esfingosina em membranas biológicas? Neste contexto, e para dar resposta a estas perguntas estabeleceu-se uma abordagem experimental baseada em técnicas complementares, nomeadamente: espectroscopia e microscopia de fluorescência e ainda técnicas de dispersão dinâmica e electroforética da luz. Utilizaram-se maioritariamente sistemas modelo de membrana, em particular, vesículas unilamelares com cerca de 100 nm, que devido à sua estabilidade, tamanho controlado e natureza unilamelar, se tornam bastante úteis em experiências como as de permeabilidade em que é necessário realizar o encapsulamento de moléculas fluorescentes no interior das vesículas. Foram ainda utilizados tampões com pH distintos na preparação das vesículas, de modo a avaliar o efeito do pH nas propriedades biofísicas das membranas.

Os resultados demonstraram que a adição de concentrações crescentes de esfingosina pode levar à formação de domínios gel, em modelos de membrana constituídos por POPC ou por POPC/esfingomielina/colesterol (modelo de jangada lipídica). A formação desses domínios depende não só da concentração de esfingosina como também da restante composição lipídica da membrana e do pH do meio envolvente. Estes domínios são mais facilmente formados em modelos de membrana a pH neutro (7.4), que mimetizam o ambiente da membrana plasmática, quando comparado com o ambiente acídico (pH 5.0) do lisossoma, no qual maiores concentrações de esfingosina são necessárias. Foi ainda demonstrado que a pH neutro, os

modelos de jangadas lipídicas contendo esfingosina (5 ou 10 mol%) apresentam a carga da membrana maioritariamente neutra, enquanto nos mesmos modelos a pH ácido a carga da membrana é positiva. Neste caso, a carga positiva da esfingosina gera repulsão eletrostática, reduzindo a sua capacidade para formar domínios gel. Os dados sugerem, deste modo, que a formação de domínios ricos em esfingosina, em membranas celulares, pode ser regulada pela carga desta base esfingóide.

Neste trabalho de doutoramento, foi desenvolvido um novo modelo designado de "lysosome-mimicking vesicles – LMVs", que mais se assemelha ao lisossoma por possuir pH acídico no interior e pH neutro no ambiente externo (gradiente de pH). Este modelo foi utilizado para avaliar os efeitos da acumulação anormal de esfingosina nos compartimentos acídicos da célula. Para avaliar as vantagens da utilização das LMVs, foi estudado o efeito da acumulação de esfingosina nas proriedades biofísicas e estruturais da membrana de lipossomas padrão (sem gradiente de pH) e LMVs constituídos por diferentes composições lipídicas, de modo a mimetizar lisossomas em condições fisiológicas normais e lisossomas com alterações do tipo NPC. Verificou-se um maior efeito da adição da esfingosina nas propriedaes biofísicas e permeabilidade de membrana das LMVs. Este efeito foi também mais evidente nas vesículas que contêm maior concentração de colesterol e esfingomielina, mimetizando as membranas lisossomais NPC. A caracterização das LMVs demonstrou a importância de se desenvolverem sistemas modelo com características o mais semelhantes possível aos sistemas biológicos em estudo, de forma a garantir uma melhor extrapolação dos resultados obtidos em sistemas artificais para o contexto biológico.

O impacto biofísico da acumulação de múltiplas espécies lipídicas em células NPC foi também avaliado, verificando-se alterações na fluidez da membrana, que são complexas e dependentes da linha celular. Observou-se ainda, tal como se tinha observado em sistemas modelo, que a esfingosina tem um efeito importante nas propriedades biofísicas da membrana, neste caso, quando externamente adicionada a células saudáveis. Este efeito, que é quase imediato, é traduzido na diminuição da fluidez da membrana, e aponta para o possível envolvimento da esfingosina na formação/estabilização de domínios especializados na membrana.

No geral, os resultados sugerem que a esfingosina quando anormalmente acumulada nas células pode alterar a fluidez da membrana e consequentemente afetar processos celulares a ela associados. Na doença NPC, a integridade da membrana lisossomal pode ficar comprometida com a acumulação de esfingosina e afetar o normal funcionamento do sistema endocítico. Estes dados, dão suporte biofísico ao papel biológico da esfingosina e podem ser tidos em consideração, aquando do desenvolvimento de novas abordagens terapêuticas para pacientes NPC.

PALAVRAS CHAVE

- ✓ Biofísica de membranas
- ✓ Domínios de membrana
- ✓ Doença de Niemann-Pick
- ✓ Esfingosina
- ✓ Modelos de membrana

INDEX

LIST OF ABBREVIATIONS

aCDase, Acid Ceramidase

ACERs, Alkaline Ceramidases

ANTS, 8-Aminonaphthalene-1,3,6-Trisulfonic Acid Disodium Salt

aSMase, Acid Sphingomyelinase

BMP, bis(monoacylglycero)phosphate

C1P, Ceramide-1-Phosphate

CDase, Ceramidases

CerS, Ceramide synthase

CF, Cystic Fibrosis

Chol, Cholesterol

CLSM, Confocal laser scanning microscopy

CMC, Critical micelle concentration

CoA, Coenzyme A

DAG, Diacylglycerol

Deox-dhSph, Deoxy-sphinganine

Deoxmeth-dhSph, Deoxymethyl-sphinganine

DEPE, 1,2-dielaidoyl-*sn*-glycero-3-phosphoethanolamine

DES, Dihydroceramide desaturase

DHPC, 1,2-dihexadecyl-*sn*-glycero-3-phosphocholine

DLS, Dynamic light scattering

DM, Dichroic mirror

DMPC, 1,2-dimyristoyl-*sn*-glycero-3-phosphocholine

DPH, 1,6-diphenyl-1,3,5-hexatriene

DPPC, 1,2-dipalmitoyl-*sn*-glycero-3-phosphocholine

DPPS, 1,2-dihexadecanoyl-*sn*-glycero-3-phosphoserine

DPX, p-xylene-bis-pyridinium bromide

DSC, Differential Scanning Calorimetry

ELS, Electrophoretic Light Scattering

ER, Endoplasmic reticulum

GalCer, Galactosylceramide

GlcCer, Glucosylceramide

GPI, Glycosylphosphatidylinositol

GSLs, Glycosphingolipids

GUV, Giant unilamellar vesicle

H, Hexagonal phase

H_{II}, Inverted hexagonal phase

L, Lamellar phase

l_d, Liquid disordered

LE, Late endosomal/endosome

LEDs, Single-wavelength light emitting diodes

LM, Lysosomal membrane

LMVs, Lysosome-Mimicking Vesicles

l_o, Liquid ordered

LSD, Lysosomal Storage Diseases

LUV, Large unilamellar vesicle

L_α, Liquid crystalline

L_β, Gel phase

$L_{\beta'}$, Tilted gel

MLV, Multilamellar vesicle

MS, Mass spectrometry

nCDase, Neutral ceramidase

NMR, Nuclear magnetic resonance

NPC, Niemann-Pick type C

PA, Phosphatidic acid

PC, Phosphatidylcholine

PDI, Polydispersity index

PE, Phosphatidylethanolamine

PFA, Paraformaldehyde

PG, Phosphatidylglycerol

PI, Phosphatidylinositol

PKC, Protein kinase C

PLs, Phospholipids

PM, Plasma membrane

POPC, 1-palmitoyl-2-oleoyl-*sn*-glycero-3-phosphocholine

PS, Phosphatidylserine

P_{β}, Rippled gel

S1P, Sphingosine-1-phosphate

SKs, Sphingosine kinases

SLs, Sphingolipids

SM, Sphingomyelin

s_o, Solid ordered

Sph, Sphingosine

SPT, Serine Palmitoyltransferase

SUV, Small unillamelar vesicle

T_m, Main transition temperature

TMA-DPH, 1-(4-(trimethylamino)phenyl)-6-phenylhexa-1,3,5-triene

***t*-PnA**, *trans*-parinaric acid

TRFA, Time Resolved Fluorescence and Anisotropy

WT, Wild-type

AIMS AND OUTLINE

The work presented in this dissertation is focused on the characterization of the impact of Sph in the biophysical properties of model and cell membranes. With this study new insights on Sph biological actions are expected, especially with regard to its involvement in the pathophysiology of NPC.

Through the combination of different techniques, such as fluorescence spectroscopy and microscopy, DLS and ELS, this work was conducted in order to characterize:

i) Binary lipid mixtures containing Sph and POPC, a common membrane phospholipid (Chapter II)

ii) Quaternary mixtures with a composition mimicking the most studied lipid domains - raft domains (POPC, Chol and SM) and Sph (Chapters II and III)

iii) The effect of pH changes, using an environment that mimics the plasma and lysosomal membranes (pH 7.4 and pH 5.0, respectively) (Chapters II and III)

iv) Sph-induced effect in membrane permeability (Chapter III)

v) Membrane biophysical properties of NPC cell models (Chapter IV)

vi) The biophysical impact of Sph externall addition to heathy cells (Chapter IV)

Most of the data obtained during the execution of this work has already been published in peer review scientific journals, hence a great part of this thesis comprises a compilation of the published work.

This dissertation is divided into 6 chapters. **Chapter I** comprises an overview of the thematic that contextualize the present thesis. In a first approach both the biological role and the evolution of the concept of biomembranes are introduced. The importance of the structural components of biomembranes is also addressed with a special focus in membrane lipids. A description of relevant concepts/systems used for membrane biophysics analysis is presented. Moreover, information regarding the techniques employed in the framework of this dissertation, for the analysis of membrane biophysical properties, is presented. Review articles were published with information regarding sphingolipids/Sph biophysics, from which

information was used in the writing of this chapter. After the introduction of the sphingolipids category, the metabolism, physico-chemical properties, phase behavior and biological role of Sph, the main lipid under study, are described, as well as its involvement in human disease.

Chapters II, III and IV describe the main results obtained in the studies leading to this dissertation. **Chapter II**, describes the effect of Sph in the biophysical properties of model membranes (Large Unilamellar Vesicles - LUVs) composed by POPC/Sph and POPC/SM/Chol /Sph. The experiments were performed both at neutral (pH 7.4) and acidic (pH 5.0) pH, in order to evaluate the influence of pH changes in the biophysical properties of Sph enriched membranes. To address these questions, complementary techniques including fluorescence spectroscopy, DLS and ELS were used. **Chapter III** addresses the development of a new synthetic system that more closely resembles the lysososme – the lysosome-mimicking vesicles (LMVs). The effect of Sph accumulation in membrane structure/permeability and biophysical properties was assessed in standard liposomes (no pH gradient) and in LMVs representing physiological (lower SM, Chol content) and NPC-like conditions (higher SM, Chol content). The studies were performed using fluorescence spectroscopy, DLS and ELS. **Chapter IV** is focused on the biophysical impact of lipid abnormal accumulation in NPC. The outcome of: null or down expression of NPC1 locus, the pharmacological induction of the NPC phenotype with U18666A treatment and the externall addition of Sph to healty cells was evaluated in Chinese Hamster Ovary cells (CHO-K1 and CHO-M12) and neuroblastoma cells (SH-SY5Y and their mutant counterpart down-expressing the NPC1 locus). The studies were performed using fluorescence spectroscopy and microscopy.

The overall conclusions resulting from this PhD work are presented in **Chapter V**. Briefly it is suggest that model membranes are, in fact, a valuable system to predict cell membrane properties. The need to develop model systems that more closely resemble the biological systems under study is highlighted. The impact of Sph in the biophysical properties of biological membranes, coincident with the model membrane data, further emphasizes the importance of such systems. However, when considering the more complex biological systems, other features should be taken into account, such as the changes in membrane components (e.g. lipid profile)

during differentiation and cell aging. Finally, to conclude this manuscript, future work perspectives are presented in **Chapter VI**.

CHAPTER I

INTRODUCTION

This Chapter partially comprises my contributions to the works published in:

Biological Chemistry (2015) 396: 597-609 by **Carreira A.C**.[a], Ventura A.E[a], Varela A.R.P.[a], Silva L.C. ([a]equally contributing authors)

Angel Catala (Eds). Drugs, Delivery Systems and Membrane Organization in Model and Cell Membranes (2016) Nova Science Publishers Inc, New York. pp. 53-88 by Ana E. Ventura, Tânia Santos, **Ana C. Carreira**, Nuno Martinho, João Conniot, Ana R. Varela, Rogério Gaspar, Helena Florindo, Liana C. Silva

CHAPTER 1 – INTRODUCTION

1. The biological role of biomembranes

Biomembranes are crucial components of all cells, responsible for the physical separation between the inside and outside of each cell. Contrary to prokaryotic cells, where only a single extracellular membrane exists, eukaryotic cells present in addition to an outer plasma membrane (PM), various internal membranes surrounding different compartments, such as nucleous, mitochondria, endoplasmic reticulum (ER), Golgi complex, endosomes and lysosomes[1,2]. Biological membranes are therefore responsible for cell compartmentalization, but also for all the communication established between the separated internal and external spaces[1,3,4]. The structural principle of all biomembranes is fundamentally the same: biomembranes are composed by lipids, proteins and carbohydrates, as it will be described in section 3, however, they are incredibly dynamic structures with a remarkable diversity. This is the reason why they are involved in several cellular processes. They regulate the transport of ions and molecules into and out of the cell due to their selective permeability[5,6]. Membranes are also involved in cellular energy production due to the creation of ion gradients across them[7]. Moreover, membranes are able to control the flow of messages between cells through electrical and chemical signals, being involved in cell to cell communication[8–11]. In addition, biomembranes can present different morphologies that are associated with specific functions[12]. An example of this, are the tight junctions that provide the continuous intercellular space between epithelial cells, required for the separation of tissues[13]. Another important feature to consider is the membrane compartmentalization into specialized lipid domains, which will be discussed in the next section (section 2). Duo to all the aforementioned properties, biological membranes are crucial contributors for the maintenance of cellular homeostasis.

2. The evolution of the concept of biomembrane

The evidence for an osmotic barrier separating the inner and outer face of cells appeared in the second half of the 19th century[14]. Almost in the end of the 19th century, Charles Overton discovered by studying the osmotic properties of cells that the partition coefficient of molecules between water and oil determines its permeation through membranes[14,15]. Pursuant to such studies it was suggested that the cellular membranes present properties of oil[14,15]. In 1917, it was proposed by Langmuir that in a monolayer of lipids formed at the air-water interface, the polar head groups interact with the water whereas the hydrophobic backbones avoid the liquid phase, pointing to the air phase[16]. A great contribution to cell biology was made in the early 20th century. After preparing a lipid extract from human erythrocyte, a lipid monolayer was formed in an air-water interface. By comparing the area occupied by the lipid extract with the surface area of the erythrocyte, Gorter and Grendel noticed that the area of the extracted lipids was the double of the cell surface. Through these very simple experiments, they proposed that the structural basis of the PM is a lipid bilayer[17].

In 1935, Danielli and Davson introduced a new model of biological membrane where it was considered that proteins are adsorbed to the surface of the lipid layers[18] and during the following 30 years, this static structural model prevailed. In 1959, with the progress in electronic microscopy, the model of the lipid bilayer was confirmed and this concept was extended to all organelle membranes[19]. The essential distinction between integral and peripheral proteins, only appeared in 1972, when Singer and Nicolson proposed the "fluid mosaic" model[20]: the membrane is considered a bidimensional solution in which, the proteins are completely or partially inserted in the lipidic bilayer, freely diffusing in it. The word "mosaic" refers to the random appearance of the lipid-protein composition (Fig. 1A). The "fluid mosaic" model is still the main concept of biomembrane, but with the development of new techniques that provided higher structural resolution it is nowadays recognized that the cell membrane presents different structural organization in terms of thickness, patchiness and protein/lipid composition[21,22]. It has been proposed that biological membranes are actually more mosaic than fluid[22], and that the lipid-lipid, protein-protein, lipid-protein and protein-cytoskeleton interactions are responsible for membrane organization. It is now widely accepted

that membrane components are not randomly distributed in the bilayer. Studies from Kusumi group propose that the binding of transmembrane proteins to actin-based membrane skeleton can temporarily confine or corral the transmembrane proteins in the membrane skeleton mesh – "membrane skeleton fence" model. The "anchored transmembrane protein picket" model in other hand explains the hop diffusion of phospholipids (PLs) - various transmembrane proteins are aligned and anchored along the membrane skeleton, acting as rows of pickets that hampers the free diffusion of PLs[23–25]. There is also the concept of specialized membrane lipid domains, the most extensively studied being known as lipid rafts. This concept appeared for the first time to explain the formation of glycolipid-rich apical membrane of epithelial cells[26]. The concept was then generalized as a principle of membrane subcompartmentalization, where specialized membrane regions would be responsible for the segregation of proteins and involved in crucial biological processes, such as, signal transduction and trafficking[27–31]. A clear definition of lipid rafts only appeared in 2006: rafts were defined as "small (10–200 nm), heterogeneous, highly dynamic, sterol- and sphingolipid-enriched domains that compartmentalize cellular processes. Small rafts can sometimes be stabilized to form larger platforms through protein-protein and protein-lipid interactions"[32]. It is thought that lipids present in these domains are enriched in saturated and longer hydrocarbon chain and ceramide backbones, contributing to the less fluid nature of these domains[33–35]. This more ordered lipid environment, presented both in the inner and the outer leaflets of an asymmetric cell membrane can presumably be linked across leaflets[36,37], creating transient, functional and more stable platforms that would cause the entrapment of signaling molecules, thus creating the conditions to activate signaling events[33,34]. The concept of membrane raft is still being developed and it was proposed that for a full understanding of these domains, it is crucial to consider the following raft features: i) different properties before and after stimulation; ii) variation of sizes, lifetimes and molecular constituents[25]. It should however be mentioned that the presence of these domains in live cells remains a question of debate duo to lack of suitable techniques to detect these small and short-lived domais[38–40]. Nonetheless, the crucial role of membrane lateral heterogeneity in cellular function is widely recognized[41] and efforts have been made to better characterize such membrane heterogeneity[42,43].

Kusumi and coworkers[25] proposed that the PM can be considered as a hierarchical three-tiered cooperative meso domain, in which the first tier corresponds to the actin membrane-skeleton-induced compartments – PM partitioning into domains with 40-300 nm in diameter due to its interaction with the actin based membrane skeleton and transmembrane proteins anchored to the membrane skeleton fence; the second tier corresponds to the raft domains, generally much smaller (2-20 nm) than membrane-skeleton-induced compartments and the third tier refers to dynamic, oligomeric integral protein complex domains that usually present 3 to 10 nm in diameter and that may or may not be linked to the cytoskeleton. In addition, an update "fuid mosaic" model has been proposed based on the new data that also covers concepts of membrane curvature[44] related to the geometrical and mechanical properties of lipids and proteins, lipid phases and deviations from equilibrium[45,46] (Fig. 1B). Briefly, the actual concept of biomembrane include: i) membrane associated cytoskeletal fences; ii) the formation of specialized membrane domains, such as lipid rafts and dynamic protein/glycoprotein complexes; and iii) extracellular matrix structures[45]. This additional information contributes to a better description of the structure, dynamics and functions of cellular membranes. In the crowded membrane plane, the specialized membrane domains and the transmembrane protein fences along with other membrane-associated cytoskeletal and extracellular structures contribute to the non-random mosaic macro-organization of biomembranes, while the smaller nano or sub-micro sized domains such as membrane lipid rafts and protein complexes form dynamic specialized regions in the membrane. This description/model will undoubtedly become more and more complex in the future with additional answers concerning not only composition, function and dynamics but also thermodynamic and physical explanations regarding the functional and structural activities of membrane components[45].

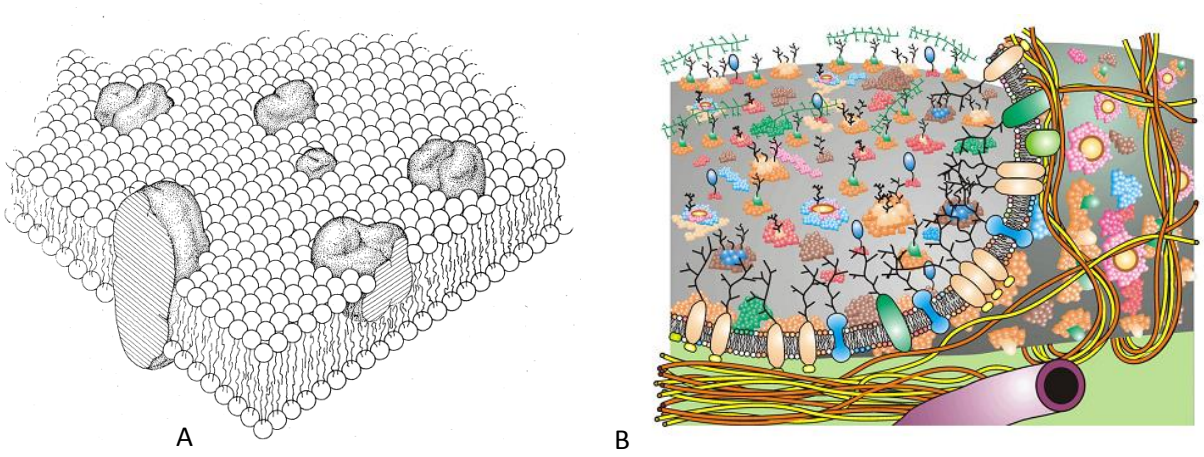

Figure 1 - (A) The "fluid mosaic" model proposed by Singer and Nicolson[20]. (B) Updated version of the "fluid mosaic" model, containing information regarding membrane domain structures and membrane-associated cytoskeletal and extracellular structures. The different colours represent different lipids, proteins, glycoproteins and oligosaccharides. Adapted from Singer and Nicolson (1972)[20] and Nicolson (2014)[45].

3. Membrane structural components

Biological membranes are composed by lipids, proteins and carbohydrates (Fig. 2). As previously referred, its structure consists of a double sheet of lipid molecules, also known as lipid bilayer. In addition to the vast repertoire of lipids that constitute biological membranes, there are also various types of membrane proteins and carbohydrates that are crucial components of the bilayer structure[47].

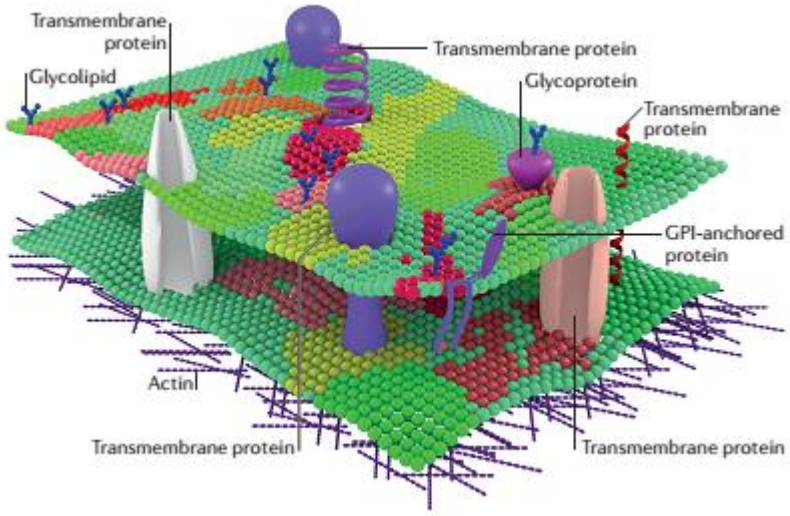

Figure 2 – Structural components of the biological membranes. Adapted from Sezgin *et al*. (2017)[34].

Lipidomics is a relatively recent scientific field dedicated to the analysis of the lipid world[48]. After more than a decade of evolution, many methods have been developed for lipidomics analysis. Among other techniques, mass spectrometry (MS) and nuclear magnetic resonance (NMR) are very useful approaches for lipid characterization[49]. Lipidomic studies enabled the identification of a wide variety of lipids[50–52]. In an eukaryotic cell, thousands of different lipid species can be present due to variation of the headgroups and aliphatic chains[48,53]. The lipid organization in the membrane allows different protein arrangements. In addition, lipids enable cells to fuse, fissure and tubulate, features that are needed for cell division and reproduction[53]. Some lipids are also recognized by their ability to act as first and second messengers in important signaling cascades[53–55]. The great diversity of lipids in cell membranes can be divided in eight categories based on their chemical and biochemical principles: fatty acyls, glycerolipids, glycerophospholipids, sphingolipids, sterol lipids, prenol lipids, saccharolipids and polyketides. These categories are then divided in classes that have diverse structural and chemical properties[56]. In the framework of this dissertation focus will be given to glycerophospholipids, sphingolipids and sterol lipids, major lipid categories used in the present study (Fig. 3). **Glycerophospholipids** are the main structural lipids in eukaryotic membranes, representing about 65 mol% of lipids in mammalian cells[57]. These lipids are derivatives of glycerol phosphate and in most of them the phosphate is at the *sn*-3 position of

the glycerol. Different classes of glycerophospholipids can be distinguished considering the group that is linked to the phosphate. Some examples are Phosphatidylcholine (PC), that accounts for more than 50% of the PLs in most eukaryotic membranes[53], Phosphatidic acid (PA), Phosphatidylethanolamine (PE), Phosphatidylserine (PS), Phosphatidylglycerol (PG) and Phosphatidylinositol (PI)[53,54,58]. 2) **Sphingolipids** (SLs), differ from the glycerophospholipids in the hydrophobic group that is ceramide. This group represents about 10 mol% of lipids in mammalian cells[55,57]. The backbone of a sphingolipid is constituted by a sphingoid base that after acylation gives rise to ceramide, which in turn can be glycosylated or linked through phosphodiester bridges to various headgroups[59], as will be described in section 6. Glycosphingolipids (GSLs) are included in this category of lipids and can vary from simple cerebrosides, GSLs containing a single carbohydrate residue – glucosylceramide (GlcCer) or galactosylceramide (GalCer) - to more complex molecules, such as glangliosides, that are constituted by an oligoside containing sialic acid linked to ceramide[60]. 3) **Sterols**, constitute the major class of non-polar lipids in biomembranes[53]. Structurally, these lipids are characterized by the presence of a steroid hydrophobic core that presents 4 rings linked to an –OH hydrophilic group. In mammalians, Chol is the predominant sterol. This lipid is highly abundant in the PM (ap. 40%)[61] and was identified as an important determinant of membrane fluidity and lateral organization. It influences the organization of other lipids[62,63], such as in the case of the membrane lipid rafts[64] and lipid-anchored membrane proteins[65].

The lipid distribution along the cell and within each membrane is strongly differentiated. The distribution of lipid molecules is distinct between the two membrane leaflets - internal and external. For instance, SLs are mainly found in the PM leaflet facing the external medium, while the aminophopholipids PS and PE are essentially located in the cytosolic leaflet[57]. The lipid distribution is also different among the distinct cellular membranes[57]. As an example, the PM is enriched in SLs and Chol[66], the inner mitochondrial membrane is enriched in cardiolipin[67] and the internal membranes of the acidic compartments are enriched in the negatively charged bis(monoacylglycero)phosphate (BMP)[68]. The distinct lipid distribution is fundamental for membrane organization into functionaly distinct areas, and thus for the compartmentalization of distinct cellular processes in different sub cellular spaces. Accordinaly, Chol is commonly

linked to the formation of membrane lipid rafts[34], while cardiolipin is associated with the mitochondrial bioenergetics, particularly it is found in membranes designed to generate an electrochemical gradient used in the production of adenosine tri-phosphate (ATP)[67]. The BMP on the other hand, is thought to play a role in GSLs degradation and Chol transport[69].

The ER and the Golgi complex are the major sites of lipid biogenesis[70,71], but there are other organelles involved in phospholipid synthesis, such as mitochondria[72] and perosixomes[72].

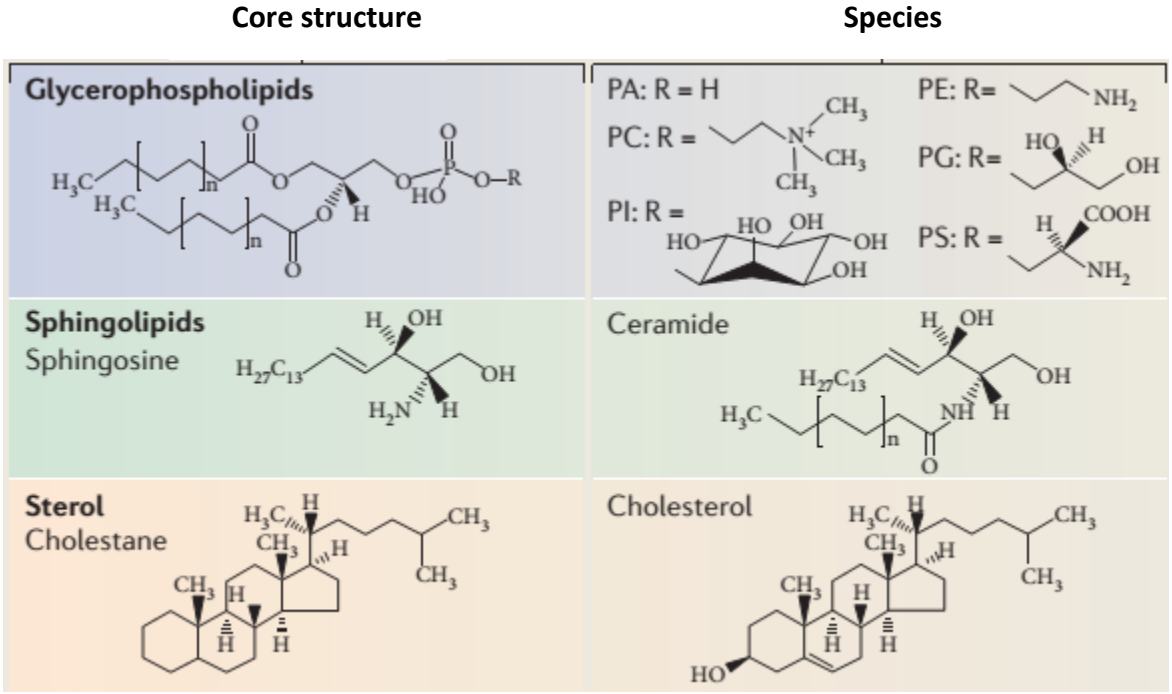

Figure 3 – Examples of lipid categories of eukaryotes and representative structures. Adapted from Saliba *et al*. (2015)[73].

In addition to the lipid bilayer, all biological membranes contain proteins and carbohydrates. Membrane proteins are fundamental for cellular function, serving as specific receptors, enzymes, transport proteins, and so on. The ratio between proteins and phospholipid molecules will depend on membrane function. Typically, a ratio of 1 protein per 25 phospholipid molecules is present in the PM, but in the mitochondrial internal membrane - specialized in energy processing, there are in average 1 protein for every 15 lipids. On the other hand, the membrane of myelin that encloses the nerve cells, uses the properties of lipids as electrical insulators and has 1 protein for 70 lipid molecules[2]. Membrane proteins are

distributed either in the surface (peripheral) or immersed (integral) in the membrane bilayer[34,74]. Integral proteins are usually attached to the lipid bilayer through hydrophobic and electrostatic interactions but some of them can also covalently attach to fatty acids or other lipid groups[2]. These proteins are folded in a way that its nonpolar hydrophobic surface interacts with the nonpolar region of the lipid bilayer, while the polar region interacts with the lipid headgroups at the membrane surface. Some of these proteins completely cross the lipid bilayer - transmembrane proteins, while others only partially integrate it (Fig. 2). Contrary to integral proteins, pheripheral proteins, do not penetrate the hydrophobic core of the lipid bilayer. They are weakly bound to the membrane surface, through electrostatic interactions with either lipid headgroups or other proteins[74]. Glycosylphosphatidylinositol (GPI)-anchored proteins are attached to the membrane through a GPI moiety, hence their designation. They are also present in membrane lipid rafts[34] but they become water soluble proteins if the lipid anchor is hydrolyzed. In eukaryotic cells, the synthesis of membrane proteins starts on the cytosolic ribosomes. In a first step, a short segment of protein is synthesized and the ribosome, mRNA and nascent protein chain associate with the ER, where the protein synthesis is finalized and simultaneously inserted into the membrane[47].

Membrane carbohydrates occur almost invariably chemically attached to either membranes lipids (glycolipids) or membrane proteins (glycoproteins) (Fig. 2). These membrane carbohydrates are synthetized in the ER and are modified in the Golgi complex, by the addition of many new monomers, to form more complex molecules[12]. These molecules are mostly located in the outer monolayer of the PM, facing the extracellular area, although some of them can also be associated to intracellular membranes. The whole group of membrane carbohydrates is known as glycocalyx. This is a dynamic structure, generically composed by glycoproteins and proteoglycans that insert their amino acid chain among the lipid fatty acids[75,76]. The composition and thickness of the glycocalyx is continuously changing in a dynamic equilibrium between the soluble components and the flowing blood[75]. This structure plays an important role in different cellular processes, being involved for instance in cell adhesion[77,78] and cellular recognition[79].

4. Membrane lipids and lyotropic phase structures

Due to their amphipathic nature, lipids form aggregates when in contact with water, protecting the hydrophobic moiety from the aqueous phase. These molecules are invariably polymorphic and, depending not only on the structure of the lipid molecule itself, but also on other parameters such as water content or degree of hydration, temperature, ionic strength, pH environment and pressure (see reference[80] and the references therein), two types of aggregates can be distinguished: the lamellar phases (L), where the lipids are organized in a bilayer, and the non-lamellar phases, where the lipids acquire hexagonal (H) or cubic (C) structures (Fig. 4)[81]. At neutral pH and physiological ionic strength most of the lipids prefer the lamellar phase, while others (e.g. PE) may prefer the inverted hexagonal (H_{II}) phase, depending on temperature and acyl chain composition[80,82]. This non-lamellar phase is usually related to transient events in the membrane (e.g. fusion, pore formation)[53]. Different types of hexagonal and cubic phases have been identified[83,84]. Among the cubic phases two classes can be distinguished: i) inverted micellar, in which spherical aggregates of lipids pack together in a cubic array; ii) bicontinuous, in which the lipid phase and the water channels are in continuous space[85]. In the hexagonal phase, hollow cylinders of lipids are formed, being the most frequent the H_{II} phase. The lipid headgroups face the cylinder interior, which is filled with water, and the acyl chains form the exterior. Each cylinder is surrounded by other six cylinders - hexagonal structure[85].

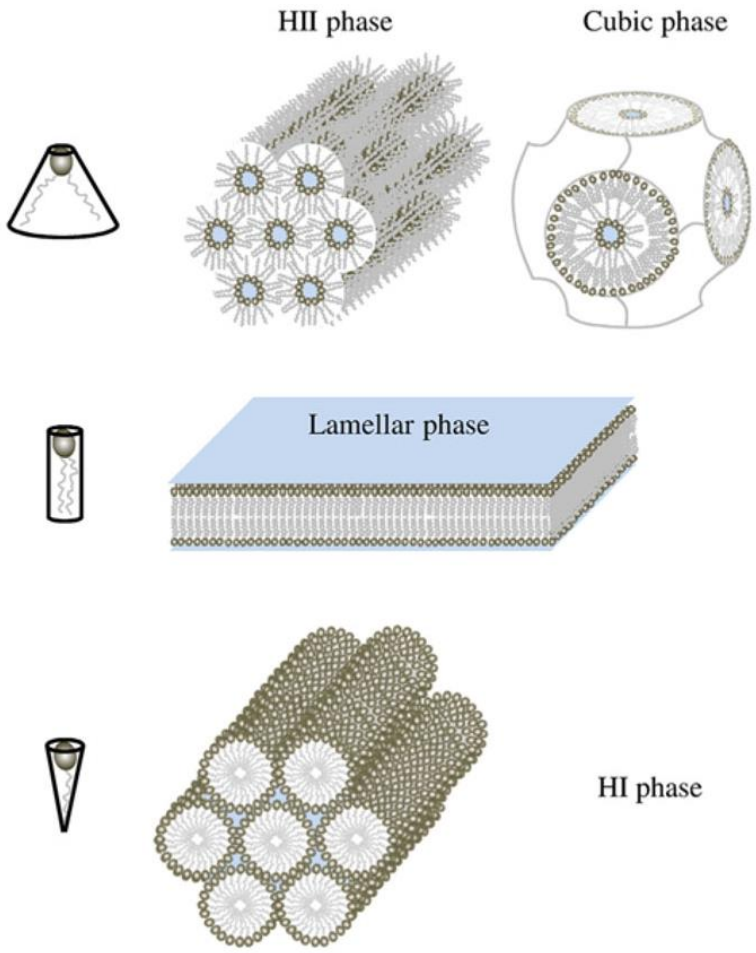

Figure 4 – The different lattice types resulting from lipid polymorphism. Lipids with a small polar head, such as PE have a molecular shape that resembles a truncated cone. They may induce a negative curvature strain and favor the organization of membranes into inverted micelles or tubular (H_{II} phases) or even cubic (bicontinuous) structures. Lipids with a bulky polar head, such as, gangliosides and only one acyl chain, such as lysoPC have a molecular shape similar to an inverted cone and induce a positive curvature strain in membranes. They favor the formation of tubular (H_I) or spheric micelles. Lipids that have similar cross-sectional areas for the polar head and hydrophobic region, such as PC assume cylindrical structures. They form lamellar phases, with no curvature. Adapted from Jouhet (2013)[81].

Lamellar phases are ubiquitous in cellular compartments and can phase-separate upon mixing lipids in different liquid-crystalline states[86]. The most relevant lamellar phases are: i)

fluid or liquid disordered (L_α or l_d), ii) gel or solid ordered (L_β or s_o), and iii) liquid ordered (l_o) (Fig. 5).

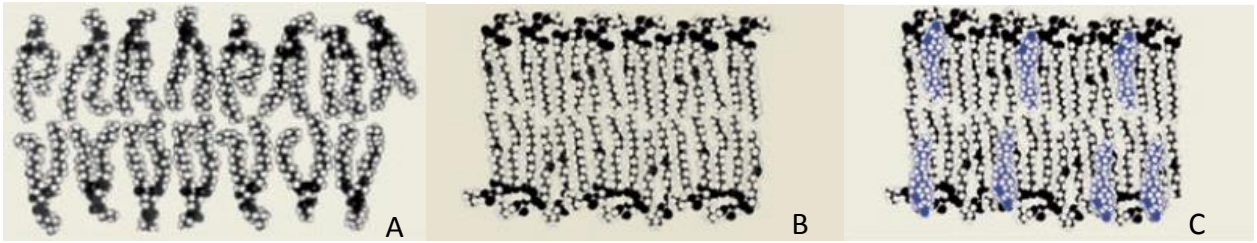

Figure 5 - Different lipid lamellar phases. Schematic representation of (A) liquid disordered (l_d), (B) gel or solid ordered (s_o) and (C) liquid ordered (l_o) phase. Adapted from van Meer *et al*., 2008[53].

Lipids with long and saturated hydrocarbon chains (e.g. SM) are frequent in more ordered phases, while lipids with unsaturated hydrocarbon chains (as most glycerophospholipids) tend to incorporate more fluid phases[53].

According to the "fluid mosaic" model, the fluid phase is considered the one that better represents the biological membrane. In this phase, in comparison to the other lamellar phases, the water content is higher, there is a larger interfacial area and the bilayer thickness is smaller. The lateral diffusion is increased concomitant with the appearance of fast rotation motions of the acyl chains. The lipids are not in a true liquid state, they are able to move with significant freedom in a parallel plane to the membrane surface, but not so extensively in a perpendicular direction[46,53]. Considering the conformational freedom of the lipids within the fluid phases, two phases can be distinguished: i) liquid-disordered (l_d) and ii) liquid-ordered (l_o), if Chol is present in the membrane[53].

In the l_o phase, the lipids are in extended conformations and tightly packed, although not as much as in the gel phase, diffusing laterally in the perpendicular axis of the bilayer, but slower when compared to the l_d phase[53]. The lipid raft domains mentioned previously, characterized by the tight packing of the lipid saturated acyl chains and Chol are thought to be in the l_o phase, coexisting with the disordered surrounding lipids (l_d phase)[87,88]. Due to the favorable packing with saturated lipids, the presence of Chol seems to stimulate this type of phase separation[88].

Even though the water content in the gel phase is usually very low, it depends on the lipid headgroup size, polarity and charge. A slow rotation along the long-axis occurs due the organization of the hydrocarbon chains in an all-*trans* conformation[53,89,90]. In this phase, the cross-sectional area is minimal and the bilayer thickness is maximal, which results in closely packed headgroups and hydrocarbon chains[91]. In order to enhance the packing, the acyl chains are perpendicular to the bilayer surface for lipids with small headgroups (e.g. ceramide)[92] (gel phase, L_β) and tilted for lipids with larger headgroups[84] (gel phase, $L_{\beta'}$), such as in the case of DPPC[93] and 1,2-distearoyl-*sn*-glycero-3-phosphatidylcholine[91].

The occurrence of fluid and gel phases as previously referred do not depend solely on the structure of the lipid molecules, but also other factors, such as temperature. For each bilayer-forming lipid, there is a specific temperature, known as main transition temperature (T_m), at which 50% of the thermotropic transition between gel and fluid phases occurs[94,95]. At that temperature the two phases coexist and some packing defects appear at the interface between the two phases[88]. In addition to a transition between a gel and fluid phase, some lipids present a pre-transition, at temperatures below the T_m, characterized by the formation of periodic ripples (P_β, rippled gel) in the membrane[96]. The L_β to L_α chain-melting phase transition has been the most intensively studied lipid phase transition[80], considering that most membrane lipids exist in the lamellar fluid phase under physiologically relevant conditions[53,97], but sometimes also in the lamellar gel phase[98].

When studying the lipid-lipid interplay, the phase transitions can be schematically represented by phase diagrams (Fig. 6)[95]. The higher the number of lipids included in the mixture, more complex is the phase behavior and usually there is a broad range of temperatures where two or more phases can coexist. To define the boundaries of a phase diagram, different techniques can be used in order to detect the lipid phase changes. These include differential scanning calorimetry (DSC), fluorescence spectroscopy and NMR[99–101].

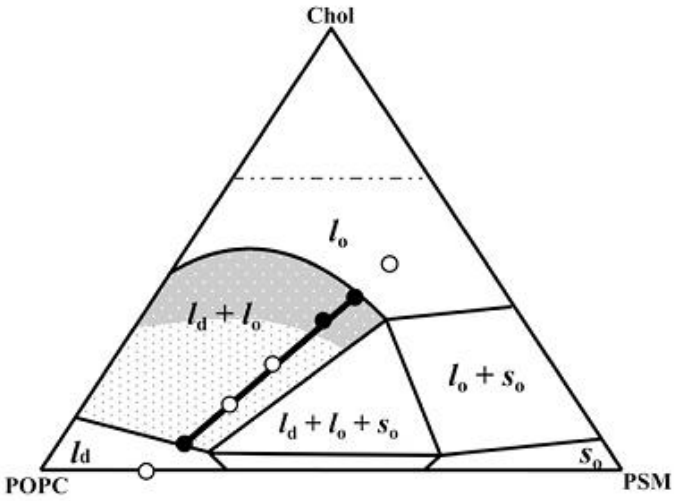

Figure 6 – Example of a ternary phase diagram determined for POPC/PSM/Chol mixtures at 24 °C. The black line corresponds to the tie line that contains the 1:1:1 POPC/PSM/Chol mixture. The grey shades represent regions of different sized raft domains. Legend: l_d, liquid disordered; l_o, liquid ordered; s_o, solid ordered. Adapted from Silva *et al*. (2007)[102].

5. Strategies to study lipid-lipid interactions and membrane properties

The biophysical properties of a membrane are determined by its composition, specifically by the lipid-lipid, lipid-protein and protein-protein interactions. The large number of different lipids and proteins, their distinct interactions and the changes that occur in the membrane due to these interactions, underlie biomembrane complexity. Due to their different structures, regarding both headgroups and chain structures, lipids are able to influence the thickness and packing of the membrane[95,103], and its dynamic organization. In addition, lipid net charge might influence the spatial location of proteins, for instance, through the electrostatic interactions between negatively charged lipids and cationic moieties of the proteins[104]. As previously referred, lateral heterogeneities in the membrane set different domains with distinct physical properties and functions from the neighboring regions[90], which might determine the regulation of conformational state and sorting of membrane proteins. Well-known examples of these specialized domains are the lipid rafts[33,105,106] and the ceramide-platforms[107,108]. A better understanding of the interdependence between the changes that occur in the different membrane domains is needed. However, due to the complex nature of biomembranes it is

difficult to study the biophysical properties of biological membranes and characterize the features of the different phases *in vivo*. Accordingly, different types of membrane model systems have been developed (see sub-section 5.1) and several studies (e.g.[109–112]) have been performed using these membrane models to better understand the interplay between different lipids in the more complex biological membranes, as well as to predict how membrane properties will change when alterations in lipid composition occur.

5.1. Model membranes

Different types of artificial systems can be used, and their composition and complexity can be manipulated according to the specific goals of the study. They can be constituted by one or more lipids, and include or not proteins[113,114]. Liposomes have been the most common model systems used in the characterization of membrane properties and the related biological processes[114] but they also have important applications in the pharmaceutical[115] and food industry[116]. This kind of vesicles can present different sizes and lamellar organization (Figure 7)[117]. For instance, multilamellar vesicles (MLV) present different overlapping layers and are spontaneously formed when bilayer-forming lipids contact with water, being very easily prepared[118,119]. Due to its high cooperativity in phase transition, this system is the most suitable to study the thermotropic properties of the membrane[120]. However, some disadvantages are also associated with these model membranes, for instance, the size and number of layers are not homogeneous, which can be responsible for an increase in light scattering, affecting photophysical studies[121]. Among other techniques[119], large unilamellar vesicles (LUV) can be obtained after the repeated extrusion of MLV through polycarbonate filters with specific pore-size[122,123]. The lipid amount is about the same in both monolayers[124] and the size of these vesicles can range from 100 nm to 1 µm. Due to their easy formation, high reproducibility, stability, controlled size and unilamellar nature, they are very useful in different types of studies, such as the trapping of solutes and drug delivery[115,125–127], being therefore a widely used model membrane system.

Small unilamellar vesicles (SUV) are smaller than 100 nm and they can be obtained mostly through MLV or LUV disruption, using sonication methods[118,128,129]. In SUV the great majority of

the lipids are located in the outside surface and the aqueous space is small. The smaller the size of the vesicle, the higher propensity for the occurrence of fusion events, in order to reduce the tension[130]. This system presents high membrane curvature that hampers the lipid packing[131], and causes low cooperativity in phase transition[132]. These vesicles can be useful in the preparation of supported lipid bilayers[133] or in membrane fusion studies[134].

Giant Unilamellar vesicles (GUVs) have diameters superior to 1 µm, being in terms of size the best cell-mimicking approach. Among other preparation methods[119], these vesicles are commonly obtained through electroformation[135]. Due to their large size, these systems are very suitable for microscopy studies and useful in the analysis of the biophysical properties of membranes, such as the observation of phase separation and membrane domains. This can be achieved through the use of fluorescent probes which have different partitions towards the phases present in the membrane[136].

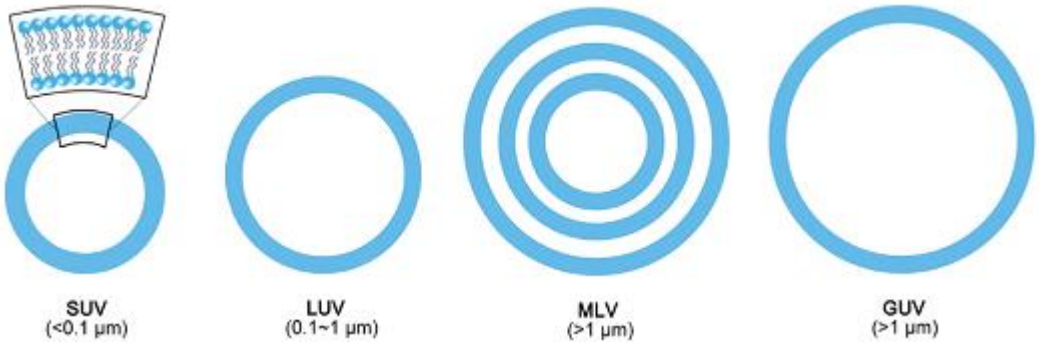

Figure 7 - Schematic representation of the most commonly applied liposomes. The drawings are not to scale. Adapted from Li *et al.* (2017)[117].

5.2. Membrane characterization

There are several techniques available to characterize the biophysical properties of model and cell membranes. Due to their complementarity, they are usually employed in a combined way in order to allow a more comprehensive characterization of the systems under investigation. Some examples are DSC, fluorescence spectroscopy and microscopic techniques (e.g. confocal microscopy and atomic force microscopy).

In this section, the principles of the main characterization techniques used in this work will be briefly described.

5.2.1. Fluorescence Spectroscopy

Fluorescence spectroscopy comprises a set of techniques often employed in biophysics. The photophysical properties of fluorophores incorporated in the membrane are evaluated, through steady-state and/or time-resolved fluorescence methodologies, giving information about the physical properties of a specific lipid environment, such as fluidity, pH, or water content[137].

Before fluorescence emission occurs, a fluorophore must enter in an excited state after light absorption, which is represented by a transition from the fundamental electronic state (S_0) to a singlet electronic state of higher energy (e.g. S_1 or S_2). Upon excitation, the energy absorbed by the fluorophore, can then be released through different processes, some of them represented in the Jablonski diagram (Fig. 8). The release of energy to the lowest exited-state energy level (S_1) generally occurs through non-radiative processes. However, this internal conversion process may also give place to a radiative process, through the emission of photons. Fluorescence, for instance, corresponds to the radiative relaxation from S_1 to S_0[138,139].

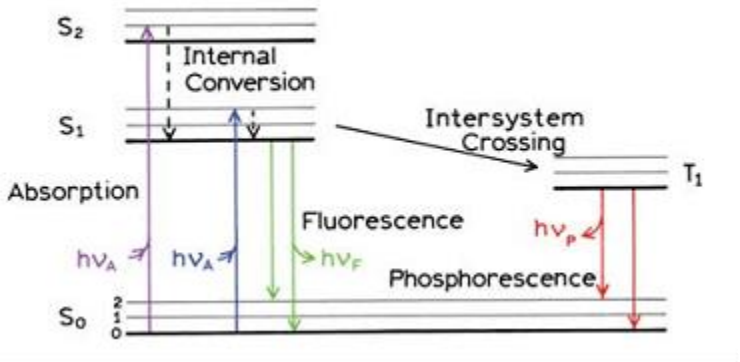

Figure 8 – One form of Jablonski diagram. The singlet electronic states are denoted as S_0, S_1, S_2 and one triplet state is represented by T_1. Adapted from Lakowicz (2006)[138].

Fluorescence Emission and excitation spectra

When a fluorophore is excited at a fixed wavelength and the fluorescence intensity is collected for a range of higher wavelengths, an emission spectrum is obtained. In order to obtain an excitation spectrum, the inverse process is carried out, i.e., the fluorophore is excited at various wavelengths and the fluorescence intensity is collected at a fixed wavelength[138].

Fluorescence spectra are sensitive to changes in the medium and for that reason might be useful to study changes in the environment in which a fluorophore is inserted[138]. The polarity of the solvent, for example, has a large effect on the spectral properties of some fluorophores. As already mentioned, upon excitation, the fluorophore rapidly losses the excess of vibrational energy and relaxes to level S_1, from where the emission occurs. This process, in which the maximum of fluorescence emission occurs at less energetic wavelengths, i.e. longer wavelengths, than that of absorption, leads to an energy gap between the absorption and the emission spectrum, termed the Stokes´shift[139]. The effect of solvent polarity displaces emission for even lower energy levels due to stabilization of the fluorophore in the exited state, lowering the energy of S_1 level (solvent relaxation). When returning to the ground state, the dipole alignment will no longer be optimal, which means that the energy in S_0 is now higher than the initial state (before excitation). This results in a lower energy gap between S_1 and S_0 manifested by emission in longer wavelengths (red shift in emission)[138,139]. However, excitation spectra are usually less suitable because no solvent relaxation takes place during extremely fast absorption process.

Steady-state fluorescence anisotropy

When a fluorophore is continuously illuminated with a lamp emitting a constant flow of photons, the concentration of excited fluorophore remains constant, which means it is in a steady-state. Steady-state fluorescence anisotropy is regularly used in membrane biophysics studies, since it can sense the environment in which the fluorophore is inserted. This methodology consists in the measurement of depolarization of emitted light. Upon excitation with polarized light, the fluorophores with a parallel transition dipole with the electric vector of excitation will absorb the photons more efficiently. Then the emitted photons are measured

after passing through a linear filter light (polarizer) that is positioned in either a parallel or a perpendicular direction of the polarized light excitation[139]. The anisotropy can be calculated using the intensities of the emitted light, through equation 1:

$$r = \frac{(I_{VV} - G \times I_{VH})}{(I_{VV} + 2G \times I_{VH})} \qquad (Eq.1)$$

where the different intensities (*I*), are the vertical and horizontal components of fluorescence emission in steady-state with vertical (I_{VV} and I_{VH}, respectively) and horizontal (I_{HV} and I_{HH}, respectively) excitation relatively to the emission axis. G factor can be determined by the I_{HV}/I_{HH} ratio and is used to correct the different sensitivity of the detector for the vertical and horizontal polarization[138].

Fluorescence anisotropy (<*r*>) measurements are performed in a spectrofluorometer equipped with polarizers, as exemplified in figure 9.

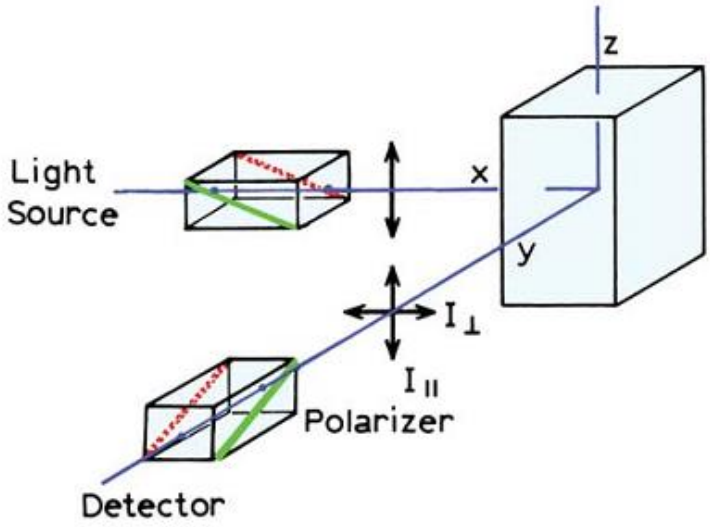

Figure 9 – Schematic representation for the measurment of fluorescence anisotropy. Adapted from Lakowicz (2006)[138].

As previously referred fluorescence anisotropy might be used in order to sense the environment in which the fluorophore is inserted. In this way, if the fluorophore is located in a rigid environment its rotational movement will be hindered and the depolarization of light is inefficient. In this case the polarization of emitted light will be intimately related with the polarization of the excitation light. On the other hand, if the fluorophore is located in a more fluid environment, its rotation is facilitated and there is no preferential polarization orientation for the emitted light[138].

In the absence of depolarization processes, a fundamental anisotropy value will vary depending on the angle between the absorption and emission transition moments. A variation from a maximum of 0.4, in a collinear situation (0°) to negative values of -0.2 for an angle of 90° can occur[138]. Considering a practical application of this concept, if we consider a fluorophore with an angle of 0° inserted in a rigid region of the membrane, like a gel phase, it will exhibit a high anisotropy value that is usually superior to 0.3. When the same fluorophore, with the same angle is located in a more fluid region of the membrane the anisotropy value decreases.

Fluorescence Lifetime of the Intensity Decay

The average time that a molecule remains in the excited state is given by its fluorescence lifetime[139]. A fluorescence intensity decay is obtained after an excitation pulse infinitely short, with enough energy for a given number of molecules to pass into the excited state. Some molecules promptly emit a photon just after being excited, however other molecules take longer times for the photon emission. This is the reason way the lifetime corresponds to a statistical average. Through the time distribution of the emitted photons, an intensity decay is obtained[138].

Fluorescence decays can be described by only one exponential (simple decays) or by a sum of exponentials (complex decays). Equation 2 describes a single exponential decay that is directly obtained from the time-dependent intensity, while equation 3 describes a multi-exponential decay with n components:

$$I(t) = I_0 \ \exp\left(-\frac{t}{\tau}\right) \qquad (Eq.2)$$

where I_0 corresponds to the intensity at time 0, and the lifetime is the inverse of total decay rate.

$$I(t) = \sum_{i=1}^{n} \alpha_i \exp\left(-\frac{t}{\tau_i}\right) \qquad (Eq.3)$$

where α_i and τ_i are the normalized amplitude and lifetime of the component *i*, respectively

The mean fluorescence lifetime of a fluorophore can be defined by equation 4:

$$< \tau >= \frac{\sum_{i=1}^{n} \alpha_i \tau_i^2}{\sum_{i=1}^{n} \alpha_i \tau_i} \qquad (Eq.4)$$

The time-correlated single-photon counting method, also known as single-photon timing is the most popular technique for lifetime determination. The principle of this technique is based on the fact that the probability of detecting a single photon at time t, after an excitation pulse, is proportional to the fluorescence intensity at that time[138]. The time between the excitation pulse and the emission of the photon is represented as a histogram (Fig. 10).

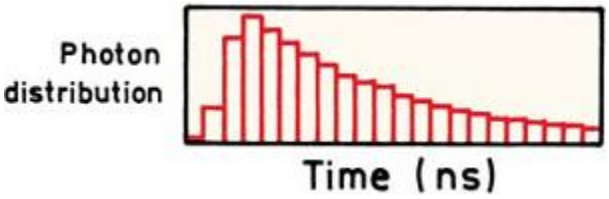

Figure 10 – Histogram representing the photon counting over time in order to obtain the average fluorescence lifetime of a fluorophore. Adapted from Lakowicz (2006)[138].

As for fluorescence anisotropy, the fluorescence lifetime is also dependent on different environmental factors (e.g. temperature and polarity) and it can be used as a complementary methodology in membrane biophysics. In general, fluorophores displaying longer lifetimes are usually partitioned into more rigid membrane regions, while the incorporation into more fluid areas is reflected by shorter lifetimes.

5.2.2. Fluorophores

There are a number of different fluorophores available for the study of membrane biophysical properties. The selection of those probes will depend on the specific purpose of the study. Some probes are used for labelling specific lipid molecules, others are sensitive to the hydration of the surrounding environment and there are also some probes that selectively partition into distinct membrane phases, being very useful for the study of membrane organization[40,140,141]. An example of these probes is *trans*-Parinaric Acid (*t*-PnA) which was specifically selected for this work, with the aim of studying the Sph interplay with other membrane lipids. *t*-PnA presents a preferential partion for tightly packed domains (gel phase), where it presents a high quantum yield[142]. The *t*-PnA intensity decay is usually described by a sum of 3 or 4 exponentials and the longest lifetime component that reflects the order of the highly packed domains is often used as a fingerprint for the gel phase detection (values > 30 ns)[102].

The probe 1,6-diphenyl-1,3,5-hexatriene (DPH), was also used in this work and contratry to *t*-PnA, displays an equal partition among the different membrane lipid phases (l_d, l_o and gel)[140] (Fig. 11). DPH is a very sensitive probe to evaluate membrane fluidity[143]. It presents almost no fluorescence in water, but when inserted in the membrane bilayer its fluorescence increases significantly. Despite its non-preferential partition to distinct lipid phases, this probe shows a higher anisotropy and lifetime values in l_o and gel phases, compared to the l_d phase.

TMA-DPH, the trimethylammonium derivative of DPH, has a more shallow location in the membrane compared to the hydrophobic DPH[143] and it was punctually used in this work, in an attempt to acquire additional information regarding the interaction of Sph with cell membranes.

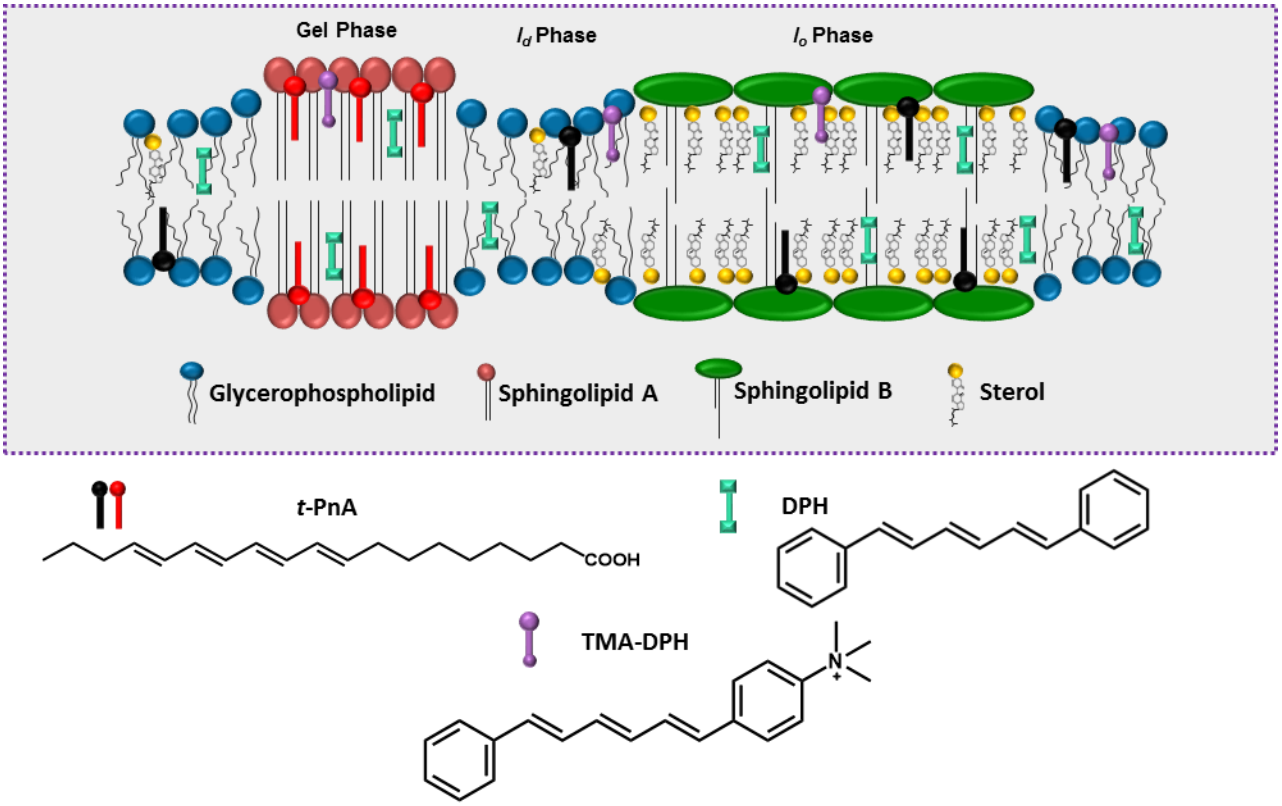

Figure 11 – Predicted location of fluorescent probes used in this work. The polar headgroups of sphingolipids are represented in purple and green) (types A and B), and that of phospholipids in blue. Sterols that are involved in the formation of l_o phases are represented by a ring system. DPH reports the global order of the membrane in the hydrophobic core; *t*-PnA reports acyl chain packing and has preferential partition for gel phases (red *t*-PnA), but can also be found in l_o and l_d phases where it presents a lower quantum yield (black *t*-PnA); TMA-DPH, similar to DPH, reports the global order of the membrane, but is anchored at the membrane surface by the TMA group and is more sensitive to hydration. Adapted from Marquês *et al*. (2015)[144].

5.2.3. Electrophoretic and dynamic light scattering measurements

Dynamic Light Scattering (DLS)

Particle size can be determined by measuring the random changes in the intensity of light scattered from a suspension or solution. This technique is known as DLS and it takes in account

that the random motion of molecules, known as Brownian motion, at room temperature, occurs at a velocity that depends on the size of the vesicles[145–147].

Through the use of a laser beam focused in a small area of the sample, it is possible to perform the measurement of the intensity fluctuations resulting from the light that is scattered by the particles, in this case the vesicles, crossing the focused area (Fig. 12A). The vesicles scatter the light in a way dependent of its hydrodynamic diameter. Moreover, the velocity of the Brownian motion is defined by a property known as translational diffusion coefficient. Through this coefficient, the size of the vesicles can be calculated using the Stokes-Einstein equation:

$$d(H) = \frac{kT}{3\pi\eta D} \qquad (Eq.5)$$

where d(H) is the hydrodynamic diameter, D is the translational diffusion coefficient, k is the Boltzmann constant, T is the absolute temperature and η corresponds to the medium viscosity[145].

The scattered light provides a correlation function from which vesicle size distribution can be obtained (Fig. 12B). This value is accompanied by a polydispersity index (PDI), which provides information about the homogeneity of the size distribution of the sample. The PDI varies between 0 and 1, where values close to zero indicate nearly homogeneous monodisperse solutions and values close to 1 represent heterogeneous populations with a broad distribution of macromolecular sizes, for example, vesicles with different sizes or vesicle aggregation[145,146].

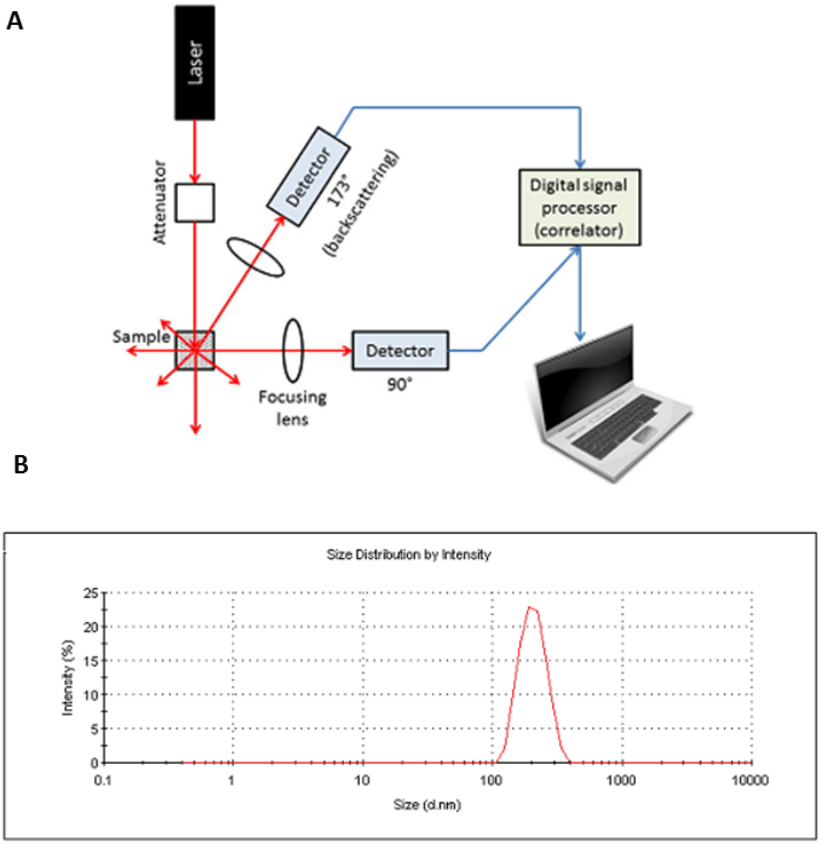

Figure 12 – Dynamic light scattering. (A) Schematic representation of DLS instrumentation. (B) Example of a size distribution plot. Adapted from Bhattacharjee (2016)[147] and Malvern Instruments (2013)[145].

Electrophoretic light scattering (ELS)

The net charge at the vesicle surface affects the distribution of the ions in the surrounding medium. An increased concentration of counter ions occurs in the surface interfacial region and the liquid surrounding the vesicle can be divided into two parts: the Stern layer, an inner region, where the ions are strongly bound and an outer region where the ions are attached less firmly. This means that around each vesicle an electrical double layer exists. In the outer, more diffuse layer, there is a boundary (slipping plane) inside which a stable group of ions is formed. The ions inside this boundary will follow the vesicle movement, contrary to the ones that are located beyond it. The potential that exists at this boundary is known as ζ-potential (Fig. 13)[145,147].

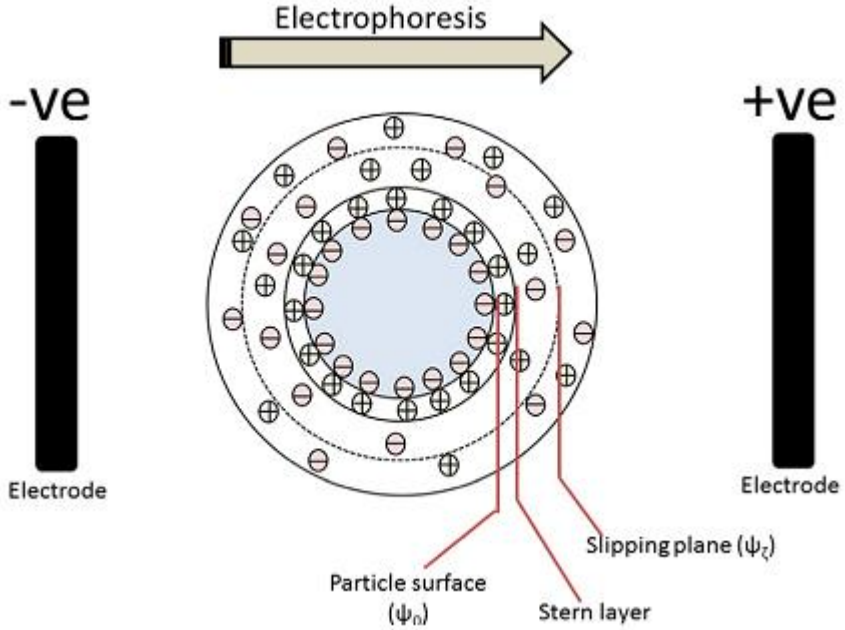

Figure 13 – Representation of the potentials found in a particle in suspension. Adapted from Bhattacharjee (2016)[147].

The technique used to determine the ζ-potential, consists in a micro electrophoresis. An electric field is applied across an electrolyte and the charged vesicles in suspension will be attracted and move towards the electrode of the opposite charge (Fig. 13)[147]. The velocity at which the vesicles move will depend on the strength of the electric field, the dielectric constant of the medium, the viscosity of the medium and the ζ-potential. By applying the Henry equation it is possible to obtain the ζ-potential:

$$u = \frac{\varepsilon\zeta}{\eta} f(KR_S) \qquad (Eq. 6)$$

where ζ is the ζ-potential, $_U$ is the electrophoretic mobility, ε is the dielectric constant, η is the viscosity of the medium and f (KR_s) is the Henry´s function[145].

5.2.4. Permeability studies

In order to evaluate the Sph-induced alterations in membrane permeability, leakage experiments were performed. This methodology is based on the encapsulation of fluorescent probes inside the vesicles. In this work, a well-known fluorophore 8-Aminonaphthalene-1,3,6-Trisulfonic Acid Disodium Salt (ANTS) and its quencher p-xylene-bis-pyridinium bromide (DPX) were used[148]. Both these molecules are entrapped inside the vesicles. If membrane permeabilization occurs after exposing the vesicles to the molecule under study, ANTS and DPX become diluted into the external medium and they hardly interact, which can be reflected by an increase in ANTS fluorescence intensity (Fig. 14).

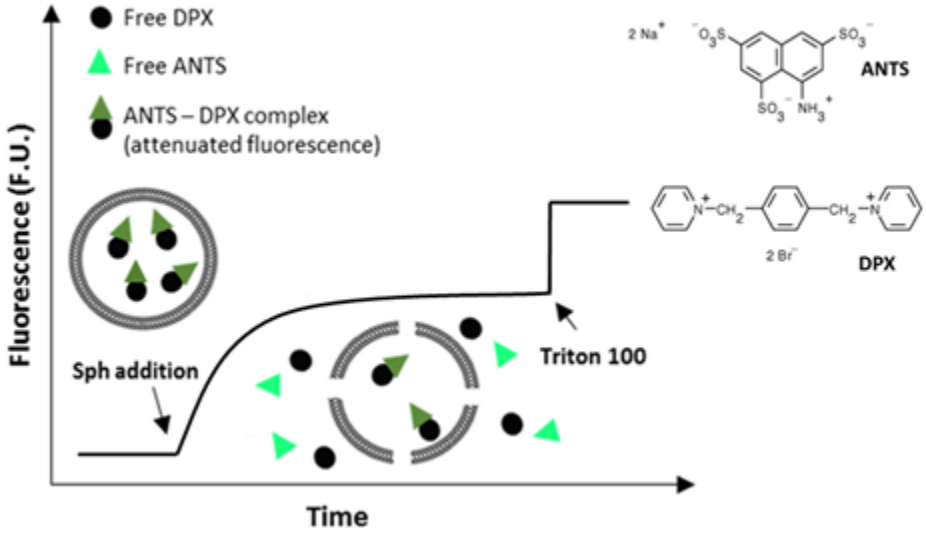

Figure 14 – Schematic representation of an ANTS/DPX leakage assay. The ANTS maximum fluorescence intensity (100% leakage) is obtained after the addition of Triton X-100 in the end of the experiment.

5.2.5. Fluorescence microscopy

Fluorescence microscopy, represents a powerful tool in cell and molecular biology. This technique allows the detection of the fluorescence from a sample itself (auto-fluorescence) or more commonly from fluorophores that are used to detect specific targets. These fluorescent labels can be attached to the molecules/structures of interest with high specificity, providing a strong intensity contrast in the microscopic image of the sample[149]. There are a myriad of

fluorophore molecules[150,151] and fluorophore bioconjugates[152] available in the market and the use of fluorescent proteins[153,154] is also wide-spread.

Different variants of fluorescence microscopy techniques can be used, from the basic widefield microscopy, to confocal laser scanning microscopy (CLSM) and the super-resolution techniques[155] that revealed to be very useful in the study of structures with sizes comprised under the diffraction limit of conventional fluorescent microscopes, such as viruses[156]. These techniques allowed the breaking of the diffraction limit while maintaining the advantages of the fluorescence readout such as non-invasive live-cell imaging and labelling specificity. With such a big diversity of fluorescence microscopy approaches[157] different biological processes can be studied, including cell signaling[158], endocytic trafficking[159], spatial location of proteins/receptors[160], lipid phase separation[140,161] and membrane domains[38,161–163]. A fluorescence microscope is used to separate the emitted light from excitation light as it can be observed in figure 15. Briefly, a dichroic mirror (DM) that is located in an excitation filter cube directs the excitation light that commonly is provided by mercury, xenon, halogen, arc lamps or single-wavelength light emitting diodes (LEDs)[164,165] to the sample or specimen and passes the emitted fluorescence to the emission cube, where it will be separated. To prevent the excitation light from reaching the detectors, a filter barrier is used (marked with the letter B in the image). A second DM is used to separate the emitted fluorescence into two beams and the emission filters (Em 1 and Em 2) block unwanted light. For the detection of fluorescence, cameras in the case of widefield microscopy or photomultiplier tubes in the case of CLSM are used (Fig. 15A). In the CLSM, the DM and the objective lens reflects and focus the laser light in the specimen. Then the laser excites the fluorescence throughout the specimen, which will pass the DM and be focused onto the image plane. Only the light from the confocal plane of the specimen will reach the photomultiplier tube, through the use of a pinhole (Fig. 15B). In CLSM only a small point of the specimen is illuminated and the laser beam needs to scan across it to create an image. In widefield microscopy, the whole specimen is illuminated simultaneously by a parallel beam of light to excite the fluorophore(s). The simplicity of this technique conjugated with diffraction limited optics and the projection of out of focus light onto the single image plane of the camera, can result in images with low spatial resolution and low contrast[166].

However, widefield microscopy is still commonly used and the success of its use depends mainly in the selection of the sample. The selection of thin samples, such as a monolayer of cells, or macroscopic structures such as organelles are preferable in order to reduce the material outside the focus plane[166]. To consider the sample thickness the use of confocal microscopy can be more suitable, since it is able to reject the out of focus light from the image using a pinhole as previously referred, which may result in images with higher resolution[167]. Multiphoton microscopy can also be used to observe far deeper into a thick sample. This technique resort to the use of fentosencond pulsed laser and the simultaneous absorption of two long wavelengths photons in a single event[168,169]. The advantage is that, while maintaining the three-dimensional resolution of an ideal confocal microscope, a higher level of penetration in the sample is achieved with a lower level of photobleaching and photodamage (no absorption and fluorescence above and below the plane of focus), which is fundamental for the visualization of living cells and tissues[169].

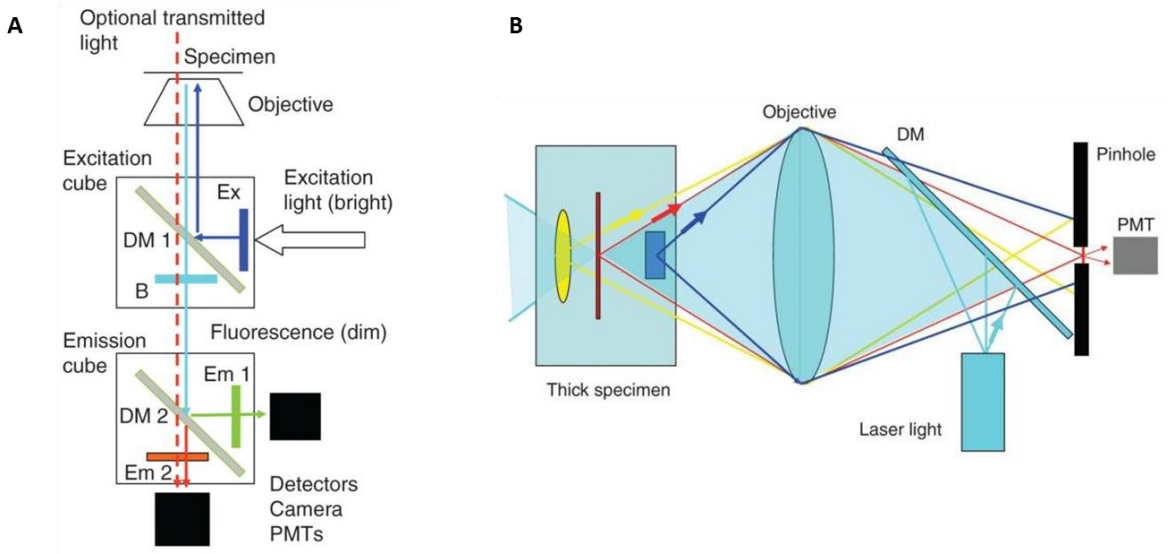

Figure 15 – Fluorescence microscopy principle. A) The basic light paths of a fluorescence microscope and B) operation of a laser scanning confocal microscope. Adapted from Sanderson (2014)[166].

In the present work widefield, LSCM and two-photon microscopy were used for the observation of cellular phenotypes associated with lipid abnormal accumulation.

6. Sphingolipids: Diversity, metabolism and biological role

From a lipidomic analysis, it is estimated that more than thousands of SLs can exist. All of them are encompassed in the LIPID MAPS Structure Database[170], which is regularly updated. The complexity of SLs (Fig. 16) is based on the diversity of the 3 structural components, namely the headgroup, the fatty acyl chain and the sphingoid base.

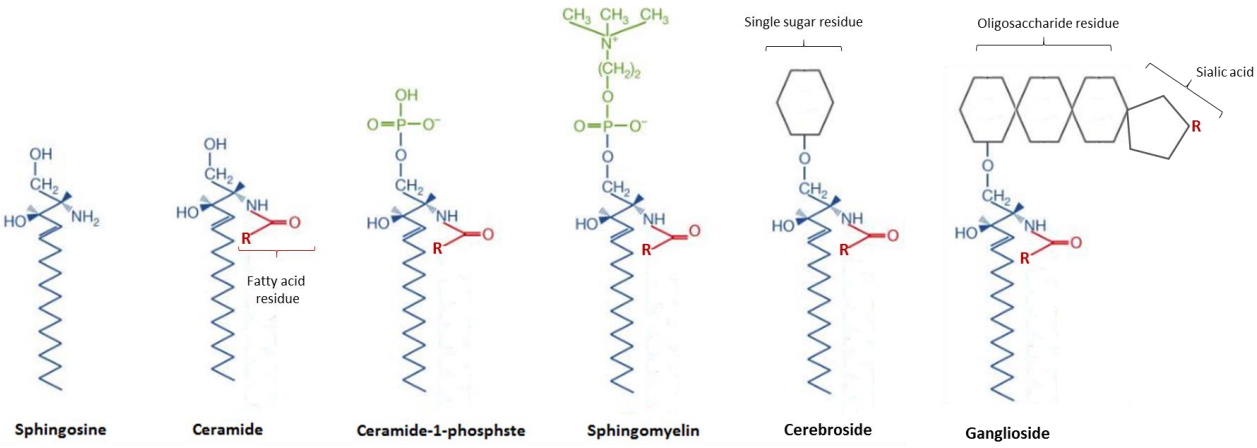

Figure 16 – Representative structures of sphingolipids. Adapted from Futerman and Hannun (2004)[171].

In mammalians, sphingoid basis with a chain length of 18 carbons, such as Sph (2S,3R-D-erythro-2-amino-1,3-octadec-4E-ene-diol, also known as *trans*-4-sphingenine) (Fig. 17), sphinganine (2S,3R-D-erythro-2-amino-1,3-octadecane diol) and phytosphingosine (2S,3S,4R-erythro-2-amino-1,3,4-octadecane triol, also known as 4-hydroxysphinganine), are the most prevalent backbones of SLs, but a number of other sphingoid bases exists and evidence points to more than 60 variants[172,173]. Sphingoid bases with alkyl chain lengths varying from 12 to 26 carbon atoms have been reported[174,175] but variation in the number and position of double bonds and hydroxyl groups also occur[173].

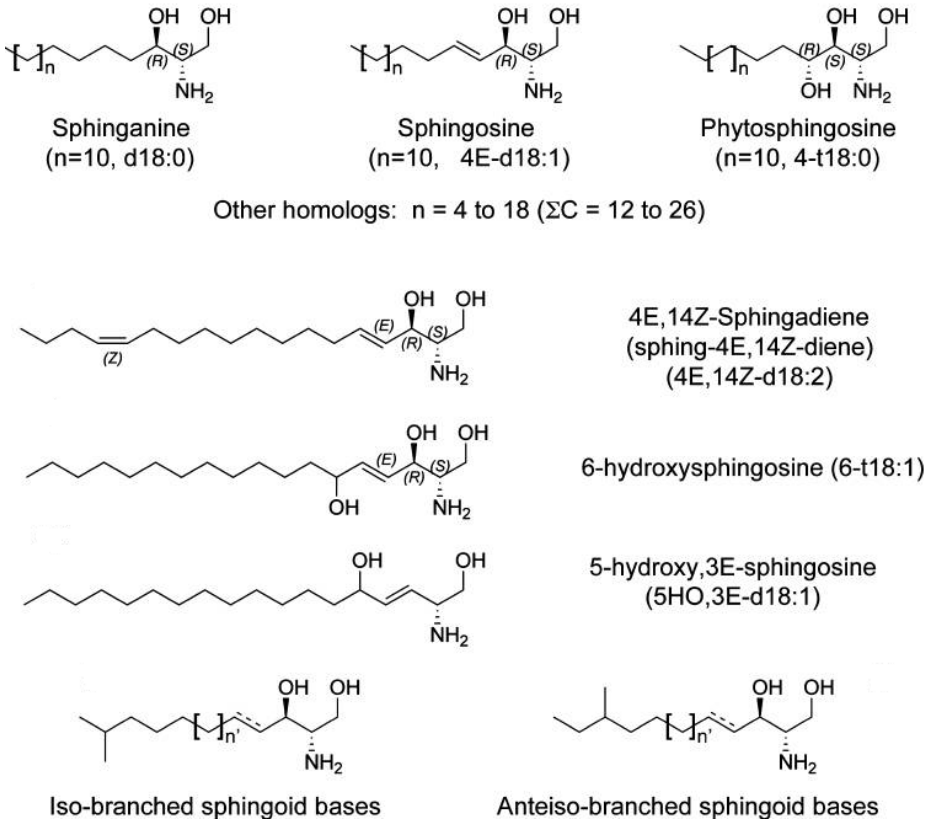

Figure 17 – Examples of sphingoid bases found in mammalian tissues. Adapated from Pruett *et al*. (2008)[173].

The sphingoid base simplified nomenclature created by analogy with fatty acids, considers 3 aspects in the lipid backbone[173]:

i) the number of hydroxyl groups (e.g. “d” for 2 and “t” for 3 hydroxyl groups)

ii) the number of carbon atoms (after hydroxyl groups)

iii) the number of double bonds (including location and configuration; as a prefix or suffix)

Long chain bases with 20 carbon atoms can be found in brain gangliosides and a fine regulation of these molecules must be maintained in order to avoid detrimental effects in the nervous tissues[176]. In human skin, 6-hydroxy-sphingosine is one of the possible sphingoid backbone of ceramide, in addition to Sph and phytosphingosine[177]. The unusual sphingoid bases 3-ethoxy-d15:0, 3-ethoxy-d17:0 and 9-methyl-3-ethoxy-d15:0, can be found in milk

gangliosides[178] and the uncommon 5-hydroxy,3E-sphingosine is obtained through the acid hydrolization of brain extracts[179]. Deoxy-sphinganine (deox-dhSph) and deoxymethyl-sphinganine (deoxmeth-dhSph) belong to a class of 1-deoxy-sphingolipids that lack the C1-OH group of the normal sphingoid bases[180,181]. This results from the ability of serine palmitoyltransferase (SPT) to metabolize different amino acids (Fig. 18). While the conjugation of alanine forms deox-dhSph, the conjugation of glycine forms deoxmeth-dhSph. 1-deoxysphingoid bases can be metabolised to deoxy-ceramides, but neither converted to complex SLs nor degraded by the canonical catabolic pathway due to the missing C1-OH group[182,183]. The accumulation of these atypical SLs is reflected by cytotoxic effects and the development of pathological situations, reason why they are considered important biomarkers for different diseases, such as diabetes[182,184,185], hereditary sensory and autonomic neuropathy [186].

The concentration of free sphingoid bases in cells is low[187,188] due to its rapid metabolization into other lipid species. SL metabolism is an extremely complex and organized system involving several enzymes and isoenzymes which has been extensively described[181]. The central molecule of SL metabolism is ceramide (Fig. 18). Ceramide is a very simple molecule (Fig. 16), but very important in terms of cellular function. The intervention of ceramide as second-signal effector molecule in diverse biological processes, such as apoptosis[189,190], proliferation[190] and senescence[191], have been demonstrated. In mammalians, the generation of ceramide, can occur in the ER through the *de novo pathway* (Fig. 18). In a first step SPT catalyzes the condensation of palmitoyl-coenzyme A (CoA) with serine, forming 3-keto-sphinganine. Then, the formation of the sphingoid base sphinganine, is followed by the attachment of a fatty acid to generate dihydroceramide, catalyzed by ceramide synthase (CerS). The final step corresponds to the insertion of a 4,5-trans double bound, by the enzyme dihydroceramide desaturase (DES)[192]. Different CerS isoforms with differential preferences for acyl-CoA and acyl chains, reside in the ER and contribute for the generation of ceramides with distinct acyl chains lengths[193,194], with different impacts in the biophysical properties of membranes [195–197]. After ceramide generation in the ER, this lipid can be transported by either vesicular transport or the action of ceramide transfer protein to the Golgi complex where the

formation of more complex SLs will occur[198–200]. SM is formed through the transfer of a phosphorylcholine headgroup from PC to the C-1 of ceramide (Fig. 18) in the trans Golgi nertwork[201]. This is the most common sphingolipid in mammalian PM, where it interacts with Chol forming, the lipid raft domains (section 2). SM can be hydrolyzed to ceramide and phosphocholine (*sphingomyelinase pathway*, Fig. 18) through the action of different sphingomyelinases, with different subcellular locations[202].

Another way to obtain ceramide is through the *salvage pathway* (Fig. 18). Sph coming from the sub-cellular acidic compartments (LE and lysosomes), where most SLs are cleaved into their building blocks[203] can be converted into ceramide and its derivatives[204], or be phosphorylated by sphingosine kinases (SK) to form sphingosine-1-phosphate (S1P) (Fig. 18) an highly bioactive lipid[205–209]. Similarly to Sph, ceramide can also be phosphorylated through the action of ceramide kinase to yield ceramide-1-phosphate (C1P)[210], another important signaling molecule[209,211]. The de-phosphorylation of S1P and C1P by S1P and C1P phosphatase generates Sph and ceramide, respectively.

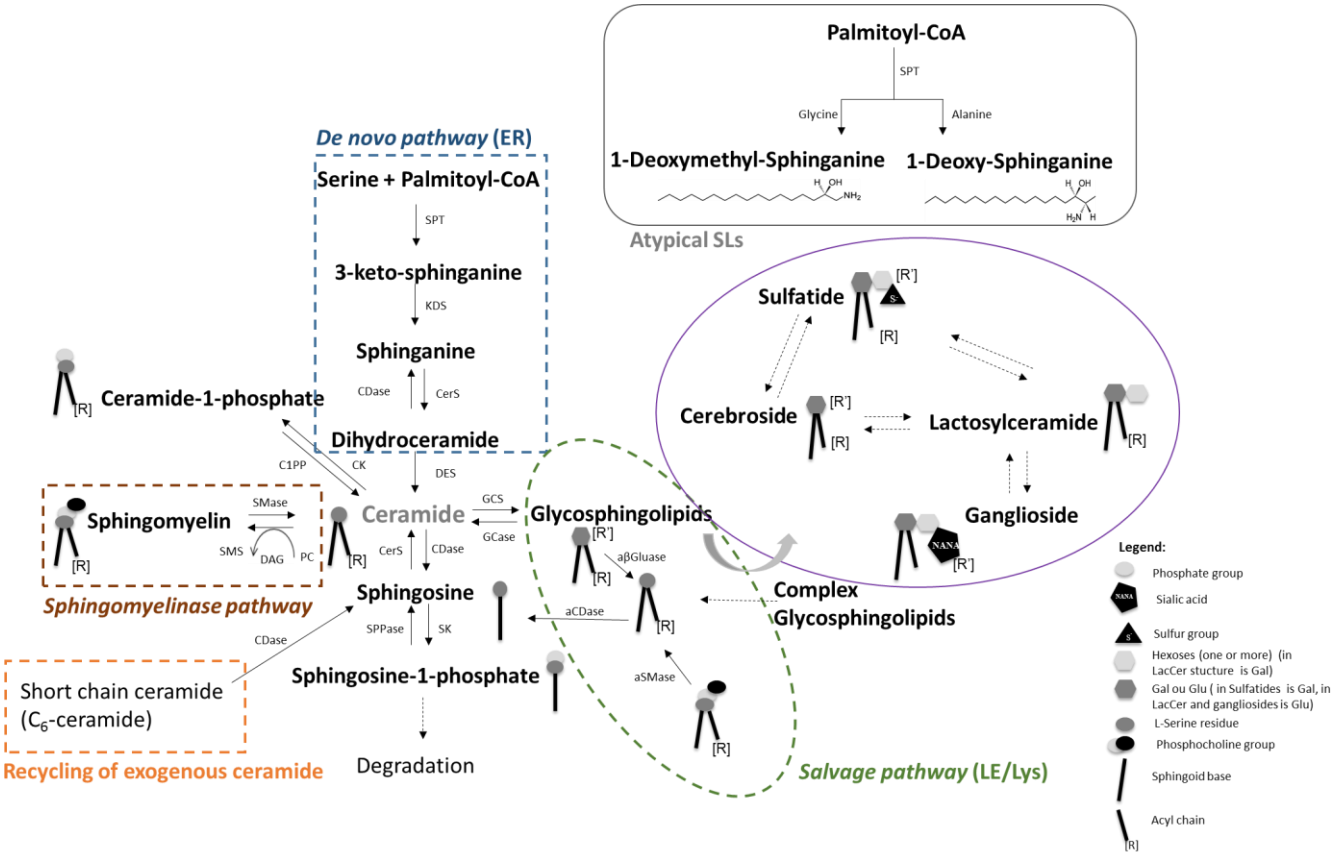

Figure 18 – Simplified schematic representation of the SL metabolism. Ceramide synthesis can be achieved through the *de novo pathway*, *sphingomyelinase pathway*, *salvage pathway* and the exogenous recycling of ceramide. Ceramide is a central molecule in the SLs metabolism and it can be used for the synthesis of more complex SLs, such as SM and GSLs or be degraded to form Sph. The formation of the atypical sphingoid bases, 1-deoxy-sphinganine and 1-deoxymethyl-sphinganine is possible through the conjugation of palmitoyl-CoA with alanine and glycine, respectively. Abbreviations: aβGluase, acid β-glucosidase; aCDase, acid ceramidase; aSMase, acid sphingomyelinase; C1PP, ceramide-1-phosphate phosphatase; CDase, ceramidase; CerS, ceramide synthase; CK, ceramide kinase; DAG, Diacylglycerol; DES, dihydroceramide desaturase; ER, endoplasmic reticulum; GCase, glucosylceramidase; GCS, glucosylceramide synthase; KDS, ketosphinganine reductase; LE, Late endosomes; Lys, Lysosomes; PC, Phosphatidylcholine; SK, sphingosine kinase; SMase, sphingomyelinase; SMS, sphingomyelin synthase; SPPase, sphingosine phosphate phosphatase; SPT, serine palmitoyltransferase.

As previously reffered GSLs are formed by a ceramide backbone covalently linked to a glycan moiety (section 3). The simpler molecules belonging to this group of SLs are the cerebrosides that are formed upon the addition of a glucose or a galactose to the ceramide backbone, forming GlcCer and GalCer, respectively. While GalCer is formed in the ER and then transported to the Golgi complex[212], GlcCer is synthesized in the *cis*-Golgi network[213]. Sulfatides are derived from GalCer via esterification of a sulfate group to the 3-hydroxyl of the galactose moiety[212] and are important acidic glycolipids with relevant roles in the nervous system, immune system, insulin secretion and virus infection, among others[214]. The addition of galactose to a GlcCer gives origin to lactosylceramide, the structural unit of gangliosides and globosides[215]. The classification of the vast majority of GSLs structures is based on seven common tetrasacharide neutral sugar cores. The ones sharing the same neutral core belong to the same "series": ganglio, lacto, neolacto, globo, isoglobo, mollu or arthro. The most representative "series" in the vertebrates are the ganglio (Fig. 19), globo, and neolacto series[216]. The GSLs are further sub-classified as neutral, if no charged sugars or ionic groups are present; sialylated (gangliosides), if one or more sialic acid residues are present or sulfated.

The official nomenclature of GSLs can be complex[217] and for that reason simplified nomenclature is also used. This is the case of Svennerholm[218] abbreviations for brain gangliosides. In the case of the ganglioside Galβ1-3GalNAcβ1-4(Neu5Acα2-3)Galβ1-4GlcβCer, also known as GM1, the first letter "G" corresponds to the serie ganglio, the second letter "M" refers the number of sialic acid residues (M=1) and the number refers to the order of migration of the compound in thin layer chromatography[60,216].

Several enzymes are involved in the synthesis of GSLs in the Golgi complex[216]. After their synthesis, these molecules are transported by vesicular transport to the PM[219], where they play different biological roles, acting as membrane receptors or modulators of other membrane components in order to change signal transduction[220]. GSLs can then undergo endocytosis and be recycled back from the early endosomes; sorted from the endosomes to the Golgi complex for re-glycosylation or they can be totally or partially degraded in the lysosomes[221].

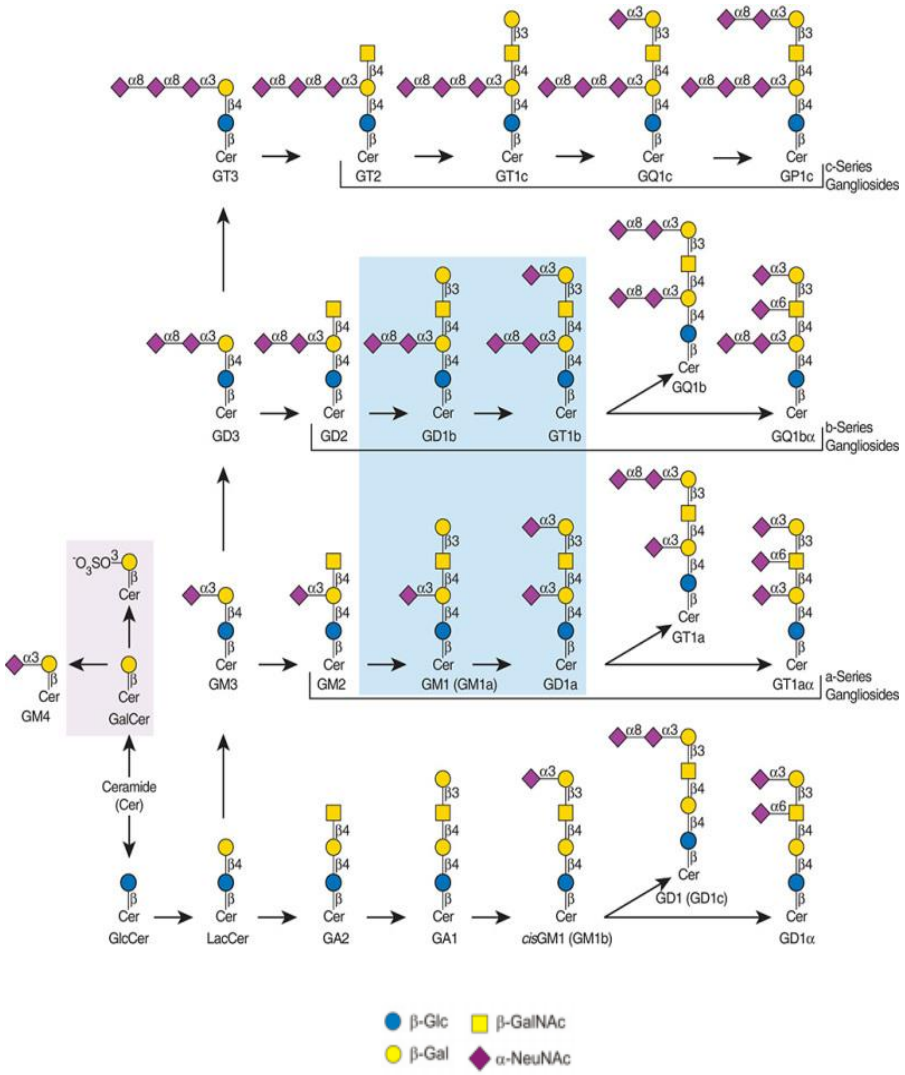

Figure 19 – Biosynthetic pathways of ganglio series drived GSLs. Adapted from Schnaar and Kinoshita (2015)[216]. The abbreviations are given according to the recommendations of the International Union of Pure and Applied Chemistry – International Union of Biochemistry Joint Commission on Biochemical Nomenclature of Glycolipids[217].

SLs in general play a fundamental role in withstand the eukaryotic life. GSLs, in particularly are crucial for the development of complex multicellular organisms[222]. Their importance was noticed when a knock-out of glucosylceramide synthase, that catalyze the GlcCer synthesis, proved to be embryonic lethal[223]. A correlation between GSLs expression and the cellular events that lead to the development of the vertebrate nervous system has been reported[224–226]. GSLs can interact with growth factor receptors, having a role in growth,

differentiation and modulation of signal transduction[213]. GSLs are also important for cell adhesion and motility[227]. The involvement of some GSLs in membrane organization[112,161,228,229] and formation of specialized membrane domains[34,230] has also been demonstrated.

It is known that alterations in SL metabolism can be related with different pathologies[231,232] and in order to preserve normal cell function it becomes clear that the cellular levels of SLs must be finely balanced. As previously referred, these bioactive lipids can be involved in the regulation of different cellular processes, such as proliferation[233], differentiation[234], inflammation[235,236], apoptosis[237] and autophagy[238]. Some SLs, including S1P, C1P and GlcCer are important regulators of cell proliferation and survival, while Sph and ceramide have an antagonistic effect contributing to growth suppression and apoptosis[239]. Recent evidence suggested that the enzymes of the SL rheostat do not function merely by directly changing the cell fate through the balance between pro-apoptotic ceramide and pro-survival S1P, as initially conceived in the rheostat model[240], but also by the differential activation of a myriad, often opposing, signaling pathways[241]. Thus, a new rheostat model was proposed[241] considering the local production, secretion and the signaling mediated by these metabolites. The SL rheostat is therefore a fundamental control system that has a profound effect in cellular function[241].

7. Sphingosine

As previously referred, Sph is the most abundant sphingoid base in mammals. It was first described by J. L. W. Thudichum in 1884 and structurally characterized as 2S,3R,4E-2-aminooctadec-4-ene-1,3-diol[242].

7.1. Metabolism

Sph is formed by deacylation of ceramide through the action of different ceramidases (CDase) that act in different subcellular locations, being classified by the optimum pH of activity (reviewed in Gault *et al*. (2010)[202]). Briefly, in the acidic environment of the lysosome, acid ceramidase (aCDase) is responsible for the deacylation of ceramides that result from the

degradation of PM SLs[202]. At neutral pH, the most active CDase is neutral ceramidase (nCDase), a soluble protein that can peripherally associate with the outer leaflet of PM, participating in the regulation of Sph and S1P synthesis in that subcellular location[202,243]. There is also a family of CDase that presents optimum activity at alkaline pH. This family of alkaline ceramidases (ACERs) is constituted by three different members (ACERs 1, 2, 3) with different subcellular positions and substrate specificities. ACER1, with several putative transmembrane domains is located in the ER[244]. It is highly expressed in the epidermis[245] and has a manifest substrate specificity for very long chain ceramide species, especially C24 and C24:1[246]. ACER2 presents also several putative transmembrane domains, but is located in the Golgi complex[202,247]. It is highly expressed in the placenta, but most of the tissues have a lower expression of this enzyme[202]. Compared to ACER1, ACER2 have a less limited substrate specificity, being able to metabolize other long chain ceramides (e.g. C16, C18, C20)[202]. Finally, ACER3 is located both in ER and Golgi complex and curiously it has a higher substrate preference for phytoceramide species and unsaturated fatty acid ceramides (≤C20)[202,248]. Similarly, to ACER2, it is broadly expressed in different tissues, with a higher level of expression in placenta[202].

As referred in the previous section, Sph can be recycled in the *salvage pathway* (Fig. 18) where a number of enzymes are involved (e.g. sphingomyelinases, cerebrosidases, CDase, and CerS), and it can be phosphorylated through the action of two SKs, cytosolic enzymes that peripherally associate with membranes. These enzymes, similarly to CDase, have different subcellular locations and substrate specificities[202]. The irreversibly degradation of Sph to hexadecenal and phosphoethanolamine by S1P lyase can occur in the ER[202].

7.2. Physico-chemical properties

In the last two decades, different groups performed studies on the physico-chemical properties of the most abundant sphingoid base, Sph[249–252]. Due to its amphipatic nature, Sph is able to form micelles when dispersed in aqueous solutions. However, a large disparity on the critical micelle concentration (CMC) values of Sph has been reported[109,251,253]. For instance, CMC values obtained by studies based on fluorescence measurements range from 18 μM to 112 μM[109,251]. These differences were attributed to the non-ideal mixing of the fluorophore

with sphingoid base and the possible disruption of the micelle. Lower CMC values (0.99 ± 0.12 μM[252]) were reported in studies performed by DLS at neutral pH. Such differences may also be inherent to the techniques used and the specific conditions in which the measurements were performed, particularly pH and ionic strength, which may influence dramatically the ionization state and hydrogen bonding ability[252]. Indeed, Sasaki et al[252] showed that alterations in pH strongly affected the aggregation behavior of Sph, for instance, by driving an increase in the CMC of the protonated Sph due to changes in the ionic and hydrogen-bonding states. In addition, it is known that free Sph is found in the micromolar range in the body fluids. In the blood, for instance, it is possible to have both Sph and its phosphorylated form in concentrations ranging from 0.1 to 1 μM[59]. This points for the possible existence of Sph micelles under physiological conditions.

The pKa value of Sph is also controversial. The amino group of the sphingoid base should be the major determinant of Sph pKa. A simple alkylamine has a pKa between 7 and 8 in both Triton X-100 and octyl-β-D-glucopyranoside micelles[250], a value considerably lower to that determined in water[250]. For more complex amines, it is likely that the pKa is even more dependent on the environment. Accordingly, pKa values ranging from ∼ 6 to ∼ 9 have been reported for Sph, under different experimental conditions. NMR and DSC were used to determine Sph pKa in mixtures with 1,2-dihexadecanoyl-*sn*-glycero-3-phosphoserine (DPPS). An apparent pKa of 9.1 was reported[254]. However, DPPS is anionic in the pH range of reported pKa values for Sph, and therefore it is expected to stabilize the protonated form of the sphingoid base. On the other hand, pKa values of 6.7[250] and 8.5[249] were determined for Sph in Triton X-100 micelles. The former value is in the same range as the one determined for Sph aggregates in the absence of detergents or other lipids (6.61 ± 0.03)[252]. This latter value would be consistent with an uncharged Sph under physiological conditions in the PM[250,252], becoming charged when in acidic cell compartments. However, when mixed with POPC, a lipid that contains a zwitterionic headgroup, over a wide pH range[255], Sph provides a positively charged surface both at neutral (pH 7.4) and acidic conditions (pH 5.0)[256]. Moreover, in quaternary POPC/SM/Chol/Sph vesicles at pH 7.4, increase in Sph concentration (10 mol%) gradually causes a shift in membrane surface charge into positive values (close to neutrality)[256]. Once the

differences in hydration and/or hydrogen bonding affect the pK of the amino group[254] it is not surprising that very different pKa values have been reported for Sph in solution, micelles and membranes. Accordingly, it was reported that changes in pH from an acidic to a neutral environment promotes alterations in the hydrogen-bonding network of Sph aggregates, from intramolecular to intermolecular[252].

DSC studies revealed that Sph displays a single phase transition centered at 39 ^{o}C[251]. However, studies using fluorescence spectroscopy, suggest that the gel to fluid phase transition of Sph occurred at ap. 53 °C under neutral conditions (pH 7.4), being reduced to ap. 48 °C under acidic conditions (pH 5.0)[256]. These results although distinct, probably due to the differences in the experimental conditions (e.g. techniques, Sph concentration) suggest that Sph potentially exists in the gel phase at physiological temperature. Therefore, Sph is a good candidate to induce changes in membrane fluidity and to participate in the formation of ordered lipid domains.

7.3. Phase behavior in model membranes

There are a few studies suggesting that Sph interacts directly to cellular proteins[257,258]. However, there are also increasing evidence that it might exert its biological actions through the modulation of the physical state of cell membranes[109,111]. Indeed, several studies have addressed the effect of Sph in bilayer membranes and its ability to change membrane biophysical properties, by promoting changes in fluidity[109,111,251,254,259,260], formation of domains[111,261] or by changing membrane permeability[109,260,262].

Studies in model membranes performed using an array of methodologies, such as DSC[251,254,259,263], NMR[254,259], Fourier-transform infrared spectroscopy[263], fluorescence spectroscopy[109,260] and fluorescence microscopy[111] point towards a Sph-induced rigidifying effect in membranes. This effect has been observed in model membranes containing saturated PLs, such as DPPS, 1,2-dipalmitoyl-*sn*-glycero-3-phosphocholine (DPPC), 1,2-dimyristoyl-*sn*-glycero-3-phosphocholine (DMPC)[251,254,259], and unsaturated PLs, namely PC[111], but also in more complex mixtures containing Chol and SM[109,111,260] as will be discussed below.

The effects of Sph on membrane properties are complex and depend on membrane lipid composition, the protonation state of Sph and its concentration. For instance, protonated Sph (pH 6.0) is able to increase the T_m of DPPC[259]. The same observation was made for DPPC/Sph mixtures at pH 7.4, supporting the ability of Sph to stabilize DPPC gel domains[251]. According to the authors, hydrogen bonding between Sph hydroxyls and the lipid phosphate, changes in membrane hydration due to Sph and electrostatic interactions between the lipid phosphate and the at least partially protonated amino group of Sph are possible explanations[251]. For instance, interaction with Sph could promote the reorientation of the PC headgroups which would decrease the lipid cross-sectional area and promote tighter intermolecular packing in the mixtures[251,259]. Indeed, it was suggested that Sph-induced condensation of POPC monolayers might originate among other factors from a reorientation of the P^- - N^+ dipole of the POPC headgroup from a parallel to a more vertical orientation in relation to the membrane plane[264]. This phenomenon might resemble to a certain extent what has been already hypothesized for Chol[265] and for ceramide[266], where the reduction of the steric repulsion between the bulky headgroups of the co-lipids, tends to maximize chain-chain interactions and bring the lipids closer together. It is therefore interesting to hypothesize that in biological membranes Sph might be able to intercalate between other membrane lipids and concomitantly increasing the packing of the membrane, maybe enhancing the formation of ordered lipid domains, such as the widely described lipid rafts[33]**.** However, the concentration dependent effect of Sph on membrane packing[251,259], suggests that Sph might have multiple effects on membrane properties depending on its local concentration.

Sph-induced increase in the T_m was also reported for artificial membranes, composed of DMPC and the diether lipid 1,2-dihexadecyl-*sn*-glycero-3-phosphocholine (DHPC)[251] Interestingly, Sph was shown to abolish the pre-transition of DMPC and DHPC, having a different impact on the stability of the gel phase formed by both lipids. While for DHPC a decrease in the pre-transition temperature was observed, suggesting that Sph does not favor the formation of the interdigitated gel phase formed by DHPC, for DMPC the pre-transition temperature increased until merging with the T_m, estabilizing the DMPC L_β phase[251]. An increase in the transition temperature was also shown for DPPC/Chol, SM/Chol and SM/Chol/PE

mixtures containing Sph[109], which was associated to a global rigidifying effect of Sph. This Sph rigidifying effect has also been noticed in other lipid mixtures. For instance, when mixing Sph with egg PC[261] POPC[256] and POPC/SM/Chol[256,267]. In contrast, Sph promotes a decrease in the T_m of 1,2-dielaidoyl-*sn*-glycero-3-phosphoethanolamine (DEPE)[259]. This suggests that mixtures formed by protonated Sph and DEPE are essentially non-ideal. In addition, in mixtures containing high Sph concentration, the abolishment of the L_α to H_{II} transition of DEPE was observed, resulting in a direct transition to what is thought to be an isotropic phase in the ^{31}P-NMR spectra[259]. This means that Sph could have a detergent-like action, leading to the formation of very small, highly curved vesicles, or even mixed micelles of Sph/DEPE. Whether a similar situation occurs in biological membranes is to date unknown. However, such structural features would be compatible with cellular events that involve vesicle formation and membrane sorting, such as the endo-lysosomal pathway and exosome formation. It should be stressed that these effects are again dependent on Sph concentration: the lamellar to hexagonal phase transition is not affected by low Sph molar fractions[259], whereas at high Sph content, the formation of the hexagonal phase may be impeded by the opposite curvature between the PE and the protonated sphingoid base[259].

Protonated Sph was also shown to affect the thermotropic behavior of acidic PLs[251,254]. In the low Sph concentration range, mixtures of DPPS/Sph form laterally homogeneous bilayers characterized by higher phase transition temperatures than the pure lipid components[251,254]. This thermal stabilization of the membrane derives from a tighter packing promoted by increased hydrogen bonding and/or electrostatic interactions between the negatively charged PLs and the cationic Sph. This effect is, however, abolished in mixtures containing high Sph concentration, resulting in a reduction of DPPS T_m[251,254], likely due to the formation of DPPS/Sph lamellar phases that coexist with an isotropic component (^{31}P-NMR spectra)[254]. Another remarkable effect of Sph in these DPPS membranes is on the deprotonation of the carboxyl group of DPPS, which results on the shift of DPPS apparent pKa to lower values due to the electrostatic interactions established between the two lipids[263]. These interactions also contribute to an overall electrostatic charge neutralization preventing the binding between the positively charged Ca^{2+} and the negatively charged headgroup[263], suggesting that positively

charged Sph might prevent the binding of proteins to membranes in a cellular context. Similar changes in the thermotropic behavior of mixtures composed by Sph and the acidic PLs dimyristoylphosphatidic acid and egg PA, were noticied[251]. Moreover, it was shown that the interaction between Sph and PA lead to transient non-lamellar structures, namely cubic phases, which can underline Sph induced membrane permeability[260]. In studies aiming to develop stable and efficient delivery systems for nucleic acid particles, it was also suggested that, after endocytosis, the cationic lipids (e.g. 1,2-dilinoleyloxy-3-dimethylaminopropane) used in formulations interact with the naturally occurring anionic lipids present in the endosomal membrane, forming ion pars that facilitate the membrane disruption through the formation of nonbilayer structures[268]. This effect, if perpetrated by positively charged Sph can be of major biological relevance considering that certain biological membranes, such as the inner leaflet of the PM[57] and the intralysosomal membranes[68], are enriched in negatively charged lipids. Sph also has remarkable structural effects on membrane curvature. This lipid tends to favor the positive curvature of the membrane, and when in interaction with lipids that have an opposite effect, e.g. Chol, it can compensate the negative curvature, stabilizing regions of the membrane that are already more organized, i.e., the l_o and the gel phases[109]. This might be due to the interplay between the positively charged Sph and Chol, as suggested by studies performed in monolayers[269]. Indeed, Garmy and coworkers[269], suggested that Sph and Chol can form pairwise condensed complexes that interact by hydrogen bonds formed between the protonated Sph amino group and the Chol hydroxyl group. From a structural perspective, this agrees with an opposite cone-shape for these two molecules, the sterol having only a hydroxyl group as the polar part, and a bulky four ring structure for the hydrophobic one. In such a situation, the formation of these complexes in a cellular context would greatly depend on the sub-cellular location of these lipids becoming particularly favorable in acidic compartments where Sph is likely to exist in its protonated state. Thus could be extremely relevant in the context of NPC disease, where lysosomal accumulation of both Sph and Chol occurs[270]**.** Despite their strong interaction, Sph/Chol interplay cannot solely dictate the formation of the l_o phase, being SM or saturated PLs also required. This might be correlated with the lack of the phosphocholine head group in Sph, which seems to be essential for the formation of the

SM/Chol-enriched l_o phase[111]. In mixtures containing SM (SM/Chol and SM/Chol/PE), Sph enables the formation of more rigid domains[109]. In fact, it was shown that Sph can have a stabilizing effect in lipid domain formation, particularly in the sterol/SM-enriched l_o domains[111,271]. Both Sph and sphinganine contribute to a higher melting temperature of Chol/SM-containing mixtures and to the formation of more rigid and stable domains[271]. Additionally, it seems that when SM is present in the membrane, it can compete with Sph for the interaction with Chol. The Sph-SM and Sph-Chol interactions, might favor the gel phase formation or increase the Sph solubility in the l_o phase, respectively[109,111]. Altogether this evidence supports the hypothesis that Sph is a good candidate to participate in the formation of ordered lipid raft domains.

7.4. Structural and morphological alterations induced by sphingosine

Membrane domains are maintained through strong van der Waals interactions between the saturated hydrocarbon chains of the SLs and electrostatic repulsions between the lipid charges[272]. The latter are particularly important for SLs with net charge, such as, the positively-charged Sph and the negatively-charged gangliosides and sulfatides[111,273,274].

The shapes and the sizes of SL-enriched domains are defined by a conjugation of different factors, including the balance between the domain line tension and dipole-dipole repulsion. If the dipole-dipole repulsion is stronger than the line tension, flower-shape domains are formed; if the opposite occurs, round-shaped domains are predominant[275]. The balance between these factors is dependent on the type of phases forming the interface of the domains. Accordingly, flower-shape domains (Fig. 20A) are typically observed when gel-fluid phases coexist[276,277], as in mixtures of PLs with Sph[111,261]. Round-shape domains (Fig. 20B) result from fluid-fluid (l_d/l_o) phase separation[277], such as observed in complex mixtures containing Chol, SM and Sph (POPC/SM/Chol/Sph)[111]. In addition to formation of membrane domains, Sph and other SLs, such as ceramide can also promote structural changes on the membrane, which might alter their permeability properties. An increase in membrane permeability in model and cell membranes containing Sph[260] and ceramide[278] has been related to the formation of nonlamellar inverted structures. The reinforcement of the membrane rigid domains was also

pointed as a key phenomenon for Sph-induced membrane permeability[109]. In addition, the formation of membrane pores was also pointed as a possible mechanism underlying the Sph and ceramide permeabilizing effect[262].

The molecular mechanisms underlying these alterations are yet not fully resolved and one of the goals of thesis is to further address this issue.

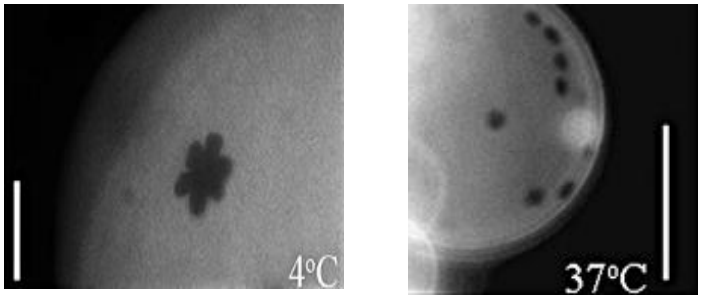

A B

Figure 20 – Morphological aspect of different phase separation in GUVs. (A) Gel/l_d phase separation in egg-yolk PC/Sph (80/20 mol%). (B) l_o/l_d phase separation in a egg-yolk PC/Sph/egg-yolk SM/Chol (30/20/30/20 mol%). Bar 20 µm. Adapted from Georgieva *et al*. (2010)[111].

7.5. Biological actions

Most studies on the biological function of Sph have been developed by Hannun[279] and Merrill[187,280,281]. Protein kinase C (PKC) was the first direct target of Sph to be identified in a study showing that Sph has the ability to inhibit PKC activity and phorbol dibutyrate binding[279]. PKC is a main regulatory enzyme that responds to numerous hormones, growth and differentiation factors and also tumor promoters[281], therefore having an important role in cell response, with an important role in cell growth regulation. For instance, Weiss et al. (1991)[282] have shown that Sph has the ability to reverse growth inhibition in vascular smooth muscle cells caused by the activation of PKC, through the interference that it causes in the binding of phorbol esters or other activators to this enzyme. Another study suggests that the accumulation of endogenous Sph in NPC fibroblasts is directly related to the inhibition of PKC, since the specific binding of [20-3H] phorbol 12,13-dibutyrate to the regulatory domain of the enzyme was significantly reduced in fibroblasts from NPC patients compared to control

fibroblasts. It was suggested that when in high concentrations (> 5-fold increase in relation to healthy control patients) Sph could act through a competitive inhibitory process, in contrast to what happens when present in lower concentrations. In this later case, Sph might directly interact with other membrane lipids, possibly with PS that is negatively charged, or inhibit the release of PKC activators, such as Ca^{2+} [283]. In fact, shortly after the discovery of the impact of Sph in PKC activity, it was hypothesized that inhibition of PKC by Sph could arise from electrostatic neutralization of the negatively charged PS required for the activation of the enzyme[284]. Furthermore, it was suggested that Sph can be involved in the regulation of PKC-dependent phosphorylation in the nucleus by modulating the association of membrane PLs to PKC, or its substrates[285]. Also, considering studies from Zeidan and Hannun (2007)[286] it seems that PKC inhibition by Sph may in turn regulate the phosphorylation of acid sphingomyelinase (aSMase) within lysosomes. This would alter aSMase activity and adjust the flux of SM being broken down into Sph, which might in turn regulate the *salvage pathway* and also lysosomal stability.

Sph has also been implicated in the modulation of the activity of other protein kinases[287–289]. Sph was shown to inhibit calmodulin-dependent kinase and insulin receptor tyrosine kinase[288], but also to enhance diacylglycerol (DAG), and casein kinase II activities[279,289]. Sph is further known for being a strong activator of Sph-dependent protein kinases, which phosphorylate a variety of cellular proteins, like 14-3-3 proteins[290], chaperones, glucose-regulated protein and heat shock proteins[291]. It has been suggested that Sph effect on these kinases might occur via changing the electrostatic interactions between the enzymes and membrane lipids[284,288,289]. Apart from its effect on the activity of protein kinases, Sph can reduce the activity of phosphatidate phosphohydrolases that have a role in the synthesis of triacylglycerols and the formation of DAG[292]. Sph can also stimulate the hydrolysis of PC into PA in a dose dependent manner, suggesting the activation of phospholipase D[293]. In addition, Sph is capable of interfering with the cellular calcium homeostasis, through the inhibition of Ca^{2+} channels, particularly the PM Ca^{2+}-ATPase[294], and also decreasing the amount of Ca^{2+} stored in the cellular acidic compartments, contributing to disease states, such as NPC1[270,295], as

discussed below. Moreover, it was recently suggested that Sph and SK1 have crucial roles in the regulation of endocytic membrane trafficking[296].

Sph also mediates cell growth arrest, apoptosis and response to chemotherapy[297,298]. Some studies have pointed to an active role of Sph in the induction of cell dead[297]. In U937 human monoblastic leukemia cells, Sph activates Jun amino-terminal kinases and inhibits extracellular signal-regulated kinases leading to apoptosis[299]. In human neutrophils treated with tumor necrosis factor-α, the concentration of ceramide and Sph increases. While ceramide did not cause apoptosis, Sph induced morphological changes characteristic of apoptotic cells and DNA fragmentation. It was proposed that the apoptotic effect of Sph could be related with the inhibition of PKC[300]. In human hepatoma cells, Sph increases caspase-3 activity, inducing apoptosis[301]. Another study revealed that caspase-7 and -8 are also involved in Sph triggered apoptosis, in human hepatoma cells[302]. Suzuki et al. proposed that Sph-dependent apoptosis is based on multiple mechanisms that operate in a concerted manner[303].

Sph can also be a positive modulator of cell growth. In concentrations ranging between 0.2 and 10 μM, Sph induces the proliferation of quiescent Swiss 3T3 fibroblasts, by stimulating DNA synthesis and potentiating the mitogenic response of growth factors[304].

7.6. Sphingosine involvement in human disease

SLs are important players not only in cell physiology but also in pathophysiology. When the normal sphingolipid metabolism is altered, some of the intervenient molecules can accumulate in the lysosomes, leading to the development of lysosomal storage diseases (LSD). By identifying the sphingolipid that abnormally accumulates in the cell, it is possible to distinguish different diseases. Some examples are Fabry, Farber and Gaucher, which are characterized by the primary accumulation of globotriaosylceramide, ceramide, and GlcCer, respectively[305]. NPC, is also included in this group of storage diseases, being associated with the primary accumulation of Sph and a secondary storage of multiple lipid species (e.g. Chol, SM, GSLs)[270]. Sphingolipidoses are inherited rare diseases, but with high mortality rates. It is expected that a better understanding of the biology of SLs that are in the basis of these diseases can lead to the development of new therapeutic strategies[172,306].

7.6.1. Niemann-Pick type C1 disease

Studies from Platt's group showed that Sph storage might be an initiating factor in neurodegenerative NPC1 disease[270,307]. This disease is a rare - incidence at conception of 1.12:100 000[308] - inherited atypical LSD, characterized by mutations in one of two genes, NPC1 in approximately 95% of the cases or NPC2[309]. Both proteins have been related with Chol transport in the endo-lysosomal system[310,311]. NPC1, a transmembrane protein, is also involved in the lysosomal efflux of the ebola virus[312]. In addition, this protein was suggested to be responsible for mediating the lysosomal efflux of Sph, a necessary process considering the protonated state of Sph at acid pH and the potentially lysosomotropic effects of Sph upon the lysosomal membrane[270,307]. Being involved in lysosomal efflux of Sph, NPC1 would be a key component of the SL *salvage pathway* and a regulator of S1P generation, however, further work is necessary to confirm this hypothesis.

The phenotype of NPC deficient cells is characterized by intra-lysosomal accumulation of Sph as well as Chol, GSLs and SM[313]. Interestingly, NPC1 is the only human disease associated with elevated levels of lysosomal Sph. Moreover, defective NPC1 function at the cellular level not only affects the storage of lipids, but also reduces the levels of lysosomal Ca^{2+} and causes unique endocytic transport and fusion defects[270]. There are evidence showing that NPC1 cells have normal ER and mitochondrial Ca^{2+} but lower Ca^{2+} in the acidic compartments[270]. A reduction of approximatly 69% in NPC1 mutant cell nicotinic acid adenine dinucleotide phosphate (NAADP)-induced Ca^{2+} release was observed. These lysosomal Ca^{2+} signaling defects were shown to cause defects in endocytic transport which in turn leads to the secondary accumulation of Chol, SM and GSLs in NPC1 cells. It was proposed that the cause of the Ca^{2+} defect in NPC1 was the primary accumulation of Sph. Furthermore, exogenous addition of Sph to normal cells induces the appearance of all NPC1 cellular phenotypes[270], and reduction in Sph levels in NPC1 cells using the SPT inhibitor myriocin reversed all the NPC1 cellular phenotypes[270]. An atypical feature of NPC, relative to other LSD, is the high complexity of storage material. Sph is an unusual lipid because it is stored in all NPC1 disease tissues, but not in any other LSD[283,314,315]. Although the total Sph storage levels in brain and peripheral tissues are low, Sph displays the greatest fold elevation compared to the other lipids that are stored in

this disease[307], in addition, it is a more potent signaling lipid at far lower concentrations compared to the other lipids stored in NPC1 disease. It was suggested that the defect in lysosomal Ca^{2+} storage filling caused by Sph abnormal storage, may be related with its inhibitory effect against PKC, calcium ATPases and Na^{+}/Ca^{2+} exchangers or similar mechanisms[270,316]. A further study[317] has indicated that inhibition of PKC mediated by Sph could be responsible for the defects in Rab9 trafficking observed in NPC disease via a defect in phosphorylation of vimentin, further indicating that the accumulation of Chol, which is ameliorated by over-expression of Rab9, is a secondary defect in this disease.

A link between NPC disease and tuberculosis was also established[318]. It was observed that the infection of WT murine and human macrophages can induce NPC phenotypes, including lipid storage and reduced Ca^{2+} release. These phenotype changes can also be achieved using lipids from mycobacteria cell walls. It was suggested that the NPC1 protein can be involved in this lipid-mediated inhibition[318]. Furthermore, it was shown that mycobacteria are able to inhibit the host NPC pathway through the accumulation of Sph, which in turn reduces LE/lysosome-mediated Ca^{2+} release preventing host phagosome-lysosomal fusion, and thereby facilitating their intracellular survival[318].

NPC has a variable age of onset, and is clinically characterized by a range of non-specific visceral, neurological and psychiatric features that progress at different rates, in different stages of the disease[309,319]. Some stabilizing therapeutic approaches might delay the progression of the disease or attenuate clinical symptoms[320]. For instance, Miglustat is used to limit the accumulation of gangliosides through the inhibition of GlcCer synthase, and is able to delay neurological manifestations of the disease[320]. Despite this, currently there is no effective therapy for NPC and several studies have been developed in an attempt to find new insights into the molecular and cellular mechanisms of the disease. These studies resort to different animal models[321–323], patients tissues[324,325], mutant cells[326,327] or even the pharmacological induction of the NPC phenotype, for instance with the commonly used cationic steroid U18666A[328]. Structurally U18666A drug is similar to Chol (Fig. 21) and it is able to bind to the sterol sensing domain of NPC1 protein interfering with the Chol transport out of lysosomes[329].

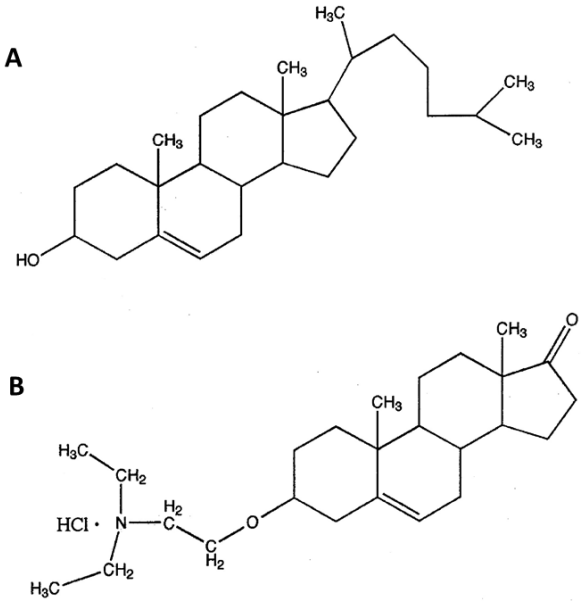

Figure 21 – Structures of (A) cholesterol and (B) U18666A. Adapted from Cenedella *et al*. (2004)[330].

7.6.2. Other roles in disease and therapeutic potential

Sph might be important in the prevention of disease and/or disease related complications. There is increasing evidence for the protective antibacterial action of sphingoid bases and other lipids in infection[331]. Sph was shown to be crucial for the host defense against *Pseudomonas aeruginosa* and other lung infections[332,333]. Cystic fibrosis (CF) is an autosomal recessive disorder caused by mutations in the cystic fibrosis transmembrane conductance regulator gene[334]. Despite the multisystemic implications of this mutation, the major cause of dead relies on chronic pulmonary infections. Different microorganisms are involved in the lung infections of CF patients. In particular *P. aeruginosa* infections are incident in these patients[335]. Due to the long term antibiotics treatments the number of resistant *P. aeruginosa* strains is increasing, which asks for alternative therapeutic approaches. It was shown that ceramide levels are elevated in the respiratory tract of CF patients[336,337], which in turn is reflected by lower Sph levels and a diminished antibacterial response[332]. Increasing Sph levels either by the inhalation of Sph or the Sph analog FTY720 (fingolimod), or by treatment with acid CDase has a positive effect in CF mice[332,333]. It is thus suggested to be a preventive/therapeutic measure to

reduce bacterial infections in CF patients[332]. Although the molecular mechanisms related to the protection of Sph against bacterial infection are not still clearly defined, it is known that PKC signaling is involved in *P. aeruginosa* elastase-induced epithelial barrier disruption[338], which indicates that Sph-induced protection against infection might be related to PKC inhibition[338]. Other hypothesis is that Sph induces bacterial cell wall damage by increasing membrane permeability and defects in adherence, similarly to what has been suggested for sphinganine[331,339].

Sph, together with sphinganine, has also been related to protection mechanisms against cancer. By inhibiting proliferation and inducing apoptosis in different cancer cell lines, these molecules assume a special importance acting as tumor suppression mediators[300,340–342] Furthermore, they have also the ability to overcome radio- or chemo-resistance in many types of cancer (reviewed in Cuvillier & Levade, 2003[340]). In fact, the potential capacity of Sph to act as a tumor suppressor has led to the development of synthetic Sph derivatives - N,N-dimethylsphingosine and N,N,N-trimethylsphingosine - that showed promising effects on lung metastasis. On the molecular level they inhibit PKC, resulting in antimetastatic effects[343–345]. Sph elevation induces cell death via either Golgi fragmentation or lysosomal rupturing[346,347] indicating a key role in programmed cell death. In contrast, it has been reported that Sph might also function as a positive modulator of cell growth[304], as previously referred (section 7.5). These contradictory effects might somehow be related with the rapid interconversion of ceramide, Sph and S1P in the SL rheostat[241].

8. References

1. Alberts, B. *et al. Molecular Biology of the Cell*. (Garland Science, 2002).
2. Purves, W. K., Sadava, D., Orians, G. H. & Heller, H. C. *Life: The Science of Biology*. (Sinauer Associates, Inc., 2004).
3. Habibi, I., Emamian, E. S. & Abdi, A. Quantitative analysis of intracellular communication and signaling errors in signaling networks. *BMC Syst. Biol.* **8,** 89 (2014).
4. Paolicelli, R. C., Bergamini, G. & Rajendran, L. Cell-to-cell Communication by Extracellular Vesicles: Focus on Microglia. *Neuroscience* (2018). doi:10.1016/j.neuroscience.2018.04.003
5. Ek-Vitorin, J. F. & Burt, J. M. Structural basis for the selective permeability of channels made of communicating junction proteins. *Biochim. Biophys. Acta* **1828,** 51–68 (2013).
6. Shinoda, W. Permeability across lipid membranes. *Biochim. Biophys. Acta - Biomembr.* **1858,** 2254–2265 (2016).
7. Osellame, L. D., Blacker, T. S. & Duchen, M. R. Cellular and molecular mechanisms of

mitochondrial function. *Best Pract. Res. Clin. Endocrinol. Metab.* **26,** 711–23 (2012).
8. Uings, I. J. & Farrow, S. N. Cell receptors and cell signalling. *Mol. Pathol.* **53,** 295–9 (2000).
9. Kennedy, M. B. Synaptic Signaling in Learning and Memory. *Cold Spring Harb. Perspect. Biol.* **8,** a016824 (2013).
10. Hoffmann, A. Immune Response Signaling: Combinatorial and Dynamic Control. *Trends Immunol.* **37,** 570–572 (2016).
11. Thurley, K., Wu, L. F. & Altschuler, S. J. Modeling Cell-to-Cell Communication Networks Using Response-Time Distributions. *Cell Syst.* **6,** 355–367.e5 (2018).
12. Heald, R. & Cohen-Fix, O. Morphology and function of membrane-bound organelles. *Curr. Opin. Cell Biol.* **26,** 79–86 (2014).
13. Giepmans, B. N. G. & van IJzendoorn, S. C. D. Epithelial cell–cell junctions and plasma membrane domains. *Biochim. Biophys. Acta - Biomembr.* **1788,** 820–831 (2009).
14. Lombard, J. Once upon a time the cell membranes: 175 years of cell boundary research. *Biol. Direct* **9,** 32 (2014).
15. Kleinzeller, A. in *Current Topics in Membranes* **48,** 1–22 (Academic Press, 1999).
16. Langmuir, I. The constitution and fundamental properties of solids and liquids. *J. Am. Chem. Soc.* **38,** 1848–1906 (1917).
17. Gorter, E. & Grendel, F. On Bimolecular Layers of Lipoids on the Chromocytes of the Blood. *J. Exp. Med.* **41,** 439–443 (1925).
18. Danielli, J. F. & Davson, H. A contribution to the theory of permeability of thin films. *J. Cell. Comp. Physiol.* **5,** 495–508 (1935).
19. Robertson, J. D. The ultrastructure of cell membranes and their derivatives. *Biochem. Soc. Symp.* **16,** 3–43 (1959).
20. Singer, S. J. & Nicolson, G. L. The fluid mosaic model of the structure of cell membranes. *Science* **175,** 720–731 (1972).
21. Feigenson, G. W. Phase behavior of lipid mixtures. *Nat. Chem. Biol.* **2,** 560–563 (2006).
22. Engelman, D. M. Membranes are more mosaic than fluid. *Nature* **438,** 578–580 (2005).
23. Kusumi, A. & Sako, Y. Cell surface organization by the membrane skeleton. *Curr. Opin. Cell Biol.* **8,** 566–74 (1996).
24. Fujiwara, T., Ritchie, K., Murakoshi, H., Jacobson, K. & Kusumi, A. Phospholipids undergo hop diffusion in compartmentalized cell membrane. *J. Cell Biol.* **157,** 1071–1082 (2002).
25. Kusumi, A. *et al.* Membrane mechanisms for signal transduction: The coupling of the meso-scale raft domains to membrane-skeleton-induced compartments and dynamic protein complexes. *Semin. Cell Dev. Biol.* **23,** 126–144 (2012).
26. Simons, K. & Van Meer, G. Lipid sorting in epithelial cells. *Biochemistry* **27,** 6197–6202 (1988).
27. Brown, D. A. & Rose, J. K. Sorting of GPI-anchored proteins to glycolipid-enriched membrane subdomains during transport to the apical cell surface. *Cell* **68,** 533–544 (1992).
28. Simons, K. & Toomre, D. Lipid rafts and signal transduction. *Nat. Rev. Mol. Cell Biol.* **1,** 31–39 (2000).
29. Pike, L. J. Lipid rafts: bringing order to chaos. *J. Lipid Res.* **44,** 655–667 (2003).
30. Helms, J. B. & Zurzolo, C. Lipids as Targeting Signals: Lipid Rafts and Intracellular Trafficking. *Traffic* **5,** 247–254 (2004).
31. Simons, K. & Ikonen, E. Functional rafts in cell membranes. *Nature* **387,** 569–572 (1997).
32. Pike, L. J. Rafts defined: a report on the Keystone Symposium on Lipid Rafts and Cell Function. *J. Lipid Res.* **47,** 1597–1598 (2006).
33. Simons, K. & Sampaio, J. L. Membrane Organization and Lipid Rafts. *Cold Spring Harb. Perspect. Biol.* **3,** a004697–a004697 (2011).
34. Sezgin, E., Levental, I., Mayor, S. & Eggeling, C. The mystery of membrane organization:

composition, regulation and roles of lipid rafts. *Nat. Rev. Mol. Cell Biol.* **18,** 361–374 (2017).
35. Sonnino, S. & Prinetti, A. Membrane domains and the 'lipid raft' concept. *Curr. Med. Chem.* **20,** 4–21 (2013).
36. Kiessling, V., Wan, C. & Tamm, L. K. Domain coupling in asymmetric lipid bilayers. *Biochim. Biophys. Acta* **1788,** 64–71 (2009).
37. Raghupathy, R. *et al.* Transbilayer Lipid Interactions Mediate Nanoclustering of Lipid-Anchored Proteins. *Cell* **161,** 581–594 (2015).
38. Wheeler, G. & Tyler, K. M. Widefield microscopy for live imaging of lipid domains and membrane dynamics. *Biochim. Biophys. Acta* **1808,** 634–641 (2011).
39. Klotzsch, E. & Schütz, G. J. A critical survey of methods to detect plasma membrane rafts. *Philos. Trans. R. Soc. Lond. B. Biol. Sci.* **368,** 20120033 (2013).
40. Klymchenko, A. S. & Kreder, R. Fluorescent Probes for Lipid Rafts: From Model Membranes to Living Cells. *Chem. Biol.* **21,** 97–113 (2014).
41. Carquin, M., D'Auria, L., Pollet, H., Bongarzone, E. R. & Tyteca, D. Recent progress on lipid lateral heterogeneity in plasma membranes: From rafts to submicrometric domains. *Prog. Lipid Res.* **62,** 1–24 (2016).
42. Sarangi, N. K., Ayappa, K. G. & Basu, J. K. Complex dynamics at the nanoscale in simple biomembranes. *Sci. Rep.* **7,** 11173 (2017).
43. Morigaki, K. & Tanimoto, Y. Evolution and development of model membranes for physicochemical and functional studies of the membrane lateral heterogeneity. *Biochim. Biophys. Acta - Biomembr.* (2018). doi:10.1016/J.BBAMEM.2018.03.010
44. McMahon, H. T. & Boucrot, E. Membrane curvature at a glance. *J. Cell Sci.* **128,** 1065–70 (2015).
45. Nicolson, G. L. The Fluid—Mosaic Model of Membrane Structure: Still relevant to understanding the structure, function and dynamics of biological membranes after more than 40 years. *Biochim. Biophys. Acta - Biomembr.* **1838,** 1451–1466 (2014).
46. Goñi, F. M. The basic structure and dynamics of cell membranes: An update of the Singer–Nicolson model. *Biochim. Biophys. Acta - Biomembr.* **1838,** 1467–1476 (2014).
47. Watson, H. Biological membranes. *Essays Biochem.* **59,** 43–69 (2015).
48. Brown, H. A. & Murphy, R. C. Working towards an exegesis for lipids in biology. *Nat. Chem. Biol.* **5,** 602–606 (2009).
49. Li, M., Yang, L., Bai, Y. & Liu, H. Analytical methods in lipidomics and their applications. *Anal. Chem.* **86,** 161–75 (2014).
50. Wenk, M. R. Lipidomics: New tools and applications. *Cell* **143,** 888–895 (2010).
51. Wenk, M. R. The emerging field of lipidomics. *Nat. Rev. Drug Discov.* **4,** 594–610 (2005).
52. Shevchenko, A. & Simons, K. Lipidomics: coming to grips with lipid diversity. *Nat. Rev. Mol. Cell Biol.* **11,** 593–598 (2010).
53. van Meer, G., Voelker, D. R. & Feigenson, G. W. Membrane lipids: where they are and how they behave. *Nat. Rev. Mol. Cell Biol.* **9,** 112–124 (2008).
54. van Meer, G. Cellular lipidomics. *EMBO J.* **24,** 3159–3165 (2005).
55. van Meer, G. & Hoetzl, S. Sphingolipid topology and the dynamic organization and function of membrane proteins. *FEBS Lett.* **584,** 1800–1805 (2010).
56. Lydic, T. A. & Goo, Y.-H. Lipidomics unveils the complexity of the lipidome in metabolic diseases. *Clin. Transl. Med.* **7,** 4 (2018).
57. van Meer, G. & de Kroon, A. I. P. M. Lipid map of the mammalian cell. *J. Cell Sci.* **124,** (2010).
58. Hishikawa, D., Hashidate, T., Shimizu, T. & Shindou, H. Diversity and function of membrane glycerophospholipids generated by the remodeling pathway in mammalian cells. *J. Lipid Res.* **55,** 799–807 (2014).
59. Zheng, W. *et al.* Ceramides and other bioactive sphingolipid backbones in health and disease:

lipidomic analysis, metabolism and roles in membrane structure, dynamics, signaling and autophagy. *Biochim. Biophys. Acta* **1758,** 1864–1884 (2006).
60. Kolter, T. Ganglioside Biochemistry. *ISRN Biochem.* **2012,** 1–36 (2012).
61. Ayuyan, A. G. & Cohen, F. S. The Chemical Potential of Plasma Membrane Cholesterol: Implications for Cell Biology. *Biophys. J.* **114,** 904–918 (2018).
62. Chabanel, A., Flamm, M. & Sung, K. L. P. Influence of cholesterol content on red cell membrane viscoelasticity and fluidity. *Biophys. J.* **44,** 171–176 (1983).
63. Mukherjee, S. & Maxfield, F. R. Membrane domains. *Annu. Rev. Cell Dev. Biol.* **20,** 839–866 (2004).
64. Silvius, J. R. Role of cholesterol in lipid raft formation: Lessons from lipid model systems. *Biochimica et Biophysica Acta - Biomembranes* **1610,** 174–183 (2003).
65. Grouleff, J., Irudayam, S. J., Skeby, K. K. & Schiøtt, B. The influence of cholesterol on membrane protein structure, function, and dynamics studied by molecular dynamics simulations. *Biochim. Biophys. Acta - Biomembr.* **1848,** 1783–1795 (2015).
66. Brown, D. A. & London, E. Functions of lipid rafts in biological membranes. *Annu. Rev. Cell Dev. Biol.* **14,** 111–136 (1998).
67. Paradies, G., Paradies, V., De Benedictis, V., Ruggiero, F. M. & Petrosillo, G. Functional role of cardiolipin in mitochondrial bioenergetics. *Biochim. Biophys. Acta - Bioenerg.* **1837,** 408–417 (2014).
68. Kolter, T. & Sandhoff, K. Lysosomal degradation of membrane lipids. *FEBS Lett.* **584,** 1700–12 (2010).
69. Akgoc, Z. *et al.* Bis(monoacylglycero)phosphate: a secondary storage lipid in the gangliosidoses. *J. Lipid Res.* **56,** 1006–13 (2015).
70. Fagone, P. & Jackowski, S. Membrane phospholipid synthesis and endoplasmic reticulum function. *J. Lipid Res.* **50 Suppl,** S311-6 (2009).
71. Jacquemyn, J., Cascalho, A. & Goodchild, R. E. The ins and outs of endoplasmic reticulum-controlled lipid biosynthesis. *EMBO Rep.* **18,** 1905–1921 (2017).
72. Osman, C., Voelker, D. R. & Langer, T. Making heads or tails of phospholipids in mitochondria. *J. Cell Biol.* **192,** 7–16 (2011).
73. Saliba, A.-E., Vonkova, I. & Gavin, A.-C. The systematic analysis of protein–lipid interactions comes of age. *Nat. Rev. Mol. Cell Biol.* **16,** 753–761 (2015).
74. Stillwell, W. & Stillwell, W. Membrane Proteins. *An Introd. to Biol. Membr.* 89–110 (2016). doi:10.1016/B978-0-444-63772-7.00006-3
75. Reitsma, S., Slaaf, D. W., Vink, H., van Zandvoort, M. A. M. J. & oude Egbrink, M. G. A. The endothelial glycocalyx: composition, functions, and visualization. *Pflugers Arch.* **454,** 345–59 (2007).
76. Gao, L. & Lipowsky, H. H. Composition of the endothelial glycocalyx and its relation to its thickness and diffusion of small solutes. *Microvasc. Res.* **80,** 394–401 (2010).
77. Boettiger, D. & Wehrle-Haller, B. Integrin and glycocalyx mediated contributions to cell adhesion identified by single cell force spectroscopy. *J. Phys. Condens. Matter* **22,** 194101 (2010).
78. Lipowsky, H. H. The endothelial glycocalyx as a barrier to leukocyte adhesion and its mediation by extracellular proteases. *Ann. Biomed. Eng.* **40,** 840–8 (2012).
79. Varki, A. Biological roles of glycans. *Glycobiology* **27,** 3–49 (2017).
80. Lewis, R. N. A. H. & McElhaney, R. N. Membrane lipid phase transitions and phase organization studied by Fourier transform infrared spectroscopy. *Biochim. Biophys. Acta - Biomembr.* **1828,** 2347–2358 (2013).
81. Jouhet, J. Importance of the hexagonal lipid phase in biological membrane organization. *Front. Plant Sci.* **4,** 494 (2013).

82. Lewis, R. N. & McElhaney, R. N. Surface charge markedly attenuates the nonlamellar phase-forming propensities of lipid bilayer membranes: calorimetric and (31)P-nuclear magnetic resonance studies of mixtures of cationic, anionic, and zwitterionic lipids. *Biophys. J.* **79,** 1455–1464 (2000).
83. Funari, S. S. & Rapp, G. A continuous topological change during phase transitions in amphiphile/water systems. *Proc. Natl. Acad. Sci. U. S. A.* **96,** 7756–7759 (1999).
84. Seddon, J. M. & Templer, R. H. in *Handbook of Biological Physics* (eds. Lipowsky, R. & Sackmann, E.) **1,** 97–160 (Elsevier Science B.V, 1995).
85. Dopico, A. *Methods in Membrane Lipids*. *ChemBioChem* **9,** (2006).
86. Tresset, G. The multiple faces of self-assembled lipidic systems. *PMC Biophys.* **2,** 3 (2009).
87. Elson, E. L., Fried, E., Dolbow, J. E. & Genin, G. M. Phase separation in biological membranes: integration of theory and experiment. *Annu. Rev. Biophys.* **39,** 207–226 (2010).
88. M'Baye, G., Mély, Y., Duportail, G. & Klymchenko, A. S. Liquid ordered and gel phases of lipid bilayers: fluorescent probes reveal close fluidity but different hydration. *Biophys. J.* **95,** 1217–1225 (2008).
89. Nagle, J. F. & Tristram-Nagle, S. Structure of lipid bilayers. *Biochim. Biophys. Acta* **1469,** 159–95 (2000).
90. Sonnino, S. & Prinetti, A. Lipids and membrane lateral organization. *Front. Physiol.* **1,** 153 (2010).
91. Hartkamp, R. *et al.* Investigating the Structure of Multicomponent Gel-Phase Lipid Bilayers. *Biophys. J.* **111,** 813–823 (2016).
92. Ekman, P. *et al.* Formation of an ordered phase by ceramides and diacylglycerols in a fluid phosphatidylcholine bilayer — Correlation with structure and hydrogen bonding capacity. *Biochim. Biophys. Acta - Biomembr.* **1848,** 2111–2117 (2015).
93. Erbe, A. & Sigel, R. Tilt angle of lipid acyl chains in unilamellar vesicles determined by ellipsometric light scattering. *Eur. Phys. J. E* **22,** 303–309 (2007).
94. Loura, L. M. S. & de Almeida, R. F. M. *Tópicos de Biofísica de Membranas*. (Lidel - edições técnicas, Lda., 2004).
95. Heberle, F. A. & Feigenson, G. W. Phase separation in lipid membranes. *Cold Spring Harb. Perspect. Biol.* **3,** a004630 (2011).
96. Riske, K. A. *et al.* Lipid bilayer pre-transition as the beginning of the melting process. *Biochim. Biophys. Acta - Biomembr.* **1788,** 954–963 (2009).
97. Mouritsen, O. G. The liquid-ordered state comes of age. *Biochim. Biophys. Acta - Biomembr.* **1798,** 1286–1288 (2010).
98. Aresta-Branco, F. *et al.* Gel domains in the plasma membrane of Saccharomyces cerevisiae: highly ordered, ergosterol-free, and sphingolipid-enriched lipid rafts. *J. Biol. Chem.* **286,** 5043–5054 (2011).
99. de Almeida, R. F. M., Fedorov, A. & Prieto, M. Sphingomyelin/phosphatidylcholine/cholesterol phase diagram: boundaries and composition of lipid rafts. *Biophys. J.* **85,** 2406–2416 (2003).
100. Goñi, F. M. *et al.* Phase diagrams of lipid mixtures relevant to the study of membrane rafts. *Biochim. Biophys. Acta* **1781,** 665–84 (2008).
101. Engberg, O. *et al.* Lipid Interactions and Organization in Complex Bilayer Membranes. *Biophysj* **110,** 1563–1573 (2016).
102. Silva, L. C., de Almeida, R. F. M., Castro, B. M., Fedorov, A. & Prieto, M. Ceramide-domain formation and collapse in lipid rafts: membrane reorganization by an apoptotic lipid. *Biophys. J.* **92,** 502–516 (2007).
103. Kucerka, N., Nieh, M.-P., Pencer, J., Sachs, J. N. & Katsaras, J. What determines the thickness of a biological membrane. *Gen. Physiol. Biophys.* **28,** 117–25 (2009).
104. Pöyry, S. Role of charged lipids in membrane structures — Insight given by simulations. *Biochim.*

Biophys. Acta - Biomembr. **1858,** 2322–2333 (2016).
105. Niemela, P. S., Ollila, S., Hyvonen, M. T., Karttunen, M. & Vattulainen, I. Assessing the nature of lipid raft membranes. *PLoS Comput. Biol.* **3,** 0304–0312 (2007).
106. Staubach, S. & Hanisch, F.-G. Lipid rafts: signaling and sorting platforms of cells and their roles in cancer. *Expert Rev. Proteomics* **8,** 263–77 (2011).
107. Bollinger, C. R., Teichgräber, V. & Gulbins, E. Ceramide-enriched membrane domains. *Biochimica et Biophysica Acta - Molecular Cell Research* **1746,** 284–294 (2005).
108. Stancevic, B. & Kolesnick, R. Ceramide-rich platforms in transmembrane signaling. *FEBS Lett.* **584,** 1728–1740 (2010).
109. Contreras, F. X., Sot, J., Alonso, A. & Goñi, F. M. Sphingosine increases the permeability of model and cell membranes. *Biophys. J.* **90,** 4085–4092 (2006).
110. Pinto, S. N., Silva, L. C., de Almeida, R. F. M. & Prieto, M. Membrane domain formation, interdigitation, and morphological alterations induced by the very long chain asymmetric C24:1 ceramide. *Biophys. J.* **95,** 2867–2879 (2008).
111. Georgieva, R., Koumanov, K., Momchilova, A., Tessier, C. & Staneva, G. Effect of sphingosine on domain morphology in giant vesicles. *J. Colloid Interface Sci.* **350,** 502–510 (2010).
112. Varela, A. R. P. *et al.* Influence of intracellular membrane pH on sphingolipid organization and membrane biophysical properties. *Langmuir* **30,** 4094–4104 (2014).
113. Chan, Y.-H. M. & Boxer, S. G. Model membrane systems and their applications. *Curr. Opin. Chem. Biol.* **11,** 581–587 (2007).
114. Siontorou, C. *et al.* Artificial Lipid Membranes: Past, Present, and Future. *Membranes (Basel).* **7,** 38 (2017).
115. Zylberberg, C. & Matosevic, S. Pharmaceutical liposomal drug delivery: a review of new delivery systems and a look at the regulatory landscape. *Drug Deliv.* **23,** 3319–3329 (2016).
116. Mirafzali, Z., Thompson, C. S. & Tallua, K. Application of Liposomes in the Food Industry. *Microencapsul. Food Ind.* 139–150 (2014). doi:10.1016/B978-0-12-404568-2.00013-3
117. Li, H., Zhao, T. & Sun, Z. Analytical techniques and methods for study of drug-lipid membrane interactions. *Rev. Anal. Chem.* **37,** 1–23 (2017).
118. Jesorka, A. & Orwar, O. Liposomes: Technologies and Analytical Applications. *Annu. Rev. Anal. Chem.* **1,** 801–832 (2008).
119. Alavi, M., Karimi, N. & Safaei, M. Application of Various Types of Liposomes in Drug Delivery Systems. *Adv. Pharm. Bull.* **7,** 3–9 (2017).
120. Marsh, D., Watts, A. & Knowles, P. F. Cooperativity of the phase transition in single- and multibilayer lipid vesicles. *Biochim. Biophys. Acta* **465,** 500–514 (1977).
121. Castanho, M. A. R. B., Santos, N. C. & Loura, L. M. S. Separating the turbidity spectra of vesicles from the absorption spectra of membrane probes and other chromophores. *Eur. Biophys. J.* **26,** 253–259 (1997).
122. MacDonald, R. C. *et al.* Small-volume extrusion apparatus for preparation of large, unilamellar vesicles. *Biochim. Biophys. Acta - Biomembr.* **1061,** 297–303 (1991).
123. Zhu, T. F. & Szostak, J. W. Preparation of large monodisperse vesicles. *PLoS One* **4,** e5009 (2009).
124. Mayer, L. D., Hope, M. J. & Cullis, P. R. Vesicles of variable sizes produced by a rapid extrusion procedure. *Biochim. Biophys. Acta* **858,** 161–168 (1986).
125. Clary, L., Verderone, G., Santaella, C. & Vierling, P. Membrane permeability and stability of liposomes made from highly fluorinated double-chain phosphocholines derived from diaminopropanol, serine or ethanolamine. *Biochim. Biophys. Acta - Biomembr.* **1328,** 55–64 (1997).
126. Sercombe, L. *et al.* Advances and Challenges of Liposome Assisted Drug Delivery. *Front. Pharmacol.* **6,** 286 (2015).

127. Yingchoncharoen, P., Kalinowski, D. S. & Richardson, D. R. Lipid-Based Drug Delivery Systems in Cancer Therapy: What Is Available and What Is Yet to Come. *Pharmacol. Rev.* **68,** 701–87 (2016).
128. Ulrich, A. S. Biophysical aspects of using liposomes as delivery vehicles. *Biosci. Rep.* **22,** 129–150 (2002).
129. Akbarzadeh, A. *et al.* Liposome: classification, preparation, and applications. *Nanoscale Res. Lett.* **8,** 102 (2013).
130. Lin, C.-M., Li, C.-S., Sheng, Y.-J., Wu, D. T. & Tsao, H.-K. Size-Dependent Properties of Small Unilamellar Vesicles Formed by Model Lipids. *Langmuir* **28,** 689–700 (2012).
131. Vanni, S., Hirose, H., Barelli, H., Antonny, B. & Gautier, R. A sub-nanometre view of how membrane curvature and composition modulate lipid packing and protein recruitment. *Nat. Commun.* **5,** 4916 (2014).
132. Gruenewald, B., Stankowski, S. & Blume, A. Curvature influence on the cooperativity and phase transition enthalpy of lecithin vesicles. *FEBS Lett.* **102,** 227–229 (1979).
133. Richter, R. P. & Brisson, A. R. Following the Formation of Supported Lipid Bilayers on Mica: A Study Combining AFM, QCM-D, and Ellipsometry. *Biophys. J.* **88,** 3422–3433 (2005).
134. Witkowska, A. & Jahn, R. Rapid SNARE-Mediated Fusion of Liposomes and Chromaffin Granules with Giant Unilamellar Vesicles. *Biophys. J.* **113,** 1251–1259 (2017).
135. Pereno, V. *et al.* Electroformation of Giant Unilamellar Vesicles on Stainless Steel Electrodes. *ACS Omega* **2,** 994–1002 (2017).
136. Wesołowska, O., Michalak, K., Maniewska, J. & Hendrich, A. B. Giant unilamellar vesicles - a perfect tool to visualize phase separation and lipid rafts in model systems. *Acta Biochim. Pol.* **56,** 33–9 (2009).
137. Sezgin, E. & Schwille, P. Fluorescence techniques to study lipid dynamics. *Cold Spring Harb. Perspect. Biol.* **3,** a009803 (2011).
138. Lakowicz, J. R. *Principles of Fluorescence Spectroscopy*. (Springer US, 2006). doi:10.1007/978-0-387-46312-4
139. Shanker, N. & Bane, S. L. in *Methods in cell biology* **84,** 213–242 (2008).
140. Baumgart, T., Hunt, G., Farkas, E. R., Webb, W. W. & Feigenson, G. W. Fluorescence probe partitioning between Lo/Ld phases in lipid membranes. *Biochim. Biophys. Acta* **1768,** 2182–94 (2007).
141. Demchenko, A. P., Mély, Y., Duportail, G. & Klymchenko, A. S. Monitoring biophysical properties of lipid membranes by environment-sensitive fluorescent probes. *Biophys. J.* **96,** 3461–70 (2009).
142. Sklar, L. A., Hudson, B. S., Petersen, M. & Diamond, J. Conjugated polyene fatty acids on fluorescent probes: spectroscopic characterization. *Biochemistry* **16,** 813–819 (1977).
143. do Canto, A. M. T. M. *et al.* Diphenylhexatriene membrane probes DPH and TMA-DPH: A comparative molecular dynamics simulation study. *Biochim. Biophys. Acta - Biomembr.* **1858,** 2647–2661 (2016).
144. Marquês, J. T., Antunes, C. A. C., Santos, F. C. & de Almeida, R. F. M. in *Advances in Planar Lipid Bilayers and Liposomes* **22,** 65–96 (Academic Press, 2015).
145. Malvern Instruments. ZetaSizer Nano - User Manual. (2013). Available at: https://www.malvernpanalytical.com/en/search?q=manuals&start=51. (Accessed: 20th June 2018)
146. Stetefeld, J., McKenna, S. A. & Patel, T. R. Dynamic light scattering: a practical guide and applications in biomedical sciences. *Biophys. Rev.* **8,** 409–427 (2016).
147. Bhattacharjee, S. DLS and zeta potential – What they are and what they are not? *J. Control. Release* **235,** 337–351 (2016).
148. Ellens, H., Bentz, J. & Szoka, F. C. H+- and Ca2+-induced fusion and destabilization of liposomes. *Biochemistry* **24,** 3099–3106 (1985).

149. Fernández-Suárez, M. & Ting, A. Y. Fluorescent probes for super-resolution imaging in living cells. *Nat. Rev. Mol. Cell Biol.* **9,** 929–943 (2008).
150. Terai, T. & Nagano, T. Small-molecule fluorophores and fluorescent probes for bioimaging. *Pflügers Arch. - Eur. J. Physiol.* **465,** 347–359 (2013).
151. Zhou, L. *et al.* Rational Development of Near-Infrared Fluorophores with Large Stokes Shifts, Bright One-Photon, and Two-Photon Emissions for Bioimaging and Biosensing Applications. *Chem. - A Eur. J.* **23,** 8736–8740 (2017).
152. Sarkar, I. & Mishra, A. K. Fluorophore tagged bio-molecules and their applications: A brief review. *Appl. Spectrosc. Rev.* **53,** 552–601 (2018).
153. Kremers, G.-J., Gilbert, S. G., Cranfill, P. J., Davidson, M. W. & Piston, D. W. Fluorescent proteins at a glance. *J. Cell Sci.* **124,** 157–60 (2011).
154. Miyawaki, A. & Niino, Y. Molecular Spies for Bioimaging—Fluorescent Protein-Based Probes. *Mol. Cell* **58,** 632–643 (2015).
155. Schermelleh, L., Heintzmann, R. & Leonhardt, H. A guide to super-resolution fluorescence microscopy. *J. Cell Biol.* **190,** 165–175 (2010).
156. Chojnacki, J. & Eggeling, C. Super-resolution fluorescence microscopy studies of human immunodeficiency virus. *Retrovirology* **15,** 41 (2018).
157. Combs, C. A. & Shroff, H. in *Current Protocols in Neuroscience* **79,** 2.1.1-2.1.25 (John Wiley & Sons, Inc., 2017).
158. Cebecauer, M., Humpolíčková, J. & Rossy, J. Advanced Imaging of Cellular Signaling Events. *Methods Enzymol.* **505,** 273–289 (2012).
159. Weigert, R. Imaging the dynamics of endocytosis in live mammalian tissues. *Cold Spring Harb. Perspect. Biol.* **6,** a017012 (2014).
160. Sengupta, P., Van Engelenburg, S. & Lippincott-Schwartz, J. Visualizing cell structure and function with point-localization superresolution imaging. *Dev. Cell* **23,** 1092–1102 (2012).
161. Varela, A. R. P. *et al.* Effect of glucosylceramide on the biophysical properties of fluid membranes. *Biochim. Biophys. Acta - Biomembr.* **1828,** 1122–1130 (2013).
162. Owen, D. M., Magenau, A., Williamson, D. & Gaus, K. The lipid raft hypothesis revisited - New insights on raft composition and function from super-resolution fluorescence microscopy. *Bioessays* 739–747 (2012). doi:10.1002/bies.201200044
163. Owen, D. M. & Gaus, K. Imaging lipid domains in cell membranes: the advent of super-resolution fluorescence microscopy. *Front. Plant Sci.* **4,** 503 (2013).
164. Albeanu, D. F., Soucy, E., Sato, T. F., Meister, M. & Murthy, V. N. LED arrays as cost effective and efficient light sources for widefield microscopy. *PLoS One* **3,** e2146 (2008).
165. Robertson, J. B., Zhang, Y. & Johnson, C. H. Light-emitting diode flashlights as effective and inexpensive light sources for fluorescence microscopy. *J. Microsc.* **236,** 1–4 (2009).
166. Sanderson, M. J., Smith, I., Parker, I. & Bootman, M. D. Fluorescence microscopy. *Cold Spring Harb. Protoc.* **2014,** pdb.top071795 (2014).
167. Wilson, T. Resolution and optical sectioning in the confocal microscope. *J. Microsc.* **244,** 113–121 (2011).
168. Denk, W., Strickler, J. H. & Webb, W. W. Two-photon laser scanning fluorescence microscopy. *Science* **248,** 73–6 (1990).
169. Benninger, R. K. P. & Piston, D. W. Two-photon excitation microscopy for the study of living cells and tissues. *Curr. Protoc. cell Biol.* **Chapter 4,** Unit 4.11.1-24 (2013).
170. Sud, M. *et al.* LMSD: LIPID MAPS structure database. *Nucleic Acids Res.* **35,** D527-32 (2007).
171. Futerman, A. H. & Hannun, Y. A. The complex life of simple sphingolipids. *EMBO Rep.* **5,** 777–782 (2004).
172. Lahiri, S. & Futerman, A. H. The metabolism and function of sphingolipids and glycosphingolipids.

Cell. Mol. Life Sci. **64,** 2270–2284 (2007).
173. Pruett, S. T. *et al.* Biodiversity of sphingoid bases ('sphingosines') and related amino alcohols. *J. Lipid Res.* **49,** 1621–1639 (2008).
174. Farwanah, H. *et al.* Separation and mass spectrometric characterization of covalently bound skin ceramides using LC/APCI-MS and Nano-ESI-MS/MS. *J. Chromatogr. B Anal. Technol. Biomed. Life Sci.* **852,** 562–570 (2007).
175. Stewart, M. E. & Downing, D. T. Free sphingosines of human skin include 6-hydroxysphingosine and unusually long-chain dihydrosphingosines. *J. Invest. Dermatol.* **105,** 613–618 (1995).
176. Zhao, L. *et al.* Elevation of 20-carbon long chain bases due to a mutation in serine palmitoyltransferase small subunit b results in neurodegeneration. *Proc. Natl. Acad. Sci. U. S. A.* **112,** 12962–7 (2015).
177. Kendall, A. C., Kiezel-Tsugunova, M., Brownbridge, L. C., Harwood, J. L. & Nicolaou, A. Lipid functions in skin: Differential effects of n-3 polyunsaturated fatty acids on cutaneous ceramides, in a human skin organ culture model. *Biochim. Biophys. Acta* **1859,** 1679–1689 (2017).
178. Martín, M. J., Martín-Sosa, S. & Hueso, P. Bovine milk gangliosides: changes in ceramide moiety with stage of lactation. *Lipids* **36,** 291–298 (2001).
179. Kadowaki, H., Bremer, E. G., Evans, J. E., Jungalwala, F. B. & McCluer, R. H. Acetonitrile-hydrochloric acid hydrolysis of gangliosides for high performance liquid chromatographic analysis of their long chain bases. *J. Lipid Res.* **24,** 1389–1397 (1983).
180. Bode, H. *et al.* HSAN1 mutations in serine palmitoyltransferase reveal a close structure–function–phenotype relationship. *Hum. Mol. Genet.* **25,** 853–865 (2016).
181. Hannun, Y. A. & Obeid, L. M. Sphingolipids and their metabolism in physiology and disease. *Nat. Rev. Mol. Cell Biol.* **19,** 175–191 (2017).
182. Zuellig, R. A. *et al.* Deoxysphingolipids, novel biomarkers for type 2 diabetes, are cytotoxic for insulin-producing cells. *Diabetes* **63,** 1326–39 (2014).
183. Ferreira, C. R. *et al.* Deoxysphingolipid precursors indicate abnormal sphingolipid metabolism in individuals with primary and secondary disturbances of serine availability. *Mol. Genet. Metab.* **124,** 204–209 (2018).
184. Othman, A. *et al.* Plasma 1-deoxysphingolipids are predictive biomarkers for type 2 diabetes mellitus. *BMJ Open Diabetes Res. Care* **3,** e000073 (2015).
185. Mwinyi, J. *et al.* Plasma 1-deoxysphingolipids are early predictors of incident type 2 diabetes mellitus. *PLoS One* **12,** e0175776 (2017).
186. Ernst, D. *et al.* Novel HSAN1 mutation in serine palmitoyltransferase resides at a putative phosphorylation site that is involved in regulating substrate specificity. *Neuromolecular Med.* **17,** 47–57 (2015).
187. Merrill, A. H. Sphingolipid and glycosphingolipid metabolic pathways in the era of sphingolipidomics. *Chem. Rev.* **111,** 6387–422 (2011).
188. Knapp, M., Baranowski, M., Lisowska, A. & Musiał, W. Decreased free sphingoid base concentration in the plasma of patients with chronic systolic heart failure. *Adv. Med. Sci.* **57,** 100–105 (2012).
189. Pettus, B. J., Chalfant, C. E. & Hannun, Y. A. Ceramide in apoptosis: An overview and current perspectives. *Biochim. Biophys. Acta - Mol. Cell Biol. Lipids* **1585,** 114–125 (2002).
190. Saddoughi, S. A. & Ogretmen, B. Diverse Functions of Ceramide in Cancer Cell Death and Proliferation. *Adv. Cancer Res.* **117,** 37–58 (2013).
191. Venable, M. E. & Yin, X. Ceramide induces endothelial cell senescence. *Cell Biochem. Funct.* **27,** 547–551 (2009).
192. Huang, X., Withers, B. R. & Dickson, R. C. Sphingolipids and lifespan regulation. *Biochim. Biophys. Acta* **1841,** 657–64 (2014).

193. Cingolani, F., Futerman, A. H. & Casas, J. Ceramide synthases in biomedical research. *Chem. Phys. Lipids* **197,** 25–32 (2016).
194. Wegner, M.-S., Schiffmann, S., Parnham, M. J., Geisslinger, G. & Grösch, S. The enigma of ceramide synthase regulation in mammalian cells. *Prog. Lipid Res.* **63,** 93–119 (2016).
195. Maula, T., Artetxe, I., Grandell, P.-M. M. & Slotte, J. P. P. Importance of the sphingoid base length for the membrane properties of ceramides. *Biophys. J.* **103,** 1870–1879 (2012).
196. Pinto, S. N. *et al.* Changes in membrane biophysical properties induced by sphingomyelinase depend on the sphingolipid *N* -acyl chain. *J. Lipid Res.* **55,** 53–61 (2014).
197. Maula, T., Al Sazzad, M. A. & Slotte, J. P. Influence of Hydroxylation, Chain Length, and Chain Unsaturation on Bilayer Properties of Ceramides. *Biophys. J.* **109,** 1639–51 (2015).
198. Hanada, K. Intracellular trafficking of ceramide by ceramide transfer protein. *Proc. Jpn. Acad. Ser. B. Phys. Biol. Sci.* **86,** 426–37 (2010).
199. Kajiwara, K. *et al.* Osh proteins regulate COPII-mediated vesicular transport of ceramide from the endoplasmic reticulum in budding yeast. *J. Cell Sci.* **127,** 376–87 (2014).
200. Prashek, J. *et al.* Interaction between the PH and START domains of ceramide transfer protein competes with phosphatidylinositol 4-phosphate binding by the PH domain. *J. Biol. Chem.* **292,** 14217–14228 (2017).
201. Deng, Y., Rivera-Molina, F. E., Toomre, D. K. & Burd, C. G. Sphingomyelin is sorted at the trans Golgi network into a distinct class of secretory vesicle. *Proc. Natl. Acad. Sci. U. S. A.* **113,** 6677–82 (2016).
202. Gault, C. R., Obeid, L. M. & Hannun, Y. A. An overview of sphingolipid metabolism: From synthesis to breakdown. *Advances in Experimental Medicine and Biology* **688,** 1–23 (2010).
203. Kolter, T. A view on sphingolipids and disease. *Chem. Phys. Lipids* **164,** 590–606 (2011).
204. Kitatani, K., Idkowiak-Baldys, J. & Hannun, Y. A. The sphingolipid salvage pathway in ceramide metabolism and signaling. *Cell. Signal.* **20,** 1010–1018 (2008).
205. Singh, A. T., Dharmarajan, A., Aye, I. L. M. H. & Keelan, J. A. Sphingosine-sphingosine-1-phosphate pathway regulates trophoblast differentiation and syncytialization. *Reprod. Biomed. Online* **24,** 224–234 (2012).
206. Calise, S. *et al.* Sphingosine 1-phosphate stimulates proliferation and migration of satellite cells: role of S1P receptors. *Biochim. Biophys. Acta* **1823,** 439–50 (2012).
207. Olivera, A. & Spiegel, S. Sphingosine-1-phosphate as second messenger in cell proliferation induced by PDGF and FCS mitogens. *Nature* **365,** 557–560 (1993).
208. Spiegel, S. Sphingosine 1-phosphate: a prototype of a new class of second messengers. *J. Leukoc. Biol.* **65,** 341–344 (1999).
209. Hait, N. C. & Maiti, A. The Role of Sphingosine-1-Phosphate and Ceramide-1-Phosphate in Inflammation and Cancer. *Mediators Inflamm.* **2017,** 1–17 (2017).
210. Boath, A. *et al.* Regulation and Traffic of Ceramide 1-Phosphate Produced by Ceramide Kinase. *J. Biol. Chem.* **283,** 8517–8526 (2008).
211. Arana, L., Gangoiti, P., Ouro, A., Trueba, M. & Gómez-Muñoz, A. Ceramide and ceramide 1-phosphate in health and disease. *Lipids Health Dis.* **9,** 15 (2010).
212. Compostella, F., Panza, L. & Ronchetti, F. The mammalian sulfated glycolipid sulfatide: Synthesis and biological implications. *Comptes Rendus Chim.* **15,** 37–45 (2012).
213. D'Angelo, G., Capasso, S., Sticco, L. & Russo, D. Glycosphingolipids: Synthesis and functions. *FEBS Journal* **280,** 6338–6353 (2013).
214. Takahashi, T. & Suzuki, T. Role of sulfatide in normal and pathological cells and tissues. *J. Lipid Res.* **53,** 1437–50 (2012).
215. Tokuda, N. *et al.* 4GalT6 is involved in the synthesis of lactosylceramide with less intensity than 4GalT5. *Glycobiology* **23,** 1175–1183 (2013).

216. Schnaar, R. L. & Kinoshita, T. *Glycosphingolipids*. *Essentials of Glycobiology* (Cold Spring Harbor Laboratory Press, 2015). doi:10.1101/GLYCOBIOLOGY.3E.011
217. Chester, M. A. IUPAC-IUB Joint Commission on Biochemical Nomenclature (JCBN). Nomenclature of glycolipids--recommendations 1997. *Eur. J. Biochem.* **257,** 293–8 (1998).
218. Svennerholm, L. Chromatographic Separation of Human Brain Gangliosides. *J. Neurochem.* **10,** 613–623 (1963).
219. De Matteis, M. A. & Luini, A. Exiting the Golgi complex. *Nat. Rev. Mol. Cell Biol.* **9,** 273–284 (2008).
220. Lingwood, C. A. Glycosphingolipid functions. *Cold Spring Harb. Perspect. Biol.* **3,** a004788 (2011).
221. Daniotti, J. L. & Iglesias-Bartolomé, R. Metabolic pathways and intracellular trafficking of gangliosides. *IUBMB Life* **63,** 513–520 (2011).
222. Holthuis, J. C., Pomorski, T., Raggers, R. J., Sprong, H. & Van Meer, G. The organizing potential of sphingolipids in intracellular membrane transport. *Physiol. Rev.* **81,** 1689–1723 (2001).
223. Yamashita, T., Wada, R. & Proia, R. L. Early developmental expression of the gene encoding glucosylceramide synthase, the enzyme controlling the first committed step of glycosphingolipid synthesis. *Biochim. Biophys. Acta - Gen. Subj.* **1573,** 236–240 (2002).
224. Kracun, I. *et al.* Human brain gangliosides in development, aging and disease. *Int. J. Dev. Biol.* **35,** 289–295 (1991).
225. McJarrow, P., Schnell, N., Jumpsen, J. & Clandinin, T. Influence of dietary gangliosides on neonatal brain development. *Nutr. Rev.* **67,** 451–463 (2009).
226. Mocchetti, I. Exogenous gangliosides, neuronal plasticity and repair, and the neurotrophins. *Cell. Mol. Life Sci.* **62,** 2283–2294 (2005).
227. Todeschini, A. & Hakomori, S. I. Functional role of glycosphingolipids and gangliosides in control of cell adhesion, motility, and growth, through glycosynaptic microdomains. *Biochim. Biophys. Acta - Gen. Subj.* **1780,** 421–433 (2008).
228. Prinetti, A., Loberto, N., Chigorno, V. & Sonnino, S. Glycosphingolipid behaviour in complex membranes. *Biochim. Biophys. Acta - Biomembr.* **1788,** 184–193 (2009).
229. Varela, A. R. P. *et al.* Pathological levels of glucosylceramide change the biophysical properties of artificial and cell membranes. *Phys. Chem. Chem. Phys.* **19,** 340–346 (2017).
230. Gupta, G. & Surolia, A. Glycosphingolipids in microdomain formation and their spatial organization. *FEBS Letters* **584,** 1634–1641 (2010).
231. Pralhada Rao, R. *et al.* Sphingolipid metabolic pathway: an overview of major roles played in human diseases. *J. Lipids* **2013,** 178910 (2013).
232. Borodzicz, S., Czarzasta, K., Kuch, M. & Cudnoch-Jedrzejewska, A. Sphingolipids in cardiovascular diseases and metabolic disorders. *Lipids Health Dis.* **14,** 55 (2015).
233. Bernhart, E. *et al.* Interference with distinct steps of sphingolipid synthesis and signaling attenuates proliferation of U87MG glioma cells. *Biochem. Pharmacol.* **96,** 119–30 (2015).
234. Bieberich, E. Ceramide in stem cell differentiation and embryo development: novel functions of a topological cell-signaling lipid and the concept of ceramide compartments. *J. Lipids* **2011,** 610306 (2011).
235. Napolitano, G. & Karin, M. Sphingolipids: the oil on the TRAFire that promotes inflammation. *Sci. Signal.* **3,** pe34 (2010).
236. Maceyka, M. & Spiegel, S. Sphingolipid metabolites in inflammatory disease. *Nature* **510,** 58–67 (2014).
237. Tirodkar, T. S. & Voelkel-Johnson, C. Sphingolipids in apoptosis. *Exp. Oncol.* **34,** 231–42 (2012).
238. Young, M. M., Kester, M. & Wang, H.-G. Sphingolipids: regulators of crosstalk between apoptosis and autophagy. *J. Lipid Res.* **54,** 5–19 (2013).
239. Ekiz, H. A. & Baran, Y. Therapeutic applications of bioactive sphingolipids in hematological

malignancies. *Int. J. Cancer* **127,** 1497–1506 (2010).
240. Cuvillier, O. *et al.* Suppression of ceramide-mediated programmed cell death by sphingosine-1-phosphate. *Nature* **381,** 800–803 (1996).
241. Newton, J., Lima, S., Maceyka, M. & Spiegel, S. Revisiting the sphingolipid rheostat: Evolving concepts in cancer therapy. *Exp. Cell Res.* **333,** 195–200 (2015).
242. Thudichum, J. L. W. *Treatise on the Chemical Constitution of Brain*. (Bailliere, Tindall, and Cox, London, 1884).
243. Tani, M., Igarashi, Y. & Ito, M. Involvement of Neutral Ceramidase in Ceramide Metabolism at the Plasma Membrane and in Extracellular Milieu. *J. Biol. Chem.* **280,** 36592–36600 (2005).
244. Mao, C. *et al.* Cloning and Characterization of a Mouse Endoplasmic Reticulum Alkaline Ceramidase. *J. Biol. Chem.* **278,** 31184–31191 (2003).
245. Houben, E. *et al.* Differentiation-associated expression of ceramidase isoforms in cultured keratinocytes and epidermis. *J. Lipid Res.* **47,** 1063–1070 (2006).
246. Sun, W. *et al.* Upregulation of the Human Alkaline Ceramidase 1 and Acid Ceramidase Mediates Calcium-Induced Differentiation of Epidermal Keratinocytes. *J. Invest. Dermatol.* **128,** 389–397 (2008).
247. Xu, R. *et al.* Golgi alkaline ceramidase regulates cell proliferation and survival by controlling levels of sphingosine and S1P. *FASEB J.* **20,** 1813–1825 (2006).
248. Mao, C. *et al.* Cloning and Characterization of a Novel Human Alkaline Ceramidase. A mammalian enzyme that hydrolyzes phytoceramide. *J. Biol. Chem.* **276,** 26577–26588 (2001).
249. Bottega, R., Epand, R. M. & Ball, E. H. Inhibition of protein kinase C by sphingosine correlates with the presence of positive charge. *Biochem. Biophys. Res. Commun.* **164,** 102–107 (1989).
250. Merrill, A. H. *et al.* Structural requirements for long-chain (sphingoid) base inhibition of protein kinase C in vitro and for the cellular effects of these compounds. *Biochemistry* **28,** 3138–3145 (1989).
251. Kõiv, A., Mustonen, P. & Kinnunen, P. K. Influence of sphingosine on the thermal phase behaviour of neutral and acidic phospholipid liposomes. *Chem. Phys. Lipids* **66,** 123–134 (1993).
252. Sasaki, H., Arai, H., Cocco, M. J. & White, S. H. pH dependence of sphingosine aggregation. *Biophys. J.* **96,** 2727–2733 (2009).
253. Deguchi, H., Yegneswaran, S. & Griffin, J. H. Sphingolipids as bioactive regulators of thrombin generation. *J. Biol. Chem.* **279,** 12036–12042 (2004).
254. López-García, F., Micol, V., Villalaín, J. & Gómez-Fernández, J. C. Interaction of sphingosine and stearylamine with phosphatidylserine as studied by DSC and NMR. *Biochim. Biophys. Acta* **1153,** 1–8 (1993).
255. Lee, A. G. G. in *Membrane Fluidity in Biology* (ed. Aloia, R. C.) 59 (Academic Press, New York, 1983).
256. Zupancic, E., Carreira, A. C., de Almeida, R. F. M. & Silva, L. C. Biophysical implications of sphingosine accumulation in membrane properties at neutral and acidic pH. *J. Phys. Chem. B* **118,** 4858–66 (2014).
257. Woodcock, J. M. *et al.* Sphingosine and FTY720 directly bind pro-survival 14-3-3 proteins to regulate their function. *Cell. Signal.* **22,** 1291–1299 (2010).
258. Riento, K. *et al.* Flotillin proteins recruit sphingosine to membranes and maintain cellular sphingosine-1-phosphate levels. *PLoS One* **13,** e0197401 (2018).
259. López-García, F., Villalaín, J. & Gómez-Fernández, J. C. A phase behavior study of mixtures of sphingosine with zwitterionic phospholipids. *Biochim. Biophys. Acta* **1194,** 281–288 (1994).
260. Jiménez-Rojo, N. *et al.* Membrane permeabilization induced by sphingosine: effect of negatively charged lipids. *Biophys. J.* **106,** 2577–2584 (2014).
261. Watanabe, C., Puff, N., Staneva, G., Seigneuret, M. & Angelova, M. I. Antagonism and synergy of

single chain sphingolipids sphingosine and sphingosine-1-phosphate towards lipid bilayer properties. Consequences for their role as cell fate regulators. *Langmuir* **30,** 13956–13963 (2014).
262. Siskind, L. J., Fluss, S., Bui, M. & Colombini, M. Sphingosine forms channels in membranes that differ greatly from those formed by ceramide. *J. Bioenerg. Biomembr.* **37,** 227–236 (2005).
263. López-García, F., Villalaín, J. & Gómez-Fernández, J. C. Effect of sphingosine and stearylamine on the interaction of phosphatidylserine with calcium. A study using DSC, FT-IR and 45Ca(2+)-binding. *Biochim. Biophys. Acta* **1236,** 279–288 (1995).
264. Säily, V. M. J., Alakoskela, J.-M., Ryhänen, S. J., Karttunen, M. & Kinnunen, P. K. J. Characterization of Sphingosine−Phosphatidylcholine Monolayers: Effects of DNA. *Langmuir* **19,** 8956–8963 (2003).
265. Björkbom, A. *et al.* Effect of sphingomyelin headgroup size on molecular properties and interactions with cholesterol. *Biophys. J.* **99,** 3300–8 (2010).
266. Massey, J. B. Interaction of ceramides with phosphatidylcholine, sphingomyelin and sphingomyelin/cholesterol bilayers. *Biochim. Biophys. Acta - Biomembr.* **1510,** 167–184 (2001).
267. Carreira, A. C., de Almeida, R. F. M. & Silva, L. C. Development of lysosome-mimicking vesicles to study the effect of abnormal accumulation of sphingosine on membrane properties. *Sci. Rep.* **7,** 3949 (2017).
268. Semple, S. C. *et al.* Rational design of cationic lipids for siRNA delivery. *Nat. Biotechnol.* **28,** 172–176 (2010).
269. Garmy, N., Taïeb, N., Yahi, N. & Fantini, J. Interaction of cholesterol with sphingosine: physicochemical characterization and impact on intestinal absorption. *J. Lipid Res.* **46,** 36–45 (2005).
270. Lloyd-Evans, E. *et al.* Niemann-Pick disease type C1 is a sphingosine storage disease that causes deregulation of lysosomal calcium. *Nat. Med.* **14,** 1247–1255 (2008).
271. Alanko, S. M. K., Halling, K. K., Maunula, S., Slotte, J. P. & Ramstedt, B. Displacement of sterols from sterol/sphingomyelin domains in fluid bilayer membranes by competing molecules. *Biochim. Biophys. Acta - Biomembr.* **1715,** 111–121 (2005).
272. Bandekar, A. & Sofou, S. Floret-shaped solid domains on giant fluid lipid vesicles induced by pH. *Langmuir* **28,** 4113–4122 (2012).
273. Saxena, K., Duclos, R. I., Sripada, P. K. & Shipley, G. G. Unusual hydration properties of C16:0 sulfatide bilayer membranes. *Biophys. J.* **79,** 385–393 (2000).
274. Cantu, L., Corti, M., Brocca, P. & Del Favero, E. Structural aspects of ganglioside-containing membranes. *Biochim. Biophys. Acta* **1788,** 202–8 (2009).
275. Perkovic, S. & McConnell, H. M. Cloverleaf monolayer domains. *J. Phys. Chem. B* **101,** 381–388 (1997).
276. Blanchette, C. D., Lin, W.-C., Ratto, T. V & Longo, M. L. Galactosylceramide domain microstructure: impact of cholesterol and nucleation/growth conditions. *Biophys. J.* **90,** 4466–4478 (2006).
277. Fidorra, M., Duelund, L., Leidy, C., Simonsen, A. C. & Bagatolli, L. A. Absence of fluid-ordered/fluid-disordered phase coexistence in ceramide/POPC mixtures containing cholesterol. *Biophys. J.* **90,** 4437–4451 (2006).
278. Montes, L. R., Ruiz-Argüello, M. B., Goñi, F. M. & Alonso, A. Membrane restructuring via ceramide results in enhanced solute efflux. *J. Biol. Chem.* **277,** 11788–11794 (2002).
279. Hannun, Y. A. *et al.* Sphingosine inhibition of protein kinase C activity and of phorbol dibutyrate binding in vitro and in human platelets. *J. Biol. Chem.* **261,** 12604–12609 (1986).
280. Merrill, A. H. De novo sphingolipid biosynthesis: a necessary, but dangerous, pathway. *J. Biol. Chem.* **277,** 25843–6 (2002).
281. Merrill Jr., L. A. H. & Sandhoff, K. in *Biochemistry of Lipids. Lipoproteins and Membranes* (eds.

Vance, D. E. & Vance, J. E.) 373–406 (Elsevier Science B.V., 2002).
282. Weiss, R. H., Huang, C.-L. & Ives, H. E. Sphingosine reverses growth inhibition caused by activation of protein kinase c in vascular smooth muscle cells. *J. Cell. Physiol.* **149,** 307–312 (1991).
283. Rodriguez-Lafrasse, C. *et al.* Modulation of protein kinase C by endogenous sphingosine: inhibition of phorbol dibutyrate binding in Niemann-Pick C fibroblasts. *Biochem. J.* **325 (Pt 3),** 787–91 (1997).
284. Bazzi, M. D. & Nelsestuen, G. L. Mechanism of protein kinase C inhibition by sphingosine. *Biochem. Biophys. Res. Commun.* **146,** 203–7 (1987).
285. Katoh, N. Modulation by sphingosine of phosphorylation of substrate proteins by protein kinase C in nuclei from cow mammary gland. *J. Vet. Med. Sci.* **66,** 1237–42 (2004).
286. Zeidan, Y. H. & Hannun, Y. A. Activation of acid sphingomyelinase by protein kinase Cdelta-mediated phosphorylation. *J. Biol. Chem.* **282,** 11549–61 (2007).
287. Jefferson, A. B. & Schulman, H. Sphingosine inhibits calmodulin-dependent enzymes. *J. Biol. Chem.* **263,** 15241–4 (1988).
288. Arnold, R. S. & Newton, A. C. Inhibition of the insulin receptor tyrosine kinase by sphingosine. *Biochemistry* **30,** 7747–54 (1991).
289. Mcdonald, B., Hannunjll, Y. A., Reynolds, C. H. & Sahyoun, N. Activation of casein kinase II by sphingosine. *J. Biol. Chem.* **266,** 21773–21776 (1991).
290. Megidish, T., Cooper, J., Zhang, L., Fu, H. & Hakomori, S. A novel sphingosine-dependent protein kinase (SDK1) specifically phosphorylates certain isoforms of 14-3-3 protein. *J. Biol. Chem.* **273,** 21834–21845 (1998).
291. Megidish, T. *et al.* Endogenous Substrates of Sphingosine-Dependent Kinases (SDKs) Are Chaperone Proteins: Heat Shock Proteins, Glucose-Regulated Proteins, Protein Disulfide Isomerase, and Calreticulin †. *Biochemistry* **38,** 3369–3378 (1999).
292. Gomez-Munoz, A., Hamza, E. H. & Brindley, D. N. Effects of sphingosine, albumin and unsaturated fatty acids on the activation and translocation of phosphatidate phosphohydrolases in rat hepatocytes. *Biochim. Biophys. Acta - Lipids Lipid Metab.* **1127,** 49–56 (1992).
293. Natarajan, V., Jayaram, H. N., Scribner, W. M. & Garcia, J. G. Activation of endothelial cell phospholipase D by sphingosine and sphingosine-1-phosphate. *Am. J. Respir. Cell Mol. Biol.* **11,** 221–229 (1994).
294. Colina, C., Cervino, V. & Benaim, G. Ceramide and sphingosine have an antagonistic effect on the plasma-membrane Ca2+-ATPase from human erythrocytes. *Biochem. J.* **362,** 247–51 (2002).
295. Höglinger, D. *et al.* Intracellular sphingosine releases calcium from lysosomes. *Elife* **4,** (2015).
296. Lima, S., Milstien, S. & Spiegel, S. Sphingosine and Sphingosine Kinase 1 Involvement in Endocytic Membrane Trafficking. *J. Biol. Chem.* **292,** 3074–3088 (2017).
297. Cuvillier, O. Sphingosine in apoptosis signaling. *Biochim. Biophys. Acta - Mol. Cell Biol. Lipids* **1585,** 153–162 (2002).
298. Woodcock, J. Sphingosine and ceramide signalling in apoptosis. *IUBMB Life* **58,** 462–6 (2006).
299. Jarvis, W. D. *et al.* Coordinate regulation of stress- and mitogen-activated protein kinases in the apoptotic actions of ceramide and sphingosine. *Mol. Pharmacol.* **52,** 935–947 (1997).
300. Ohta, H., Yatomi, Y., Sweeney, E. A., Hakomori, S. & Igarashi, Y. A possible role of sphingosine in induction of apoptosis by tumor necrosis factor-alpha in human neutrophils. *FEBS Lett* **355,** 267–70. (1994).
301. Hung, W. C., Chang, H. C. & Chuang, L. Y. Activation of caspase-3-like proteases in apoptosis induced by sphingosine and other long-chain bases in Hep3B hepatoma cells. *Biochem. J.* **338 (Pt 1,** 161–166 (1999).
302. Chang, H. C., Hsu, C., Hsu, H. K. & Yang, R. C. Functional role of caspases in sphingosine-induced

apoptosis in human hepatoma cells. *IUBMB Life* **55,** 403–407 (2003).
303. Suzuki, E., Handa, K., Toledo, M. S. & Hakomori, S. Sphingosine-dependent apoptosis: a unified concept based on multiple mechanisms operating in concert. *Proc. Natl. Acad. Sci. U. S. A.* **101,** 14788–14793 (2004).
304. Zhang, H., Buckley, N. E., Gibson, K. & Spiegel, S. Sphingosine stimulates cellular proliferation via a protein kinase C-independent pathway. *J. Biol. Chem.* **265,** 76–81 (1990).
305. Ozkara, H. A. Recent advances in the biochemistry and genetics of sphingolipidoses. *Brain Dev.* **26,** 497–505 (2004).
306. Ozbayraktar, F. & Ulgen, O. K. Molecular facets of sphigolipids: mediators of disease. *Biotechnol. J.* **4,** 1028–1041 (2009).
307. Lloyd-Evans, E. & Platt, F. M. Lipids on trial: the search for the offending metabolite in Niemann-Pick type C disease. *Traffic* **11,** 419–428 (2010).
308. Wassif, C. A. *et al.* High incidence of unrecognized visceral/neurological late-onset Niemann-Pick disease, type C1, predicted by analysis of massively parallel sequencing data sets. *Genet. Med.* **18,** 41–8 (2016).
309. Vanier, M. T. Niemann-Pick disease type C. *Orphanet J. Rare Dis.* **5,** 16 (2010).
310. Enkavi, G., Mikkolainen, H., Güngör, B., Ikonen, E. & Vattulainen, I. Concerted regulation of npc2 binding to endosomal/lysosomal membranes by bis(monoacylglycero)phosphate and sphingomyelin. *PLOS Comput. Biol.* **13,** e1005831 (2017).
311. Li, X. *et al.* 3.3 Å structure of Niemann–Pick C1 protein reveals insights into the function of the C-terminal luminal domain in cholesterol transport. *Proc. Natl. Acad. Sci.* **114,** 9116–9121 (2017).
312. Qiu, S. *et al.* Ebola virus requires phosphatidylinositol (3,5) bisphosphate production for efficient viral entry. *Virology* **513,** 17–28 (2018).
313. Platt, N. *et al.* Immune dysfunction in Niemann-Pick disease type C. *J. Neurochem.* **136 Suppl 1,** 74–80 (2016).
314. Goldin, E. *et al.* Type C Niemann-Pick disease: A murine model of the lysosomal cholesterol lipidosis accumulates sphingosine and sphinganine in liver. *Biochim. Biophys. Acta - Lipids Lipid Metab.* **1127,** 303–311 (1992).
315. te Vruchte, D. *et al.* Accumulation of glycosphingolipids in Niemann-Pick C disease disrupts endosomal transport. *J. Biol. Chem.* **279,** 26167–26175 (2004).
316. Pandol, S. J., Schoeffield-Payne, M. S., Gukovskaya, A. S. & Rutherford, R. E. Sphingosine regulates Ca2+-ATPase and reloading of intracellular Ca2+ stores in the pancreatic acinar cell. *Biochim. Biophys. Acta - Biomembr.* **1195,** 45–50 (1994).
317. Walter, M., Chen, F. W., Tamari, F., Wang, R. & Ioannou, Y. A. Endosomal lipid accumulation in NPC1 leads to inhibition of PKC, hypophosphorylation of vimentin and Rab9 entrapment. *Biol. Cell* **101,** 141–153 (2009).
318. Fineran, P. *et al.* Pathogenic mycobacteria achieve cellular persistence by inhibiting the Niemann-Pick Type C disease cellular pathway. *Wellcome open Res.* **1,** 18 (2016).
319. Vanier, M. T. *et al.* Diagnostic tests for Niemann-Pick disease type C (NP-C): A critical review. *Mol. Genet. Metab.* **118,** 244–254 (2016).
320. Santos-Lozano, A. *et al.* Niemann-Pick disease treatment: a systematic review of clinical trials. *Ann. Transl. Med.* **3,** 360 (2015).
321. Somers, K. L. *et al.* Effects of dietary cholesterol restriction in a feline model of Niemann-Pick type C disease. *J. Inherit. Metab. Dis.* **24,** 427–36 (2001).
322. Walkley, S. U. & Suzuki, K. Consequences of NPC1 and NPC2 loss of function in mammalian neurons. *Biochim. Biophys. Acta - Mol. Cell Biol. Lipids* **1685,** 48–62 (2004).
323. Gómez-Grau, M. *et al.* New murine Niemann-Pick type C models bearing a pseudoexon-generating mutation recapitulate the main neurobehavioural and molecular features of the

disease. *Sci. Rep.* **7,** 41931 (2017).
324. Woś, M. *et al.* Mitochondrial dysfunction in fibroblasts derived from patients with Niemann-Pick type C disease. *Arch. Biochem. Biophys.* **593,** 50–59 (2016).
325. Bergamin, N. *et al.* A human neuronal model of Niemann Pick C disease developed from stem cells isolated from patient's skin. *Orphanet J. Rare Dis.* **8,** 34 (2013).
326. Millard, E. E., Srivastava, K., Traub, L. M., Schaffer, J. E. & Ory, D. S. Niemann-Pick Type C1 (NPC1) Overexpression Alters Cellular Cholesterol Homeostasis. *J. Biol. Chem.* **275,** 38445–38451 (2000).
327. Rodríguez-Pascau, L., Coll, M. J., Casas, J., Vilageliu, L. & Grinberg, D. in *JIMD reports* **4,** 29–37 (2011).
328. Vázquez, M. C., Martínez, P., Alvarez, A. R., González, M. & Zanlungo, S. Increased copper levels in in vitro and in vivo models of Niemann-Pick C disease. *BioMetals* **25,** 777–786 (2012).
329. Lu, F. *et al.* Identification of NPC1 as the target of U18666A, an inhibitor of lysosomal cholesterol export and Ebola infection. *Elife* **4,** e12177 (2015).
330. Cenedella, R. J. *et al.* Direct perturbation of lens membrane structure may contribute to cataracts caused by U18666A, an oxidosqualene cyclase inhibitor. *J. Lipid Res.* **45,** 1232–41 (2004).
331. Fischer, C. L. *et al.* Antibacterial Activity of Sphingoid Bases and Fatty Acids against Gram-Positive and Gram-Negative Bacteria. *Antimicrob. Agents Chemother.* **56,** 1157–1161 (2012).
332. Pewzner-Jung, Y. *et al.* Sphingoid long chain bases prevent lung infection by Pseudomonas aeruginosa. *EMBO Mol. Med.* **6,** 1205–1214 (2014).
333. Tavakoli Tabazavareh, S. *et al.* Lack of Sphingosine Causes Susceptibility to Pulmonary Staphylococcus Aureus Infections in Cystic Fibrosis. *Cell. Physiol. Biochem.* **38,** 2094–2102 (2016).
334. WHO. Human Genetics Programme Chronic Diseases and Health Promotion World Health Organization The molecular genetic epidemiology of cystic fibrosis Report of a joint meeting of WHO/ECFTN/ICF(M)A/ECFS. (2002).
335. Valderrey, A. D. *et al.* Chronic colonization by Pseudomonas aeruginosa of patients with obstructive lung diseases: cystic fibrosis, bronchiectasis, and chronic obstructive pulmonary disease. *Diagn. Microbiol. Infect. Dis.* **68,** 20–27 (2010).
336. Becker, K. A., Tümmler, B., Gulbins, E. & Grassmé, H. Accumulation of ceramide in the trachea and intestine of cystic fibrosis mice causes inflammation and cell death. *Biochem. Biophys. Res. Commun.* **403,** 368–374 (2010).
337. Brodlie, M. *et al.* Ceramide Is Increased in the Lower Airway Epithelium of People with Advanced Cystic Fibrosis Lung Disease. *Am. J. Respir. Crit. Care Med.* **182,** 369–375 (2010).
338. Clark, C. A., Thomas, L. K. & Azghani, A. O. Inhibition of Protein Kinase C Attenuates *Pseudomonas aeruginosa* Elastase–Induced Epithelial Barrier Disruption. *Am. J. Respir. Cell Mol. Biol.* **45,** 1263–1271 (2011).
339. Bibel, D. J., Aly, R. & Shinefield, H. R. Inhibition of microbial adherence by sphinganine. *Can. J. Microbiol.* **38,** 983–5 (1992).
340. Cuvillier, O. & Levade, T. Enzymes of sphingosine metabolism as potential pharmacological targets for therapeutic intervention in cancer. *Pharmacol. Res.* **47,** 439–445 (2003).
341. Ahn, E. H. & Schroeder, J. J. Induction of apoptosis by sphingosine, sphinganine, and C(2)-ceramide in human colon cancer cells, but not by C(2)-dihydroceramide. *Anticancer Res.* **30,** 2881–4 (2010).
342. Hossain, Z., Sugawara, T. & Hirata, T. Sphingoid bases from sea cucumber induce apoptosis in human hepatoma HepG2 cells through p-AKT and DR5. *Oncol. Rep.* **29,** 1201–1207 (2013).
343. Edsall, L. C., Van Brocklyn, J. R., Cuvillier, O., Kleuser, B. & Spiegel, S. N,N-Dimethylsphingosine is a potent competitive inhibitor of sphingosine kinase but not of protein kinase C: modulation of cellular levels of sphingosine 1-phosphate and ceramide. *Biochemistry* **37,** 12892–8 (1998).
344. Edsall, L. C., Pirianov, G. G. & Spiegel, S. Involvement of sphingosine 1-phosphate in nerve growth

factor-mediated neuronal survival and differentiation. *J. Neurosci.* **17,** 6952–60 (1997).
345. Huwiler, A., Kolter, T., Pfeilschifter, J. & Sandhoff, K. Physiology and pathophysiology of sphingolipid metabolism and signaling. *Biochim. Biophys. Acta* **1485,** 63–99 (2000).
346. Hu, W. *et al.* Golgi fragmentation is associated with ceramide-induced cellular effects. *Mol. Biol. Cell* **16,** 1555–67 (2005).
347. Villamil Giraldo, A. M., Appelqvist, H., Ederth, T. & Öllinger, K. Lysosomotropic agents: impact on lysosomal membrane permeabilization and cell death. *Biochem. Soc. Trans.* **42,** 1460–1464 (2014).

CHAPTER II

BIOPHYSICAL IMPLICATIONS OF SPHINGOSINE ACCUMULATION IN MEMBRANE PROPERTIES AT NEUTRAL AND ACIDIC PH

This Chapter comprises the work published in The Journal of Physical Chemistry B (2014) 118: 4858-4866 by Eva Zupancic[*], **Ana C. Carreira**[*], Rodrigo F. M. de Almeida, and Liana C. Silva (*equally contributing authors)

CHAPTER II – BIOPHYSICAL IMPLICATIONS OF SPHINGOSINE ACCUMULATION IN MEMBRANE PROPERTIES AT NEUTRAL AND ACIDIC PH

THE JOURNAL OF PHYSICAL CHEMISTRY B

Article

pubs.acs.org/JPCB

Biophysical Implications of Sphingosine Accumulation in Membrane Properties at Neutral and Acidic pH

Eva Zupancic,[§,∥] Ana C. Carreira,[§,‡,∥] Rodrigo F. M. de Almeida,[‡] and Liana C. Silva*[,§]

[§]iMed.UL - Research Institute for Medicines and Pharmaceutical Sciences, Faculdade de Farmácia da Universidade de Lisboa, 1649-003 Lisboa, Portugal

[‡]Centro de Química e Bioquímica, DQB, Faculdade de Ciências da Universidade de Lisboa, Campo Grande, 1749-016 Lisboa, Portugal

1. Abstract

Sphingosine (Sph) is a simple lipid involved in the regulation of several biological processes. When accumulated in the late endosomal/lysosomal compartments, Sph causes changes in ion signaling and membrane trafficking, leading to the development of Niemann-Pick disease type C. Little is known about Sph interaction with other lipids in biological membranes; however, understanding the effect of Sph in the physical state of membranes might provide insights into its mode of action. Using complementary established fluorescence approaches we show that Sph accumulation leads to the formation of Sph-enriched gel domains in 1-palmitoyl-2-oleoyl-*sn*-glycero-3-phosphocholine (POPC) and POPC/Sphingomyelin (SM)/Cholesterol (Chol) model membranes. These domains are more easily formed in membrane models mimicking the neutral pH plasma membrane environment (PM) as compared to the acidic lysosomal membrane environment (LM), where higher Sph concentrations (or lower temperatures) are required. Electrophoretic light scattering measurements further revealed that in PM-raft models (POPC/SM/Chol), Sph is mainly neutral, whereas in LM models, the positive charge of Sph leads to electrostatic repulsion, reducing the Sph ability to form gel domains. Thus, formation of Sph-enriched domains in cellular membranes might be strongly regulated by Sph charge.

2. Introduction

Sphingosine ((2S, 3R, 4E)-2-amino-4-octadecen-1,3-diol) is a bioactive metabolite resulting from ceramide degradation by aCDase in lysosomes.[1,2] It is the most common sphingoid base in mammalian sphingolipids and influences a variety of cellular activities, such as growth, differentiation and apoptosis.[3–5] Sphingosine (Sph) may act directly through enzyme binding or indirectly through changes in cell membrane properties[6]. This lipid is responsible for activation and inhibition of various kinases, including PKC.[7–10] Some of these enzymes do not contain a Sph-binding site, and the direct effect of Sph on their activity can be ruled out. Therefore, it is feasible that the impact of Sph on some enzymes, receptors and other cellular components could be due to its effect on the physical state of cell membranes.[11]

Sph is preferentially partitioned into the membrane[12], and despite its biological importance, little is known about its effect on the lipid bilayer structure and interaction with other lipids. Studies in model and biological membranes have revealed that Sph is able to change the permeability and rigidity of the membrane[6,11,13,14], which might have impact in signalling, sorting of proteins and lipids and membrane trafficking.[6]

It has been reported that the protonation state of Sph is altered within the range of neutral or acidic pH, values found within different cellular compartments.[15–17] When in neutral pH, Sph can present a non-protonated form and rapidly move across and between biological membranes.[18] On the contrary, when released into the lysosomal acidic environment, Sph has the particularity of being positively charged[15], reducing its ability to pass through membranes. Crossing the lysosomal membrane to reach ER, where it is responsible for ceramide and S1P generation, is essential but currently there is no known Sph transporter in the lysosomal membrane.[19]

In the endo-lysosomal pathway, changes from neutral to acidic environment occur, and the alteration of Sph protonation state could be relevant, once it is likely to promote changes in the electrostatic lipid-lipid and lipid-protein interactions.[19] Understanding the effects of Sph on membrane organization is important also because it is described that accumulation of Sph in the late endosome/lysosomal (LE/Ly) compartments is an early event in the development of Niemann-Pick disease type C (NPC). NPC is a rare and usually fatal lysosomal storage disorder,

inherited in an autosomal recessive manner[20], which is characterized by the accumulation of multiple lipid species, including Sph, Chol, GSLs and Sphingomyelin (SM).[19] Accumulation of Sph in NPC is associated with impaired Ca^{2+} homeostasis, defective endocytic membrane trafficking and secondary storage of lipids.[21] Despite this, little is known about Sph role in the lysosome, particularly regarding the biophysical implications of Sph accumulation. In this work we investigate the interaction of Sph with POPC-containing membranes and with a ternary system that was previously characterized, and represents a well-defined raft-model mixture constituted by POPC/SM/Chol.[22,23] To this end, a multiparameter fluorescence spectroscopy approach was used, being the analysis performed at neutral (pH 7.4) and acidic (pH 5.0) pH, in order to mimic the plasma (PM) and the lysosomal (LM) membrane environment, respectively. The results show that Sph-gel like domains are formed through Sph accumulation in model membranes and that the formation of these domains is facilitated at neutral pH compared to acidic pH, due to intermolecular electrostatic repulsions of the positively charged Sph molecules at acidic pH.

3. Experimental section

3.1. Materials

1-palmitoyl-2-oleoyl-*sn*-glycero-3-phosphocholine (POPC), Sphingomyelin (SM) (Egg, Chicken) and D-erythro-sphingosine (Sph) were obtained from Avanti Polar Lipids, Inc. (Alabaster, AL, USA). Chol was obtained from Sigma-Aldrich (St. Louis, MO, USA). DPH (1,6-diphenyl-1,3,5-hexatriene) and *t*-PnA (trans-parinaric acid) were from Molecular Probes/Invitrogen (Eugene, OR, USA). All spectroscopic solvents were from Fluka (St. Louis, MO, USA).

3.2. Liposome preparation

Multilamellar (MLV) and large unilamellar (LUV) lipid vesicles (both with 0.2 mM total lipid concentration) were prepared by standard procedures.[24] As suspension medium, Hepes buffer (10 mM Hepes with 150 mM NaCl, pH 7.4) and Citrate Phosphate buffer (0.1 M citric acid and 0.2M Na2HPO4, pH 5.0) were used. The suspensions were equilibrated by freeze thaw

cycles (T> 50 °C) and kept overnight at 4°C protected from light. The probe to lipid (P/L) ratio was 1:200 for DPH and 1:500 for t-PnA. Before starting the analysis, the samples were incubated for at least 1 h at room temperature and protected from light. The composition of the ternary POPC/SM/Chol mixtures was selected to span the tie line containing the 1:1:1 equimolar mixture taken from the ternary POPC/SM/Chol phase diagram[22]. The ternary mixtures used in this study were 71.6:23.3:5.1; 59.7:26.3:14; 45.1:29.9:25; 34:32.7:33.3 and 25.4:34.8:39.8 (POPC/SM/Chol). The effect of Sph on these mixtures was studied by adding 5 or 10 mol% of Sph.

POPC and SM concentration in stock solutions were confirmed by phosphorus analysis[25]. The concentration of Chol and Sph stock solutions were determined gravimetrically with a high precision balance (Mettler Toledo UMT2). Probe concentrations were determined spectrophotometrically using ε (t-PnA, 299.4 nm, ethanol) = 89 x 103 M^{-1} cm^{-1} [26], ε (DPH, 355 nm, chloroform) = 80.6 x 103 M^{-1} cm^{-1}.[27]

3.3. Fluorescence measurements

The fluorescence measurements were carried out on a Spex Fluorolog 3-22/Tau 3 spectrofluorometer equipped with double grating monochromators in both excitation and emission light paths from Horiba Jobin Yvon.[28] Excitation/emission wavelengths (nm) were 358/430 and 303/404 for DPH and *t*-PnA, respectively. All measurements were performed in 1.0 cm x 0.4 cm quartz cuvettes, at room temperature (24°C), with the exception of thermotropic studies. For measurements performed at different temperatures, the heating rate was always below 0.2°C/min and the temperature was achieved by a Braun 852 circulating water bath and controlled with 0.1 °C precision directly inside the cuvette with a PT100.

The fluorescence intensity decay measurements were obtained by a single photon counting technique as previously described.[28] For *t*-PnA the excitation wavelength was 315 nm (using a NanoLED source, model: N-320; Horiba Jobin-Yvon), being the emission collected at 404 nm. To analyze the experimental decays and obtain the fitting curves the TRFA software (Scientific Software Technologies Center, Minsk, Belarus) was used. Fluorescence decays were described by a sum of exponentials, where α_i is the normalized pre-exponential, and τ_i is the

lifetime of the decay component i. The mean fluorescence lifetime <τ> is given by <τ> $= \sum_i \alpha_i \tau_i^2 / \sum_i \alpha_i \tau_i$.

3.4. Dynamic light scattering measurements

The vesicle sizes were determined by performing DLS analysis on a Zetasizer Nano S equipment (Malvern Instruments). Size measurement was made using patented NIBS (Non-Invasive Back Scatter) technology. Samples were placed in 12 mm square polystyrene cuvettes and then in a chamber maintained at 25°C. The data analysis was performed by the accompanying software and expressed as Z-Average size or size distribution by intensity. The polydispersion index (PDI) for each sample was also calculated using the same software. In each experiment the measurements were done in triplicate.

3.5. Electrophoretic light scattering measurements

The electrophoretic mobilities were analyzed through M3-PALS technology on a ZetaSizer Nano Z equipment (Malvern Instruments). Samples were placed in clear disposable zeta cells and then in a thermostated sample chamber maintained at 25°C. The data analysis was performed by the accompanying software and the measurements were done in triplicate in each experiment.

4. Results

4.1. Phase behavior of POPC/Sph mixtures

To evaluate the effect of Sph in a fluid membrane, two types of fluorescent probes with different phase-related properties were used: *t*-PnA that has preferential partitioning towards the gel phase[29,30] and DPH that has a similar partitioning between the gel and the fluid phase.[28] To fully understand the system behavior, the entire composition range from 0 to 100 mol% of Sph was spanned. Figure 1A shows the fluorescence anisotropy of *t*-PnA in POPC/Sph mixtures at neutral and acidic pH. At pH 7.4, a pH value resembling the environment of the PM, *t*-PnA anisotropy presents a gradual increase with increasing content of Sph, reaching a plateau for

X_{Sph} > 40 mol%. In contrast, at pH 5.0 (resembling the lysosomal pH environment), *t*-PnA anisotropy slightly increases with Sph content up to 40 mol% and higher Sph content is required to induce a sharp increase in *t*-PnA anisotropy. Nevertheless, the high anisotropy values suggest that Sph is able to form gel domains in the fluid POPC matrix, in a manner dependent on pH environment and Sph content. This is further supported by the high mean fluorescence lifetime values of *t*-PnA, (Figure 1B) that are typical of a gel phase.[31] Figure 1B shows that Sph ability to form gel domains is enhanced at neutral pH compared to acidic pH, as shown by the increase in *t*-PnA mean fluorescence lifetime for lower Sph content in models mimicking the PM environment. In addition, the longer fluorescence lifetime suggests a tighter packing of Sph- gel phase under a neutral pH environment.

The probe DPH was also used to further characterize the phase behavior of these binary mixtures under neutral and acidic conditions (Figure 1C). DPH anisotropy increases with Sph content showing the ability of this lipid to increase the order of the membrane. At neutral pH and in mixtures containing higher Sph content, the anisotropy of DPH is higher and typical of a gel phase, further supporting the stronger ability of Sph to segregate into gel-domains at pH 7.4 compared to acidic pH. The differences in the anisotropy of DPH at neutral and acidic pH are not as strong as those observed with *t*-PnA because DPH, in contrast to *t*-PnA, displays an equal partition between the gel and the fluid phases.[22,28]

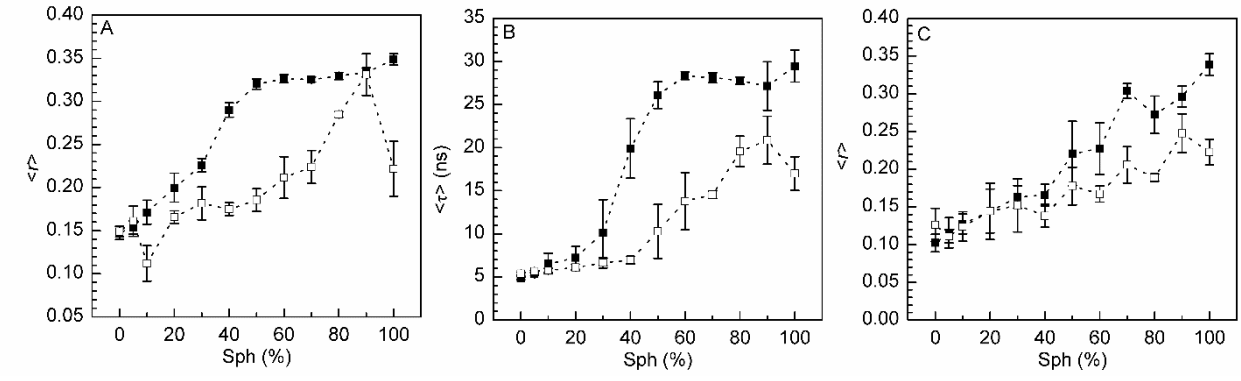

Figure 1. Effect of Sph on fluid POPC membranes. (A,C) Steady-state fluorescence anisotropy of (A) *t*-PnA and (C) DPH, and (B) Mean fluorescence lifetime of *t*-PnA at pH 7.4 (solid symbols) and pH 5.0 (open symbols) as a function of Sph molar fraction. Values are means ± SD of at least three independent experiments. The lines act merely as guides to the eye.

4.2. Thermotropic behavior of POPC/Sph mixtures

To investigate the thermotropic properties of the binary POPC/Sph mixtures, the steady-state fluorescence anisotropy of *t*-PnA and DPH was measured as a function of temperature. The thermotropic characterization of Sph is shown in Figure 2A. It can be observed that *t*-PnA anisotropy is high and typical of a gel phase in the low temperature range. Increasing the temperature decreases the anisotropy to values typical of a fluid phase. At neutral pH, the onset and completion of the gel-to-fluid phase transition occurs at higher temperatures, showing that the T_m of Sph is pH dependent (Figure 2A), decreasing from ~ 53 °C at pH 7.4 to ~ 48 °C at pH 5.0. Differences in the thermotropic behavior with pH environment were also observed in POPC/Sph mixtures, particularly for Sph content above 30 mol% (Figure 2B). In addition, as shown in Figure 2B, increasing the Sph content in the mixtures leads to an increase in the temperature at which the complete melting of gel domains occurs. Similar results were obtained in thermotropic studies using the probe DPH (Figure S1 in the Supporting Information). From these results, it is possible to determine the partial binary phase diagram of POPC/Sph mixtures in neutral and acidic pH (Figure 2C). To determine the *liquidus* boundary (gel+fluid-to-fluid transition) data from *t*-PnA anisotropy was used. This is because of the strong partition of this probe towards the gel phase which therefore can be detected even when present in very small fractions. Accordingly, it is the most suitable probe to determine the complete melting of gel phase. To determine the *solidus* boundary, DPH data was used. The equal partition of this probe towards the gel and the fluid phases allows a better estimation of the onset of the melting of the gel phase.

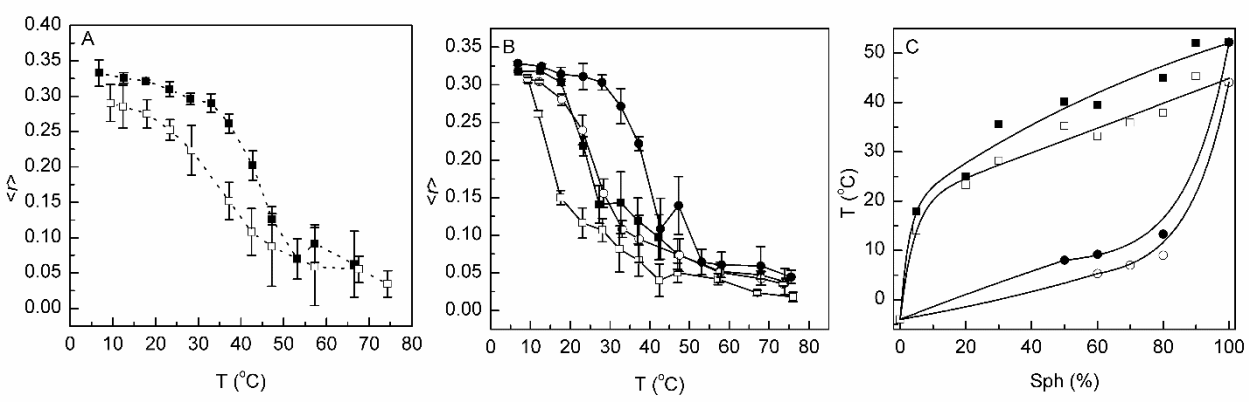

Figure 2. Thermotropic behavior of POPC/Sph mixtures. Steady-state fluorescence anisotropy <*r*> of *t*-PnA as a function of temperature in MLV composed of (A) pure Sph and (B) POPC/Sph mixtures containing 30 (squares) and 70 (circles) mol% of Sph at neutral (solid symbols) and acidic (open symbols) pH. (C) Partial binary phase diagram of POPC/Sph mixtures at neutral (solid symbols) and acidic (open symbols) pH: the gel+fluid-to-fluid transition (*liquidus* boundary) was obtained from *t*-PnA anisotropy; the *solidus* boundary was determined from DPH anisotropy data (see text for further details). The point for pure POPC is from Curatolo *et al*.[32] Values are means ± SD of at least three independent experiments.

4.3. Characterization of POPC/Sph vesicles by electrophoretic and dynamic light scattering

Dynamic and electrophoretic light scattering were used to further evaluate the characteristics of POPC/Sph vesicles. Zeta potential values shown in Figure 3A reveal that for low Sph content (up to 30 mol % Sph), the vesicles present a higher net positive charge at acidic pH. However, for Sph molar fractions above 40%, the surface charge at neutral pH continues to increase, whereas at pH 5.0, no further increase in the positive charge is observed. Figure 3B shows that POPC/Sph vesicles size is mainly comprised in the 100−150 nm range, but a tendency for vesicle aggregation and/or fusion can be noticed for high Sph content. In the absence of POPC, an increase in size and polydispersity index (PDI) is observed at both neutral and acidic pH, even though a higher instability is observed in the latter, suggesting a different organization and/or interaction of the Sph molecules at different pH environments. These results are reinforced by the high scattering intensities (I/I_0) recorded in the range of 0.5 −10 μm (Figures 3C,D), in the presence of higher Sph contents (X_{Sph} > 50%), especially at pH 5.0.

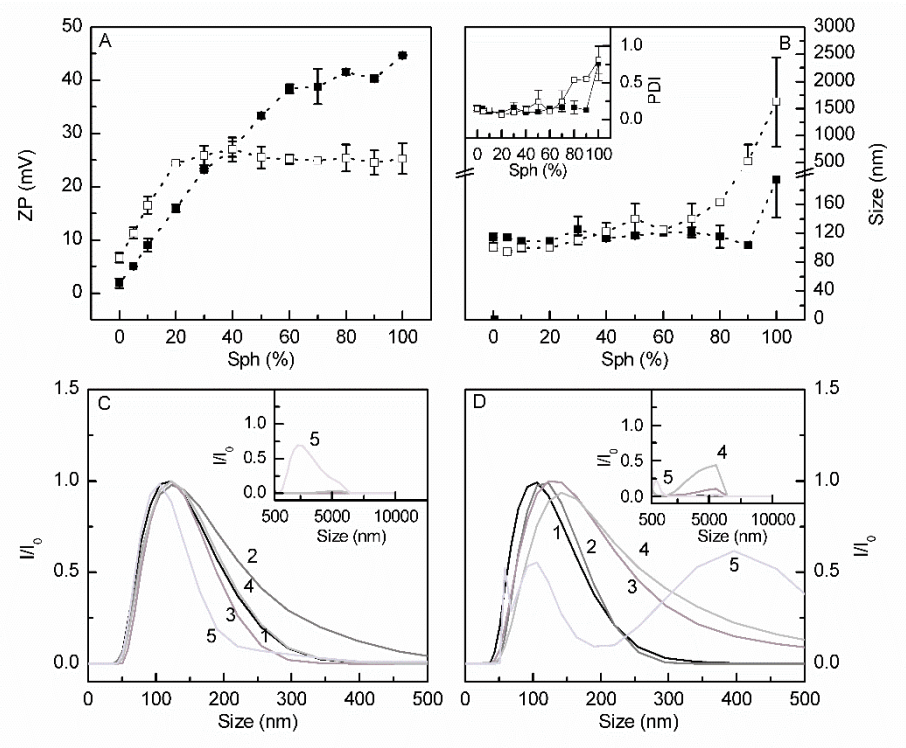

Figure 3 - Characterization of POPC/Sph binary mixtures by electrophoretic and dynamic light scattering measurements. (A) ζ-potential and (B) Particle mean size and polydispersity index (PDI, inset) of binary POPC/Sph mixtures at neutral (pH 7.4, solid squares) and acidic pH (pH 5.0, open squares). Error bars represent SD resulting from at least 3 independent experiments. In the point that represents 100% Sph, at pH 5.0, the SD associated to vesicle size is ± 825 nm. (C) and (D) Normalized scattered light intensity of binary mixtures as a function of particle size (nm) at pH 7.4 and pH 5.0, respectively. Results shown correspond to mixtures containing 0 (line 1), 30 (line 2), 50 (line 3), 70 (line 4) and 100 (line 5) mol% Sph. Values are the average ± SD (A, B) or the median (C, D) of at least 3 independent experiments. The lines act merely as guides to the eye.

4.4. Effect of Sph on the biophysical properties of raft-mimicking mixtures

In addition to Sph, Chol and SM also accumulate in LE/Ly in NPC disease. Accordingly, it is important to understand the interplay between Sph, Chol and SM to gain further insight into the biophysical alterations that these lipids might promote on the LE/Ly. The phase behavior of POPC/SM/Chol mixtures at room temperature and at different pH environments was evaluated. Figure 4A shows the fluorescence anisotropy of *t*-PnA as a function of l_o fraction, $X\,l_o$, for the

ternary mixtures. The anisotropy of *t*-PnA presents a linear increase with X_{I_o} in both pH environments. However, slightly lower anisotropy values were obtained at pH 5.0. Similar results were obtained with *t*-PnA mean fluorescence lifetime: an increase in <τ> towards values typical of I_o phase[22] was observed and longer lifetimes were obtained at neutral pH environment (Figure 4B). These results suggest that the packing properties of the I_o phase are affected by changes in pH environment.

ζ-potential measurements of the POPC/SM/Chol mixtures show that the vesicles present a non-zero net charge at both pH 7.4 and 5.0 (Figure 4C). The structures of both POPC and SM include the same hydrophilic phosphorylcholine head group, which is zwitterionic over a wide range of pH (approximately 3-12).[33] At neutral pH the vesicles showed a small negative net charge in accordance with other studies reporting that liposomes made from zwitterionic lipids carry a negative charge at neutral pH.[34,35,36] An increase in the ζ-potential from – 5 mV to + 4 mV was observed when the pH decreased from 7.4 to 5.0. Regardless of the pH environment, changes in ζ-potential with the lipid composition of the ternary mixtures were minimal.

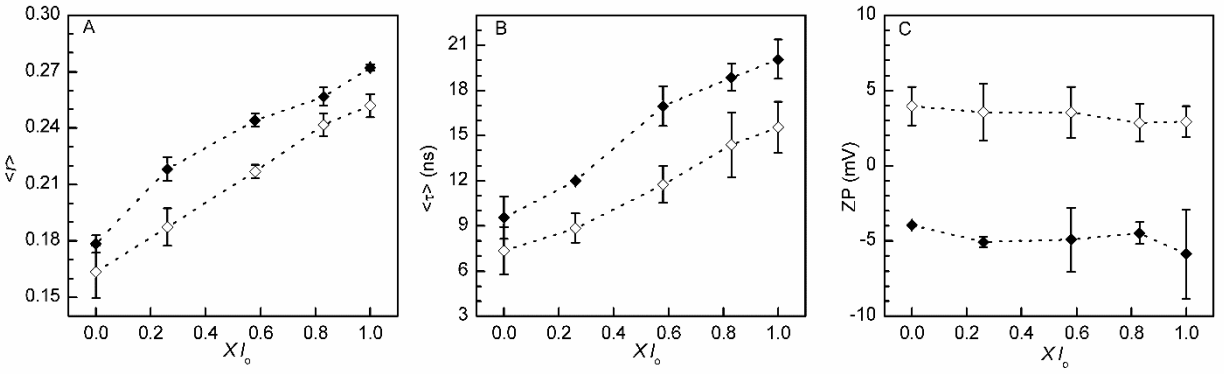

Figure 4. Characterization of POPC/SM/Chol raft-like mixtures in neutral and acidic pH. (A) Fluorescence anisotropy and (B) long lifetime component of *t*-PnA, and (C) ζ-potential in ternary POPC/SM/Chol mixtures at pH 7.4 (solid symbols) and pH 5.0 (open symbols). The values are the mean ± SD of at least three independent experiments. The lines act merely as guides to the eye.

Figure 5 (A - H) shows the variation of fluorescence anisotropy and of the long lifetime component of *t*-PnA in ternary POPC/SM/Chol mixtures with different Sph contents at both neutral and acidic pH. Normally the intracellular Sph levels are very low, but in some situations,

like in NPC cells, Sph abnormally accumulate.[2,19] Accordingly, it is important to elucidate the effect of Sph accumulation in the membrane biophysical properties. To better evaluate the impact of Sph on the organization and properties of raft-mimicking membranes, the data was represented as a function of $X\ l_o$. Our studies showed that at pH 7.4 (Figures 5A,B) and for the lower l_o fraction, the addition of 10 mol% Sph causes a substantial increase in the anisotropy (Figure 5A), mean fluorescence lifetime (See Figure S2 in the Supporting Information) and long lifetime component (Figure 5B) of *t*-PnA, suggesting that under these conditions Sph induces the formation of more ordered phases with gel-like properties, as suggested by the very long lifetime component of *t*-PnA fluorescence intensity decay (Figure 5B)[30]. The extent of gel phase formation is, however, low as suggested by the small pre-exponential (α_i) associated to the long component lifetime of *t*-PnA (See Figure S3 in the Supporting Information). Gel domain formation becomes less pronounced as the Chol concentration increases and, for the mixtures with the highest l_o fraction, the ordering effect of Sph on membrane properties is no longer observed. At pH 5.0 the effect of increasing Sph content in the ternary mixtures is not so marked (Figures 5C,D), and both the anisotropy values and the long lifetime component of *t*-PnA are lower comparing with pH 7.4, even when in the presence of lower l_o fractions and higher Sph content (Figures 5E,H). This suggests that when Sph accumulates in acidic vesicles, its ability to form gel domains diminishes.

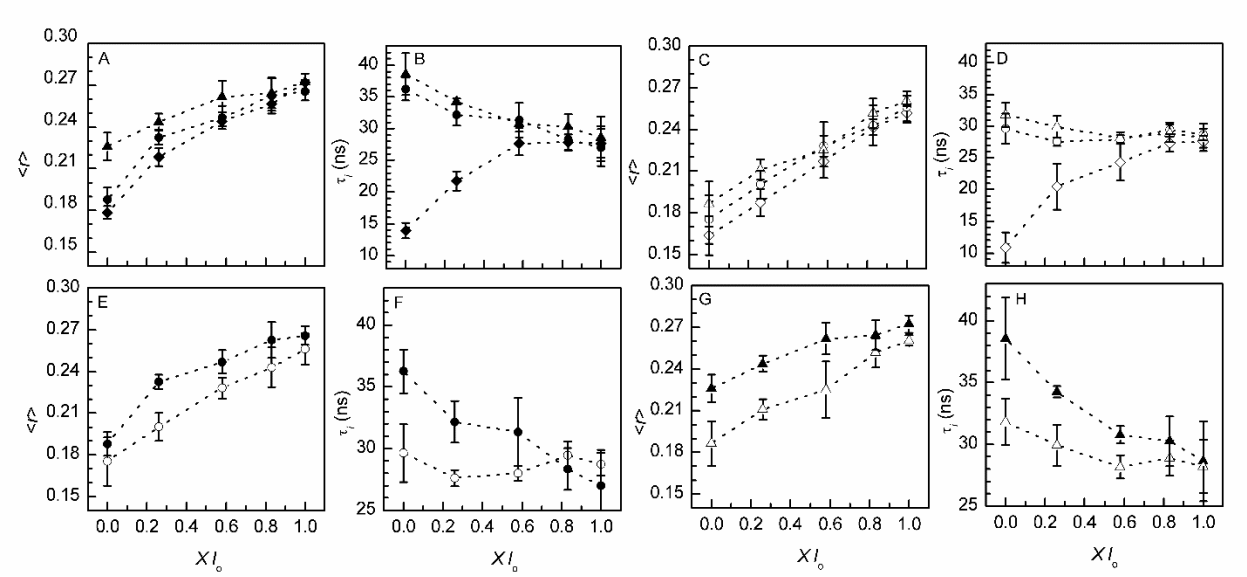

Figure 5. Interplay between Sph, Chol, and SM in lipid raft-mimicking mixtures. Panels A-D show the variation in *t*-PnA (A, C) fluorescence anisotropy and (B, D) long lifetime component in ternary POPC/SM/Chol mixtures (diamonds) and POPC/SM/Chol mixtures containing 5 (circles) and 10 (triangles) mol% of Sph at (A, B) pH 7.4 and (C, D) pH 5. Panels E-G show the (E, G) fluorescence anisotropy and (F, H) long lifetime component of *t*-PnA in POPC/SM/Chol mixtures containing (E, F) 5 and (G, H) 10 mol% of Sph at pH 7.4 (solid symbols) and pH 5.0 (open symbols). The values are the mean ± SD of at least three independent experiments. The lines act merely as guides to the eye.

4.5. Characterization of POPC/SM/Chol/Sph vesicles by electrophoretic and dynamic light scattering

As above mentioned, the ternary POPC/SM/Chol mixtures have a slightly negative surface charge at pH 7.4. With the increase of Sph content this charge gradually reaches positive values close to zero at 10 mol% Sph (Figure 6A). In the acidic environment (pH 5.0), the surface charge of the ternary mixtures is always positive and the net positive charge increases with increasing contents of Sph (Figure 6B), reaching ζ-potencial values close to 20 mV in the presence of 10 mol% Sph. Moreover, the presence of Sph in these mixtures leads to a small increase in the ζ-potential as the I_o fraction is increased, particularly at pH 5.0 (Figure 6B). This was not observed for the ternary mixtures in the absence of Sph (Figure 4C).

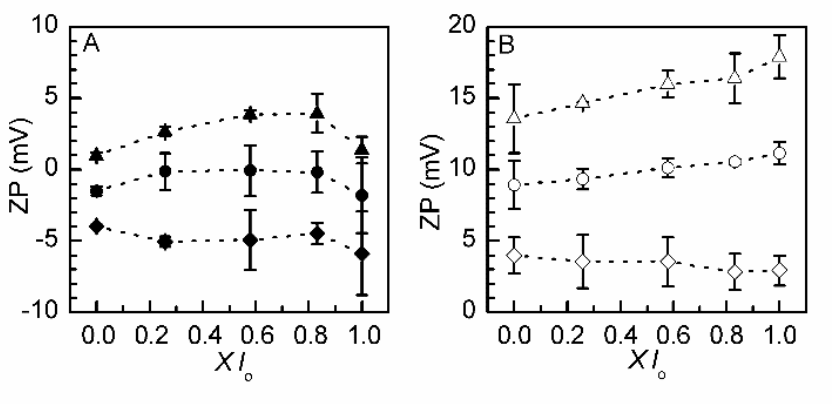

Figure 6. Surface charge characterization of POPC/SM/Chol/Sph mixtures. (A) and (B) ζ-potential at neutral (7.4) and acidic (5.0) pH, respectively. The symbols represent 0 (diamonds), 5 (circles), and 10 (triangles) mol% Sph. The values are the mean ± SD of at least 3 independent experiments. The lines act merely as guides to the eye.

Concerning the particles size (see Figure S4 in the Supporting Information), the model membranes tested in the different pH environments have generally sizes that range 100-150 nm. At pH 7.4, when the mixtures are constituted by higher Chol (higher I_o fraction) and Sph molar fractions, the PDI is higher and the particles seem to have a tendency to aggregate. Considering that at pH 7.4 the ζ-potential of the mixtures is close to neutral even in the presence of 10 mol% Sph, it is probable that in this environment the vesicles are not able to repel, which could justify their tendency to aggregate. There is also the possibility that the increase in the vesicle size is a result of different mechanical properties in vesicles with high Chol and Sph content, leading to a less efficient extrusion.[37] On the other hand, the net positive charge presented by the vesicles at acidic pH is probably responsible by repulsive forces that hamper the aggregation.

5. Discussion

Despite being a crucial lipid in cell function, little is known about Sph mode of action. In particular, the biophysical impact caused by Sph accumulation remains incompletely understood. Some studies have addressed the effect of Sph in the biophysical properties of model membranes[6,11,15,38,39], but information regarding its effect on the fluid POPC, a major

phospholipid membrane component, and an understanding of its interplay with lipids that also accumulate in the lysosomes of NPC disease, such as Chol and SM, are currently unavailable. In this study, we evaluated the influence of Sph in the biophysical and interfacial electrostatic properties of model membranes constituted by (1) POPC (fluid membrane) and (2) POPC/SM/Chol (raft model). The behavior of the artificial membranes was analyzed in neutral pH (pH 7.4) and acidic pH (pH 5.0) in order to mimic the PM and LM environments, respectively.

5.1. Impact of Sph on the physical state, thermotropic behavior and electrostatic properties of a fluid POPC membrane

Our results showed that Sph accumulation in POPC model membranes promotes the formation of Sph gel-like domains, in agreement with previous studies.[6,11,15,38,39] However, to our best knowledge, this is the first study reporting the phase behavior, thermotropic, and interfacial electrical properties of Sph-containing mixtures, in neutral and acidic pH environments. Our results demonstrated that the effect of Sph on the membrane is dependent on the pH of the hydration medium. Gel domain formation occurred with lower Sph concentrations at pH 7.4, compared to pH 5.0, and these differences are reflected in the partial binary phase diagrams of the mixtures at both pH. Sphingolipid gel domains are maintained by strong van der Waals interactions between the saturated hydrocarbon chains and electrostatic repulsive forces due to lipid dipoles.[11] In the case of Sph, the net positive charge is probably underlying the electrostatic repulsion, which certainly destabilizes domain formation. Apparently, this destabilization is higher at acidic pH, as denoted by the lower ability of Sph to form gel domains under these conditions. This could be related to differences in the ionic state of Sph. It was reported that the apparent pK of Sph might range from 6.7[40] to 9.1[15,16] depending on the environment (e.g., solution, micelles, bilayers) due to differences in hydration and hydrogen-bonding states.[16,33,34] Therefore, the assumption that Sph is positively charged at neutral pH[16,41] might not always be valid. For example, it was demonstrated that when Sph forms aggregates at neutral pH, the great majority of molecules presents a neutral net charge.[17]

Our results show that increasing Sph concentration at neutral pH increases the net positive charge of the mixtures, suggesting that under these conditions, Sph molecules are

indeed positively charged. The higher net positive charge increases the repulsive forces and prevents strong vesicle aggregation. Because Sph is protonated at acid pH, it would be expected that Sph aggregation would also be hampered in these conditions, due to the repulsive forces created by the charged groups. Interestingly, when Sph molar fraction exceeds 30%, a pH dependent change in the interfacial electrical properties of POPC/Sph vesicles is observed. The net surface charge of these vesicles (which is lower at pH 7.4 when Sph <40 mol %) continues to increase at neutral pH, although at acidic pH, the value reaches a plateau at +25 mV. Because it is not expected to have a decrease in the positive surface charge of the vesicles as the concentration of Sph is increased in the mixtures, additional alterations in the electrical and/or mechanical properties of the vesicles should account for the observed surface charge stabilization at acidic pH. One hypothesis could be the formation of structures that bury the positive charge of Sph, such as aggregated vesicles or high curvature regions rich in Sph. This would contribute to a decrease in the repulsive forces between the vesicles and increase in their aggregation (Figure 3). Alterations in the H-bonding network of Sph from intramolecular at pH 5.0 to intermolecular at pH 7.4[17] could also account for the differences observed in the thermotropic behavior of Sph and POPC/Sph mixtures at distinct pH. This would also explain the different organization of Sph molecules in the absence of POPC, particularly the larger structures formed at acidic pH.

5.2. Effect of pH environment on the biophysical and electrostatic properties of raft-mimicking mixtures

Lipid rafts are thought to exist mainly at the PM, and they are virtually absent from intracellular membranes, where the content of lipids involved in raft formation is lower.[42] A typical example is the lysosome, where the total levels of Chol are low.[43] However, this is not the case of the lysosomes of NPC, where the accumulation of both Chol and SM contribute to an increase in the levels of these raft components.[44] It has been hypothesized that lipid rafts might accumulate in the LE/Ly of NPC (and other lipidoses) and cause the impairment of LE/Ly functions.[42] However, despite the large amount of studies addressing the biophysical properties of raft-mimicking membranes,[22,23,45–48] little attention has been given to the effect of pH

environment on lipid raft organization and properties. In the present study, we showed that upon acidification there is a decrease in the ordering of the membrane, which is independent of the composition of the ternary mixtures. This was accompanied by an increase in the net surface charge, showing that pH environment affects both the physical and the electrostatic properties of the raft-mimicking mixtures. The raft model membranes showed a nonzero net charge at both pH values, resulting from the exposure of the membrane to different ions. POPC and SM contain phosphate and choline, functional groups whose electric charge distributions is determined by the binding of counterion.[49–51] At pH 5.0, vesicles have a positive ζ-potential pointing to the association of protons with groups at the membrane surface.

5.3. Impact of Sph on the physical state and electrostatic properties of POPC/SM/Chol membranes (raft model)

Our results show that Sph is able to change the physical properties of POPC/SM/Chol even when in low concentrations. These effects are more pronounced when the fraction of l_o phase is low (low Chol and SM content) and at neutral pH, but these effects are also observed at acidic pH. Comparing this effect with the effect that Sph had upon the properties of the fluid POPC vesicles, we can conclude that the ordering ability of Sph in the ternary mixtures is higher, because lower amounts of Sph already induce significant changes in the lipid packing. However, Sph-induced changes on the properties of raft-mimicking mixtures are minor when Chol content, and thus the l_o fraction, is high. This effect resembles that described for ceramide interacting with lipid-raft mixtures,[45,46] suggesting that Sph ability to increase the ordering of the membrane and segregate into Sph gel domains depends on the Chol content. This is probably a consequence of the Sph −SM and Sph –Chol interactions, which might facilitate the formation of a gel phase or increase the solubility of Sph in the l_o phase, respectively, as previously shown for ceramide.[45,46,52] It was reported that increasing the Chol content in ternary POPC/Sph/Chol mixtures favors the miscibility of Sph in the membrane.[11] In addition, it was suggested that in ternary POPC/SM/Chol mixtures, a competition between Sph and SM might occur for the interaction with Chol, and that SM leads to a decrease of Sph miscibility, possibly due to the formation of a SM/Sph-enriched gel phase.[6,11] These observations support

our hypothesis that Sph might induce changes on the biophysical properties of raft-mimicking mixtures comparable to ceramide,[45,46] (i.e., induce the formation of a gel phase in the low Chol, low l_o phase fraction range) and it may also become miscible in the l_o phase when the Chol content and the l_o phase fraction is high). However, significant differences regarding the interaction of ceramide and Sph with lipid raft mixtures can be highlighted: (i) Sph has a lower ability to form gel phase compared to ceramide. For instance, strong alterations in the properties of raft mixtures, including gel phase formation, are observed for mixtures containing ~4 mol % of ceramide;[45] however, higher amounts of Sph are required to promote comparable effects. (ii) These observations further suggest a lower synergy between SM and Sph in the formation of gel domains, compared to ceramide/SM, where formation of ceramide gel domains was enhanced by SM.[45] (iii) Moreover, the packing properties of the Sph gel differ from the ceramide gel phase. Even though Sph has an ability to form gel phase in the fluid POPC and in raft mimicking mixtures, both the extent and the packing of the gel phase is lower in Sph-containing mixtures compared to ceramide containing mixtures,[29,45] as observed by the higher content of Sph required to induce gel phase formation and the lower fluorescence lifetime of *t*-PnA in Sph-containing mixtures. In addition, information derived from studies using DPH showed that ceramide-enriched gel domains were extremely ordered, preventing the incorporation of this probe in the ceramide gel phase. This was not observed in mixtures containing Sph. In contrast, the increase in DPH anisotropy toward values typical of gel phase further supports the ability of Sph to form a less packed gel phase as compared to ceramide. The analysis of the vesicles through electrophoretic and dynamic light scattering further showed that Sph also changes the interfacial electrical properties of the raft mixtures. Our ζ-potential measurements indicate that the electrical properties of the POPC/SM/Chol membranes are affected by both Sph content and solution pH. Sph increases the surface charge at both pH values, but at pH 7.4, the net charge is mainly neutral. However, at pH 5.0, the surface charge density is positive. In addition, while the surface electrical properties of the ternary lipid vesicles seem not to be significantly affected by their lipid composition, the presence of Sph appears to change the interfacial properties in a Chol/SM content-dependent manner, particularly at pH 5.0. Indeed, at pH 5.0, the presence of Sph leads to an increase in ζ-

potential with Chol content. A possible explanation could be a lower segregation of Sph into gel domains when the l_o phase fraction is higher (Sph is more randomly dispersed in the membrane), which contributes to the stabilization of cationic Sph due to lower repulsive forces in the absence of neighboring Sph molecules (also positively charged). It is also important to notice that we are using mixtures with l_d/l_o domains which can also contribute to Sph stabilization, for example, in the interfaces between the different domains. At pH 7.4, in the presence of 100% l_o, we can verify a decrease in the surface net charge of the vesicles that can be a result of vesicle aggregation or binding of counterions, which also contributes to vesicle aggregation. At pH 5.0, the membrane is more disordered and probably the formation of 100% l_o does not occur, even for the highest Chol/SM mole fraction employed. Even though ζ-potential measurements in binary POPC/Sph mixtures at neutral pH show a Sph-dependent mild increase in the net positive surface charge density, it is possible that not all of the Sph are on a protonated form at pH 7.4. This would contribute to a decrease in the repulsive electrostatic forces between Sph molecules and would justify the increased ability of Sph to segregate into gel domains both in the binary and raft mixtures at neutral pH compared to pH 5.0. On the other hand, the electrostatic repulsion created by Sph positive charge at pH 5.0 would hinder molecule aggregation and reduce Sph ability to form gel domains in this environment. In Figure 7, where the difference of ζ-potential between pH 5.0 and pH 7.4 can be observed, it is clear that Sph changes its protonation state in the different environments and that these alterations are dependent on mixture composition. The mixtures are more charged at acidic pH and for higher l_o fractions. Probably the lipid organization, orientation of the head groups (that are also altered by Chol presence), and the alteration of Sph hydrogen-bonding states due to pH variation are the cause of the observed behaviors.

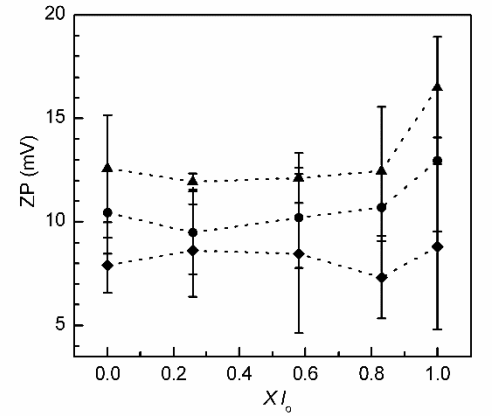

Figure 7. Difference of ζ-potential in POPC/SM/Chol/Sph mixtures between pH 5.0 and pH 7.4. The symbols represent 0 (diamonds), 5 (circles), and 10 (triangles) mol% Sph. The lines act merely as guides to the eye.

6. Conclusions

In this study, we demonstrate the impact of Sph on fluid and raft-mimicking model membranes at neutral pH (7.4) and acidic pH (5.0). Our studies revealed that Sph has an ordering effect in the fluid POPC membrane that is more pronounced in higher concentrations and at neutral pH. However, in rafts (POPC/SM/Chol membrane), its presence, even in low concentrations (5 or 10%), contributes to formation of Sph gel-like domains, in a Chol/SM content-dependent manner. These results support the hypothesis that the Sph biological role could be exerted through biophysical changes in cellular membranes.

7. Acknowledgments

Acknowledgments are addressed to Fundação para a Ciência e Tecnologia (FCT), PT: PTDC/QUI-BIQ/111411/2009, PEst-OE/QUI/UI0612/2013, SFRH/BD/88194/2012, Compromisso para a Ciência 2008, Investigador FCT 2012 (POPH, FSE).

8. References

(1) Sandhoff, K.; Kolter, T.; Van Echten-Deckert, G. Sphingolipid Metabolism. Sphingoid Analogs, Sphingolipid Activator Proteins, and the Pathology of the Cell. *Ann. N. Y. Acad. Sci.* **1998**, *845*, 139–151.

(2) Zheng, W.; Kollmeyer, J.; Symolon, H.; Momin, A.; Munter, E.; Wang, E.; Kelly, S.; Allegood, J. C.; Liu, Y.; Peng, Q.; et al. Ceramides and Other Bioactive Sphingolipid Backbones in Health and

Disease: Lipidomic Analysis, Metabolism and Roles in Membrane Structure, Dynamics, Signaling and Autophagy. *Biochim. Biophys. Acta* **2006**, *1758*, 1864–1884.

(3) Betto, R.; Teresi, A.; Fachechi-Cassano, G. Salviati, G.; Sabbadini, R. A. Sphingosine Inhibits Calcium Release from Sarcoplasmic Reticulum Membranes. *Adv. Exp. Med. Biol.* **1992**, *311*, 403–404.

(4) Spiegel, S. Sphingosine, a Breakdown Product of Cellular Sphingolipids, in Cellular Proliferation and Phospholipid Metabolism. In *Phospholipids and Signal Transmission*; Massarelli, R.; Horrocks, L. A.; Kanfer, J. N.; Löffelholz, K., Eds.; Springer: Heidelberg, 1993; pp. 189–203.

(5) Kågedal, K.; Zhao, M.; Svensson, I.; Brunk, T. Sphingosine-Induced Apoptosis Is Dependent on Lysosomal Proteases. *Biochem. J.* **2001**, *359*, 335–343.

(6) Contreras, F.-X.; Sot, J.; Alonso, A.; Goñi, F. M. Sphingosine Increases the Permeability of Model and Cell Membranes. *Biophys. J.* **2006**, *90*, 4085–4092.

(7) Megidish, T.; Cooper, J.; Zhang, L.; Fu, H.; Hakomori, S. A Novel Sphingosine-Dependent Protein Kinase (SDK1) Specifically Phosphorylates Certain Isoforms of 14-3-3 Protein. *J. Biol. Chem.* **1998**, *273*, 21834–21845.

(8) Mcdonald, B.; Hannunjll, Y. A.; Reynolds, C. H.; Sahyoun, N. Activation of Casein Kinase II by Sphingosine. *J. Biol. Chem.* **1991**, *266*, 21773–21776.

(9) Ma, Y.; Pitson, S.; Hercus, T.; Murphy, J.; Lopez, A.; Woodcock, J. Sphingosine Activates Protein Kinase A Type II by a Novel cAMP-Independent Mechanism. *J. Biol. Chem.* **2005**, *280*, 26011–26017.

(10) King, C. C.; Zenke, F. T.; Dawson, P. E.; Dutil, E. M.; Newton, A. C.; Hemmings, B. A.; Bokoch, G. M. Sphingosine Is a Novel Activator of 3-Phosphoinositide-Dependent Kinase 1. *J. Biol. Chem.* **2000**, *275*, 18108–18113.

(11) Georgieva, R.; Koumanov, K.; Momchilova, A.; Tessier, C.; Staneva, G. Effect of Sphingosine on Domain Morphology in Giant Vesicles. *J. Colloid Interface Sci.* **2010**, *350*, 502–510.

(12) López-García, F.; Villalaín, J.; Gómez-Fernández, J. C. A Phase Behavior Study of Mixtures of Sphingosine with Zwitterionic Phospholipids. *Biochim. Biophys. Acta* **1994**, *1194*, 281–288.

(13) Siskind, L. J.; Fluss, S.; Bui, M.; Colombini, M. Sphingosine Forms Channels in Membranes That Differ Greatly from Those Formed by Ceramide. *J. Bioenerg. Biomembr.* **2005**, *37*, 227–236.

(14) Jiménez-Rojo, N.; Sot, J.; Viguera, A. R.; Collado, M. I.; Torrecillas, A.; Gómez-Fernández, J. C.; Goñi, F. M.; Alonso, A. Membrane Permeabilization Induced by Sphingosine: Effect of Negatively-Charged Lipids. *Biophys. J. in press*.

(15) López-García, F.; Micol, V.; Villalaín, J.; Gómez-Fernández, J. C. Interaction of Sphingosine and Stearylamine with Phosphatidylserine as Studied by DSC and NMR. *Biochim. Biophys. Acta* **1993**, *1153*, 1–8.

(16) Goñi, F. M.; Alonso, A. Biophysics of Sphingolipids I. Membrane Properties of Sphingosine, Ceramides and Other Simple Sphingolipids. *Biochim. Biophys. Acta* **2006**, *1758*, 1902–1921.

(17) Sasaki, H.; Arai, H.; Cocco, M. J.; White, S. H. pH Dependence of Sphingosine Aggregation. *Biophys. J.* **2009**, *96*, 2727–2733.

(18) Van Meer, G.; Hoetzl, S. Sphingolipid Topology and the Dynamic Organization and Function of Membrane Proteins. *FEBS Lett.* **2010**, *584*, 1800–1805.

(19) Lloyd-Evans, E.; Platt, F. M. Lipids on Trial: The Search for the Offending Metabolite in Niemann-Pick Type C Disease. *Traffic* **2010**, *11*, 419–428.

(20) Rosenbaum, A. I.; Maxfield, F. R. Niemann-Pick Type C Disease: Molecular Mechanisms and Potential Therapeutic Approaches. *J. Neurochem.* **2012**, *116*, 789–795.

(21) Lloyd-Evans, E.; Morgan, A. J.; He, X.; Smith, D. A.; Elliot-Smith, E.; Sillence, D. J.; Churchill, G. C.; Schuchman, E. H.; Galione, A.; Platt, F. M. Niemann-Pick Disease Type C1 Is a Sphingosine Storage Disease That Causes Deregulation of Lysosomal Calcium. *Nat. Med.* **2008**, *14*, 1247–1255.

(22) De Almeida, R. F. M.; Fedorov, A.; Prieto, M. Sphingomyelin/phosphatidylcholine/cholesterol Phase Diagram: Boundaries and Composition of Lipid Rafts. *Biophys. J.* **2003**, *85*, 2406–2416.

(23) De Almeida, R. F. M.; Loura, L. M. S.; Fedorov, A.; Prieto, M. Lipid Rafts Have Different Sizes Depending on Membrane Composition: A Time-Resolved Fluorescence Resonance Energy Transfer Study. *J. Mol. Biol.* **2005**, *346*, 1109–1120.

(24) Reyes Mateo, C.; Brochon, J. C.; Pilar Lillo, M.; Ulises Acuña, A. Lipid Clustering in Bilayers Detected by the Fluorescence Kinetics and Anisotropy of Trans-Parinaric Acid. *Biophys. J.* **1993**, *65*, 2237–2247.

(25) McClare, C. W. F. An Accurate and Covenient Organic Phosphorus Assay. *Anal. Biochem.* **1971**, *39*, 527–530.

(26) Sklar, L. A.; Hudson, B. S.; Petersen, M.; Diamond, J. Conjugated Polyene Fatty Acids on Fluorescent Probes: Spectroscopic Characterization. *Biochemistry* **1977**, *16*, 813–819.

(27) Lentz, B. Membrane "fluidity" from Fluorescence Anisotropy Measurements. In *Spectroscopic membrane probes*; Loew, L., Ed.; FL: CRC Press, Boca Raton, 1988; pp. 13–41.

(28) Aresta-Branco, F.; Cordeiro, A. M.; Marinho, H. S.; Cyrne, L.; Antunes, F.; de Almeida, R. F. M. Gel Domains in the Plasma Membrane of *Saccharomyces Cerevisiae*: Highly Ordered, Ergosterol-Free, and Sphingolipid-Enriched Lipid Rafts. *J. Biol. Chem.* **2011**, *286*, 5043–5054.

(29) Silva, L.; de Almeida, R. F. M.; Fedorov, A.; Matos, A. P. A.; Prieto, M. Ceramide-Platform Formation and -Induced Biophysical Changes in a Fluid Phospholipid Membrane. *Mol. Membr. Biol.* **2006**, *23*, 137–150.

(30) Castro, B. M.; de Almeida, R. F. M.; Silva, L. C.; Fedorov, A.; Prieto, M. Formation of Ceramide/sphingomyelin Gel Domains in the Presence of an Unsaturated Phospholipid: A Quantitative Multiprobe Approach. *Biophys. J.* **2007**, *93*, 1639–1650.

(31) Sklar, L. A.; Miljanich, G. P.; Dratz, E. A. Phospholipid Lateral Phase Separation and the Partition of Cis-Parinaric Acid and Trans-Parinaric Acid among Aqueous, Solid Lipid, and Fluid Lipid Phases. *Biochemistry* **1979**, *18*, 1707–1716.

(32) Curatolo, W.; Sears, B.; Neuringer, L. A Calorimetry and Deuterium NMR Study of Mixed Model Membranes of 1-Palmitoyl-2-Oleylphosphatidylcholine and Saturated Phosphatidylcholines. *Biochim. Biophys. Acta* **1985**, *817*, 261–270.

(33) Lee, A. G. Lipid Phase Transitions and Mixtures. In *Membrane fluidity in Biology*; Aloia, R. C., Ed.; Academic Press, New York, 1983; p. 59.

(34) Makino, K.; Yamada, T.; Kimura, M.; Oka, T.; Ohshima, H.; Kondo, T. Temperature- and Ionic Strength-Induced Conformational Changes in the Lipid Head Group Region of Liposomes as Suggested by Zeta Potential Data. *Biophys. Chem.* **1991**, *41*, 175–183.

(35) Pincet, F.; Cribier, S.; Perez, E. Bilayers of Neutral Lipids Bear a Small but Significant Charge. *Eur. Phys. J. B* **1999**, *130*, 127–130.

(36) Wiedmer, S. K.; Hautala, J.; Holopainen, J. M.; Kinnunen, P. K.; Riekkola, M. L. Study on Liposomes by Capillary Electrophoresis. *Electrophoresis* **2001**, *22*, 1305–1313.

(37) Hunter, D. G.; Frisken, B. J. Effect of Extrusion Pressure and Lipid Properties on the Size and Polydispersity of Lipid Vesicles. *Biophys. J.* **1998**, *74*, 2996–3002.

(38) Kõiv, A.; Mustonen, P.; Kinnunen, P. K. Influence of Sphingosine on the Thermal Phase Behaviour of Neutral and Acidic Phospholipid Liposomes. *Chem. Phys. Lipids* **1993**, *66*, 123–134.

(39) López-García, F.; Villalaín, J.; Gómez-Fernández, J. C. Effect of Sphingosine and Stearylamine on the Interaction of Phosphatidylserine with Calcium. A Study Using DSC, FT-IR and 45Ca(2+)-Binding. *Biochim. Biophys. Acta* **1995**, *1236*, 279–288.

(40) Merrill, A. H.; Nimkar, S.; Menaldino, D.; Hannun, Y. A.; Loomis, C.; Bell, R. M.; Tyagi, S. R.; Lambeth, J. D.; Stevens, V. L.; Hunter, R. Structural Requirements for Long-Chain (sphingoid) Base

Inhibition of Protein Kinase C in Vitro and for the Cellular Effects of These Compounds. *Biochemistry* **1989**, *28*, 3138–3145.

(41) Merrill Jr., L. A. H.; Sandhoff, K. Sphingolipids: Metabolism and Cell Signaling. In *Biochemistry of Lipids. Lipoproteins and Membranes*; Vance, D. E.; Vance, J. E., Eds.; Elsevier Science B.V.: Amsterdam, 2002; pp. 373–407.

(42) Simons, K.; Gruenberg, J. Jamming the Endosomal System: Lipid Rafts and Lysosomal Storage Diseases. *Trends Cell Biol.* **2000**, *10*, 459–462.

(43) Möbius, W.; van Donselaar, E.; Ohno-Iwashita, Y.; Shimada, Y.; Heijnen, H. F. G.; Slot, J. W.; Geuze, H. J. Recycling Compartments and the Internal Vesicles of Multivesicular Bodies Harbor Most of the Cholesterol Found in the Endocytic Pathway. *Traffic* **2003**, *4*, 222–231.

(44) Chang, T.-Y.; Reid, P. C.; Sugii, S.; Ohgami, N.; Cruz, J. C.; Chang, C. C. Y. Niemann-Pick Type C Disease and Intracellular Cholesterol Trafficking. *J. Biol. Chem.* **2005**, *280*, 20917–20920.

(45) Silva, L. C.; de Almeida, R. F. M.; Castro, B. M.; Fedorov, A.; Prieto, M. Ceramide-Domain Formation and Collapse in Lipid Rafts: Membrane Reorganization by an Apoptotic Lipid. *Biophys. J.* **2007**, *92*, 502–516.

(46) Silva, L. C.; Futerman, A. H.; Prieto, M. Lipid Raft Composition Modulates Sphingomyelinase Activity and Ceramide-Induced Membrane Physical Alterations. *Biophys. J.* **2009**, *96*, 3210–3222.

(47) Nicolini, C.; Kraineva, J.; Khurana, M.; Periasamy, N.; Funari, S. S.; Winter, R. Temperature and Pressure Effects on Structural and Conformational Properties of POPC/SM/cholesterol Model Raft Mixtures--a FT-IR, SAXS, DSC, PPC and Laurdan Fluorescence Spectroscopy Study. *Biochim. Biophys. Acta* **2006**, *1758*, 248–258.

(48) Rawicz, W.; Smith, B. A.; McIntosh, T. J.; Simon, S. A.; Evans, E. Elasticity, Strength, and Water Permeability of Bilayers That Contain Raft Microdomain-Forming Lipids. *Biophys. J.* **2008**, *94*, 4725–4736.

(49) Zhou, Y.; Raphael, R. M. Solution pH Alters Mechanical and Electrical Properties of Phosphatidylcholine Membranes: Relation between Interfacial Electrostatics, Intramembrane Potential, and Bending Elasticity. *Biophys. J.* **2007**, *92*, 2451–2462.

(50) Sachs, J. N.; Nanda, H.; Petrache, H. I.; Woolf, T. B. Changes in Phosphatidylcholine Headgroup Tilt and Water Order Induced by Monovalent Salts: Molecular Dynamics Simulations. *Biophys. J.* **2004**, *86*, 3772–3782.

(51) Marquês, J. T.; de Almeida, R. F. M.; Viana, A. S. Biomimetic Membrane Rafts Stably Supported on Unmodified Gold. *Soft Matter* **2012**, *8*, 2007.

(52) Castro, B. M.; Silva, L. C.; Fedorov, A.; de Almeida, R. F. M.; Prieto, M. Cholesterol-Rich Fluid Membranes Solubilize Ceramide Domains: Implications for the Structure and Dynamics of Mammalian Intracellular and Plasma Membranes. *J. Biol. Chem.* **2009**, *284*, 22978–22987.

9. Supporting Information for: Biophysical Implications of Sphingosine Accumulation in Membrane Properties at Neutral and Acidic pH

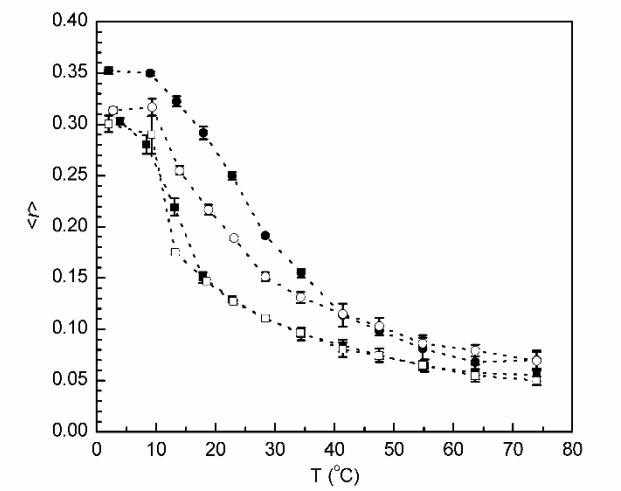

Figure S1. Thermotropic behavior of POPC/Sph mixtures. Steady-state fluorescence anisotropy of DPH as a function of temperature in MLV composed of POPC/Sph mixtures containing 30 (squares) and 80 (circles) mol% Sph at pH 7.4 (solid symbols), pH 5.0 (open symbols). Values are means ± SD of at least three independent experiments.

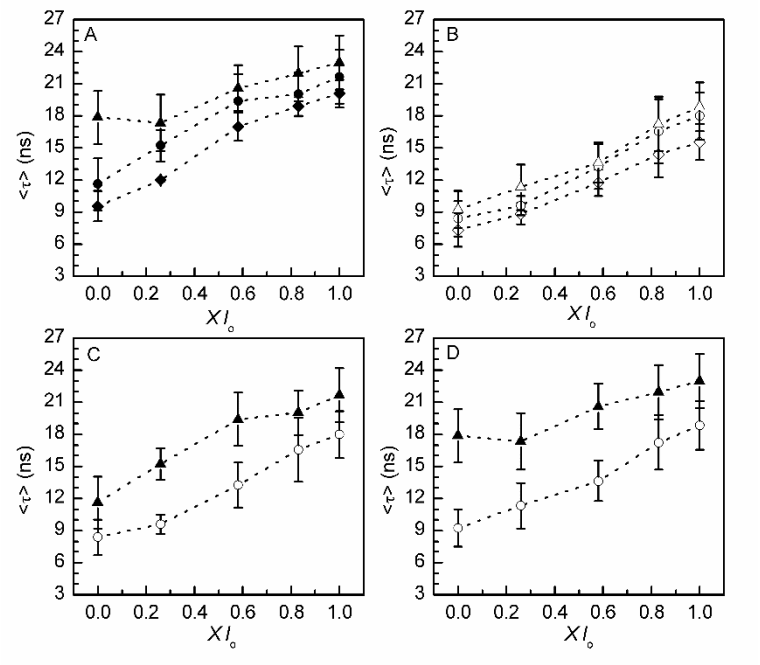

Figure S2. Mean fluorescence lifetime of *t*-PnA in POPC/SM/Chol/Sph mixtures. Mean fluorescence lifetime of *t*-PnA in ternary mixtures containing 0 (diamonds), 5 (circles), and 10 (triangles) mol% Sph at (A) neutral and (B) acidic pH. Mean fluorescence lifetime in mixtures containing (C) 5 and (D) 10 mol% Sph at pH 7.4 (solid symbols) and pH 5.0 (open symbols). The values are the mean ± SD of at least three independent experiments. The lines act merely as guides to the eye.

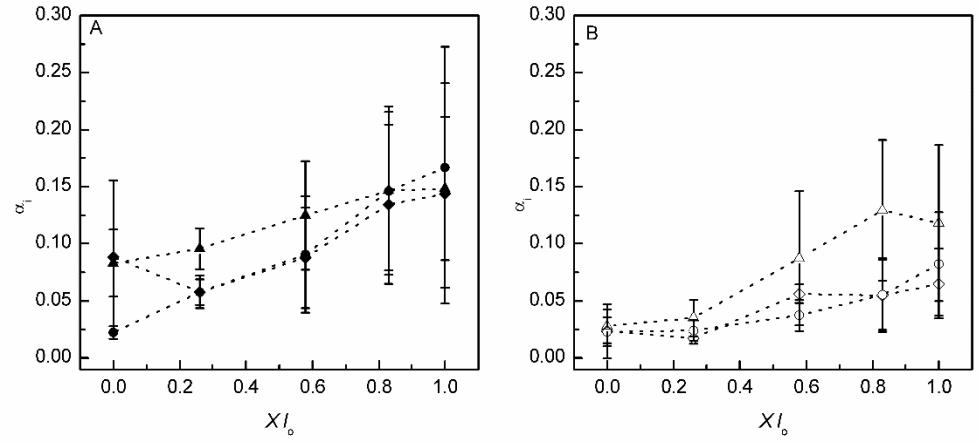

Figure S3. Normalized pre-exponential factors associated to the long component lifetime of *t*-PnA, in POPC/SM/Chol/Sph mixtures. The symbols represent 0 (diamonds), 5 (circles), and 10 (triangles) mol% Sph. The lines act merely as guides to the eye.

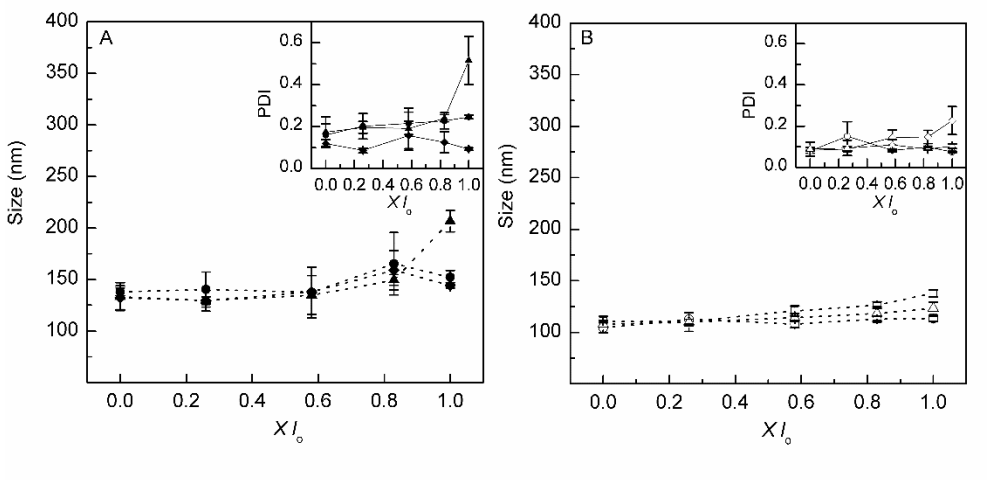

Figure S4. Size of POPC/SM/Chol/Sph mixtures as a function of $X\,l_o$. (A) and (B) size at neutral (7.4) and acidic (5.0) pH, respectively. The symbols represent ternary mixtures containing 0 (diamonds), 5 (circles), and 10 (triangles) mol% Sph. Insets: polydispersity index of the same mixtures. The values are the mean ± SD of at least 3 independent experiments. The lines act merely as guides to the eye.

CHAPTER III

DEVELOPMENT OF LYSOSOME-MIMICKING VESICLES TO STUDY THE EFFECT OF ABNORMAL ACCUMULATION OF SPHINGOSINE ON MEMBRANE PROPERTIES

This Chapter comprises the work published in Scientific Reports (2017) 7: 3949 by **Ana C. Carreira**, Rodrigo F. M. de Almeida, and Liana C. Silva

CHAPTER III – DEVELOPMENT OF LYSOSOME-MIMICKING VESICLES TO STUDY THE EFFECT OF ABNORMAL ACCUMULATION OF SPHINGOSINE ON MEMBRANE PROPERTIES

SCIENTIFIC REPORTS

OPEN

Received: 24 June 2016
Accepted: 10 May 2017
Published online: 21 June 2017

Development of lysosome-mimicking vesicles to study the effect of abnormal accumulation of sphingosine on membrane properties

Ana C. Carreira[1,2], Rodrigo F. M. de Almeida[2] & Liana C. Silva[1,3]

1. Abstract

Synthetic systems are widely used to unveil the molecular mechanisms of complex cellular events. Artificial membranes are key examples of models employed to address lipid-lipid and lipid-protein interactions. In this work, we developed a new synthetic system that more closely resembles the lysosome – the lysosome-mimicking vesicles (LMVs) – displaying stable acid-to-neutral pH gradient across the membrane. To evaluate the advantages of this synthetic system, we assessed the distinct effects of sphingosine (Sph) accumulation in membrane structure and biophysical properties of standard liposomes (no pH gradient) and in LMVs with lipid composition tuned to mimic physiological- or NPC1-like lysosomes. Ternary 1-palmitoyl-2-oleoyl-*sn*-glycero-3-phosphocholine (POPC)/Sphingomyelin (SM)/Cholesterol (Chol) mixtures with, respectively, low and high Chol/SM levels were prepared. The effect of Sph on membrane permeability and biophysical properties was evaluated by fluorescence spectroscopy, electrophoretic and dynamic light scattering. The results showed that overall Sph has the ability to cause a shift in vesicle surface charge, increase membrane order and promote a rapid increase in membrane permeability. These effects are enhanced in NPC1 - LMVs. The

results suggest that lysosomal accumulation of these lipids, as observed under pathological conditions, might significantly affect lysosomal membrane structure and integrity, and therefore contribute to the impairment of cell function.

2. Introduction

Sphingosine (2*S*,3*R*-D-erythro-2-amino-1,3-octadec-4*E*-ene-diol) is one of the most abundant sphingoid backbone in mammalian sphingolipids (SLs)[1]. It results from the degradation of ceramide (Cer) by ceramidases in different sub-cellular locations[2]. In the lysosome, Sph is generated through the hydrolysis of Cer by aCDase. The amino group of Sph is protonated under acidic conditions and therefore it needs a transporter (currently unknown) to facilitate its egress from the acidic compartments[3]. Free Sph levels are generally maintained low, due to its rapid further metabolization into important signaling molecules. This lipid can be converted into S1P through the phosphorylation of C1 hydroxyl group or acylated through the action of different ceramide synthases to produce ceramide[2,4,5].

Sph is itself a bioactive lipid and it plays an active role in different biological processes, such as differentiation[6], and apoptosis[7,8]. Moreover, Sph has been implicated in the regulation of the activity of various enzymes, including protein kinases[7,9-13]. Most of these enzymes do not have a *bona fide* Sph-binding site identified. They are amphitropic proteins, a feature that is important for their activity and regulation[14]. This suggests that the regulatory effect of Sph can in part be exerted at the membrane level, namely through physical changes that might affect the distribution of lipids and proteins and consequently trigger different cellular events.

As an important bioactive molecule, Sph has its cellular levels tightly regulated[15]. However, in some situations, like in Niemann Pick Disease type C1 (NPC1), Sph abnormally accumulates in the LE and lysosomes of cells, inducing the secondary accumulation of Chol, SM and other SLs[16]. These lipid changes might have important consequences at the level of membrane structure, organization and properties, which might influence lysosomal-associated events[3,17] or even compromise lysosomal integrity[18,19].

In recent years, efforts have been made in order to understand the impact of Sph in membrane organization. It was demonstrated that Sph has the ability to change the membrane

physical organization, promoting the formation of more ordered domains[18,20-26]. The order of these domains depends not only on the membrane lipid composition but also on the surrounding pH environment[21,26,27]. It is likely that Sph-induced alterations in membrane properties are closely related to the physico-chemical changes experienced by this lipid. The protonation state[23,28] and thus the H-bonding network of Sph[29] are susceptible to pH changes occurring within the range of different physiological pH environments, suggesting that Sph might have a different behavior depending on its sub-cellular location. For instance, the fact that Sph might become more positively charged in the acidic conditions of the lysosome may strongly affect its interaction with the surrounding lipids and interfere with the formation and maintenance of Sph domains. It was recently shown that by interacting with negatively charged lipids, commonly found in biological membranes, including lysosomal membranes, Sph contributes to the formation of transient non-lamellar phases, which affect membrane permeability[18]. This might be of biological relevance, especially when considering disorders, such as NPC1, where Sph, which is a positive regulator of calcium release from the acidic stores, abnormally accumulates in acidic compartments[16,30]. Other mechanisms have been suggested in order to explain this Sph-induced permeability, including the formation of structural defects at the interfaces between biophysically distinct lipid domains[20], and the formation of pores[31]. Despite this, the molecular mechanisms underlying this phenomenon are not yet completely understood. In addition, most of the model systems used to address the physico-chemical impact of Sph in the membranes fail to mimic the biological properties of one of the most important subcellular locations of Sph – the lysosome – not only in terms of lipid composition, but especially concerning the pH gradient across the lysosomal membrane. Therefore, in the present work, we developed and characterized a synthetic membrane system - the LMVs - in which Sph encounters two different pH environments: an internal acidic pH (pH 5.0), mimicking the lysosomal lumen, and an external neutral pH (7.4), mimicking the lysosomal outer leaflet, i.e., pH $5.0_{in}/7.4_{out}$ (Fig. 1). The LMVs were then used to address the biological relevant question of how Sph accumulation in the lysosome, as observed in NPC1[16], changes lysosomal membrane properties, both in dynamic and in thermodynamic equilibrium conditions (Fig. 1). The lipid composition of the vesicles has been manipulated in order to compare the effects of

Sph on membrane permeability and biophysical properties under situations that more closely resemble the physiological conditions, i.e., low Chol content[32,33], and NPC1-like pathological conditions, i.e., high levels of Chol and SLs[3,16]. Our results showed that Sph has a more dramatic impact on membrane organization and permeability in NPC1-mimicking conditions, compared to physiological-like situations. Moreover, our data further showed significant differences in the effects caused by Sph in LMVs and standard vesicles (with no pH gradient, Fig. 1), further supporting the notion that adequate synthetic systems should be used to address lipid-lipid interactions in conditions that better mimic the biological context.

3. Methods

3.1. Materials

Sph, POPC and SM from Egg, Chicken were obtained from Avanti Polar Lipids, Inc. (Alabaster, AL, USA). Chol and TX-100 were obtained from Sigma-Aldrich (St. Louis, MO, USA). *trans*-parinaric acid (*t*-PnA) and pyranine were purchased from Molecular Probes/Invitrogen (Eugene, OR, USA). 8-Aminonaphthalene-1,3,6-Trisulfonic Acid, Disodium Salt (ANTS) and *p*-xylene-bis-pyridinium bromide (DPX) were supplied by Life Technologies (Carlsbad, CA, USA). The organic solvents were obtained from Fluka (St. Louis, MO, USA).

The concentration of the lipid and of the probes stock solutions were determined as previously described[26].

3.2. Liposome preparation

The lipids were dissolved in chloroform or absolute ethanol (in the case of Sph) and mixed in the required proportions. The following ternary mixtures have been used: 71.6:23.3:5.1; 59.7:26.3:14; 45.1:29.9:25; 34:32.7:33.3 and 25.4:34.8:39.8 (POPC/SM/Chol). These mixtures span the tie line containing the 1:1:1 equimolar mixture of the ternary POPC/SM/Chol phase diagram[34]. For simplicity, data are represented as a function of the I_o phase fraction of the mixtures: 0; 0.26; 0.58; 0.83 and 1, respectively. To evaluate the effect of Sph on membrane properties, 5 and 10 mol% Sph were also used in the preparation of some samples. Vesicles in thermodynamic equilibrium with pre-incorporated Sph and the dynamic interaction of Sph

(external addition) with POPC/SM/Chol vesicles were studied. The solvent was evaporated under a stream of nitrogen and the samples were left under vacuum overnight in order to remove traces of solvent. As suspension medium, Hepes buffer (10 mM Hepes and 150 mM NaCl, pH 7.4) and Citrate Phosphate buffer (0.1 M citric acid and 0.2M Na_2HPO_4, pH 5.0) were used. The lipid suspensions were equilibrated by freeze thaw cycles (T > 50 °C) before LUVs preparation. LUVs (0.2 or 3 mM total lipid concentration, depending on the experiment) were then prepared by standard procedures[47] e.g. using Nuclepore polycarbonate filters of 0.1 µm pore diameter, at a temperature above the transition temperature of all the individual lipids present in the mixtures (T > 50 °C).

3.3. Preparation of lysosome-mimicking vesicles

To obtain the LMVs, LUVs with a total lipid concentration of 3 mM were prepared with Citrate Phosphate buffer (pH 5.0). To change the external pH environment, LUVs were separated through a Sephadex G-25 gel filtration column (GE Healthcare, Little Chalfont, UK) using Hepes buffer (pH 7.4) as elution buffer. To prevent vesicle burst during gel filtration chromatography, the osmolarity of the buffers was measured using an osmometer (Knauer, Berlin), and when necessary sucrose was added to the elution buffer in order to have identical internal and external buffer osmolarity. Liposomes with pH 5.0 in the internal medium and pH 7.4 in the external medium were recovered mainly in fractions 3 and 4 (1 mL each), as confirmed by absorption, fluorescence and dynamic light scattering measurements (data not shown). The liposomes were then diluted to approximately 0.2 mM lipid concentration.

3.4. Determination of the partition coefficient of *t*-PnA between aqueous and lipidic phases at different pH conditions

POPC and POPC/SM/Chol (26% I_o) vesicles were prepared with different total lipid concentrations (0.001; 0.003; 0.005; 0.01; 0.025; 0.05; 0.1; 0.15; 0.2; 0.25; 0.3; 0.4; 0.5; 1; 2 and 3 mM). The samples were placed in 96 well opaque plates and fluorescence intensity measurements of *t*-PnA (0.4 µM) were performed at 24 °C, in a microplate reader (Spectramax Gemini EM), using 303 and 404 nm as the excitation and emission wavelengths, respectively.

The data analysis software GraFit (Erithacus Software) was used to perform the non linear fitting of equation 1 to the experimental data.

$$\Delta I = \frac{(Imax - I0) \times Kp \times [L]}{[W] + Kp \times [L]} \qquad \text{Eq. 1}$$

In this equation, $\Delta I = I - I_0$, stands for the difference between the steady-state fluorescence intensity of the probe measured in the presence (I) and in the absence of lipid vesicles (I_o). I_{max} is the limiting value of I measured upon increasing the lipid concentration, [L], of the solution, and [W] corresponds to the molar concentration of water at 24 °C (approximately 55.5 M)[35].

3.5. Characterization of membrane biophysical properties

To characterize the biophysical properties of the membranes, steady-state and time resolved fluorescence spectroscopy measurements of *t*-PnA were performed. Lipid vesicles were incubated with *t*-PnA (probe to lipid ratio of 1:500) at 24 ºC for at least 1h.

Fluorescence measurements were carried out in a Spex Fluorolog 3-22/Tau 3 spectrofluorometer equipped with double grating monochromators in both excitation and emission light paths from Horiba Jobin Yvon. The *t*-PnA excitation/emission wavelengths (nm) were 303/404. The fluorescence anisotropy (<r>) was calculated as previously described[48].

The fluorescence intensity decay measurements were obtained by the single photon counting technique, as previously described[48]. The excitation wavelength was 315 nm (using a NanoLED source, model N-320; Horiba Jobin-Yvon), and the emission was collected at 404 nm. To analyze the experimental decays and obtain the fitting curves, the TRFA software (Scientific Software Technologies Center, Minsk, Belarus) was used. Fluorescence decays were described by a sum of exponentials, where α_i is the normalized pre-exponential, and τ_i is the lifetime of the decay component *i*. The mean fluorescence lifetime <τ> is given by:

$$< \tau > = \frac{\sum \alpha_i \tau_i^2}{\sum \alpha_i \tau_i} \qquad \text{Eq. 2}$$

All measurements were performed in 1.0 cm × 0.4 cm quartz cuvettes, at 24 °C. Constant temperature was maintained using a Braun 852 circulating water bath.

3.6. Leakage studies

LUVs with 3 mM total lipid concentration were prepared (as above described) using Hepes or Citrate Phosphate buffer: (pH 7.4 or pH 5.0, respectively) containing 12.5 mM of ANTS and 45 mM of DPX (leakage buffers)[49]. The non-encapsulated fluorescent probe was separated from the vesicle suspension using a Sephadex G-25 gel filtration column. Buffers with the same osmolarity (adjusted with sucrose as described above) of the leakage buffer but without ANTS/DPX was used as eluent. Liposomes encapsulating ANTS/DPX were recovered mainly in fractions 3 and 4 (1 mL each), as confirmed by absorption, fluorescence and dynamic light scattering measurements (data not shown). Liposome final concentration was determined by lipid phosphorous analysis[50], for the samples prepared in Hepes buffer. The liposomes were then diluted to approximately 0.2 mM lipid concentration and fluorescence measurements were performed at 24 °C, in 1 cm x 0.4 cm quartz cuvettes under continuous stirring. To evaluate the effect of Sph on membrane permeability, 5 and 10 mol% of Sph, dissolved in a small volume of absolute ethanol (ethanol was kept below to 1% v/v to prevent vesicle destabilization) were added to lipid vesicle suspensions that were in continuous stirring. The same volume of ethanol, without Sph was used as a control. At this ethanol concentration, the permeability change was negligible. Membrane leakage was evaluated by following the increase in the fluorescence intensity of ANTS upon its release from the liposome. To this end, ANTS fluorescence intensity was recorded over time using the same set up described in 3.4, using 355/520 nm as the excitation/emission wavelengths. The fluorescence intensity corresponding to full leakage was obtained by adding 0.1 % (v/v) of Triton X-100 to the samples at the end of the experiment, i.e., approximately 30 minutes after Sph addition.

The extent of leakage was determined as: % release = $(F_t - F_0)/(F_{100} - F_0)$ x 100, where F_t is the value of fluorescence intensity at time *t*, F_0 is the initial fluorescence of the vesicle suspension, and F_{100} is the fluorescence intensity value after the addition of Triton X-100.

3.7. Studies with pyranine

Pyranine is a pH sensitive probe that was used in this work to test the stability of the pH gradient in LMVs. The maximum absorption wavelengths for the acid (protonated) and the base (unprotonated) forms of pyranine are 405 nm and 450 nm, respectively[51]. The fluorescence intensity of pyranine excited at 450 nm is high at pH 7-8 but near background at acidic pH, while the inverse is true for the fluorescence produced by 405 nm excitation[52]. Ratiometric measurements using an excitation ratio of 450/405 nm are for that reason frequently used to provide information about the pH of a determined solution. This is an advantageous method since it not depends on pyranine concentration and is directly related with pyranine ionization degree.

LMVs/LUVs with 3 mM total lipid concentration were prepared using Hepes or Citrate Phosphate buffer (pH 7.4 or pH 5.0, respectively), as above described. These vesicles contained 0.5 mM pyranine encapsulated[35]. The following (POPC/SM/Chol ternary mixtures were used: 59.7:26.3:14 ($X/_o$ = 26) and 34:32.7:33.3 ($X/_o$ = 0.83). Liposomes encapsulating pyranine were recovered (after separation through a Sephadex G-25 column) mainly in fractions 3 and 4 (1 mL each). Liposome final concentration was determined by lipid phosphorous analysis[50], for the samples prepared in Hepes buffer. The liposomes were then diluted to approximately 0.2 mM lipid concentration in 96 well opaque plates and fluorescence measurements were performed at 24 °C, in a microplate reader (Spectramax Gemini EM), using 405 and 450 nm as the excitation wavelengths and 510 nm as emission wavelength. The auto mix option of the microplate reader was selected to mix the samples 5 seconds before the first read and 3 seconds between reads. To evaluate the stability of the pH gradient in LMVs, the fluorescence measurements were performed during *ap.* 5 hours. After this time, triton X-100 (0.1% (v/v)) was added to the samples in order to obtain the fluorescence intensity induced by an immediate burst of the vesicles. Some of the wells with LMVs (without the addition of triton X-100) were left overnight and measurements were also performed next day, to observe if the pH gradient remained stable. No significant changes were observed (data not shown). Samples with acidic and neutral pH both inside and outside the vesicles were prepared to obtain the fluorescence intensity of pyranine at only acidic and neutral conditions (control samples). The

stability of the LMVs was evaluated in the absence and presence of Sph (pre-incorporation of 10 mol% Sph and external addition of 10 mol% Sph). In the external addition studies, Sph was dissolved in a small volume of absolute ethanol (ethanol was kept below to 1% v/v to prevent vesicle destabilization) and added to lipid vesicle suspensions (the auto mix option of the microplate reader was selected to mix the samples 5 seconds before the first read and 3 seconds between reads). Control experiments were also performed by adding the same volume of ethanol, without Sph.

3.8. Electrophoretic and Dynamic Light Scattering Measurements

The electrophoretic mobilities were analyzed through M3-PALS technology on a ZetaSizer Nano Z equipment (Malvern Instruments, UK). Samples were placed in clear disposable zeta cells and then in sample chamber maintained at 24 °C. Data analysis was performed using the accompanying software, and the measurements were done in triplicate in each experiment.

Vesicle sizes were determined by performing dynamic light scattering analysis on a Zetasizer Nano S equipment (Malvern Instruments, UK). Size measurements were performed using patented non-invasive back scatter (NIBS) technology. Samples were placed in 12 mm square polystyrene cuvettes and then in a chamber maintained at 24 °C. Data analysis was performed using the accompanying software and expressed as Z average size or size distribution by intensity. The PDI for each sample was also calculated using the same software. For each sample, the measurements were done in triplicate.

3.9. Statistical analysis

The statistical analysis was performed using Student´s t-test. Mean values were considered significantly different for *p* values below 0.05.

4. Results

4.1. Rationale

The present study aimed at developing synthetic systems that more closely resembled the lysosome, to more accurately address the impact of lipid changes on the biophysical properties of lysosomal membranes in physiological and pathological (NPC1-like) situations. Therefore, to mimic the lysosomal compartment, we developed a model bilayer – the LMVs (Fig. 1) - where the pH environment is acid for the inner membrane leaflet and neutral for the outer membrane leaflet, i.e., pH $5.0_{in}/7.4_{out}$. In addition, we took advantage of the well-characterized POPC/SM/Chol ternary mixtures[34] in order to evaluate the effect of Sph on the properties of membranes containing low (physiological-like) or high (NPC1-like) levels of Chol and SLs (Fig. 1 and supplementary table S1). Studies were performed to address the effects of Sph when in conditions of thermodynamic equilibrium (i.e., pre-incorporated in the membrane prior to vesicle preparation, Fig. 1a.2,b.2,c.2) and upon dynamic interaction with the membrane (i.e., externally added to pre-formed vesicles, Fig. 1a.3,b.3,c.3). In addition, to further show the importance of developing adequate synthetic systems to address lipid-lipid interactions, comparison with standard vesicles (without pH gradient across the membrane) prepared under neutral, i.e., pH $7.4_{in}/7.4_{out}$, and acidic, pH $5.0_{in}/5.0_{out}$, conditions, was performed (Fig. 1), based both on new as well as available literature data[26].

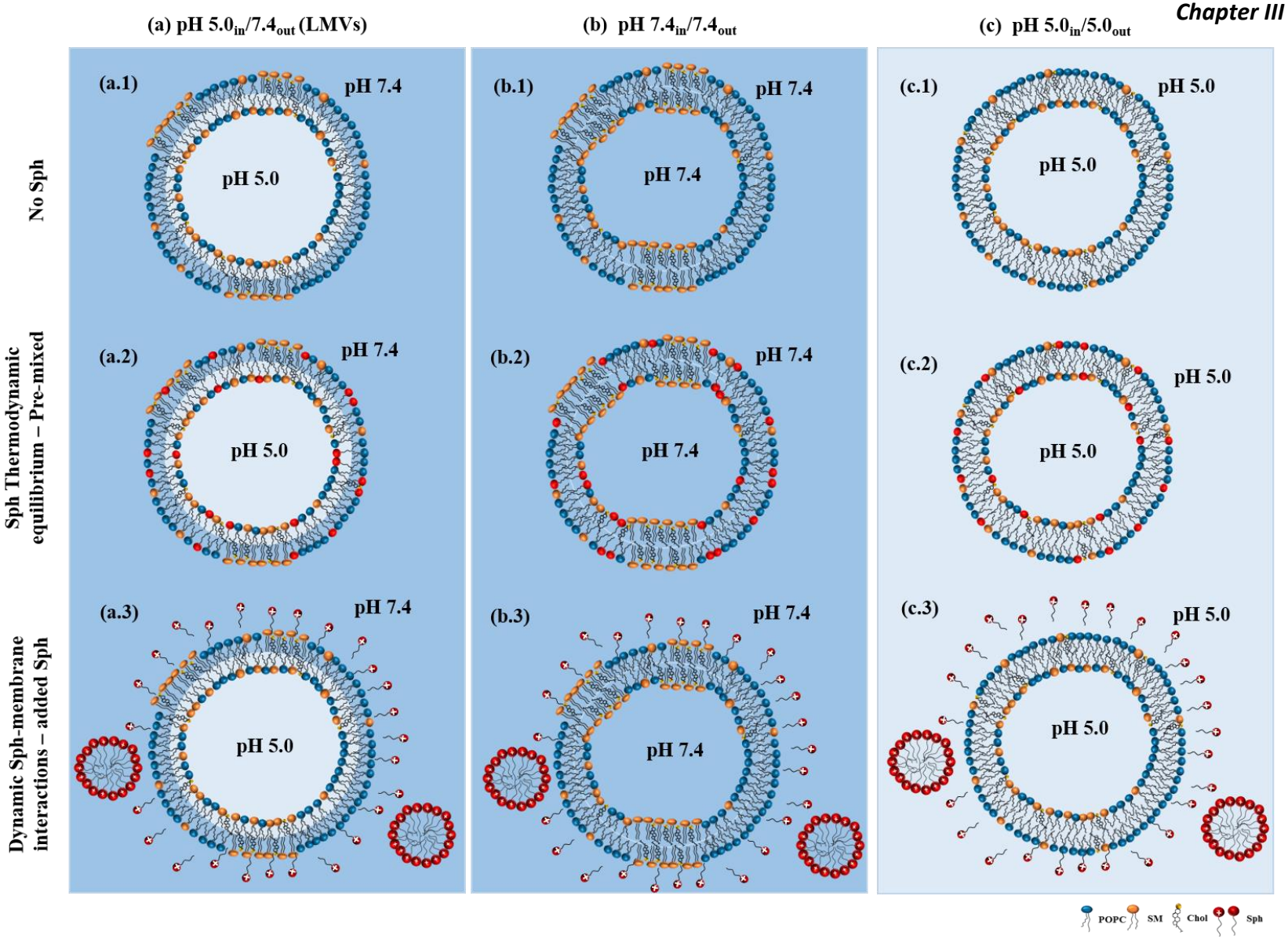

Figure 1 – See legend in the next page.

Figure 1 – Schematic representation of the synthetic systems used in this study. Artificial membrane systems composed by POPC/SM/Chol were prepared at different pH conditions. (a) A new synthetic system that more closely resembles the lysosome – the lysosome-mimicking vesicles (LMVs), displaying internal acidic pH and external neutral pH (pH5.0_{in}/7.4_{out}) was prepared through buffer exchange by gel filtration and compared with data from simpler systems prepared at (b) pH7.4_{in}/7.4_{out} and (c) pH5.0_{in}/5.0_{out}. To address the effects of Sph in the membrane, studies were performed in equilibrated sample conditions (a.2, b.2, c.2) (i.e., pre-incorporated in the membrane prior to vesicle preparation) and (a.3, b.3, c.3) upon dynamic interaction with the membrane (i.e., externally added to pre-formed POPC/SM/Chol vesicles. In addition, vesicles with different lipid compositions were prepared in order to evaluate the effect of Sph on the properties of membranes containing low (physiological-like) or high (NPC1-like) levels of Chol and SLs. The higher the levels of Chol and SM of the mixtures the higher the l_o phase fraction (Xl_o) (see methods section and supplementary table S1 for further details).

4.2. Preparation and characterization of lysosome-like models (LMVs)

The preparation of LMVs (pH 5.0_{in}/7.4_{out}) (Fig. 1a) is complex involving size exclusion chromatography to create a pH gradient across the bilayer. To test whether this experimental set up would compromise the stability of the vesicles altering its size, and to evaluate if the expected changes in surface charge were taking place upon changing the outer membrane pH from an acidic to a neutral environment[26], analysis of vesicle size and surface charge was performed before and after separating the vesicles through the chromatographic column (Fig. 2) The ζ-potential of the ternary POPC/SM/Chol mixtures before size exclusion chromatography (i.e., when displaying pH 5.0_{in}/5.0_{out}) was slightly positive, as expected since these lipid mixtures are at pH of 5.0[26]. A change in ζ-potential towards slightly negative values was observed upon creation of the pH gradient across the bilayer (Fig. 2a), reflecting the charge behavior of these mixtures at pH 7.4[26]. Changes in the surface charge of the LMVs (Fig. 2a) upon creation of the pH gradient were accompanied by only a slight increase in the size of the vesicles (Fig. 2b), showing that LMVs are stable and not prone to aggregation.

To demonstrate the pH gradient stability of the LMVs (pH 5.0_{in}/7.4_{out}) we took advantage of the fluorescence properties of the pH-sensitive dye pyranine[35]. The pH gradient

in POPC/SM/Chol LMVs was stable over several hours, as shown by the constant ratio of the fluorescence intensity of pyranine (Fig. 2c,d).

To characterize the biophysical properties of the LMVs, fluorescence spectroscopy measurements of *t*-PnA were performed. The partition coefficient (K_p) of *t*-PnA to POPC and POPC/SM/Chol vesicles at pH $5.0_{in}/5.0_{out}$ and pH $7.4_{in}/7.4_{out}$ was determined as described in Methods section and no significant differences were noticed, regarding both lipid composition and pH environment (See supplementary table S2), showing that probe interaction with the membrane is independent of these parameters. The results of the steady-state and time-resolved fluorescence spectroscopy measurements of *t*-PnA are represented in Fig. 2 (panels (e) and (f)). An increase in the fluorescence anisotropy (Fig. 2e) and mean fluorescence lifetime (Fig. 2f) of *t*-PnA was observed in LMVs containing higher l_o phase fraction (Xl_o), reflecting an increase in the order of the membrane as the levels of Chol and SM in the mixtures are increased. Moreover, *t*-PnA anisotropy (Fig. 2e) and mean fluorescence lifetime (Fig. 2f) in LMVs (pH $5.0_{in}/7.4_{out}$), are in general slightly higher compared to the same mixtures where the internal/external pH was either pH $7.4_{in}/7.4_{out}$ or pH $5.0_{in}/5.0_{out}$[26] (e.g. the fluorescence anisotropy values for ternary mixtures with no l_o phase are 0.164 at pH $5.0_{in}/5.0_{out}$; 0.179 at pH $7.4_{in}/7.4_{out}$ and 0.187 at pH $5.0_{in}/7.4_{out}$; Supplementary Fig. S1)[26], showing that the creation of the pH gradient across the membrane changes lipid-lipid interactions. Therefore, the overall membrane order and organization of the mixtures change with possible consequences for the phase boundaries of the POPC/SM/Chol ternary phase diagram[34].

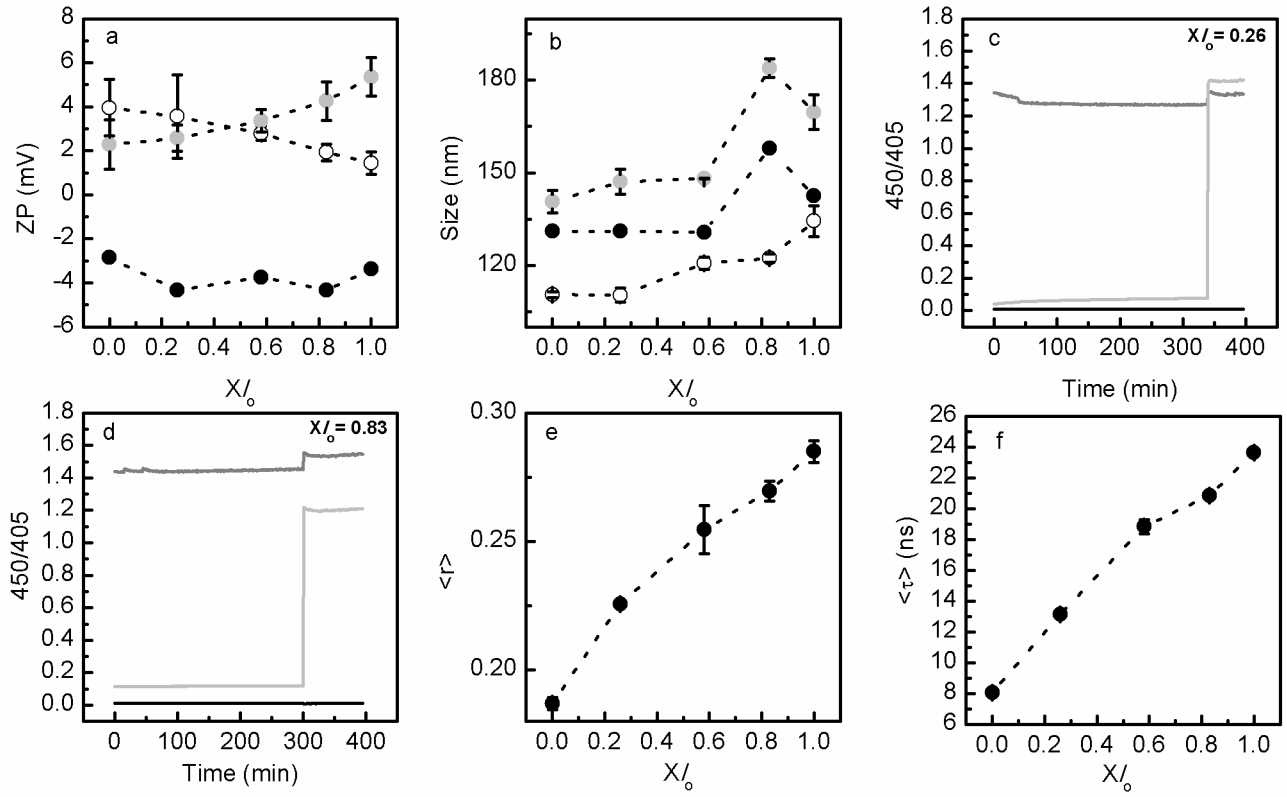

Figure 2 – **Characterization of POPC/SM/Chol LMVs (pH 5.0$_{in}$ /7.4$_{out}$).** (a) Surface charge and (b) size characterization of POPC/SM/Chol vesicles, containing increasing fractions of I_o phase (see Supplementary table S1). The open circles in (a) and (b) represent the samples before chromatography (pH 5.0$_{in}$/5.0$_{out}$), the solid symbols represent the same samples after chromatography (pH 5.0$_{in}$/7.4$_{out}$). The light grey symbols represent the external addition of 10 mol% Sph to POPC/SM/Chol LMVs. (c) and (d) pH gradient stability of LMVs (pH 5.0$_{in}$/7.4$_{out}$) composed by (c) XI_o = 0.26 and (d) XI_o = 0.83 was evaluated overtime through ratiometric measurements of pyranine excited at 450 and 405 nm (450/405). After approximately 300 minutes, triton X-100 (0.1% (v/v)) was added to samples. The light grey line represents LMVs (pH 5.0$_{in}$/7.4$_{out}$) (Fig. 1a.1), while the black and grey lines represent control vesicles prepared with pH 5.0$_{in}$/pH 5.0$_{out}$ (Fig. 1c.1) and pH 7.4$_{in}$/pH 7.4$_{out}$ (Fig. 1b.1), respectively. The vesicles contained 0.5 mM encapsulated pyranine. These experiments were repeated at least three independent times and the values are median representative curves of those experiments. Panels (e) and (f) show the variation in (e) steady-state fluorescence anisotropy and (f) mean fluorescence lifetime of *t*-PnA in ternary POPC/SM/Chol LMVs. In (a,b,e,f) the values are the mean ± SD of at least three independent experiments. The lines act merely as guides to the eye.

4.3. Effect of Sph on membrane properties under thermodynamic equilibrium

To investigate the effects of Sph in membrane properties under thermodynamic equilibrium conditions, 5 or 10 mol% of Sph was pre-incorporated in the lipid mixtures prior to vesicle preparation (see Fig. 1 and Methods for further details). Pre-incorporation of Sph into the LMVs does not significantly change the fluorescence anisotropy or mean fluorescence lifetime of *t*-PnA compared to LMVs without Sph (See supplementary Fig. S2). This is in contrast to what has been previously reported for identical mixtures characterized either at pH $7.4_{in}/7.4_{out}$ or pH $5.0_{in}/5.0_{out}$, where a significant increase in membrane order was observed upon pre-incorporation of Sph, particularly in mixtures containing low Chol and SM content[26]. This suggests that under pH conditions mimicking the lysosome, pre-incorporation of Sph at those small molar ratios has no significant effect on the overall membrane order. However, pre-incorporated Sph increases the packing of the ordered phase of the LMVs, as observed by the increase in the long lifetime component of *t*-PnA fluorescence intensity decay (Fig. 3a). The effect is more pronounced in mixtures containing higher levels of Chol/SM. For these mixtures, the fluorescence lifetime of *t*-PnA is very long and typical of gel phase[36]. These results differ from our previous observations performed in standard vesicles with no pH gradient (i.e., pH $5.0_{in}/5.0_{out}$ and pH $7.4_{in}/7.4_{out}$), where it was concluded that Sph-ability to form gel domains was higher in mixtures displaying lower I_o fraction, thus less Chol/SM[26]. This observation further shows that Sph-induced changes on membrane organization are highly dependent on pH.

Surface charge analysis showed that the ζ-potential of the Sph-containing vesicles before size exclusion chromatography, i.e., pH $5.0_{in}/5.0_{out}$, is positive (Fig. 3b) and similar to what we have previously reported[26]. Upon creation of the pH gradient (pH $5.0_{in}/7.4_{out}$) the ζ-potential decreases towards values close to neutrality, which are only slightly lower compared to those previously obtained for Sph pre-incorporated in vesicles prepared at pH 7.4[26]. The creation of the pH gradient also resulted in a shift in the population size towards larger vesicles (Fig. 3c), which was accompanied by a significant PDI increase (from < 0.1 to >1.5) (data not shown), especially for the mixtures with higher Chol/SM concentration (higher I_o fraction). This is

probably due to increased propensity for vesicle fusion and/or aggregation, as suggested by the scattering intensities (I/I_0) recorded in the 1-10 µm range (Fig. 3d). The presence of pre-incorporated Sph in LMVs (Fig. 1a.2) might cause transient membrane instability due to changes in the surface charge and/or redistribution of Sph molecules upon creation of the pH gradient. Nonetheless, pre-incorporation of Sph into LMVs does not affect the pH gradient stability, as shown by the constant ratio of the fluorescence intensity of pyranine (Fig. 3 e,f).

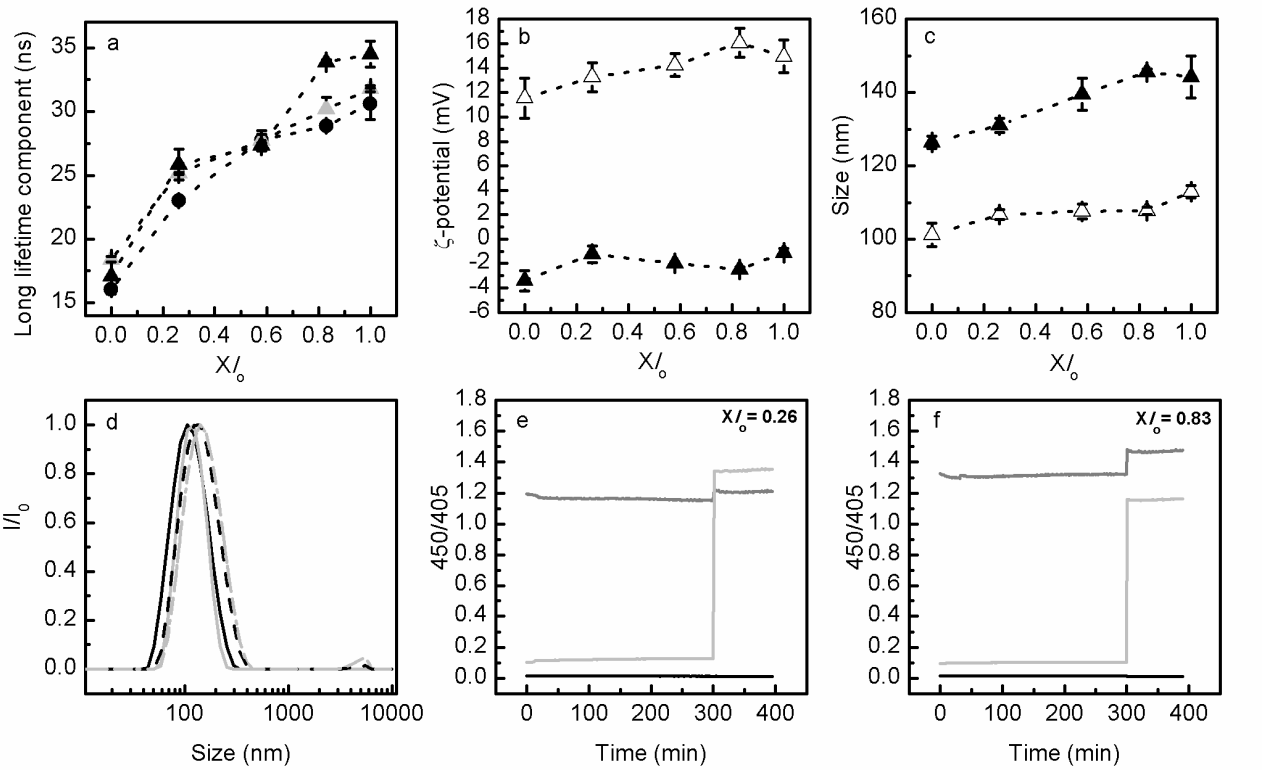

Figure 3 – Characterization of POPC/SM/Chol/Sph LMVs (pH 5.0_{in} /7.4_{out}). Panel (a) show the variation in long lifetime component of *t*-PnA in ternary POPC/SM/Chol LMVs (black circles) and POPC/SM/Chol LMVs containing 5 (grey triangles) and 10 (black triangles) mol% of Sph (pre-incorporated in the vesicles) (Fig. 1a.2). (b) Surface charge and (c) size characterization of POPC/SM/Chol/Sph (10 mol%, pre-incorporation) vesicles. The open symbols represent the samples before chromatography (pH $5.0_{in}/5.0_{out}$) and the solid symbols represent the same samples after chromatography (pH $5.0_{in}/7.4_{out}$). Panel (d) represent the normalized scattered light intensity of POPC/SM/Chol/Sph (10 mol%, pre-incorporation) (Fig. 1a.2) vesicles containing $X/_o$ = 0.26 (black lines) and $X/_o$ = 0.83 (light grey lines) as a function of particle size (nm). The measurements were also made before (solid lines) and after (dash

lines) size exclusion chromatography. In panels (a) to (c) data are represented as a function of the l_o phase fraction (Xl_o): the higher the Xl_o the higher the levels of Chol and SM of the mixtures (see methods and supplementary table S1 for further details). The values are the mean ± SD of at least three independent experiments. The lines act merely as guides to the eye. In panels (e) and (f) the pH gradient stability of POPC/SM/Chol/Sph (10 mol% pre-incorporated) LMVs (pH $5.0_{in}/7.4_{out}$) (Fig. 1a.2) composed by (e) Xl_o = 0.26 and (f) Xl_o = 0.83 was evaluated overtime through ratiometric measurements of pyranine excited at 450 and 405 nm (450/405). After approximately 300 minutes, triton X-100 (0.1% (v/v)) was added to samples. The light grey line represents LMVs (pH $5.0_{in}/7.4_{out}$) (Fig. 1a.2), while the black and grey lines represent control vesicles prepared with pH $5.0_{in}/5.0_{out}$ (Fig. 1c.2) and pH $7.4_{in}/7.4_{out}$ (Fig. 1b.2), respectively. The vesicles contained 0.5 mM encapsulated pyranine. These experiments were repeated at least three independent times and the values are median representative curves of those experiments.

4.4. Dynamic interaction of Sph with LMVs and POPC/SM/Chol vesicles with no pH gradient

To evaluate the dynamic interaction of Sph with the membrane and consequent alterations in membrane properties, Sph was externally added to the already formed lipid vesicles (see Fig. 1 and Methods for further details). To address the importance of adequate model systems in the study of lipid-lipid interactions, studies were performed both in LMVs (i.e., pH $5.0_{in}/7.4_{out}$) (Fig. 1a.3) and in standard liposomes display identical internal/external pH (i.e., pH $7.4_{in}/7.4_{out}$ (Fig. 1b.3) and pH $5.0_{in}/5.0_{out}$ (Fig. 1c.3).

Surface charge

Incorporation of Sph in the lipid bilayer upon its addition to the vesicles is expected to cause a change in their surface charge properties, due to the positive nature of Sph. Therefore, from these experiments it is also possible to evaluate the ability of Sph to incorporate the different type of mixtures.

Addition of Sph to LMVs caused a change in vesicle surface charge towards positive values (Fig. 2a). The ζ-potential values obtained under these conditions are in general comparable to those previously obtained at pH $7.4_{in}/7.4_{out}$ for identical mixtures where the

same amount of Sph has been initially incorporated in the lipid bilayer prior to liposome preparation[26]. This charge variation reflects the increase in positively charged lipids in the bilayer as a result of Sph incorporation.

The effect of adding Sph to standard liposomes prepared under neutral (pH $7.4_{in}/7.4_{out}$, Fig 4a) and acidic (pH $5.0_{in}/5.0_{out}$, Fig. 4d) conditions, was also evaluated. A Sph-concentration dependent increase in the surface charge of both types of vesicles was observed upon adding Sph, reflecting the incorporation of Sph in the membrane. It should, however, be stressed that, while ζ-potential values obtained at pH $5.0_{in}/5.0_{out}$ (Fig. 4d) are similar to those previously reported for POPC/SM/Chol mixtures containing pre-incorporated Sph[26], the net surface charge of the vesicles at pH $7.4_{in}/7.4_{out}$ is much higher (Fig. 4a) and comparable to the one measured at pH $5.0_{in}/5.0_{out}$ (Fig. 4d). This difference could be due to a preferential accumulation of Sph in the outer membrane leaflet and/or slow transbilayer movement to the inner membrane leaflet, due to the different protocols used. This would be a valid explanation if the increase of ζ-potential in the presence of Sph was ca. half for pre-incorporation of what was measured for the external addition. However, the ζ-potential increase observed upon external addition is ≈ 3-fold larger for external addition than for pre-incorporation. This can only be explained if Sph is mostly charged when externally added, and not when pre-incorporated. This can be rationalized considering that when the pre-incorporation protocol is used, Sph in the dry lipid - i.e. not ionized - is hydrated together with the other lipids and therefore it is never found in a bulk aqueous environment. In the less polar lipid environment the pKa can shift several units, because the charged form is not being stabilized by the strong ionic character of water[37].

Vesicle size

The external addition of 10 mol% Sph to LMVs led to an increase in vesicle size, especially in mixtures containing higher l_o content (Fig. 2b). The relatively high PDI (ap. 0.2, data not shown) and the scattering intensities (I/I_0) showing a population of particles in the 1-10 µm range (See supplementary Fig. S3) indicate that these vesicles are prone to fusion and/or aggregation similarly to the observed for LMVs with pre-incorporated Sph (Fig. 3c,d). A

similar behavior was observed after the external addition of Sph to POPC/SM/Chol vesicles prepared at pH $7.4_{in}/7.4_{out}$ (Fig. 4b,c) but not for the vesicles prepared at pH $5.0_{in}/5.0_{out}$ (Fig. 4e,f). At pH 5.0 the surface charge of the membranes is slightly positive, becoming more positive upon adding Sph. Therefore, adding Sph will increase repulsion between the liposomes. In case of external pH 7.4, whether the internal pH is 5.0 as in LMVs or 7.4, the initial incorporation of Sph will create areas of the membrane surface that are positively charged, whereas other areas of the membrane still retain the negative surface charge they had prior to Sph addition. This will favor electrostatic attraction between vesicles, and probably facilitate aggregation/fusion events[38]. These events will be limited, occurring only until the distribution of Sph is equilibrated and all the vesicles acquire a similar charge along their surface, and justify the appearance of a population of very large particles in both situations where external pH is 7.4.

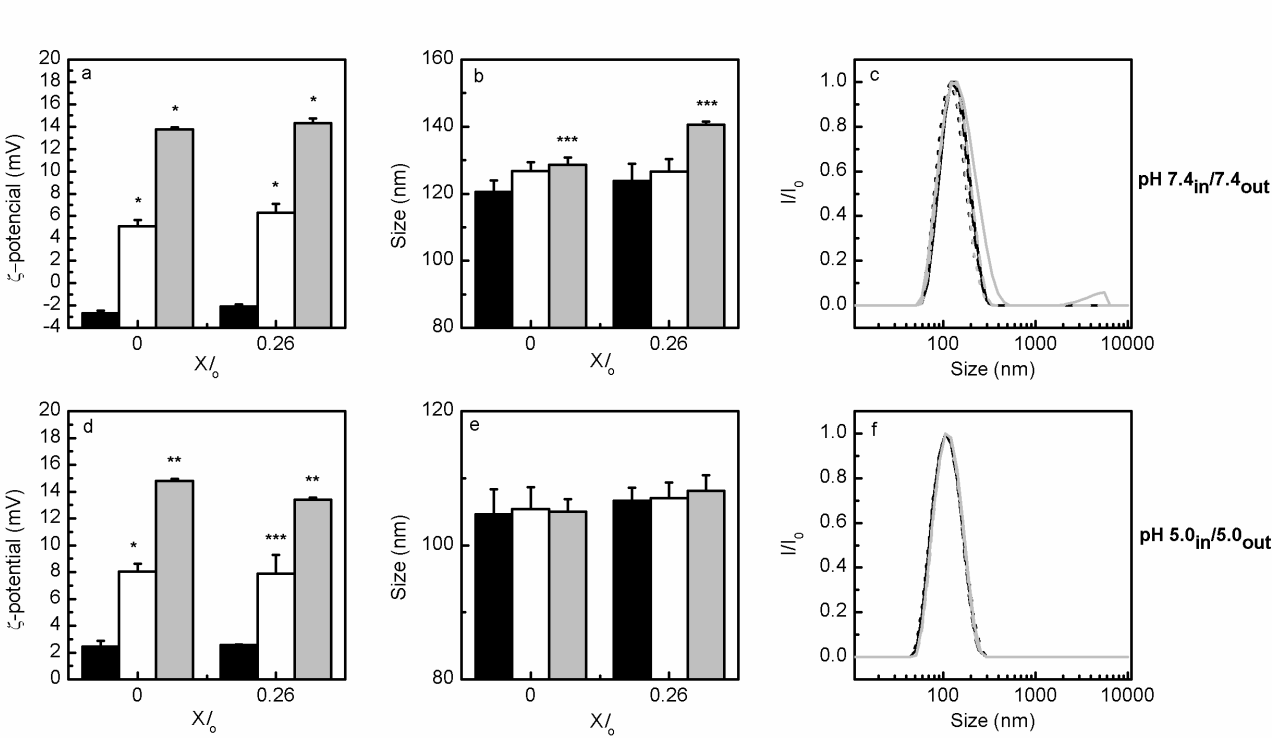

Figure 4 – Electrophoretic and dynamic light scattering characterization of POPC/SM/Chol vesicles with no pH gradient. (a,d) Surface charge and (b,c,e,f) size characterization of POPC/SM/Chol vesicles displaying (upper panels) pH $7.4_{in}/7.4_{out}$ (Fig. 1b.1,b.3) and (lower panels) pH $5.0_{in}/5.0_{out}$ (Fig. 1c.1,c.3). (a,b,d,e) The characterization was made before (black) and after the addition of 5 (white) and 10 (light

grey) mol% Sph to vesicles containing Xl_o = 0 and Xl_o = 0.26. Panels (c,f) represent the normalized scattered light intensity as a function of particle size (nm). The measurements were made before (dot lines) and after the external addition of 5 (dash lines) and 10 (solid lines) mol% Sph to vesicles containing 0 (black lines) and 0.26 (light grey lines) Xl_o phase. The values are the mean (± SD) of at least three independent experiments. *, $p < 0.001$ *versus* 0% Sph; **, $p < 0.01$ *versus* 0% Sph; ***$p < 0.05$ *versus* 0% Sph.

pH gradient and membrane permeability

The external addition of 10 mol% Sph to pre-formed LMVs (Fig. 5a,b) changed membrane stability and the pH gradient, showing that Sph addition to the vesicles causes membrane permeabilization. This effect was more pronounced for vesicles containing higher l_o phase fraction (Xl_o = 0.83, Fig. 5b), suggesting that Sph-induced changes in membrane permeability might depend on the initial membrane lipid composition and biophysical properties.

To further address this issue the well-established ANTS/DPX assay was used[18,20]. Ternary POPC/SM/Chol vesicles were loaded with the fluorescence emitter/quencher pair ANTS/DPX. The release of ANTS/DPX into the aqueous medium results in an increase in the fluorescence intensity of ANTS due to dissociation of the emitter/quencher complex. Therefore, changes in fluorescence intensity are a measure of membrane permeability. The addition of Sph to LMVs, i.e., pH $5.0_{in}/7.4_{out}$, leads to an initial and rapid increase in membrane permeability (up to 2-3 minutes), after which no further changes are observed (Fig. 5c,d). The extent of membrane permeabilization depends both on Sph concentration (Fig. 5c-f) and membrane lipid composition (Fig. 5e,f). Interestingly, and in agreement with the pH gradient stability assays (Fig. 5a,b), the effect of Sph is slightly more pronounced for membranes containing higher content of Chol and SM (Fig. 5f), i.e., in NPC1-like lysosomes, suggesting that accumulation of Sph and Chol in NPC1 lysosomes might lead to higher changes in lysosomal membrane permeability. Control experiments showed that membrane permeability did not change significantly upon addition of ethanol, confirming that increased membrane permeabilization was due to Sph (Fig. 5a-f).

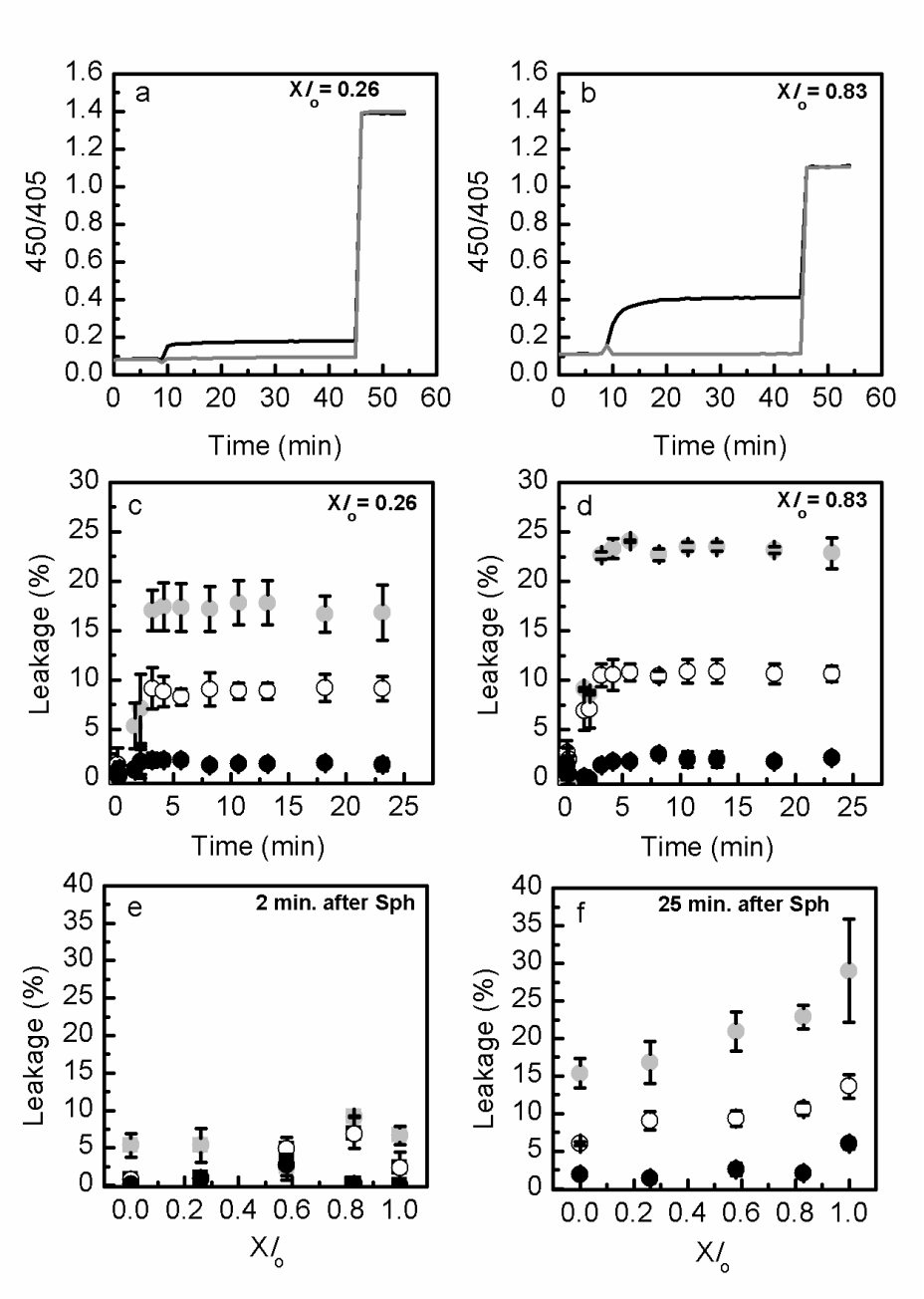

Figure 5 – Characterization of POPC/SM/Chol LMVs (pH $5.0_{in}/7.4_{out}$) upon dynamic interaction with Sph. (a,b) The pH gradient stability of LMVs (pH $5.0_{in}/7.4_{out}$) composed by (a) $X/_o = 0.26$ and (b) $X/_o = 0.83$ was evaluated overtime through ratiometric measurements of pyranine excited at 450 and 405 nm (450/405), after the external addition of 10 mol% Sph (Fig. 1a.3). After approximately 45 minutes, triton X-100 (0.1% (v/v)) was added to samples. The light grey lines correspond to LMVs after the addition of ethanol (control samples) and the black lines correspond to LMVs after the external addition of 10 mol% Sph (ap. 10 minutes after LMVs preparation). The vesicles contain 0.5 mM pyranine encapsulated. These experiments were repeated independently, at least three times and

these are median representative curves of those experiments. (c,d) Sph-induced membrane permeability was evaluated overtime upon adding 5 (white circles) and 10 (light grey circles) mol% of Sph, or ethanol (black circles) to LMVs containing (c) X_{l_o} = 0.26 and (d) X_{l_o} = 0.83. (e) and (f) show the extent of Sph-induced leakage (e) 2 and (f) 25 minutes after adding 5 and 10 mol% of Sph, or ethanol (control). The symbols are the same used in panels c and d. The values are the mean ± SD of at least three independent experiments. The lines act merely as guides to the eye.

To address whether the effect of Sph was influenced by the pH environment of the vesicles, studies were also performed in vesicles displaying pH $7.4_{in}/7.4_{out}$ (Fig. 1b.3) and pH $5.0_{in}/5.0_{out}$ (Fig. 1c.3). Fig. 6 shows that Sph-induced permeability depends on Sph concentration, membrane lipid composition of the vesicles and pH environment. At pH 7.4 the extent of Sph-induced membrane permeabilization is very low, particularly when 5 mol% Sph are added to the vesicles (Fig. 6a,b). The addition of 10 mol% Sph to the mixtures resulted in a higher leakage, being this effect more pronounced when the l_o phase is predominant (Fig. 6b), i.e., higher levels of Chol and SM. The extent of leakage induced by Sph under this experimental conditions is comparable to that obtained by Contreras et al[20], in SM/Chol (80/20) mixtures (pH 7.4) after the addition of the same molar proportions of Sph. Similar results were obtained at acidic pH (Fig. 6c,d), but the extent of leakage is higher at pH 5.0 compared to pH 7.4.

As observed for LMVs (Fig. 5c,d) the effect of Sph addition to vesicles with no gradient is immediate, but at pH 7.4 and pH 5.0 a slight increase in leakage is observed overtime (Fig. 6a,c). However, a similar trend is observed when ethanol is added to the vesicles, suggesting that this small variation is only reflecting the overall permeability properties of the vesicles.

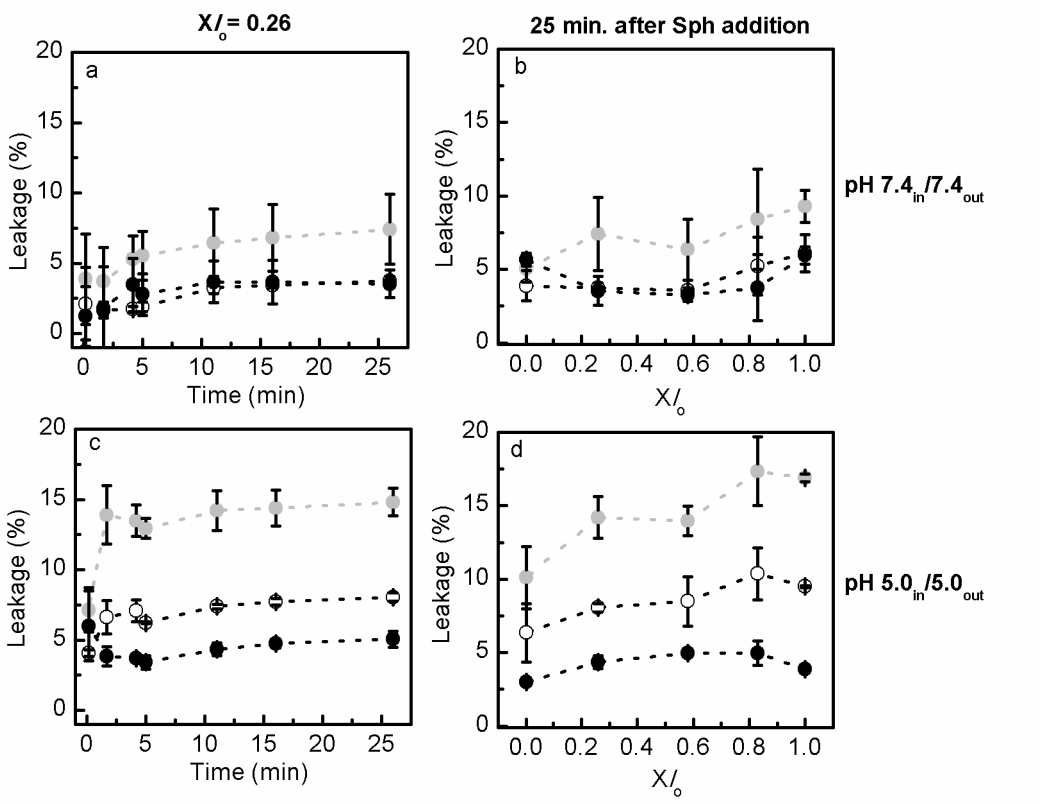

Figure 6 – Sph-induced membrane permeability on POPC/SM/Chol vesicles with no pH gradient. (a,c) Sph-induced membrane permeability was evaluated upon adding 5 (white circles) and 10 (light grey circles) mol% of Sph, or ethanol (control, black circles) to POPC/SM/Chol vesicles displaying (upper panels) pH $7.4_{in}/7.4_{out}$ (Fig. 1b.3) and (lower panels) pH $5.0_{in}/5.0_{out}$ (Fig. 1c.3) containing $X/_o$ = 0.26. (b,d) Show the extent of Sph-induced leakage 25 minutes after adding 5 (white circles) and 10 (light grey circles) mol% of Sph, or ethanol (control, black circles). The values are the mean ± SD of at least three independent experiments. The lines act merely as guides to the eye.

Further comparison of the effects of Sph on membrane permeability under different pH conditions showed that the extent of leakage was in general lower for vesicles with pH $7.4_{in}/7.4_{out}$, and higher for vesicles mimicking the lysosomal compartment (pH $5.0_{in}/7.4_{out}$) (Fig. 7 and Supplementary Fig. S4). The extent of leakage induced by Sph at pH $5.0_{in}/5.0_{out}$ is intermediate between the two other pH conditions, although closer to the situation mimicking the lysosomal compartment. This suggests that Sph-induced membrane permeabilization is facilitated at acidic conditions. This is further supported by data showing that indeed the initial extent of leakage is higher at pH $5.0_{in}/5.0_{out}$ compared to pH $7.4_{in}/7.4_{out}$ or pH $5.0_{in}/7.4_{out}$, in

which Sph first interacts with the membrane exposed to a neutral pH (Fig. 7c and Supplementary Fig. S4c). Indeed, data obtained at pH $7.4_{in}/7.4_{out}$ and pH $5.0_{in}/7.4_{out}$ are very similar (2 minutes after Sph addition; Fig. 7c), which reflects the similar neutral pH conditions sensed by Sph upon its addition to the vesicles prepared at $7.4_{in}/7.4_{out}$ and pH $5.0_{in}/7.4_{out}$. After this initial slower destabilization, a larger increase in the extent of leakage is observed for the LMVs (Fig. 7d and Supplementary Fig. S4d), which is probably due to increased destabilization of the membranes that are exposed to the pH gradient. Therefore, there is a conjugation of different factors that all together contribute to the observed increase in membrane permeabilization upon adding Sph to the LMVs.

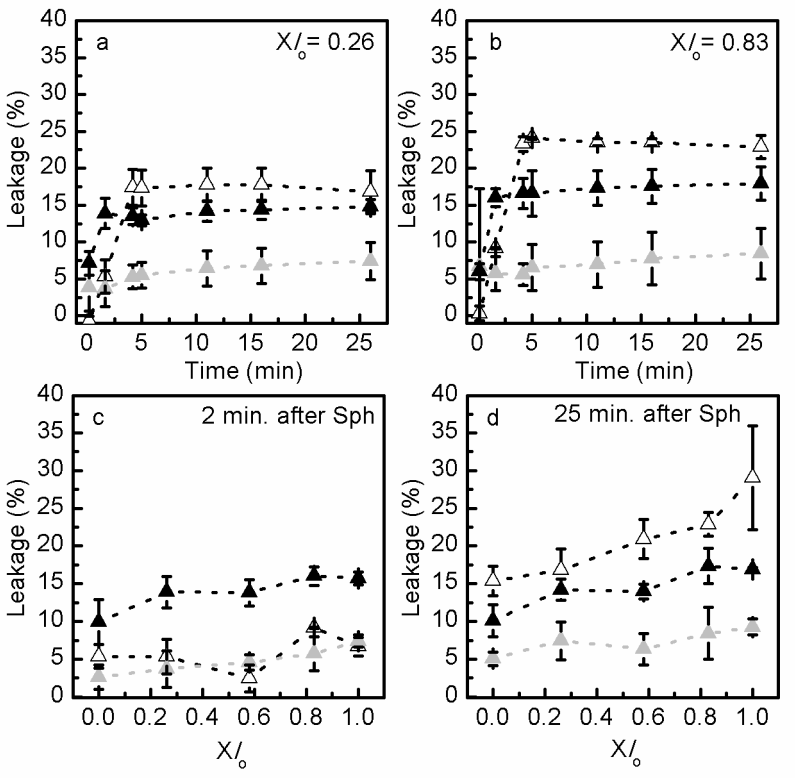

Figure 7 – Comparison of Sph-induced membrane permeability in LMVs and POPC/Chol/SM vesicles with no pH gradient. (a,b) Sph-induced membrane permeability was evaluated overtime, at pH $5.0_{in}/7.4_{out}$ (white triangles) (Fig. 1a.3), pH $7.4_{in}/7.4_{out}$ (Fig. 1b.3) (light grey triangles) and pH $5.0_{in}/5.0_{out}$ (Fig. 1c.3) (black triangles) after the addition of 10 mol% Sph to POPC/SM/Chol vesicles containing (a) $X/_o = 0.26$ and (b) $X/_o = 0.83$. (c,d) The extent of Sph-induced leakage was determined in POPC/SM/Chol vesicles containing increasing fractions of I_o phase (c) 2 and (d) 25 minutes after Sph addition. The

values are the mean ± SD of at least three independent experiments. The lines act merely as guides to the eye.

Sph-induced changes on membrane fluidity and lateral organization

It has been previously suggested that Sph-induced membrane permeability could be due to Sph-pore formation[31] or due to increased membrane packing defects as a consequence of lipid phase separation[18,20]. Therefore, to further characterize the biophysical impact of adding Sph to LMVs, the fluorescence anisotropy and lifetime of *t*-PnA was measured and compared with the effect of adding Sph to vesicles with no pH gradient (Fig. 8 and Supplementary Fig. S5). The studies were performed for mixtures where a high impact of Sph on membrane properties was observed previously[26], i.e., mixtures containing lower l_o phase fraction. For the LMVs, the *t*-PnA fluorescence anisotropy was measured 30 minutes (Supplementary Fig. S6), 24h (data not shown) and immediately (approximately 1 minute) after (Fig. 8a and Supplementary Fig. S6) Sph addition. No significant differences were observed between the different time points, suggesting that the effect of Sph on membrane properties is immediate, likely due to a fast interaction/partition to the membrane.

Addition of Sph to the vesicles caused a Sph-concentration dependent increase in *t*-PnA fluorescence anisotropy (Fig. 8a-c), irrespective of the pH environment. However, the effect was more pronounced for higher Sph concentrations, at pH $5.0_{in}/7.4_{out}$ (Fig. 8a) and pH $7.4_{in}/7.4_{out}$ (Fig. 8b), reflecting the higher tendency of Sph to increase membrane order at neutral pH[26]. A similar trend of variation was observed upon measuring *t*-PnA mean fluorescence lifetime (Supplementary Fig. 5a,b), further supporting these conclusions.

To gain further information on the differences in membrane ordering of the mixtures, analysis of the long lifetime component of *t*-PnA was performed (Fig. 8d-f). Addition of Sph caused a significant increase in *t*-PnA long lifetime component, particularly at pH $5.0_{in}/7.4_{out}$ (Fig. 8d) and pH $7.4_{in}/7.4_{out}$ (Fig. 8e), in agreement with the observation that Sph-induced membrane ordering is facilitated at neutral pH.

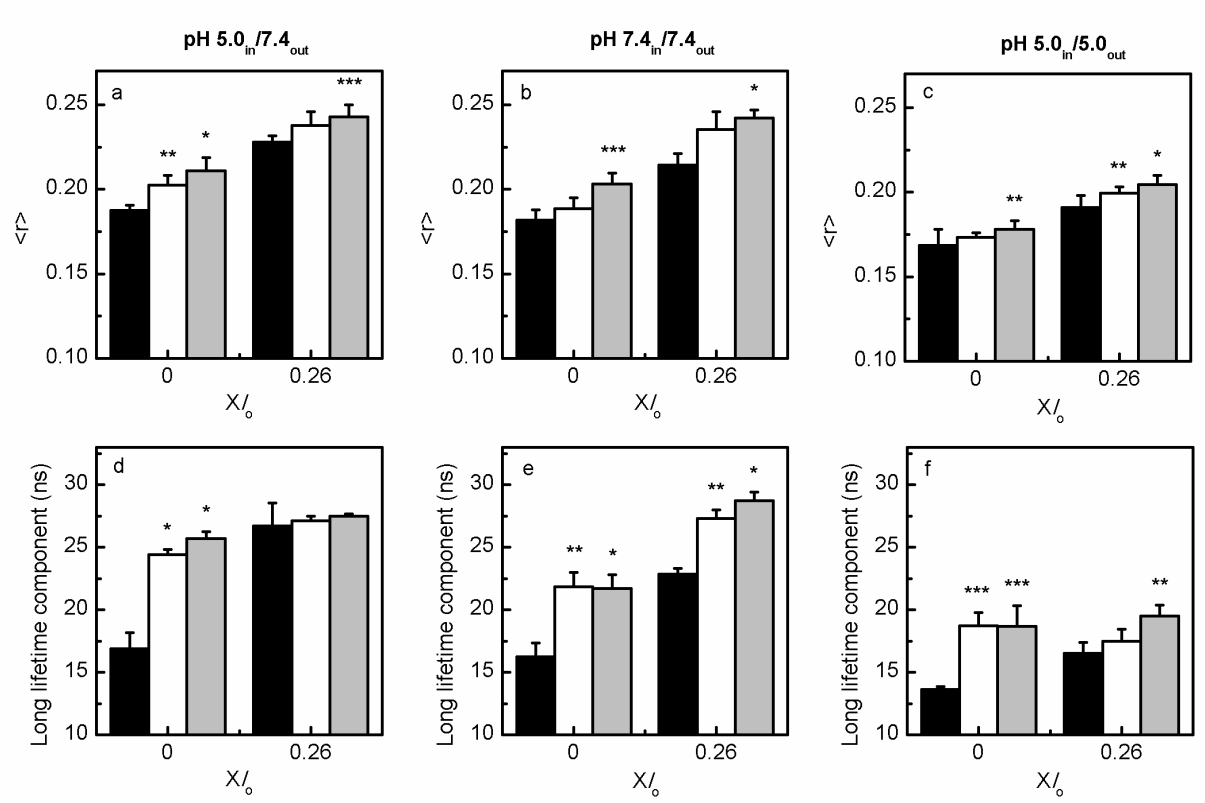

Figure 8 – Sph-induced alterations in the biophysical properties of LMVs and POPC/SM/Chol vesicles with no pH gradient. (a-c) Steady-state fluorescence anisotropy and (d-f) long lifetime component of *t*-PnA in ternary POPC/SM/Chol vesicles containing $X/_o$ = 0 and $X/_o$ = 0.26 before (black) and immediately after addition of 5 (white) and 10 (light grey) mol % of Sph. (left panels, a,d) pH $5.0_{in}/7.4_{out}$ (Fig. 1a.3), (middle panels, b,e) pH $7.4_{in}/7.4_{out}$ (Fig. 1b.3) and (right panels, c,f) pH $5.0_{in}/5.0_{out}$ (Fig. 1c.3). The values are the mean ± SD of at least three independent experiments. *, $p < 0.001$ *versus* 0% Sph; **, $p < 0.01$ *versus* 0% Sph; ***$p < 0.05$ *versus* 0% Sph.

5. Discussion

5.1. LMVs: novel lysosome-mimicking systems

To unravel the molecular mechanisms underlying complex cellular events it is often necessary to take advantage of more simple systems that can mimic certain cell features. Artificial membranes are a key example of synthetic systems widely used to address lipid-lipid and lipid-protein interactions, among others[39-41]. The composition of these membranes can be tuned so that specific interactions can be individually studied. The major goal of the present study was to develop a synthetic system with features that more closely resemble one of the

major organelles responsible for lipid synthesis and recycling – the lysosome. Such synthetic system constitutes an ideal tool to study how changes in lipid composition derived from both normal and impaired lysosomal lipid metabolism influence membrane structure and biophysical properties. Considering that Sph is a lipid mainly formed by degradation of ceramide in the lysosome, and implicated in human disease upon its accumulation in the lysosome[16], we took advantage of the LMVs (pH $5.0_{in}/7.4_{out}$) (Fig. 1a) to investigate Sph-mediated changes in membrane properties. To this end, the lipid composition of the vesicles was tuned in order to establish a comparison between the effects of Sph in systems mimicking physiological- and NPC1-like conditions.

The LMVs developed in the present study displayed a stable pH gradient across the bilayer, with internal acidic pH (pH 5.0) and external neutral pH (pH 7.4). The surface charge characteristics of the system reflect the neutral pH environment of the outer membrane. The LMVs were stable and not prone to aggregation as verified by vesicle size analysis. The order of the membranes showed differences relative to vesicles with identical lipid composition at only neutral (pH $7.4_{in}/7.4_{out}$) (Fig. 1b) or acidic (pH $5.0_{in}/5.0_{out}$) (Fig. 1c) pH, both in the absence or presence of Sph. This might be due to changes in the lipid-lipid and lipid-solvent interactions[42,43]. These observations further support that lipid organization, and consequently membrane fluidity, are highly influenced by the surrounding pH environment, and therefore suitable systems to address lipid interactions in a specific subcellular location should be developed to account for organelle-specific features. This is particularly relevant for Sph, where it is already known that this lipid presents different H-bonding states depending on the surrounding environment, shifting from intramolecular to intermolecular between pH 6.7 and 9.9[29]. In addition, it is likely that lipid organization both in the plane of the membrane and across membrane leaflets reflect membrane pH gradient, contributing to the differences in the overall packing of the lipids in the LMVs.

5.2. Application of LMVs to unravel the biophysical impact of abnormal Sph lysosomal accumulation

Our data clearly indicates that the synthetic systems developed herein, with features closer to lysosomes, display distinct properties compared to standard vesicles with no pH gradient. Therefore, those models should be employed to elucidate specific molecular interactions that enable gaining further insight into the biophysical effects derived from Sph lysosomal accumulation under pathological conditions. Hence, we addressed both the dynamic behavior of Sph and its effects under thermodynamic equilibrium conditions, by comparing changes in the ζ-potential, and on the fluorescence properties of the probes. While the ζ-potential relates to the surface charge of the vesicles, and therefore is sensitive to the changes occurring in the outer leaflet of the vesicles, the fluorescent probes are incorporated and distributed within both bilayer leaflets, thus providing biophysical information over the entire bilayer.

The data obtained in the present work pinpoint that the interaction of Sph with the membrane, as well as its effects on membrane order and permeability, strongly depend on the pH environment, inasmuch, as an initial faster permeabilization was observed at acidic pH (pH $5.0_{in}/5.0_{out}$), but the extent of vesicle permeabilization was higher in LMVs (pH $5.0_{in}/7.4_{out}$). Moreover, the results suggest that an increased membrane order, as observed in vesicles presenting an external neutral pH (i.e., LMVs and pH $7.4_{in}/7.4_{out}$ vesicles), can be crucial for an initial protection against membrane destabilization/permeabilization promoted by addition of Sph. Interestingly, data indicate that after the initial minutes upon Sph addition, it seems to exist no direct correlation between Sph-induced changes on membrane order and Sph-induced permeability. Indeed, addition of Sph to the vesicles caused an increase in the overall membrane order, being this effect more pronounced in LMVs and pH $7.4_{in}/7.4_{out}$ vesicles. However, Sph-induced membrane permeabilization was almost negligible in pH $7.4_{in}/7.4_{out}$ vesicles, in contrast to the LMVs that showed the highest extent of membrane permeabilization. Moreover, smaller changes in membrane order were detected in pH $5.0_{in}/5.0_{out}$ vesicles, even though the extent of membrane permeabilization was still significant. Therefore, this suggests that the increase in membrane permeability might not be

solely due to structural defects that could be formed at the interface between different phases upon addition of Sph to the vesicles as suggested by other groups[18,20]. In addition, the hypothesis of permanent pore formation seems to be excluded, since after the initial vesicle destabilization promoted by Sph addition, the pH gradient of the vesicles remained practically unchanged. The extent of Sph-induced membrane permeability might be related not only with membrane order and pH environment, but also to the amount of Sph molecules able to incorporate into the membrane as well as with their distribution between the two membrane leaflets. Indeed, the amphiphilic nature of Sph determines its partition into the membrane.

It is expected that several factors determine the equilibrium between Sph molecules in the aqueous medium and in the membrane. Sph might exist in water both as monomeric species and in the form of micelles, even though the CMC values of Sph were not yet ascertained (e.g., CMC values ranging from ca. 1 μM to 112 μM have been reported[20,22,29,44]. In addition, Sph partition into the membrane is likely to be affected by the phase properties of the membrane, the electrostatic forces, as well as the properties of the surrounding environment (pH, ion composition, etc). Due to the complexity of this equilibrium it is difficult to correctly determine the extent of Sph membrane partition. In this way, we rationalized our data providing only a qualitative description of the effects of adding Sph to the different vesicles. Thus, we only attempted to compare the effects of externally added Sph to the effect of the same amount of Sph pre-incorporated in vesicles with the same lipid composition. These two scenarios enable comparing the dynamic effects of Sph incorporation on a model of lysosomes, to a situation mimicking a lysosomal membrane enriched in Sph. The former would therefore represent the situation occurring in cells upon interaction of aqueous (free or aggregated) Sph with the lysosomal membrane, which clearly showed that this lipid has the ability to change membrane organization, permeability and surface charge. The latter case would provide the biophysical properties of the membrane with the maximum retention of Sph and with symmetrical distribution of the sphingoid base across the two bilayer leaflets.

Our data shows that irrespective of the pH environment, Sph-induced permeability tends to increase with the extent of l_o phase present in the vesicles, which seems to be in accordance with the observation made by Contreras et al[20], that the presence of l_o regions in

the membrane makes it a target for Sph-induced permeabilization. This suggests that Sph interaction with the membrane is facilitated upon increasing the l_o phase fraction of the vesicles. This could be due to electrostatic forces created between the positively charged Sph and the more electronegative membranes enriched in Chol. Indeed, it has been shown that membranes with higher Chol content are more electronegative due to a lower ability of cations to interact with Chol hydroxyl (-OH) groups[42]. However, the ζ-potential remained constant in LMVs and vesicles with no pH gradient regardless of the Chol content, which may reflect the occurrence of different conformational changes or lipid-lipid interactions[26,45,46]. Nonetheless, the external addition of Sph to these vesicles resulted in a larger ζ-potential increase for vesicles with higher Chol content, which suggests a higher incorporation of Sph in the membrane when Chol content is higher. These observations suggest that Sph partition to the membrane is not solely driven by electrostatic forces but it also depends on the lipid composition and membrane biophysical properties.

Indeed, POPC/SM/Chol vesicles have a more disordered membrane at acidic pH, which can favor a faster incorporation of Sph within the membrane, leading to the observed higher initial rate of membrane permeabilization. In contrast, the higher membrane order of the vesicles exposed to an outer neutral pH (LMVs and pH $7.4_{in}/7.4_{out}$ vesicles) might decrease the rate of Sph membrane incorporation, resulting in a lower initial membrane destabilization compared to acidic conditions. In vesicles with no pH gradient across the bilayer, the externally added positively charged Sph tends itself to create a gradient across the membrane, followed by *flip-flop* movement, until equilibrium is reached. Conversely, in the LMVs, the pH gradient present across the bilayer might decrease the driving force for Sph incorporation. Sph is positively charged and it will not readily move against the charge gradient, that is more positive (<pH) in the interior of the vesicles compared to the external environment (>pH). Thus, the asymmetry between the inner and the outer leaflets created upon the incorporation of Sph in the external monolayer contributes to transient membrane stress and instability (Fig. 9).

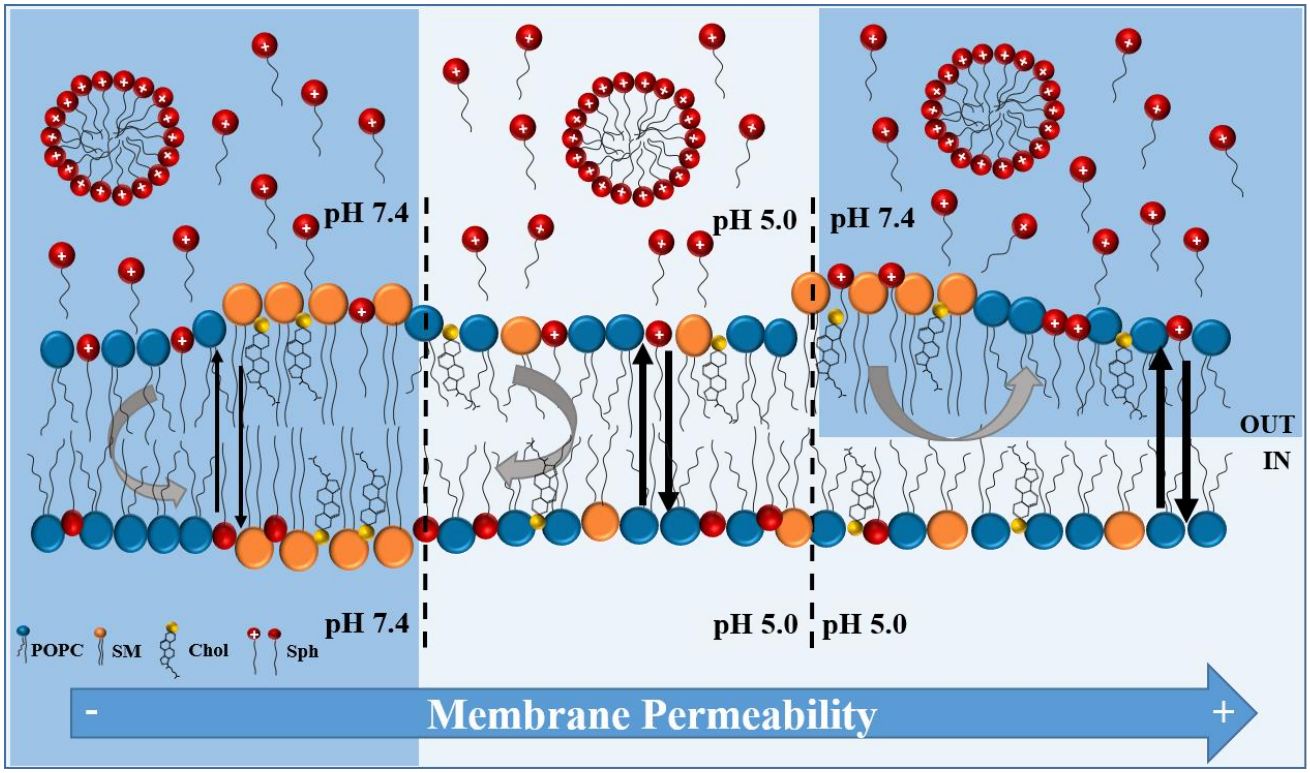

Figure 9 – Schematic representation of the effects of external addition of Sph to POPC/SM/Chol vesicles, at different physiological pH conditions. Sph that might exist in water both as monomeric species and in the form of micelles has different patterns of incorporation in the membrane, depending on the pH environment. For pH $7.4_{in}/7.4_{out}$ and pH $5.0_{in}/5.0_{out}$ vesicles the inexistence of a pH gradient across the membrane, favors the creation of a gradient by the positively charged Sph molecules inserted in the outer leafleat, promoting their *flip-flop* movement to the inner leaflet, until the gradient is cancelled and the system reaches the equilibrium. In contrast, the pH gradient across the LMVs (pH $5.0_{in}/7.4_{out}$) bilayer decreases the driving force for Sph incorporation. In this case, the distribution of positively charged Sph molecules in the external leaflet of LMVs might generate asymmetries and curvature stress at the membrane. Together with the fact that the inner leaflet of the LMVs is more disordered than the external leaflet, this could justify the increase in membrane permeability. The membrane of the pH $5.0_{in}/5.0_{out}$ vesicles is indeed more disordered compared with the membrane of pH $7.4_{in}/7.4_{out}$ vesicles. Thus, the higher fluidity of the former can favor a faster incorporation of Sph within the membrane and result in an increased rate of membrane permeabilization. The more ordered outer membranes exposed to pH 7.4, would on the contrary

contribute to a slower rate of Sph incorporation and prevent membrane destabilization, which is reflect by a lower membrane permeabilization. Thin vertical black arrows: low membrane permeability; thicker black arrows: increased membrane permeability. Curved vertical grey arrows: favorable Sph incorporation in the membrane bilayer through *flip-flop* movement; horizontal curved arrows: lower driving force for Sph incorporation in the membrane bilayer/higher initial distribution of Sph in the external leaflet. Drawn from left to right: (pH $7.4_{in}/7.4_{out}$) vesicles displaying higher membrane order in both leaflets; (pH 5.0_{in}/pH5.0_{out}) displaying lower membrane order in both leaflets; and LMVs (pH 5.0_{in}/pH7.4_{out}) displaying higher membrane order in the external leaflet compared to the inner leaflet.

Besides changes in membrane permeability, Sph incorporation in the membrane also caused alterations in membrane biophysical properties, leading to an increase in the overall order of the membrane, particularly in the packing of the ordered phase, irrespective of the pH environment. However, Sph was unable to drive gel-fluid phase separation, as previously observed for identical mixtures containing pre-incorporated Sph[26]. This might be due to an effective smaller number of Sph molecules incorporated in the membrane and therefore not enough to induce gel-fluid phase separation. In addition, Sph positive charges can hinder the formation of Sph domains due to the repulsive forces between Sph molecules. According to our surface charge analysis, a significant amount of Sph is located in the outer membrane leaflet, which might create repulsive electrostatic forces that prevent close association between Sph molecules in a gel phase. Sph positive charge might also interfere with the orientation of the head groups and curvature of the neighboring lipids[24], causing additional defects responsible for increased membrane permeability. As an example the interaction of positively charged Sph with negatively charged PLs induce membrane permeabilization through formation of non-lamellar structures[18].

6. Conclusions

The results in the present study highlight the importance of the development of synthetic systems that closely resemble physiological environments. These systems are helpful for better understanding specific molecular interactions that occur in more complex scenarios,

namely at the cell level, and even cellular dynamics. Particularly in this study, where systems mimicking physiological and NPC1 like conditions were used to address the interaction of Sph with the membrane, it was possible to detect significant differences as compared to standard vesicles with no pH gradient. Indeed, stronger changes in membrane biophysical properties and permeability were observed upon addition of Sph to vesicles that closely resemble the lysosomal environment (pH $5.0_{in}/7.4_{out}$). This effect was also more pronounced for the vesicles containing higher Chol and SM concentrations, thus mimicking NPC1-membranes. Overall, the results suggest that the abnormal accumulation of lipids in the acidic compartments of diseased cells, might significantly compromise the lysosomal membrane integrity, and consequently affect the normal function of the endolysosomal pathway, and support the further use of LMVs to understand physiological and pathological processes involving the lysosomal membrane.

7. Acknowledgments

This work was supported by Fundação para a Ciência e Tecnologia (FCT), Portugal: PTDC/BBB-BQB/0506/2012, PTDC/BBB-BQB/3710/2014, UID/00612/2013, SFRH/BD/88194/2012 to ACC and *Investigador FCT* to RFMA (IF/00317/2012) and LCS (IF/00437/2014).

8. References

1. Pruett, S. T. *et al.* Biodiversity of sphingoid bases ("sphingosines") and related amino alcohols. *J Lipid Res* **49**, 1621-1639 (2008).
2. Gault, C. R., Obeid, L. M. & Hannun, Y. A. An overview of sphingolipid metabolism: from synthesis to breakdown. *Adv Exp Med Biol* **688**, 1-23 (2010).
3. Lloyd-Evans, E. & Platt, F. M. Lipids on trial: the search for the offending metabolite in Niemann-Pick type C disease. *Traffic* **11**, 419-428 (2010).
4. Kitatani, K., Idkowiak-Baldys, J. & Hannun, Y. A. The sphingolipid salvage pathway in ceramide metabolism and signaling. *Cell signal* **20**, 1010-1018 (2008).
5. Blom, T., Li, Z., Bittman, R., Somerharju, P. & Ikonen, E. Tracking sphingosine metabolism and transport in sphingolipidoses: NPC1 deficiency as a test case. *Traffic* **13**, 1234-1243 (2012).
6. Zhang, H., Buckley, N. E., Gibson, K. & Spiegel, S. Sphingosine stimulates cellular proliferation via a protein kinase C-independent pathway. *J Biol Chem* **265**, 76-81 (1990).
7. Kanno, T., Gotoh, A. & Nishizaki, T. Sphingosine arrests the cell cycle and induces apoptosis by targeting sphingosine-dependent protein kinase and protein kinase Cδ in vitro. *Personalized Medicine Universe* **3**, 22-27 (2014).

8. Sweeney, E. A. *et al.* Sphingosine and its methylated derivative N,N-dimethylsphingosine (DMS) induce apoptosis in a variety of human cancer cell lines. *Int J Cancer* **66**, 358-366 (1996).
9. Hannun, Y. A., Loomis, C. R., Merrill, A. H., Jr. & Bell, R. M. Sphingosine inhibition of protein kinase C activity and of phorbol dibutyrate binding in vitro and in human platelets. *J Biol Chem* **261**, 12604-12609 (1986).
10. King, C. C. *et al.* Sphingosine is a novel activator of 3-phosphoinositide-dependent kinase 1. *J Biol Chem* **275**, 18108-18113 (2000).
11. Ma, Y. *et al.* Sphingosine activates protein kinase A type II by a novel cAMP-independent mechanism. *J Biol Chem* **280**, 26011-26017 (2005).
12. McDonald, O. B., Hannun, Y. A., Reynolds, C. H. & Sahyoun, N. Activation of casein kinase II by sphingosine. *J Biol Chem* **266**, 21773-21776 (1991).
13. Megidish, T., Cooper, J., Zhang, L., Fu, H. & Hakomori, S. A novel sphingosine-dependent protein kinase (SDK1) specifically phosphorylates certain isoforms of 14-3-3 protein. *J Biol Chem* **273**, 21834-21845 (1998).
14. Johnson, J. E. & Cornell, R. B. Amphitropic proteins: regulation by reversible membrane interactions (review). *Mol Membr Biol* **16**, 217-235 (1999).
15. Merrill, A., Jr. Cell regulation by sphingosine and more complex sphingolipids. *Journal of Bioenergetics and Biomembranes* **23**, 83-104 (1991).
16. Lloyd-Evans, E. *et al.* Niemann-Pick disease type C1 is a sphingosine storage disease that causes deregulation of lysosomal calcium. *Nat Med* **14**, 1247-1255 (2008).
17. Platt, F. M., Boland, B. & van der Spoel, A. C. Lysosomal storage disorders: The cellular impact of lysosomal dysfunction. *J Cell Biol* **199**, 723-734 (2012).
18. Jimenez-Rojo, N. *et al.* Membrane permeabilization induced by sphingosine: effect of negatively charged lipids. *Biophys J* **106**, 2577-2584 (2014).
19. Villamil Giraldo, A. M., Appelqvist, H., Ederth, T. & Ollinger, K. Lysosomotropic agents: impact on lysosomal membrane permeabilization and cell death. *Biochem Soc Trans* **42**, 1460-1464 (2014).
20. Contreras, F. X., Sot, J., Alonso, A. & Goñi, F. M. Sphingosine Increases the Permeability of Model and Cell Membranes. *Biophys J* **90**, 4085-4092 (2006).
21. Georgieva, R., Koumanov, K., Momchilova, A., Tessier, C. & Staneva, G. Effect of sphingosine on domain morphology in giant vesicles. *J Colloid Interface Sci* **350**, 502-510 (2010).
22. Koiv, A., Mustonen, P. & Kinnunen, P. K. Influence of sphingosine on the thermal phase behaviour of neutral and acidic phospholipid liposomes. *Chem Phys Lipids* **66**, 123-134 (1993).
23. Lopez-Garcia, F., Micol, V., Villalain, J. & Gomez-Fernandez, J. C. Interaction of sphingosine and stearylamine with phosphatidylserine as studied by DSC and NMR. *Biochim Biophys Acta* **1153**, 1-8 (1993).
24. Lopez-Garcia, F., Villalain, J. & Gomez-Fernandez, J. C. A phase behavior study of mixtures of sphingosine with zwitterionic phospholipids. *Biochim Biophys Acta* **1194**, 281-288 (1994).
25. Lopez-Garcia, F., Villalain, J. & Gomez-Fernandez, J. C. Effect of sphingosine and stearylamine on the interaction of phosphatidylserine with calcium. A study using DSC, FT-IR and 45Ca(2+)-binding. *Biochim Biophys Acta* **1236**, 279-288 (1995).
26. Zupancic, E., Carreira, A. C., de Almeida, R. F. & Silva, L. C. Biophysical implications of sphingosine accumulation in membrane properties at neutral and acidic pH. *J Phys Chem B* **118**, 4858-4866 (2014).
27. Watanabe, C., Puff, N., Staneva, G., Seigneuret, M. & Angelova, M. I. Antagonism and Synergy of Single Chain Sphingolipids Sphingosine and Sphingosine-1-phosphate toward Lipid Bilayer Properties. Consequences for Their Role as Cell Fate Regulators. *Langmuir* **30**, 13956-13963 (2014).

28. Merrill, A. H., Jr. *et al.* Structural requirements for long-chain (sphingoid) base inhibition of protein kinase C in vitro and for the cellular effects of these compounds. *Biochemistry* **28**, 3138-3145 (1989).
29. Sasaki, H., Arai, H., Cocco, M. J. & White, S. H. pH dependence of sphingosine aggregation. *Biophys J* **96**, 2727-2733, doi:10.1016/j.bpj.2008.12.3926 (2009).
30. Hoglinger, D. *et al.* Intracellular sphingosine releases calcium from lysosomes. *Elife* **27**, 10616 (2015).
31. Siskind, L. J., Fluss, S., Bui, M. & Colombini, M. Sphingosine forms channels in membranes that differ greatly from those formed by ceramide. *J Bioenerg Biomembr* **37**, 227-236 (2005).
32. Schulze, H., Kolter, T. & Sandhoff, K. Principles of lysosomal membrane degradation: Cellular topology and biochemistry of lysosomal lipid degradation. *Biochimica et Biophysica Acta (BBA) - Mol Cell Res* **1793**, 674-683 (2009).
33. Mobius, W. *et al.* Recycling compartments and the internal vesicles of multivesicular bodies harbor most of the cholesterol found in the endocytic pathway. *Traffic* **4**, 222-231 (2003).
34. de Almeida, R. F. M., Fedorov, A. & Prieto, M. Sphingomyelin/Phosphatidylcholine/Cholesterol Phase Diagram: Boundaries and Composition of Lipid Rafts. *Biophys J* **85**, 2406-2416 (2003).
35. Coutinho, A., Silva, L., Fedorov, A. & Prieto, M. Cholesterol and ergosterol influence nystatin surface aggregation: relation to pore formation. *Biophys J* **87**, 3264-3276 (2004).
36. Castro, B. M., de Almeida, R. F., Silva, L. C., Fedorov, A. & Prieto, M. Formation of ceramide/sphingomyelin gel domains in the presence of an unsaturated phospholipid: a quantitative multiprobe approach. *Biophys J* **93**, 1639-1650 (2007).
37. Isom, D. G., Castañeda, C. A., Cannon, B. R. & García-Moreno E., B. Large shifts in pKa values of lysine residues buried inside a protein. *P Natl Acad Sci* **108**, 5260-5265 (2011).
38. Hincha, D. K. Effects of calcium-induced aggregation on the physical stability of liposomes containing plant glycolipids. *Biochim Biophys Acta* **1**, 1-2 (2003).
39. Schwille, P. in *The Minimal Cell: The Biophysics of Cell Compartment and the Origin of Cell Functionality* (eds Pier Luigi Luisi & Pasquale Stano) 231-253 (Springer Netherlands, 2011).
40. Schwille, P. & Diez, S. Synthetic biology of minimal systems. *Crit Rev Biochem Mol Biol* **44**, 223-242 (2009).
41. Lagny, T. J. & Bassereau, P. Bioinspired membrane-based systems for a physical approach of cell organization and dynamics: usefulness and limitations. *Interface Focus* **5**, 20150038 (2015).
42. Magarkar, A. *et al.* Cholesterol level affects surface charge of lipid membranes in saline solution. *Sci Rep* **4**, 5005 (2014).
43. Hazemoto, N. *et al.* Effect of phosphatidylcholine and cholesterol on pH-sensitive liposomes. *Chem Pharm Bull* **41**, 1003-1006 (1993).
44. Deguchi, H., Yegneswaran, S. & Griffin, J. H. Sphingolipids as bioactive regulators of thrombin generation. *J Biol Chem* **279,** 12036-12042 (2004).
45. Mateo, C. R., Gómez, J., Villalaín, J. & Ros, J. M. G. *Protein-Lipid Interactions: New Approaches and Emerging Concepts*. (Springer Berlin Heidelberg, 2006).
46. Yeagle, P. L., Hutton, W. C., Huang, C. H. & Martin, R. B. Headgroup conformation and lipid--cholesterol association in phosphatidylcholine vesicles: a 31P(1H) nuclear Overhauser effect study. *P Natl Acad Sci* **72**, 3477-3481 (1975).
47. Marquês, J. T., Viana, A. S. & de Almeida, R. F. M. A Biomimetic Platform to Study the Interactions of Bioelectroactive Molecules with Lipid Nanodomains. *Langmuir* **30**, 12627-12637 (2014).
48. Aresta-Branco, F. *et al.* Gel domains in the plasma membrane of Saccharomyces cerevisiae: highly ordered, ergosterol-free, and sphingolipid-enriched lipid rafts. *J Biol Chem* **286**, 5043-5054 (2011).

49. Ellens, H., Bentz, J. & Szoka, F. C. Proton- and calcium-induced fusion and destabilization of liposomes. *Biochemistry* **24**, 3099-3106 (1985).
50. Rouser, G., Siakotos, A. N. & Fleischer, S. Quantitative analysis of phospholipids by thin-layer chromatography and phosphorus analysis of spots. *Lipids* **1**, 85-86 (1966).
51. Lakowicz, J. R. *Principles of Fluorescence Spectroscopy*. (Springer, 2006).
52. Overly, C. C., Lee, K. D., Berthiaume, E. & Hollenbeck, P. J. Quantitative measurement of intraorganelle pH in the endosomal-lysosomal pathway in neurons by using ratiometric imaging with pyranine. *P Natl Acad Sci U S A* **92**, 3156-3160 (1995).

9. Supporting information for: Development of lysosome-mimicking vesicles to study the effect of abnormal accumulation of sphingosine on membrane properties

Supplementary table S1 – Lipid composition of the vesicles used in this study. Lipid mixtures with five different lipid compositions were prepared. From 1 to 5 the content of both SM and Chol were increased, while the levels of POPC were decreased. This change in membrane lipid composition was made to evaluate the effect of Sph on the properties of membranes containing low (physiological-like) or high (NPC1-like) levels of Chol and SLs. The lipid structures were drawn using Chemdraw software.

Lipids	Lipid Mixtures (mol% of each lipid)				
	1 X_{lo}= 0	2 X_{lo}= 0.26	3 X_{lo}= 0.58	4 X_{lo}= 0.83	5 X_{lo}= 1
1-palmitoyl-2-oleoyl-sn-glycero-3-phosphocholine (POPC) 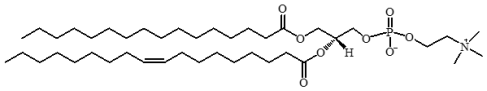	**71.6**	**59.7**	**45.1**	**34.0**	**25.4**
Sphingomyelin (SM) 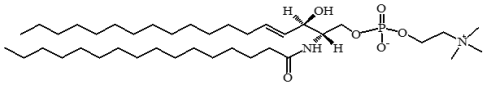	**23.3**	**26.3**	**29.9**	**32.7**	**34.8**
Cholesterol (Chol) 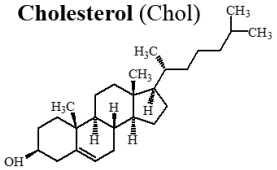	**5.1**	**14.0**	**25.0**	**33.3**	**39.8**
Sphingosine (Sph) 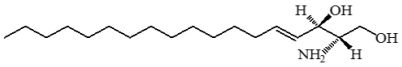	**5.0** or **10.0** mol% Sph (pre-incubation or externall addition to POPC/SM/Chol vesicles)				

Supplementary table S2 – Partition coefficient between aqueous and lipidic phases, K_p, and fluorescence intensity maximum, I_{max}, of *t*-PnA at different pH conditions.

Vesicles composition	log K_p at pH 5.0	I_{max} (a.u.) at pH 5.0	log K_p at pH 7.4	I_{max} (a.u.) at pH 7.4
POPC	4.74 ± 0.07	482 ± 12	4.30 ± 0.04	509 ± 10
POPC/SM/Chol (26% l_o)	4.60 ± 0.09	804 ± 22	4.43 ± 0.06	1125 ± 23

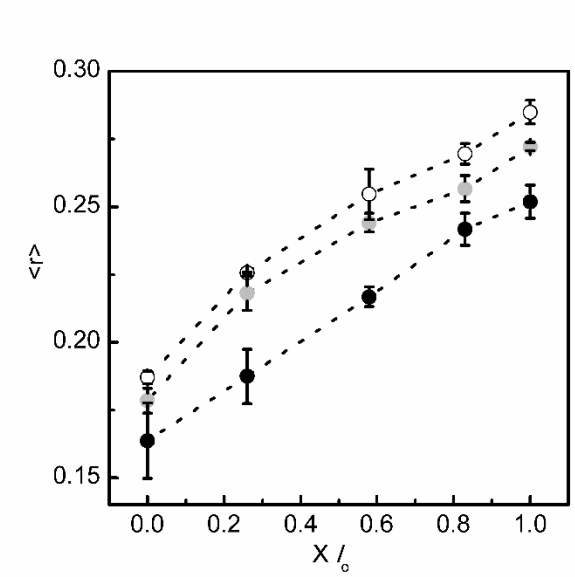

Figure S1 - pH-induced alterations in the biophysical properties of LMVs and POPC/SM/Chol vesicles with no pH gradient. The variation of *t*-PnA fluorescence anisotropy <r> in ternary POPC/SM/Chol mixtures at pH $5.0_{in}/5.0_{out}$ (black circles), pH $7.4_{in}/7.4_{out}$ (light grey circles) and pH $5.0_{in}/7.4_{out}$ (white circles) is represented as a function of l_o fraction. The values are the mean ± SD of at least three independent experiments.

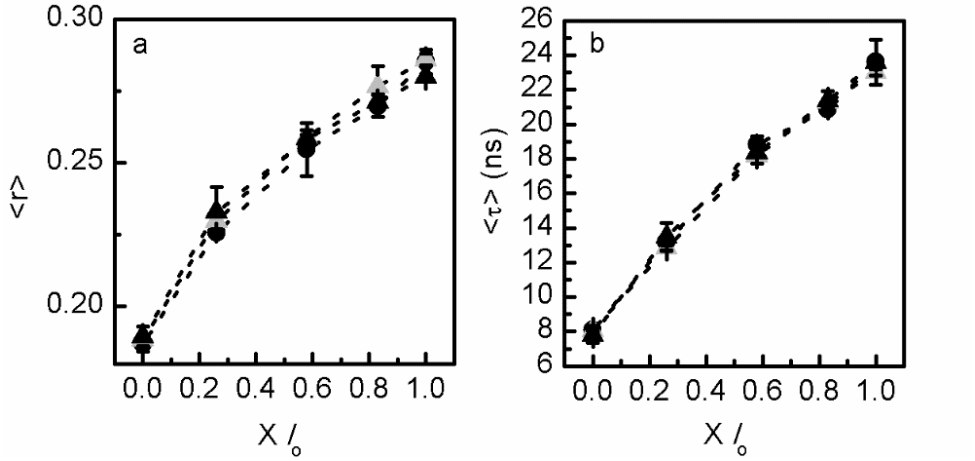

Figure S2 – Biophysical properties of LMVs (pH 5.0$_{in}$ /7.4$_{out}$) in the absence and presence of pre-incorporated Sph. Panels (a,b) show the variation in (a) steady-state fluorescence anisotropy and (b) mean fluorescence lifetime of *t*-PnA in ternary POPC/SM/Chol mixtures (black) and POPC/SM/Chol mixtures containing 5 (grey triangles) and 10 (black triangles) mol % of pre-incorporated Sph (Fig. 1a.2). Data are represented as a function of the I_o phase fraction (XI_o): the higher the *X*I_o the higher the levels of Chol and SM of the mixtures (see methods for further details). The values are the mean ± SD of at least three independent experiments. The lines act merely as guides to the eye.

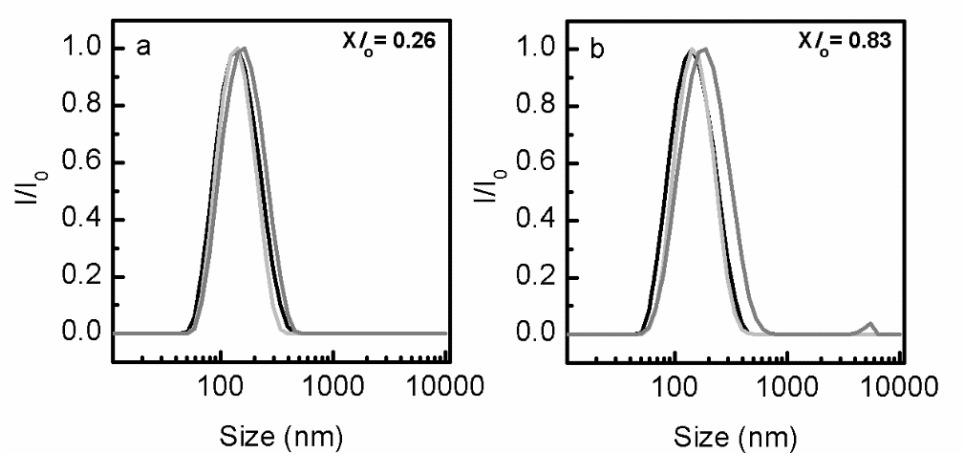

Figure S3 - Dynamic light scattering characterization of POPC/SM/Chol LMVs upon dynamic interaction with Sph. Panels (a,c) represent the normalized scattered light intensity of POPC/SM/Chol vesicles containing (a) XI_o = 0.26 and (b) XI_o = 0.83 as a function of particle size (nm). The

measurements were made before (black lines) and after (light grey lines) size exclusion chromatography, and after the addition of 10 mol% Sph to the LMVs (dark grey lines). The values are the mean (± SD) of at least three independent experiments.

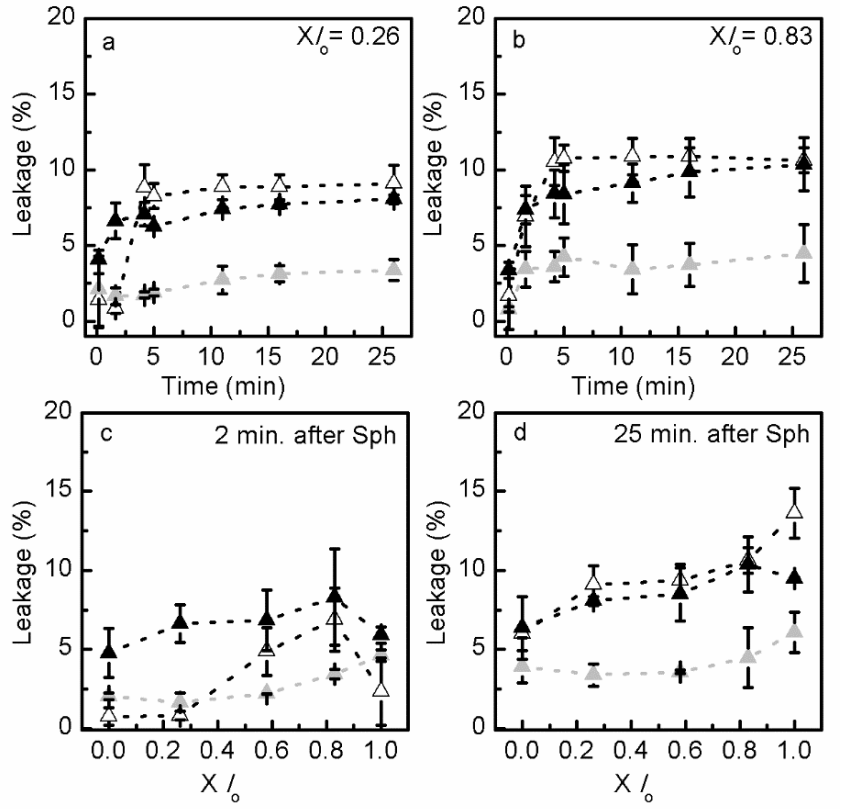

Figure S4 –Sph-induced membrane permeability in LMVs and POPC/SM/Chol vesicles with no pH gradient. (a,b) Sph-induced membrane permeability was evaluated overtime after the addition of 5 mol% of Sph to POPC/SM/Chol vesicles prepared at pH $5.0_{in}/7.4_{out}$ (white triangles), pH $7.4_{in}/7.4_{out}$ (grey triangles) and pH $5.0_{in}/5.0_{out}$ (black triangles). (a) $X/_o$ = 0.26 and (b) $X/_o$ = 0.83. (c,d) The extent of Sph-induced leakage was determined in POPC/SM/Chol vesicles containing increasing fractions of $/_o$ phase (c) 2 and (d) 25 minutes after Sph addition. The values are the mean ± SD of at least three independent experiments.

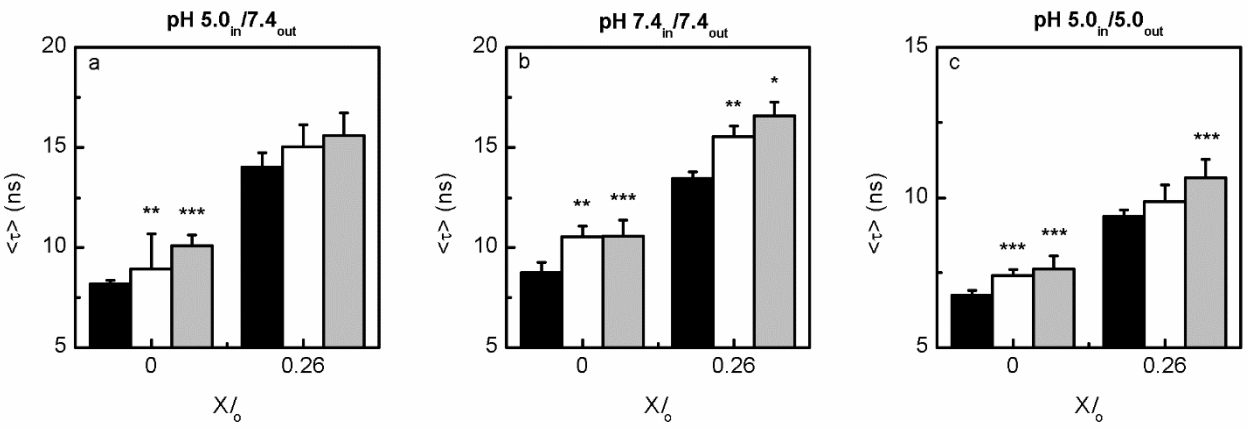

Figure S5 – Sph-induced alterations in the biophysical properties of LMVs and POPC/SM/Chol vesicles with no pH gradient. The variation in the mean fluorescence lifetime of *t*-PnA before (black) and after external addition of 5 (white) and 10 (light grey) mol% of Sph to POPC/SM/Chol vesicles is represented as a function of I_o fraction. (a) pH $5.0_{in}/7.4_{out}$, (b) pH $7.4_{in}/7.4_{out}$ and (c) pH $5.0_{in}/5.0_{out}$. The values are the mean ± SD of at least three independent experiments. *, $p < 0.001$ *versus* 0% Sph; **, $p < 0.01$ *versus* 0% Sph; ***$p < 0.05$ *versus* 0% Sph.

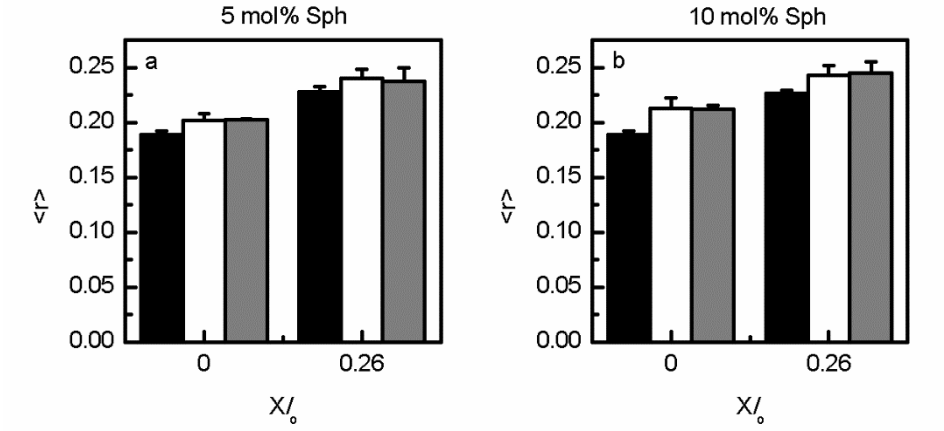

Figure S6 – Sph-induced alterations in the biophysical properties of LMVs. *t*-PnA fluorescence anisotropy was measured before (black), just after (white) and 30 minutes (grey) after the addition of (a) 5 and (b) 10 mol% Sph to LMVs containing $XI_o = 0$ and $XI_o = 0.26$. The values are the mean ± SD of at least three independent experiments.

CHAPTER IV

BIOPHYSICAL IMPACT OF LIPID ABNORMAL ACCUMULATION IN NPC1 CELL MODELS

The work in this chapter is presented as an unpublished original manuscript by **Ana C. Carreira**, Emyr Lloyd-Evans, Rodrigo F. M. de Almeida, and Liana C. Silva

CHAPTER IV – BIOPHYSICAL IMPACT OF LIPID ABNORMAL ACCUMLATION IN NPC1 CELL MODELS

1. Abstract

Niemann-Pick disease type C (NPC) is a complex and rare pathology, which is mainly associated to mutations in the NPC1 gene. This disease is phenotypically characterized by the abnormal accumulation of multiple lipid species in the cell acidic compartments. Due to the complexity of stored material, a clear molecular mechanism that explains NPC pathophysiology is still not established. Sphingosine (Sph) abnormal accumulation was suggested as the primary factor involved in the development of NPC disease, being followed by the accumulation of other lipid species (e.g. Cholesterol (Chol), Sphingomyelin (SM), Glycosphingolipids (GSLs)). With the aim to characterize the impact of the NPC phenotype in the biophysical properties of biological membranes, fluorescence spectroscopy studies were performed to evaluate the outcome of: null or down expression of NPC1 locus, the pharmacological induction of the NPC phenotype (U18666A treatment) and the addition of Sph to healthy cells. Experiments performed with Chinese Hamster Ovary (CHO) cell lines (CHO-K1 and CHO-M12) show that the abnormal accumulation of multiple lipid species in CHO NPC cells generally results in a decrease in membrane fluidity, irrespectively of the tested condition (locus, U18666A or Sph treatment). An inverse effect, i.e., an increase in membrane fluidity was observed in a mutant NPC neuroblastoma cell line down expressing the NPC locus, suggesting that changes in membrane order arising from lipid accumulation in NPC are complex and cell type dependent.

2. Introduction

NPC disease is a rare autosomal recessive disorder associated with mutations in the NPC1 or NPC2 genes. The great majority (ap. 95%) of the cases are associated with pathogenic variants of NPC1 gene[1]. This disease is phenotypically characterized by the storage of multiple lipid species, such as Sph, Chol, SM and GSLs, in the late endosomes/lysosomes of cells[2]. Due to the complexity of storage material it has been challenging to find a mechanism that clearly explains the cell biology of NPC disease. Studies have proposed different theories to explain this

unique disease, each suggesting a different NPC metabolite as the key player in the development of the NPC associated pathophysiology[3–5]. In 2008 it was suggested that Sph abnormal accumulation was the first crucial event in NPC disease[6]. It was proposed that after Sph accumulation in the acidic compartments, a calcium homeostatic defect characterized by low calcium levels occurred in those organelles, being responsible for the secondary accumulation of other lipid species, such as Chol and sphingolipids (SLs)[6]. In addition, it was shown that Sph is able to induce the NPC phenotype when added to healthy cells in concentrations found in NPC cells, which was not observed for the other lipid species that also abnormally accumulate in NPC disease[6]. Moreover, Sph was the first lipid to accumulate after the pharmacological induction of the NPC phenotype using the class II amphiphile U18666A drug that binds to NPC1 protein interfering with its cellular function[6,7].

The cellular levels of free Sph and other sphingoid bases are generally low (e.g. the blood is thought to have 0.1 to 1 μM of Sph and S1P)[8] due to its rapid metabolization into more complex molecules. Deregulation of Sph levels occurs in NPC patient organs at different extents as observed for other lipid species[2]. Despite being a minor storage lipid in NPC brain and peripheral tissues in terms of mass, it still presents the greatest fold elevation compared to other lipid species that also accumulated in NPC disease[2]. For example, increase in the levels of Sph ranging from 4-fold to 12-fold are observed in the brain and liver, respectively[2]. In addition, Sph is an important bioactive lipid with impact in different cellular processes, such as cell proliferation[9] and apoptosis[10,11]. The mechanisms behind its regulatory effect are still not clear. Although Sph is able to directly bind to cellular proteins[12,13], there are some proteins that do not have a known Sph-binding site[14,15] and evidence suggests that Sph might exert its regulatory function at the membrane level, through biophysical changes that can affect the membrane organization and consequently trigger different cellular responses[16–19]. Moreover, it is expectable that the impact of this lipid in the properties of the membranes will depend on its subcellular location, since its physico-chemical features, such as, protonation and H-bonding states, vary in different physiological pH environments[20]. In fact, it was shown that Sph has different abilities to change the biophysical properties of the membranes, depending on the pH of surrounding environment[18]: at neutral pH Sph tends to decrease membrane fluidity[16,17,21–25],

while, in acidic conditions that mimic the lysosome environment, Sph has a lower ability to decrease membrane fluidity, likely due to repulsive forces generated by the positively charged Sph molecules[18]. Another aspect to consider is the membrane lipid composition, since it was shown that Sph ability to decrease membrane fluidity is also dependent on the SM and Chol content[18,19], lipids that also accumulate in NPC disease. Considering that Sph has a strong influence in the biophysical properties of model membranes, it is tempting to hypothesize that the pathological accumulation of this lipid might have a strong impact in the properties of biological membranes. To test for this hypothesis, fluorescence spectroscopy studies were performed to evaluate different situations: cells with the NPC phenotype (null or down expressing the NPC1 locus), the pharmacological induction of the NPC phenotype (U18666A treatment) and the addition of Sph to healthy cells. Considering that NPC organs/tissues are differently affected[2], CHO-K1 cells and SH-SY5Y neuroblastoma cell lines were analyzed, together with their mutant counterparts, null (CHO-M12 cells)[26] or down-expressing (SH NPC cells)[27] the NPC1 locus. The results show that the effect of lipid abnormal accumulation in the biophysical properties of biological membranes are complex and cell type dependent. Sph, in particular, revealed to have the ability to change the fluidity of biological membranes, in a concentration dependent manner, in accordance to what was observed in model membrane studies[18,19]. After Sph treatment, an almost immediate decrease in membrane fluidity is observed both in CHO-K1 and SH-SY5Y cell membranes, suggesting a direct effect of Sph rather than a downstream metabolite. For longer incubation periods the membranes become globally more fluid, which might be due to Sph internalization, Sph metabolization into other lipid species and/or the involvement of other lipid species that also accumulate in NPC. Despite this, the present study clearly shows that Sph itself has an impact in membrane organization that is likely to be related to its role in the pathophysiology of NPC disease.

3. Materials and Methods

3.1. Materials

D-erythro-sphingosine (Sph) was obtained from Avanti Polar Lipids, Inc. (Alabaster, AL, U.S.A.). U18666A was obtained from Sigma-Aldrich (St. Louis, MO, U.S.A.). DPH (1,6-diphenyl-1,3,5-hexatriene), TMA-DPH (1-(4-(trimethylamino)phenyl)-6-phenylhexa-1,3,5-triene) and *t*-PnA (*trans*-Parinaric Acid) were from Molecular Probes/Invitrogen (Eugene, OR, EUA). All the other reagents were of the highest purity available.

The concentrations of Sph and of the probes were determined as previously described[18].

3.2. Methods

3.2.1. Cell Culture

In this work different cell lines were used: wild-type (WT) CHO-K1 and SH-SY5Y neuroblastoma cells and their mutant counterparts lacking (CHO-M12; a kind gift of Dr. Daniel Ory, Washington University, St. Louis, MO) or down expressing (SH-NPC; a kind gift of Dr. Elsa Rodrigues, Lisbon University, Lisbon, Portugal) the NPC1 locus. All this cell lines were grown in DMEM Ham F-12 (Sigma-Aldrich, Dorset, UK). The Medium was supplemented with 10% fetal bovine serum (Sigma-Aldrich, Dorset, UK), heat inactivated at 60°C for 1 hour, 1% L-glutamine (100x) (Life Technologies, California, USA) and 1% pen-strep (VWR, Pennsylvania, USA). The cells were grown as monolayers at 37 °C with 5% CO_2 in a humidified incubator.

3.2.2. Microscopy

Coverslip preparation

Glass coverslips were washed with nitric acid and kept in 100% ethanol before use. The cellular suspensions were counted and seeded onto 13 mm cover slips (VWR, PA, USA) in 24 well plates (VWR, Pennsylvania, USA). Approximately 10,000 cells were used per coverslip. Cells were grown at 37 °C with 5% CO_2 in a humidified incubator, till reach 70-80% confluence.

Cell fixation with paraformaldehyde

Cells were washed once with 1 mL of DPBS (Dulbecco's Phosphate Buffered Saline) (Sigma-Aldrich, Dorset, UK) and incubated with 300 µL of 0.4% paraformaldehyde (PFA) (VWR, Pennsylvania, USA) for 10 minutes at room temperature. PFA was removed and the cells were incubated with 1 mL of DMEM Ham F-12 complete medium for 5 minutes and washed twice with 1 mL of DPBS (1x). The cells were left in 1 mL of DPBS (1x), at 4 °C until required for staining or mounting.

Filipin staining

To visualize cholesterol in cells, fluorescent filipin that binds specifically to unesterified cholesterol was used. The stock solution of filipin was prepared by adding 2 mg of filipin (Sigma-Aldrich, Dorset, UK) to 100 µL of DMSO (Sigma-Aldrich, Dorset, UK). Filipin working solution was made by adding 7.5 µL of filipin stock solution to 1 mL of DMEM Ham F-12 complete medium. Cells were stained by adding 500 µL of filipin working solution into each well and left to incubate for 30 minutes at room temperature in the dark. After incubation, cells were washed once with complete medium and twice with DPBS (1x). The coverslips were mounted on glass slides using Mowiol and allowed to dry overnight. Excitation at 380 nm and emission at 405 nm were used for imaging.

Lysenin staining

Lysenin specifically binds to sphingomyelin and for that reason lysenin stain was performed to trace the intracellular sphingomyelin distribution. PFA fixed cells were incubated with lysenin toxin (Peptides International, Kentucky, USA) at 1:1500 dilution of a 0.5 µg/mL stock solution in blocking solution (1% bovine serum albumin (Sigma-Aldrich, Dorset, UK) and 0.1% saponin (Sigma-Aldrich, Dorset, UK) in DPBS)) and left overnight at 4 °C. After, lysenin toxin was removed by washing the cells three times for 5 minutes with DPBS (1x). Cells were incubated with lysenin primary antibody (raised in rabbit) (Peptides International, Kentucky, USA) at 1:1000 dilution in blocking solution for 1 hour at room temperature. Cells were then washed three times for 5 minutes with DPBS (1x), and stained with the fluorescent secondary

antibody DyLightR 488 Anti-Rabbit (Vector, California, USA) at 1:500 dilution in blocking solution for 30 minutes at room temperature. After incubation, cells were washed three times for 5 minutes with DPBS (1x). Excitation at 493 nm and emission at 518 nm were used for imaging.

Bis(monoacyl)glycerophosphate/lyso-bisphosphatidic acid (p-LBPA)

LBPA is a lysosome specific lipid. Fixed cells were incubated with anti-LBPA primary antibody (Echelon Biosciences, Utah, USA) at 1:1000 dilution in blocking solution (1% bovine serum albumin and 0.1% saponin in DPBS) overnight at 4 °C. After incubation, cells were washed three times for 5 minutes with DPBS (1x) and stained with the secondary antibody (DyLightR 488 Anti-Mouse (Vector, California, USA)) at 1:200 dilution in blocking solution. After 1 hour incubation at room temperature cells were washed three times for 5 minutes with DPBS (1x). Excitation at 493 nm and emission at 518 nm were used for imaging.

Cholera Toxin B staining

To trace the intracellular glycosphingolipid (ganglioside GM1) distribution the cholera toxin B stain was performed. Alexa Fluor 488 Cholera toxin subunit B (Invitrogen, Paisley, UK) protein was solubilized in DMEM Ham F-12 complete medium to make a working solution of 1 µg/mL. PFA fixed cells were incubated with Alexa Fluor 488 Cholera toxin subunit B working solution at 4 °C overnight and protected from light. When the toxin was removed, cells were washed three times for 5 minutes with DPBS (1x). Excitation at 493 nm and emission at 518 nm were used for imaging.

Nucleus staining

The counterstain of cell nucleus was performed with Hoechst (Invitrogen, Paisley, UK), a fluorescent DNA stain, solubilized in DPBS (1x) at 1:5000 dilution. The Hoechst solution was added to each well and left to incubate for 10-20 minutes at room temperature. After incubation, cells were washed three times with DPBS (1x). Excitation at 380 nm and emission at 405 nm were used for imaging.

Coverslip mounting

Stained coverslips were mounted on glass microscope slides (Fisher, Loughborough, UK) using 12 µL of Mowiol mounting solution (Calbiochem, Nottingham, UK) and left overnight to dry.

Cell visualization

Cells were visualized using Zeiss Colibri LED fluorescence microscope (Carl Zeiss, Oberkochen, Germany) and AxioVission 4.7 software (Carl Zeiss, Oberkochen, Germany) or with a Leica TCS SP5 (Leica Mycrosystems CMS GmbH, Mannheim, Germany) inverted microscope (DMI6000).

3.2.3. Cell treatments

U18666A drug[28] was used to induce an NPC1 phenotype in the healthy WT cells. A stock solution of U18666A (5 mg/mL) was prepared using sterile DMSO, aliquoted and kept frozen at -20 °C. For the microscopy studies, cells (ap. 10 000) were transferred onto a glass coverslip and for the fluorescence spectroscopy studies, cells (ap. 500 000) were grown in 90 mm petri dishes (VWR, Pennsylvania, USA). To maintain identical concentration of drug per cell number, cells were treated with a final concentration of 2µg/mL and 10µg/mL (respectively) of U18666A in DMEM Ham F-12 complete medium and grown at 37°C, during 24 hours.

To evaluate the effects of external addition of Sph, cells were grown in 90 mm petri dishes. Sph stock solutions were prepared in ethanol and kept at -20 °C. The cells were treated with a final concentration of 1, 2 or 10 µM Sph for different incubation periods: 1, 10, 20, 30, 240 (4h) or 1440 (24h) minutes. For the shorter incubation periods the Sph addition was performed directly in the fluorescence cuvettes containing approximately $1x10^6$ cells/mL and for the longer incubation periods (4 and 24h), Sph was directly added to the petri dish (containing also approximately $1x10^6$cells) and the cells were harvested only at the end of the incubation period, to perform the fluorescence measurements.

Control experiments were performed, in which ethanol or DMSO were added to the cells. The volume of ethanol and DMSO was always kept below 1% (v/v) in order to avoid possible cytotoxic effects[29].

3.2.4. Fluorescence measurements

After being suspended and counted, cells were centrifuged and re-suspended in PBS with calcium and magnesium (Life Technologies, California, USA), to obtain a final concentration of $1x10^6$cells/mL. The cell suspension was incubated for 5 minutes at 37 °C with the different probes (*t*-PnA, DPH or TMA-DPH, all at a final concentration of 2 µM). The fluorescence measurements were carried out in a Spex Fluorolog 3-22/Tau 3 spectrofluorometer equipped with double grating monochromators in both excitation and emission light paths and with a thermostated sample holder with magnetic stirring from Horiba Jobin Yvon. The measurements were performed in 1 x 0.4 cm quartz cuvettes at 37 °C under continuous stirring. For the steady-state experiments, the excitation and emission wavelengths were 360 and 430 nm for DPH and TMA-DPH, and 320 and 404 nm for *t*-PnA. The steady-state anisotropy (*r*) was calculated according to Equation 1[30]:

$$r = \frac{(I_{VV} - G \times I_{VH})}{(I_{VV} + 2G \times I_{VH})} \qquad (Eq.1)$$

in which *G* is the instrumental correction factor. Subscripts V and H represent the vertical and horizontal orientations of the polarizers, and the order of the subscripts corresponds to the excitation and emission. An adequate blank (cell suspension without probe) was subtracted from each intensity reading.

The fluorescence intensity decay measurements were obtained by the single photon counting technique[30]. A NanoLED source, model N-320 was used for *t*-PnA excitation, and the emission was collected at 404 nm. For DPH and TMA-DPH excitation, a nanoLED N-370 plus and a UGI-370 band pass filter were used, and the emission wavelength was set to 420 nm. To analyze the experimental decays and obtain the fitting curves, the TRFA software (Scientific

Software Technologies Center, Minsk, Belarus) was used. Ludox® was used as the scatterer to obtain the instrumental response function. Fluorescence decays were described by a sum of exponentials, where α_i is the normalized pre-exponential, and τ_i is the lifetime of the decay component *i*. The mean fluorescence lifetime $<\tau>$ is given by:

$$<\tau>=\frac{\sum_{i=1}^{n}\alpha_i\tau_i^2}{\sum_{i=1}^{n}\alpha_i\tau_i} \qquad (Eq.2)$$

An adequate blank was prepared and measured under the exact same conditions of the samples and subtracted from each intensity reading.

3.2.4. Statistical analysis

The statistical analysis was performed using Student's t-test. Mean values were considered significantly different for *p* values below 0.05.

4. Results

The impact of lipid abnormal accumulation in the biophysical properties of living NPC1 cell models was evaluated.

4.1. Effect of the NPC1 locus deletion

CHO-M12 is a CHO-K1 mutant cell line with a deletion of the NPC1 locus[26]. As previously referred, the NPC phenotype is associated with the accumulation of different lipid species (Chol, SM, GSLs, Sph) in the LE/lysosomes of cells, resulting from mutations in the NPC1 or NPC2 genes[1,6]. CHO-M12 cells were already shown to have a Chol trafficking defect through filipin staining[26], which is considered to be the gold standard method to establish the diagnosis in NPC patients[31]. In the present work, in addition to filipin staining, lysenin, cholera toxin and anti-LBPA stains were also performed, to trace the CHO-K1 and CHO-M12 intracellular levels of unesterified Chol, SM, the ganglioside GM1 and LBPA, respectively. Figure 1 shows that, as previously observed[26], CHO-M12 cells present a filipin-positive stain when compared to the

control CHO-K1 cells. In addition, this null NPC1 cell line was also characterized by a rise in the cellular levels of the other lipids in study, which can be observed by an increased punctate staining, suggesting an accumulation of these lipid species in the endosomal/lysosomal vesicles of CHO-M12 cells.

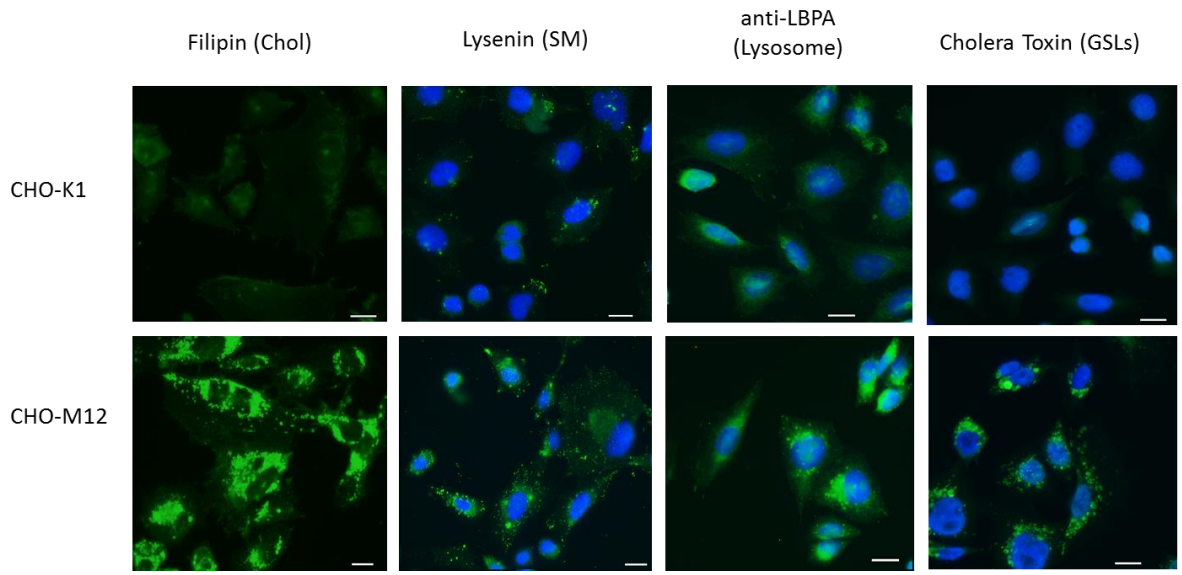

Figure 1 – Phenotypic characterization of CHO-K1 and CHO-M12 in terms of lipid content. Chol was stained with filipin, GSLs (ganglioside GM1) were stained with cholera toxin subunit B and SM was stained with lysenin. LBPA, a lipid that is present in high concentrations in the internal membrane network of endosomes and lysosomes, was also stained (anti-LBPA staining). The nucleus was contra stained with Hoechst solution (blue) after lysenin, cholera toxin and anti-LBPA stain. Scale bars, 10 µm.

To understand the consequences of this abnormal lipid accumulation in the biophysical properties of living cell membranes, fluorescence spectroscopy studies were performed, taking advantage of the photophysical properties of two fluorescent probes: *t*-PnA and DPH. *t*-PnA displays an equal partition among l_d and l_o phases similarly to DPH[32] but has strong partitioning and higher quantum yield in the presence of gel domains[33,34]. For this reason, *t*-PnA is generally used to detect ordered phases in the membrane, such as, a gel phase characterized by a very long fluorescence lifetime component[32,35] and l_o phases[36], while DPH, provides more general information of the overall fluidity of the membrane. Due to the rapid internalization of both

probes[37,38], this methodology will report alterations undergone both in the PM and internal membranes. It should be noted that the experimentally determined fluorescence parameters (anisotropy and lifetime) are weighted averages that will depend on the fraction of each phase and the partition coefficient of the probes toward that phases in the different and heterogeneous membrane environments.

Figure 2 shows that *t*-PnA (Fig. 2A) and DPH (Fig. 2D) fluorescence anisotropy is significantly higher in mutant CHO cells, suggesting an overall decrease in membrane fluidity compared to control CHO-K1 cells. The same tendency was observed upon measuring the mean fluorescence lifetime (Figs. 2B,E) and the long lifetime component (Figs. 2C,F) of the probes, although not in the same extent as observed for the anisotropy measurements. Overall the results indicate an alteration in the fluidity of the membranes of mutant CHO cells, which is compatible with an ordering effect caused by the accumulation of Sph[18,19] and other lipid species, such as Chol and SM[39], in NPC disease.

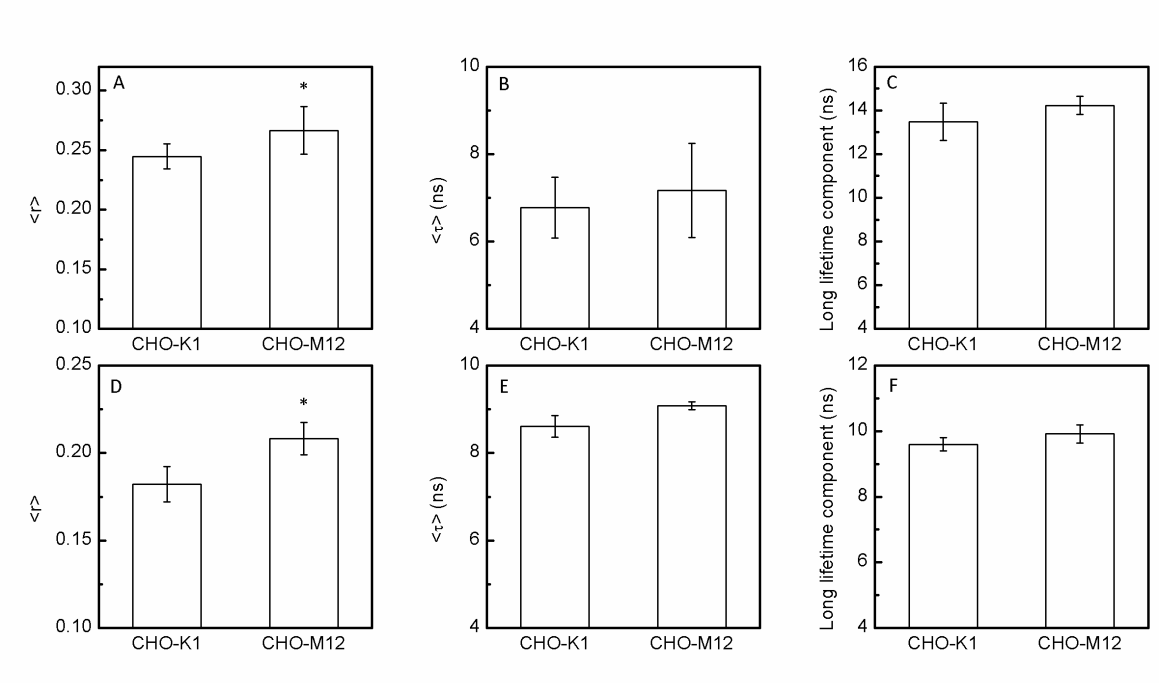

Figure 2 – Characterization of the biophysical properties of living CHO-K1 and CHO-M12 cells. (A,D) Fluorescence anisotropy <r>, (B,E) Mean fluorescence lifetime <τ> and (C,F) Long lifetime component of (A-C) *t*-PnA and (D-F) DPH. Values are means ± SD of three independent experiments.*$p < 0.01$ versus CHO-K1 cells.

4.2. Effect of U18666A treatment

The NPC phenotype can also be pharmacologically induced with the class II amphiphile U18666A (referred in this study as U-drug)[6], a cationic steroid, containing a diethylaminoethyl chain attached to the 3-hydroxyl group. Studies have shown that U-drug can directly bind to the sterol-sensing domain of NPC1 protein, blocking the movement of Chol out of the lysosomes[7], which can affect many pathophysiological events[40]. In addition, it was demonstrated that Sph is the first lipid to be elevated following inactivation of NPC1 in healthy RAW cells[6]. The elevation of Sph concentration (ap. 0.75 µM in U18666A-treated RAW cells) occured few minutes (ap. 10 minutes) after U-drug treatment and remains elevated for 24h. The secondary accumulation of Chol, SM and GSLs occured 4-8h later[6].

As expected, the phenotypic characterization of CHO-K1 cells after U-drug treatment revealed an abnormal accumulation of multiple lipid species, which was represented by an increased punctate staining (Fig. 3), similarly to what was observed for the mutant NPC CHO cells (CHO-M12).

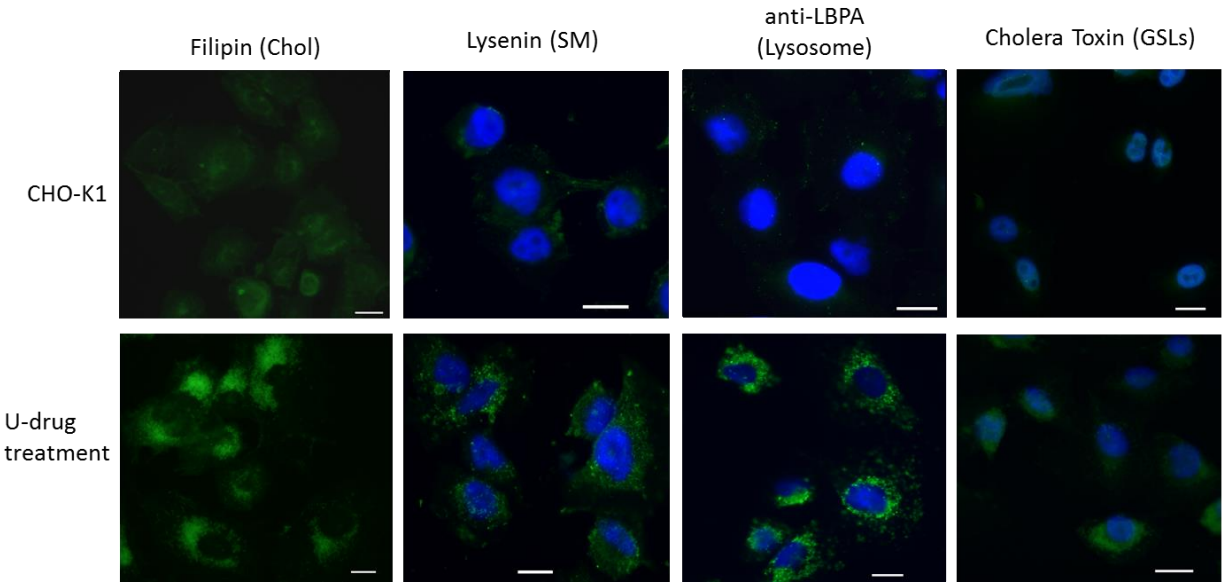

Figure 3 – Phenotypic characterization of CHO-K1 cells in terms of lipid content before and after U-drug treatment for 24h. Chol was stained with filipin, GSLs (ganglioside GM1) were stained with cholera toxin subunit B and SM was stained with lysenin. LBPA, a lipid that is present in high concentrations in the internal membrane network of endosomes and lysosomes, was also stained (anti-LBPA staining). The

nucleus was contra stained with Hoechst solution (blue) after lysenin, cholera toxin and anti-LBPA stain. Scale bars, 10 µm.

The biophysical impact of the U-drug treatment in the membranes of CHO-K1 cells was also evaluated. The results were very similar to the ones obtained for the mutant NPC cells (CHO-M12), where it was observed a decrease in membrane fluidity. This effect was represented by an increase in the fluorescence anisotropy and mean fluorescence lifetime of *t*-PnA (Figs. 4A,B) and DPH (Figs. 4D,E). A slight increase in the long lifetime component was also observed (Fig. 4C,F).

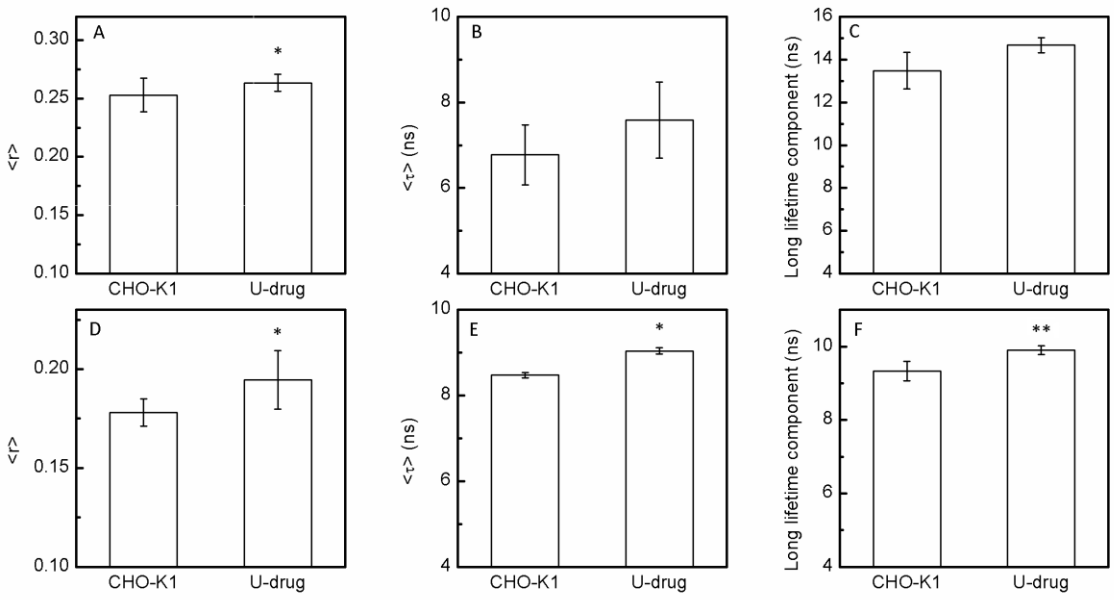

Figure 4 – Characterization of the biophysical properties of living CHO-K1 cells before and after U-drug treatment for 24h. (A,D) Fluorescence anisotropy <r>, (B,E) Mean fluorescence lifetime <τ> and (C,F) Long lifetime component of (A-C) *t*-PnA and (D-F) DPH. Values are means ± SD of three independent experiments. *$p < 0.01$ versus CHO-K1 cells; **$p < 0.05$ versus CHO-K1 cells.

4.3. Effect of Sph external addition

When added at the concentration found in NPC cells, Sph seems to be the only lipid from all the NPC1 storage lipids that induces an NPC phenotype in normal cells[6]. To evaluate if the

exogenous addition of Sph has a similar effect in the biophysical properties of CHO-K1 membranes compared with the deleterious mutation of the NPC1 locus and the altered NPC1 function through the U-drug treatment, three different Sph concentrations were tested: 1 and 2 μM, concentrations that are able to induce the NPC phenotype in healthy cells[6] and 10 μM that seems to have a rapid detergent effect in RAW macrophages[6] but was recently found to be responsible for the formation of multiple dilated intracellular vesicles in different cell lines, with an important impact in endocytic membrane trafficking[41]. The experiments were performed for short incubation periods (ap. 1, 10, 20 and 30 minutes), an intermediate period of 4h (for the lower Sph concentrations – 1 and 2 μM) and also for a period of 24h incubation with Sph.

Figure 5 shows that Sph changes the biophysical properties of CHO-K1 cell membranes through a decrease in membrane fluidity, similarly to the observed for the mutant CHO cell line (CHO-M12) that lacks the NPC1 locus (Fig. 2) and the cells treated with the U-drug (Fig. 4). Furthermore Sph-induced alterations in membrane fluidity are time and concentration dependent (Fig. 5): while 1 μM Sph did not cause significant variations in the anisotropy of *t*-PnA or DPH compared to control cells, higher Sph concentrations (2 and 10 μM) induced an immediate decrease in the overall membrane fluidity (ap. 1 min. after Sph addition). This effect was reflected by a significant increase in the fluorescence anisotropy of *t*-PnA (Fig. 5A) and a slighter increase in the fluorescence anisotropy of DPH (Fig. 5B), which reflect a lower impact in the global properties of the membranes. This could be indicative of the involvement of Sph in the formation of specialized ordered lipid domains in the PM where the levels of Chol and SM are generally high[42], in agreement with data obtained in model membranes in which the Sph interplay with Chol and SM was studied[18]. The significant increase of the fluorescence anisotropy of *t*-PnA, close to the values observed for ceramide gel phases[33] in the first minute after Sph addition, was not accompanied by a strong increase in the long lifetime component of the probe (Fig. 5C), which is considered as a "fingerprint" for the gel phase. These results suggest that such phase is not occurring in the membranes of CHO-K1 cells and that Sph is probably contributing to an increase in the l_o phase fraction without significant impact in the packing and order of the acyl chains.

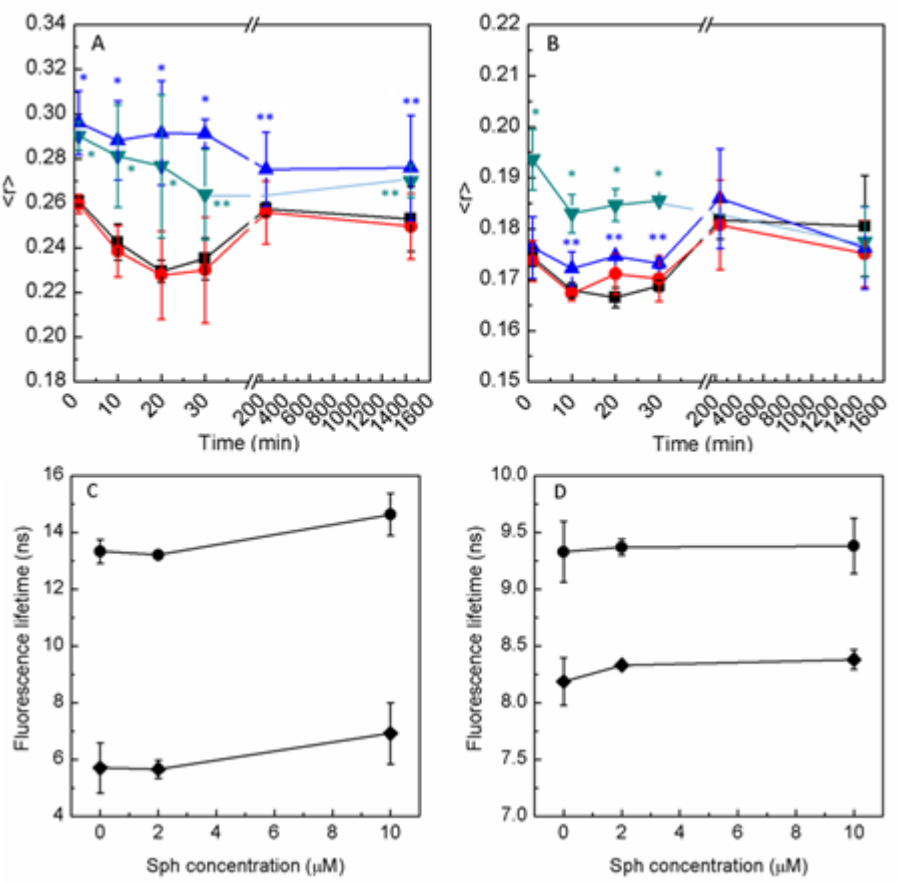

Figure 5 – Effect of Sph in the biophysical properties of CHO-K1 cells. Steady-state fluorescence anisotropy of (A) *t*-PnA and (B) DPH after ap. 1, 10, 20, 30, 240 (4h) and 1440 (24h) minutes of 1 (red circles), 2 (blue triangles) and 10 (green triangles) μM external addition of Sph. Control cells without Sph addition are represented by black squares. Mean fluorescence lifetime (black diamonds) and long lifetime component (black circles) of (C) *t*-PnA and (D) DPH were obtained after approximately 5 minutes incubation with Sph at 37 °C. Values are means ± SD of at least three independent experiments. The lines act merely as guides to the eye. *$p < 0.01$ versus control CHO-K1 cells; **$p < 0.05$ versus control CHO-K1 cells.

The membrane ordering effect was also observed, in a slightly lower extent, for longer incubation periods (4 and 24h) (Figs. 5A,5B), where the accumulation of other lipid species is also expected[6]. Figure 6 shows that irrespectively of the tested condition, i.e., lacking of NPC1

locus (CHO-M12), U-drug and Sph treatment, the biophysical impact in the membranes of CHO-K1 cells is similar and reflected by a decrease in membrane fluidity, especially with regard to the parameters obtained with the probe *t*-PnA. Sph did not have a significant effect on the DPH anisotropy (Fig. 6D) and lifetime (Fig. 6 E,F), further suggesting that the effects sensed by *t*-PnA are located into specific membrane domains.

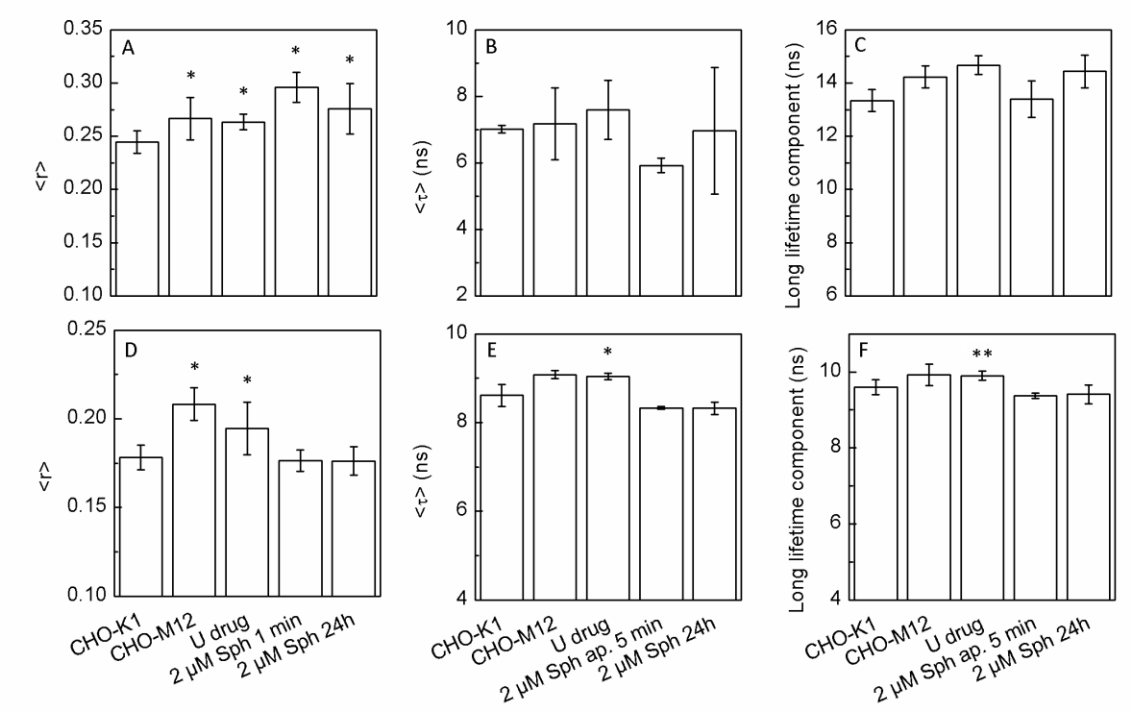

Figure 6 – Comparison between the effect of NPC1 locus deletion, U-drug treatment and Sph external addition on the biophysical properties of CHO-K1 cells. (A,D) Fluorescence anisotropy <r>, (B,E) mean fluorescence lifetime <τ > and (C,F) long lifetime component of (A,B,C) *t*-PnA and (D,E,F) DPH, respectively. The values are the mean ± SD of at least three independent experiments. Control experiments showed that membrane biophysical properties did not change significantly upon addition of ethanol (probe solvent; <r> values of 0.247±0.011 for *t*-PnA and 0.174±0.006 for DPH) or DMSO (U-drug solvent; <r> values of 0.255±0.007 for *t*-PnA and 0.174±0.010 for DPH), confirming that the observed changes in the biophysical properties of CHO-K1 cells membranes were due to Sph and the U-drug, respectively. *$p < 0.01$ versus CHO-K1 cells; **$p < 0.05$ versus CHO-K1 cells.

Interestingly, and contrary to what was observed for RAW macrophages treated with 2 μM Sph for 24 h[6], CHO-K1 cells treated with 2 μM Sph during the same incubation period, did

not result in increased Chol filipin staining (Figure S1). Nevertheless, this concentration revealed to have an effect in the membrane biophysical properties of CHO-K1 cells 24h after incubation, which suggests that the observed biophysical changes, can in fact be related to a Sph-induced effect. Sph metabolism and the involvement of other lipid species cannot, however, be ruled out.

4.4. The cell type effect

Considering the different patterns of lipid accumulation in the visceral organs and in the brain in NPC disease[2,43], a human neuronal cell model of NPC generated from a SH-SY5Y neuroblastoma cell line and down expressing the NPC1 locus[27] was also studied. The fluorescence anisotropy and lifetime of *t*-PnA, DPH and TMA-DPH were measured and the results are presented in Figure 7.

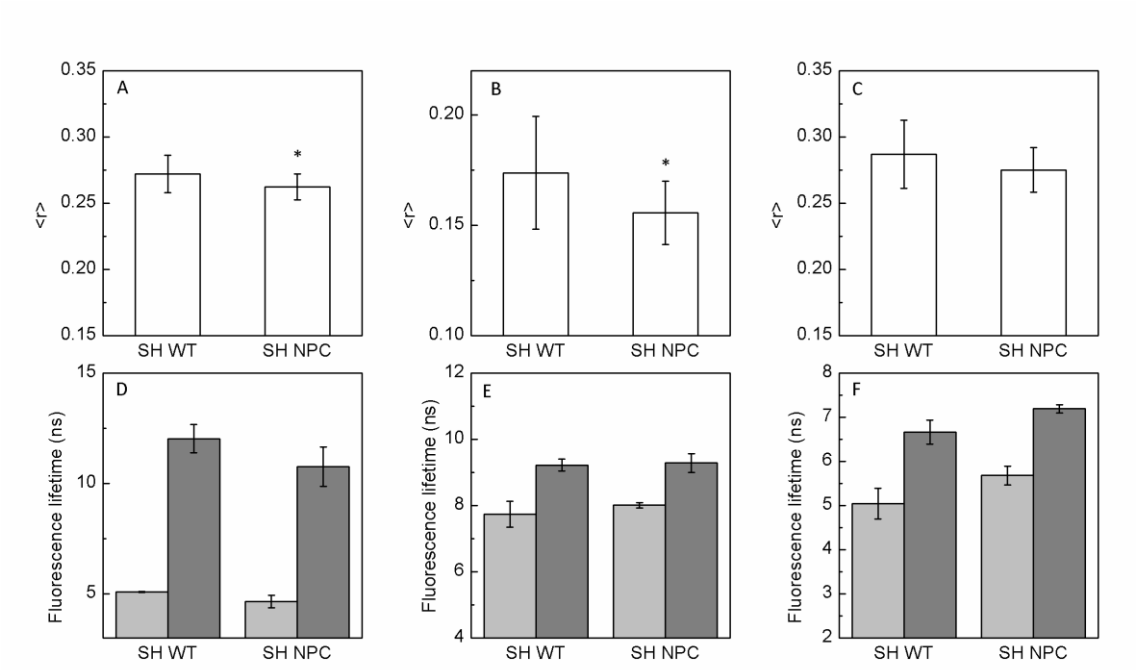

Figure 7 – Biophysical characterization of WT and NPC mutant SH-SY5Y neuroblastoma cells. (A,D) *t*-PnA; (B,E) DPH and (C,F) TMA-DPH fluorescence anisotropy <r> (A,B,C) and fluorescence lifetime (D,E,F) measured in WT and NPC mutant SH-SY5Y neuroblastoma cells, at 37 °C. In panels D, E and F the light grey bars represent the mean fluorescence lifetime, while the dark grey bars correspond to the long

lifetime component. Values are means ± SD of three independent experiments. *p < 0.01 versus SH WT cells.

Figure 7 shows that *t*-PnA (Fig. 7A) and DPH (Fig. 7B) fluorescence anisotropy are lower in mutant neuroblastoma cells, suggesting an increase in the overall membrane fluidity compared to control WT SH-SY5Y neuroblastoma cells. The lifetime of these probes followed a similar behavior, but no significant changes occurred between mutant and control cells. These results are opposite to those obtained in CHO cells, where decreased fluidity was observed in mutant cells (Fig. 2). To further characterize these cells, the DPH trimethylammonium derivative (TMA-DPH) was used. This probe has a more favorable electrostatic interaction with electronegative lipids and a slightly shallower position in the membrane compared to the hydrophobic DPH[44] and a lower rate of internalization[45], thus enabling characterizing the properties of the PM. Similarly to *t*-PnA and DPH, TMA-DPH fluorescence anisotropy is lower in mutant SH cells, compared to the WT cells (Fig. 7C), further suggesting a slight increase in membrane fluidity in mutant cells. Regarding TMA-DPH lifetime, no significant differences were observed between mutant and control cells. These results suggest that changes in membrane fluidity arising from lipid accumulation in NPC are complex and cell type dependent. This is likely to be due to differences in lipid composition of these cell lines, since the WT neuroblastoma cell line revealed to have highly ordered domains in the membranes, represented by high anisotropy values of *t*-PnA (0.272±0.014) and TMA-DPH (0.287±0.026)[46], compared to CHO-K1 cells that present a higher membrane fluidity (*t*-PnA <r> 0.243±0.010).

The effect of Sph external addition (2 μM, 1 minute and 24h incubation) and U-drug treatment (24 h) in the biophysical properties of WT neuroblastoma cells was also evaluated, taking advantage of the photophysical properties of *t*-PnA. Figure 8 shows that both U-drug and Sph treatment resulted in a decrease in membrane fluidity in WT neuroblastoma cells, as observed for CHO-K1 cells. Moreover, the effect of 2 μM Sph was also immediate and reflected by a significant increase in the fluorescence anisotropy of *t*-PnA (Fig. 9A), but not by a strong increase in the long lifetime component of *t*-PnA (Fig. 8B), as previously observed for CHO-K1 cells. This data further suggests that Sph might contribute to an increased fraction of l_o phase in

biological membranes, rather than the formation of a highly ordered and compact gel phases. After 24 h treatment with Sph an increase in membrane fluidity was observed, similarly to what was registered for the NPC neuroblastoma cell line (*t*-PnA anisotropy values are very similar, 0.262±0.01 for SH NPC (Fig. 7A) and 0.258±0.01 for cells treated with Sph during 24 h (Fig. 8A)), suggesting a change in the lipid profile, probably related to metabolization of Sph and secondary accumulation of other lipid species, as observed for RAW cells after Sph treatment[6].

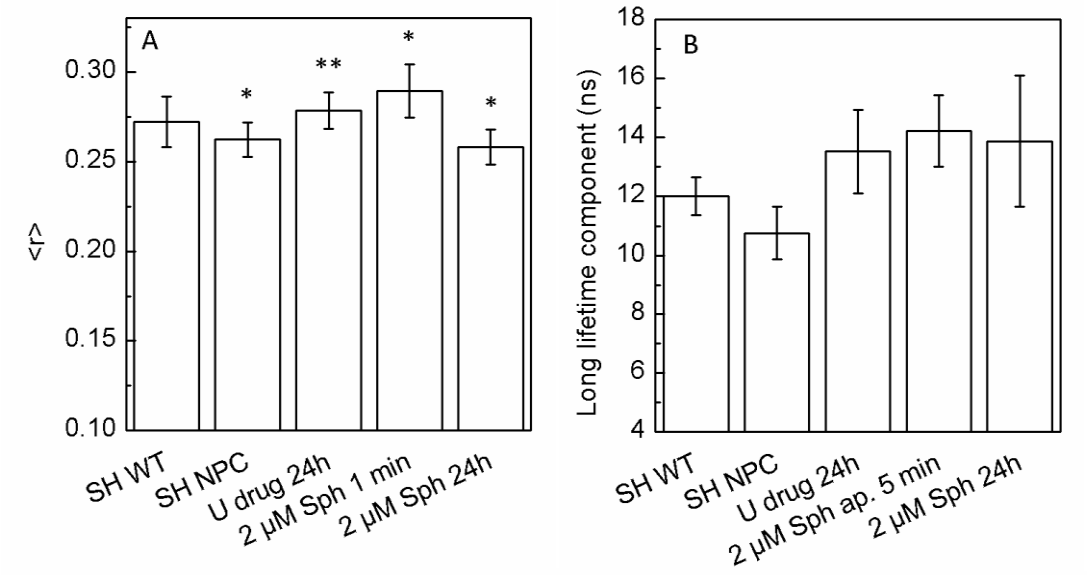

Figure 8 - Comparison between the effect of NPC1 down regulation, U-drug treatment and Sph external addition on the biophysical properties of SH-SY5Y cells (SH WT). (A) Fluorescence anisotropy <r> and (B) long lifetime component of *t*-PnA. The values are the mean ± SD of at least three independent experiments. **p* < 0.01 versus SH WT; ***p* < 0.05 versus SH WT.

5. Discussion

NPC disease is a complex LSD genetically associated with mutations in the NPC1 or NPC2 genes and phenotypically characterized by the abnormal accumulation of different lipid species, such as Chol, SM, multiple GSLs and Sph[6]. Even though a vast number of studies have been made to understand the cellular role of each accumulated lipid in the development of this disease (reviewed in Lloyd-Evans and Platt (2010)[2]) little attention has been given to the impact of an increased content of these lipids in the biophysical properties of biological membranes. In

the present study, the biophysical properties of biological membranes were evaluated in different NPC1 cell models: i) cells that are null or down expressing the NPC1 locus, ii) cells that were treated with U18666A drug to pharmacologically induce the NPC phenotype and iii) cells to which different concentrations of Sph were added. In CHO-K1 cells, it was observed that regardless the tested condition, a general decrease in membrane fluidity occurred when compared to the control WT cells. This effect was also observed in human NPC fibroblasts and mouse SPM-3T3 cells, represented by an increase of approximately 0.03 in the fluorescence anisotropy of DPH[47], that was similar to the one observed in the present study for the same probe (DPH <r>, CHO-K1: 0.18±0.01; CHO-M12: 0.21±0.01). In other lysosomal storage disorders, such as Gaucher disease a similar behavior was observed but to a higher extent. Gaucher mutant fibroblasts, enriched in GlcCer, seems to have regions of the membrane displaying properties of a gel phase[48], a behavior that was observed for other SLs, particularly ceramides, in living cells[46]. In the present study, the increase in membrane order was not accompanied by a strong increase in the long lifetime component of the fluorescence intensity decay of *t*-PnA (Fig. 2C) suggesting that such phase is not occurring in the membranes of CHO mutant cells. In addition, the data obtained with NPC mutant neuroblastoma cells revealed that the membrane biophysical changes arising from lipid abnormal accumulation in NPC cells are highly complex, and seem to depend on the specific membrane lipid composition prior to lipid accumulation, which is cell type and aging[49] dependent. The present results show that the NPC mutant neuroblastoma cell line have an increased membrane fluidity when compared to WT neuroblastoma cells and the inverse effect was observed in the NPC mutant CHO cells (CHO-M12). In fact, the cells tested in the present study have different origins and lipid patterns, particularly regarding the SLs levels and profile[50–52]. Neuronal cells are highly enriched in SLs[53]. In particular, gangliosides are usually abundant in the external leaflet of the PM of neuronal cells[50]. Since the presence of SLs, including gangliosides, in the membranes have been related to the formation and stabilization of specific membrane lipid domains with reduced fluidity[54–56], this could justify the presence of highly ordered domains in the membranes of the WT neuroblastoma cell line, compared to CHO-K1 cells. Another aspect to consider is that the mutant neuroblastoma cells (down expressing the NPC1 locus) revealed to have a 1.2 fold

increase in the ganglioside GM2 and a 2 fold increase in Chol content[27]. This increase in Chol could contribute for the destabilization of the highly ordered membranes, through a "fluidifying" effect of Chol[57,58], leading to more fluid membranes in the mutant cell line when compared to control neuroblastoma cells.

In this study it was also observed that, independently of the cell line, both the U-drug and Sph treatment resulted in changes in the biophysical properties of biological membranes, generally by decreasing membrane fluidity. The treatment of healthy cells with U-drug has been associated with abnormal accumulation of Chol[59–61] but it also interferes with the levels of other lipid species, as observed by Lloyd-Evans et al.[6] and in the present study. This cationic steroid, was already shown to have a condensing and ordering effect on membrane lipids in model membranes[62], however, the abnormal accumulation of different lipid species after the treatment of healthy cells with this drug point to the possible involvement of those lipids in the observed effects. In fact, the changes in membrane fluidity and the differences observed among locus deletion, U-drug and Sph treatment might be related with the association of lipid molecules prone to form specialized ordered domains, such as SM and Chol[63], GSLs[64,65] or ceramides[33,66,67]. Studies in model membranes have demonstrated that all the lipid species accumulated in NPC disease have the ability to change the membrane fluidity. For instance, Chol is associated to an ordering effect in fluid phases[58], contributing in association with saturated, high-melting phospho- and SLs, such as SM, to the formation of specialized lipid domains, known as lipid rafts[63]. In contrast, and as previously referred, Chol might also contribute to the destabilization of highly ordered membranes[57,58]. Moreover, our previous studies regarding the impact of Sph in the biophysical properties of model membranes[18,19], show that similarly to other SLs, such as GlcCer[48] and ceramide[35], an increased content of Sph results in a membrane ordering effect, either due to the formation of a Sph-enriched gel phase or stabilization of the l_o phase, depending on the lipid composition of the artificial membranes.

In the present study, it was possible to assess the effect of Sph in a more complex environment, i.e., in the membranes of living cells. The results showed that Sph induces a concentration and time dependent ordering effect in the membranes of CHO-K1 cells. These results are in accordance with model membrane data that, as previously reffered, predict an

increase in the packing of membranes upon increasing Sph levels[18,19]. Nonetheless, it should be considered that Sph molecules are rapidly metabolized into more complex lipids[68,69], and therefore cells might be able to partially compensate for the rapid increase in Sph levels upon its addition to cells, particularly when lower concentrations of Sph were used. This might justify why changes in fluorescence anisotropy were not observed for the lowest concentration of Sph tested. In addition, significant changes in the measured fluorescence parameters are only expected if a substantial fraction of the Sph molecules become involved in the formation of ordered phases, since the probes display an equal partition between ordered and disordered phases. It should be stressed that higher Sph concentrations induced an immediate decrease in membrane fluidity of CHO-K1 cells (2 and 10 μM Sph) and WT neuroblastoma cells (2 μM Sph), thus suggesting its involvement in the formation of ordered specialized membrane domains at the PM level. For longer incubation periods after Sph addition, a lower decrease in the fluidity of CHO-K1 cell membranes, and an increase in the fluidity of neuroblastoma cells, consistent to what was observed for NPC neuroblastoma cells, were perceived. This might be related with Sph metabolization, the accumulation of other lipid species or even the partition of Sph to internal membranes. As observed in model membranes, differences in membrane lipid composition and the protonation state of Sph in the acidic environment of the lysosomes can account for different Sph-induced biophysical changes[18,19]. In fact, if we consider that Sph abnormal accumulation is a first event in the development of NPC disease, followed by the accumulation of other lipid species (4-8h later)[6], and that a rearrangement of the cell membranes occurs, with changes in membrane lipid composition during different steps of the cell cycle[70], this time/concentration dependent effect would be expected.

Although the involvement of other lipid species that also accumulate in NPC cannot be ruled out, particularly of Chol, this study clearly shows that Sph has an important role in changing the biophysical properties of biological membranes which certainly would influence membrane associated cellular processes, such as lipid and protein trafficking, sorting and recycling. For this reason, further investigation on the biophysical changes resulting from the abnormal Sph accumulation would be of great importance for a better understanding of the molecular mechanisms underlying NPC disease.

6. Concluding remarks

The present study shows that NPC cells present altered biophysical properties that are complex and cell type dependent. Sph, in particular, seems to be very important in inducing these membrane biophysical changes, although other lipid species might also be involved. This study gives support to the hypothesis that Sph biological action might be related to Sph-induced biophysical changes in living cell membranes. This could be of great importance when considering that these biophysical changes are likely to affect several cellular processes, some of them probably involved in the pathophysiology of human disease, as in the case of NPC disease where calcium homeostasis[6,69], fusion and trafficking defects[6] occur in the endocytic pathway.

7. References

1. Vanier, M. T. et al. Diagnostic tests for Niemann-Pick disease type C (NP-C): A critical review. Mol. Genet. Metab. 118, 244–254 (2016).
2. Lloyd-Evans, E. & Platt, F. M. Lipids on trial: the search for the offending metabolite in Niemann-Pick type C disease. Traffic 11, 419–428 (2010).
3. Pentchev, P. G. et al. A defect in cholesterol esterification in Niemann-Pick disease (type C) patients. Proc. Natl. Acad. Sci. U. S. A. 82, 8247–51 (1985).
4. Zervas, M., Somers, K. L., Thrall, M. A. & Walkley, S. U. Critical role for glycosphingolipids in Niemann-Pick disease type C. Curr. Biol. 11, 1283–7 (2001).
5. Tamura, H. et al. Niemann–Pick type C disease: Novel NPC1 mutations and characterization of the concomitant acid sphingomyelinase deficiency. Mol. Genet. Metab. 87, 113–121 (2006).
6. Lloyd-Evans, E. et al. Niemann-Pick disease type C1 is a sphingosine storage disease that causes deregulation of lysosomal calcium. Nat. Med. 14, 1247–55 (2008).
7. Lu, F. et al. Identification of NPC1 as the target of U18666A, an inhibitor of lysosomal cholesterol export and Ebola infection. Elife 4, e12177 (2015).
8. Zheng, W. et al. Ceramides and other bioactive sphingolipid backbones in health and disease: lipidomic analysis, metabolism and roles in membrane structure, dynamics, signaling and autophagy. Biochim. Biophys. Acta 1758, 1864–1884 (2006).
9. Zhang, H., Buckley, N. E., Gibson, K. & Spiegel, S. Sphingosine stimulates cellular proliferation via a protein kinase C-independent pathway. J. Biol. Chem. 265, 76–81 (1990).
10. Cuvillier, O. Sphingosine in apoptosis signaling. Biochim. Biophys. Acta 1585, 153–62 (2002).
11. Ahn, E. H. & Schroeder, J. J. Induction of apoptosis by sphingosine, sphinganine, and C(2)-ceramide in human colon cancer cells, but not by C(2)-dihydroceramide. Anticancer Res. 30, 2881–4 (2010).
12. Woodcock, J. M. et al. Sphingosine and FTY720 directly bind pro-survival 14-3-3 proteins to regulate their function. Cell. Signal. 22, 1291–1299 (2010).

13. Riento, K. et al. Flotillin proteins recruit sphingosine to membranes and maintain cellular sphingosine-1-phosphate levels. PLoS One 13, e0197401 (2018).
14. Bazzi, M. D. & Nelsestuen, G. L. Mechanism of protein kinase C inhibition by sphingosine. Biochem. Biophys. Res. Commun. 146, 203–7 (1987).
15. Ma, Y. et al. Sphingosine activates protein kinase A type II by a novel cAMP-independent mechanism. J. Biol. Chem. 280, 26011–26017 (2005).
16. Contreras, F.-X., Sot, J., Alonso, A. & Goñi, F. M. Sphingosine Increases the Permeability of Model and Cell Membranes. Biophys. J. 90, 4085–4092 (2006).
17. Georgieva, R., Koumanov, K., Momchilova, A., Tessier, C. & Staneva, G. Effect of sphingosine on domain morphology in giant vesicles. J. Colloid Interface Sci. 350, 502–510 (2010).
18. Zupancic, E., Carreira, A. C., de Almeida, R. F. M. & Silva, L. C. Biophysical implications of sphingosine accumulation in membrane properties at neutral and acidic pH. J. Phys. Chem. B 118, 4858–66 (2014).
19. Carreira, A. C., de Almeida, R. F. M. & Silva, L. C. Development of lysosome-mimicking vesicles to study the effect of abnormal accumulation of sphingosine on membrane properties. Sci. Rep. 7, 3949 (2017).
20. Sasaki, H., Arai, H., Cocco, M. J. & White, S. H. pH Dependence of Sphingosine Aggregation. Biophys. J. 96, 2727–2733 (2009).
21. Kõiv, A., Mustonen, P. & Kinnunen, P. K. Influence of sphingosine on the thermal phase behaviour of neutral and acidic phospholipid liposomes. Chem. Phys. Lipids 66, 123–134 (1993).
22. López-García, F., Micol, V., Villalaín, J. & Gómez-Fernández, J. C. Interaction of sphingosine and stearylamine with phosphatidylserine as studied by DSC and NMR. Biochim. Biophys. Acta 1153, 1–8 (1993).
23. López-García, F., Villalaín, J. & Gómez-Fernández, J. C. A phase behavior study of mixtures of sphingosine with zwitterionic phospholipids. Biochim. Biophys. Acta 1194, 281–8 (1994).
24. López-García, F., Villalaín, J. & Gómez-Fernández, J. C. Effect of sphingosine and stearylamine on the interaction of phosphatidylserine with calcium. A study using DSC, FT-IR and 45Ca(2+)-binding. Biochim. Biophys. Acta 1236, 279–88 (1995).
25. Jiménez-Rojo, N. et al. Membrane permeabilization induced by sphingosine: effect of negatively charged lipids. Biophys. J. 106, 2577–2584 (2014).
26. Millard, E. E., Srivastava, K., Traub, L. M., Schaffer, J. E. & Ory, D. S. Niemann-Pick Type C1 (NPC1) Overexpression Alters Cellular Cholesterol Homeostasis. J. Biol. Chem. 275, 38445–38451 (2000).
27. Rodríguez-Pascau, L., Coll, M. J., Casas, J., Vilageliu, L. & Grinberg, D. in JIMD reports 4, 29–37 (2011).
28. Roff, C. F. et al. Type C Niemann-Pick disease: use of hydrophobic amines to study defective cholesterol transport. Dev. Neurosci. 13, 315–9 (1991).
29. Timm, M., Saaby, L., Moesby, L. & Hansen, E. W. Considerations regarding use of solvents in in vitro cell based assays. Cytotechnology 65, 887–94 (2013).
30. Lakowicz, J. R. Principles of Fluorescence Spectroscopy. (Springer US, 2006). doi:10.1007/978-0-387-46312-4
31. Vanier, M. T. & Latour, P. in Methods in cell biology 126, 357–375 (2015).
32. Aresta-Branco, F. et al. Gel domains in the plasma membrane of Saccharomyces cerevisiae: highly ordered, ergosterol-free, and sphingolipid-enriched lipid rafts. J. Biol. Chem. 286, 5043–5054 (2011).
33. Silva, L., de Almeida, R. F. M., Fedorov, A., Matos, A. P. A. & Prieto, M. Ceramide-platform formation and -induced biophysical changes in a fluid phospholipid membrane. Mol. Membr. Biol. 23, 137–150 (2006).

34. Castro, B. M., de Almeida, R. F. M., Silva, L. C., Fedorov, A. & Prieto, M. Formation of ceramide/sphingomyelin gel domains in the presence of an unsaturated phospholipid: a quantitative multiprobe approach. Biophys. J. 93, 1639–1650 (2007).
35. Silva, L. C., de Almeida, R. F. M., Castro, B. M., Fedorov, A. & Prieto, M. Ceramide-domain formation and collapse in lipid rafts: membrane reorganization by an apoptotic lipid. Biophys. J. 92, 502–16 (2007).
36. de Almeida, R. F. M., Loura, L. M. S. & Prieto, M. Membrane lipid domains and rafts: current applications of fluorescence lifetime spectroscopy and imaging. Chem. Phys. Lipids 157, 61–77 (2009).
37. Esko, J. D., Gilmore, J. R. & Glaser, M. Use of a fluorescent probe to determine the viscosity of LM cell membranes with altered phospholipid compositions. Biochemistry 16, 1881–90 (1977).
38. Schroeder, F. Fluorescence Probes as Monitors of Surface Membrane Fluidity Gradients in Murine Fibroblasts. Eur. J. Biochem. 112, 293–307 (1980).
39. de Almeida, R. F. M., Fedorov, A. & Prieto, M. Sphingomyelin/phosphatidylcholine/cholesterol phase diagram: boundaries and composition of lipid rafts. Biophys. J. 85, 2406–2416 (2003).
40. Cenedella, R. J. Cholesterol Synthesis Inhibitor U18666A and the Role of Sterol Metabolism and Trafficking in Numerous Pathophysiological Processes. Lipids 44, 477–487 (2009).
41. Lima, S., Milstien, S. & Spiegel, S. Sphingosine and Sphingosine Kinase 1 Involvement in Endocytic Membrane Trafficking. J. Biol. Chem. 292, 3074–3088 (2017).
42. van Meer, G. & de Kroon, A. I. P. M. Lipid map of the mammalian cell. J. Cell Sci. 124, (2010).
43. Walkley, S. U. & Vanier, M. T. Secondary lipid accumulation in lysosomal disease. Biochim. Biophys. Acta - Mol. Cell Res. 1793, 726–736 (2009).
44. do Canto, A. M. T. M. et al. Diphenylhexatriene membrane probes DPH and TMA-DPH: A comparative molecular dynamics simulation study. Biochim. Biophys. Acta - Biomembr. 1858, 2647–2661 (2016).
45. Illinger, D. & Kuhry, J. G. The kinetic aspects of intracellular fluorescence labeling with TMA-DPH support the maturation model for endocytosis in L929 cells. J. Cell Biol. 125, 783–94 (1994).
46. Pinto, S. N. et al. Changes in membrane biophysical properties induced by sphingomyelinase depend on the sphingolipid N -acyl chain. J. Lipid Res. 55, 53–61 (2014).
47. Koike, T. et al. Decreased membrane fluidity and unsaturated fatty acids in Niemann–Pick disease type C fibroblasts. Biochim. Biophys. Acta - Mol. Basis Dis. 1406, 327–335 (1998).
48. Varela, A. R. P. et al. Pathological levels of glucosylceramide change the biophysical properties of artificial and cell membranes. Phys. Chem. Chem. Phys. 19, 340–346 (2017).
49. Prinetti, A. et al. Changes in the Lipid Turnover, Composition, and Organization, as Sphingolipid-enriched Membrane Domains, in Rat Cerebellar Granule Cells Developing in Vitro. J. Biol. Chem. 276, 21136–21145 (2001).
50. van Echten-Deckert, G. & Herget, T. Sphingolipid metabolism in neural cells. Biochim. Biophys. Acta - Biomembr. 1758, 1978–1994 (2006).
51. Rosales Fritz, V. M., Daniotti, J. L. & Maccioni, H. J. . Chinese hamster ovary cells lacking GM1 and GD1a synthesize gangliosides upon transfection with human GM2 synthase. Biochim. Biophys. Acta - Gene Struct. Expr. 1354, 153–158 (1997).
52. Warnock, D. E. et al. Determination of plasma membrane lipid mass and composition in cultured Chinese hamster ovary cells using high gradient magnetic affinity chromatography. J. Biol. Chem. 268, 10145–53 (1993).
53. Olsen, A. S. B. & Færgeman, N. J. Sphingolipids: membrane microdomains in brain development, function and neurological diseases. Open Biol. 7, 170069 (2017).

54. Palestini, P. et al. Gel phase preference of ganglioside GM1 at low concentration in two-component, two-phase phosphatidylcholine bilayers depends upon the ceramide moiety. Biochim. Biophys. Acta - Biomembr. 1235, 221–230 (1995).
55. Sonnino, S., Mauri, L., Chigorno, V. & Prinetti, A. Gangliosides as components of lipid membrane domains. Glycobiology 17, 1R–13R (Oxford University Press, 2007).
56. Patel, D. S. et al. Influence of Ganglioside GM1 Concentration on Lipid Clustering and Membrane Properties and Curvature. Biophys. J. 111, 1987–1999 (2016).
57. Hilderson, H. J. Fluorescence Studies on Biological Membranes. (Springer US, 1988).
58. Crane, J. M. & Tamm, L. K. Role of cholesterol in the formation and nature of lipid rafts in planar and spherical model membranes. Biophys. J. 86, 2965–2979 (2004).
59. Sobo, K. et al. Late endosomal cholesterol accumulation leads to impaired intra-endosomal trafficking. PLoS One 2, e851 (2007).
60. Schweitzer, J. K., Pietrini, S. D. & D'Souza-Schorey, C. ARF6-Mediated Endosome Recycling Reverses Lipid Accumulation Defects in Niemann-Pick Type C Disease. PLoS One 4, e5193 (2009).
61. Copetti-Santos, D. et al. U18666A Treatment Results in Cholesterol Accumulation, Reduced Na+, K+-ATPase Activity, and Increased Oxidative Stress in Rat Cortical Astrocytes. Lipids 50, 937–944 (2015).
62. Cenedella, R. J. et al. Direct perturbation of lens membrane structure may contribute to cataracts caused by U18666A, an oxidosqualene cyclase inhibitor. J. Lipid Res. 45, 1232–41 (2004).
63. Sezgin, E., Levental, I., Mayor, S. & Eggeling, C. The mystery of membrane organization: composition, regulation and roles of lipid rafts. Nat. Rev. Mol. Cell Biol. 18, 361–374 (2017).
64. Rock, P., Allietta, M., Young, W. W., Thompson, T. E. & Tillack, T. W. Ganglioside GM1 and asialo-GM1 at low concentration are preferentially incorporated into the gel phase in two-component, two-phase phosphatidylcholine bilayers. Biochemistry 30, 19–25 (1991).
65. Varela, A. R. P. et al. Effect of glucosylceramide on the biophysical properties of fluid membranes. Biochim. Biophys. Acta - Biomembr. 1828, 1122–1130 (2013).
66. Zhang, Y., Li, X., Becker, K. A. & Gulbins, E. Ceramide-enriched membrane domains-Structure and function. Biochimica et Biophysica Acta - Biomembranes 1788, 178–183 (2009).
67. Castro, B. M., Silva, L. C., Fedorov, A., de Almeida, R. F. M. & Prieto, M. Cholesterol-rich fluid membranes solubilize ceramide domains: implications for the structure and dynamics of mammalian intracellular and plasma membranes. J. Biol. Chem. 284, 22978–22987 (2009).
68. Blom, T., Li, Z., Bittman, R., Somerharju, P. & Ikonen, E. Tracking sphingosine metabolism and transport in sphingolipidoses: NPC1 deficiency as a test case. Traffic 13, 1234–43 (2012).
69. Höglinger, D. et al. Intracellular sphingosine releases calcium from lysosomes. Elife 4, (2015).
70. Denz, M. et al. Cell cycle dependent changes in the plasma membrane organization of mammalian cells. Biochim. Biophys. Acta - Biomembr. 1859, 350–359 (2017).

8. Supporting information for: Biophysical impact of lipid abnormal accumulation in NPC1 cell models

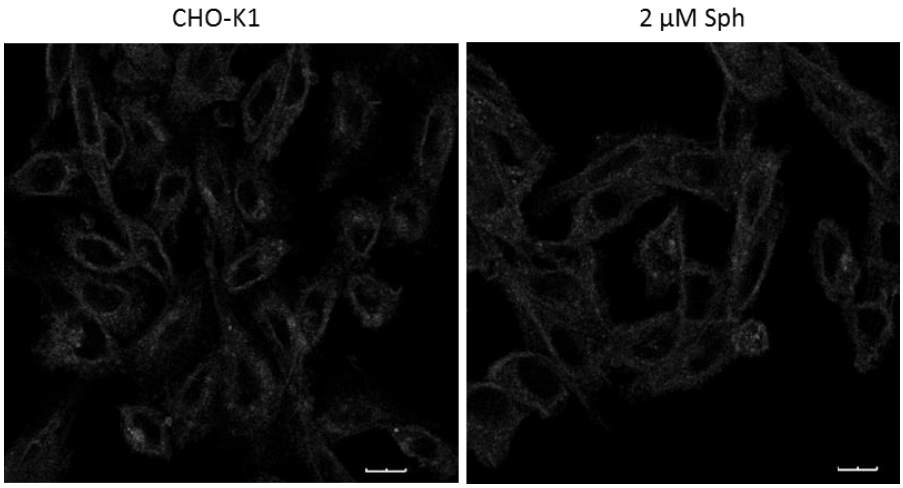

Figure S1 – Filipin staining showing the effect of 2 µM Sph on CHO-K1 cholesterol. The cells were incubated with Sph for 24h, at 37 °C, before staining. Scale bars, 10 µm

CHAPTER V

FINAL CONCLUSIONS

CHAPTER V – FINAL CONCLUSIONS

Previous studies performed by other authors[1–7] had explored the impact of Sph in the biophysical properties of membranes, mostly in artificial model membranes, though the complete picture of the biophysical properties and the molecular mechanisms underlying the biological roles of this remarkable bioactive lipid are still far from being fully elucidated. In the present work, further studies were performed regarding the biophysical impact of Sph in model membrane systems that allow to circumvent some of the difficulties and limitations of studying lipid-lipid interactions *in vivo* by using a well-defined and controlled number and proportion of lipids (or other membrane components)[8]. In addition, studies were also performed in the more complex biological environment of living cells.

The comprehensive characterization of Sph properties was performed by studying the interplay of Sph with other membrane lipids. The effect of Sph in simple fluid model membranes composed by POPC, a common membrane phospholipid (Chapter II); the influence of Sph in the biophysical behavior of model membranes containing Chol and SM, lipids that are commonly associated to membrane compartmentalization, through the formation of specialized ordered (l_o phase) membrane domains – raft domains (Chapters II and III); the effect of pH in modulating the Sph biophysical properties (Chapters II and III); the Sph-induced effect in membrane permeability (Chapter III) and the impact of Sph in the biophysical properties of living cell membranes (Chapter IV) were analyzed in the sequence of this work. In order to achieve these goals, a multi-probe and multi-parameter approach was applied and complementary techniques such as fluorescence spectroscopy and microscopy, ELS and DLS were used. The use of probes with different phase partition properties enabled the identification of different lipid phases. For instance, *t*-PnA partitions equally among l_d and l_o phases, similarly to DPH, however, it has the particularity to present a higher quantum yield and partition when in the presence of gel phases which makes this probe very useful when trying to identify such membrane phases[9,10].

In Chapter II the biophysical properties of POPC/Sph and POPC/SM/Chol/Sph vesicles were characterized, both at neutral (pH 7.4) and acidic (pH 5.0) conditions. Based in the thermotropic studies with POPC/Sph mixtures a partial binary phase diagram was determined,

which provides important information regarding the phase behavior of membranes composed by Sph and fluid lipids. An example of this could be the extrapolation for other temperatures (e.g. physiological temperature) of the biophysical state of Sph-containing membranes. In this study it was possible to conclude that Sph, in resemblance to other SLs, such as ceramide[9,11] and glucosylceramide (GlcCer)[12–14], has the ability to change the biophysical properties of membranes, by decreasing membrane fluidity and segregating into gel domains, depending on the membrane lipid composition and the pH of the surrounding environment. Our studies revealed that Sph has a membrane ordering effect that is more pronounced at higher Sph concentrations and at neutral pH. This effect seems to be related to alteration of the protonation and hydrogen bonding states of Sph in both pH environments. It is, therefore, plausible to expect that Sph can drive strong changes in the surface charge of membranes in a manner that depends both on the membrane lipid composition and on the pH. Accordingly, it would not be surprising that local membrane enrichment in Sph would affect the electrostatic membrane-proteins interactions and consequently protein activity.

Sph ability to drive gel-fluid phase separation was enhanced in ternary POPC/SM/Chol mixtures compared to binary POPC/Sph mixtures. Nonetheless, the composition of the ternary mixtures also dictates Sph phase behavior, and an increase in Chol/SM content decreases Sph-induced gel domain formation, as observed for ceramide[9] and GlcCer[14]. However, differences regarding the interaction of these lipids with raft mixtures can be pointed. Sph similarly to GlcCer[14] seems to have a lower ability to drive the formation of gel phases in raft mixtures, since higher amounts of these lipids (ap. 10 mol%) are needed to promote comparable effects to the ones induced by approximately 4 mol% of ceramide[9].

Chapter III, addressed the development of a new synthetic system that more closely resembles the lysosome - the LMVs - and the importance of the development of such mimetic systems. The effect of Sph abnormal accumulation in membrane structure/permeability and biophysical properties was assessed in standard liposomes (no pH gradient) and in LMVs representing physiological (lower SM, Chol content) and NPC-like conditions (higher SM, Chol content). The results showed a higher impact of Sph in the properties of NPC-LMVs (higher SM, Chol content), highlighting the relevance of the LMVs as a more appropriated system to study

the events occurring in that sub-cellular location. In addition, it was possible to conclude that Sph causes a shift in vesicle surface charge, increases membrane order and promote a rapid increase in membrane permeability, particularly in NPC-LMVs. This study suggested that the abnormal accumulation of lipids observed in NPC disease, might contribute to an impairment of the cell function, through significant alterations in the lysosomal membrane structure and integrity.

In Chapter IV we further investigate how the abnormal accumulation of lipids in NPC disease affects the biophysical properties of biological membranes. Considering that NPC organs/tissues are affected to different extents[15], distinct cell lines were used: CHO-K1 cells, SH-SY5Y neuroblastoma cells and their mutant counterparts lacking (CHO-M12) or down-expressing (NPC neuroblastoma cell line) the NPC1 locus. The results showed that the changes in the biophysical properties of membranes arising from lipid abnormal accumulation in NPC cells are highly complex and cell type dependent. The treatment of healthy cells with U18666A or Sph was also analyzed since it was previously associated with the induction of the NPC phenotype[16]. Both treatments had impact in the biophysical properties of living cells membranes, by decreasing membrane fluidity. Despite the involvement of other lipid species that also abnormally accumulate in NPC disease cannot be ruled out, this study clearly shows that Sph has an important effect in the biophysical properties of biological membranes. This almost immediate effect that seems to occur in a first instance at the PM level, suggests that Sph might integrate specialized membrane domains, and might interfere with different cellular processes, such as calcium homeostasis and endocytic trafficking that are affected in NPC disease[16,17]. These results are in accordance with the model membrane data that predicted an impact of Sph on membrane organization and fluidity, depending on the Sph concentration and membrane lipid composition. Overall the results suggest that membrane biophysical properties might have a role in the molecular mechanisms underlying NPC pathophysiology.

In summary, it can be concluded that:

i) Sph decreases the fluidity of POPC membranes;

ii) Sph modulates the properties of raft like membranes, suggesting its involvement in the formation of specialized membrane domains that are involved in the regulation of different biological processes;

iii) Sph has a pH dependent ordering effect, which is more pronounced at neutral pH and for higher Sph concentrations;

iv) Sph effect in the membrane biophysical properties is strongly regulated by Sph charge;

v) The development of artificial model membrane systems that more closely mimic physiological situations, are of crucial importance to better extrapolate the results obtained with these synthetic systems to the more complex biological membranes;

vi) Sph effects in membrane biophysical properties and permeability are more pronounced in LMV´s containing higher Chol and SM content, as observed in NPC disease;

vii) The biophysical changes arising from lipid abnormal accumulation in NPC cells are complex and cell type dependent;

viii) Sph has an important impact in the biophysical properties of biological membranes, leading to a decrease in the fluidity of the membrane of living cells in a concentration and time dependent manner.

The evidence obtained in the present work supports the hypothesis that Sph biological actions might in part be related to Sph-induced biophysical changes in biological membranes. New insights were obtained regarding the behavior of this lipid when integrated in membranes (artificial and biological) with different compositions. The impact of Sph in the modulation of membrane domains, suggests that Sph abnormal accumulation might directly affect the distribution of other membrane components and consequently affect cell signaling pathways and their related cellular events. Therefore, it is tempting to hypothesize that Sph-induced alterations in the biophysical properties of biological membranes might be one of the triggering mechanisms underlying NPC disease[16]. Additional studies addressing the relation between membrane biophysical changes and NPC are needed, in order to further test this hypothesis.

References

1. Kõiv, A., Mustonen, P. & Kinnunen, P. K. Influence of sphingosine on the thermal phase behaviour of neutral and acidic phospholipid liposomes. *Chem. Phys. Lipids* **66,** 123–134 (1993).
2. López-García, F., Micol, V., Villalaín, J. & Gómez-Fernández, J. C. Interaction of sphingosine and stearylamine with phosphatidylserine as studied by DSC and NMR. *Biochim. Biophys. Acta* **1153,** 1–8 (1993).
3. López-García, F., Villalaín, J. & Gómez-Fernández, J. C. A phase behavior study of mixtures of sphingosine with zwitterionic phospholipids. *Biochim. Biophys. Acta* **1194,** 281–8 (1994).
4. Contreras, F.-X., Sot, J., Alonso, A. & Goñi, F. M. Sphingosine Increases the Permeability of Model and Cell Membranes. *Biophys. J.* **90,** 4085–4092 (2006).
5. Georgieva, R., Koumanov, K., Momchilova, A., Tessier, C. & Staneva, G. Effect of sphingosine on domain morphology in giant vesicles. *J. Colloid Interface Sci.* **350,** 502–510 (2010).
6. Jiménez-Rojo, N. *et al.* Membrane permeabilization induced by sphingosine: effect of negatively charged lipids. *Biophys. J.* **106,** 2577–2584 (2014).
7. Watanabe, C., Puff, N., Staneva, G., Seigneuret, M. & Angelova, M. I. Antagonism and synergy of single chain sphingolipids sphingosine and sphingosine-1-phosphate towards lipid bilayer properties. Consequences for their role as cell fate regulators. *Langmuir* **30,** 13956–13963 (2014).
8. Siontorou, C. *et al.* Artificial Lipid Membranes: Past, Present, and Future. *Membranes (Basel).* **7,** 38 (2017).
9. Silva, L. C., de Almeida, R. F. M., Castro, B. M., Fedorov, A. & Prieto, M. Ceramide-domain formation and collapse in lipid rafts: membrane reorganization by an apoptotic lipid. *Biophys. J.* **92,** 502–516 (2007).
10. Aresta-Branco, F. *et al.* Gel domains in the plasma membrane of Saccharomyces cerevisiae: highly ordered, ergosterol-free, and sphingolipid-enriched lipid rafts. *J. Biol. Chem.* **286,** 5043–5054 (2011).
11. Silva, L., de Almeida, R. F. M., Fedorov, A., Matos, A. P. A. & Prieto, M. Ceramide-platform formation and -induced biophysical changes in a fluid phospholipid membrane. *Mol. Membr. Biol.* **23,** 137–150 (2006).
12. Varela, A. R. P. *et al.* Effect of glucosylceramide on the biophysical properties of fluid membranes. *Biochim. Biophys. Acta - Biomembr.* **1828,** 1122–1130 (2013).
13. Varela, A. R. P. *et al.* Influence of intracellular membrane pH on sphingolipid organization and membrane biophysical properties. *Langmuir* **30,** 4094–4104 (2014).
14. Varela, A. R. P. *et al.* Pathological levels of glucosylceramide change the biophysical properties of artificial and cell membranes. *Phys. Chem. Chem. Phys.* **19,** 340–346 (2017).
15. Lloyd-Evans, E. & Platt, F. M. Lipids on trial: the search for the offending metabolite in Niemann-Pick type C disease. *Traffic* **11,** 419–428 (2010).
16. Lloyd-Evans, E. *et al.* Niemann-Pick disease type C1 is a sphingosine storage disease that causes deregulation of lysosomal calcium. *Nat. Med.* **14,** 1247–1255 (2008).
17. Höglinger, D. *et al.* Intracellular sphingosine releases calcium from lysosomes. *Elife* **4,** (2015).

CHAPTER VI

FUTURE PERSPECTIVES

CHAPTER VI – FUTURE PERSPECTIVES

Sph is an important bioactive lipid with roles in cellular processes, such as apoptosis[1] and cell proliferation[2] and has been implicated in different pathologies, as a triggering[3] or preventive agent[4–6]. The mechanism by which Sph exerts its biological actions are still unclarified, but it has been suggested that Sph-induced alterations in the membrane biophysical properties might be a possible mechanism that would influence protein sorting and thus cell signaling events[7,8].

The main goal of this PhD project was to characterize, from a multidisciplinary perspective, the alterations that occur upon Sph accumulation in NPC. In a first approach we characterized the effect of different Sph concentrations on the biophysical properties, electrostatic properties and permeability of model membrane systems composed of different membrane lipids, mimicking different cellular pH environments. After this, studies were also performed at the cell level. It was concluded that Sph decreases membrane fluidity and that it might drive the formation of lipid domains. To complement the studies that were performed in this dissertation work, other model systems could be characterized in future experiments, in order to gain further insights regarding Sph interaction with other bioactive lipids and how those interactions would influence the membrane properties. An example of this would be the characterization of the interaction of Sph with SLs that also accumulate in NPC, such as, GSLs derived from GlcCer[9]. These lipids are highly abundant in the nervous system[10], one of the systems most affected in NPC[11]. In resemblance with the previous studies a multiprobe/multiparameter combined fluorescence spectroscopy approach can be used complemented by confocal microscopy studies with GUVs, which allow to image shape and phase separation.

In addition to those studies, a further characterization of the biophysical properties of cell membranes and vesicles prepared from lipid extracts of patient cells could be performed. In particular, it would be interesting to explore changes in the membrane properties of cells derived from patients with different ages of onset, with only systemic manifestations and with both systemic and neurological disease, since this is a disease with an extremely heterogeneous clinical presentation[11]. In addition, organelle purification could also be performed to analyze if

changes in membrane properties are more pronounced in specific subcellular locations. In particular, studies with purified lysosomes, the organelles where the accumulation of different lipid species occurs, including Sph, and therefore, where more notorious changes in membrane properties are expected. A methodological approach based on magnetic separation is currently being implemented in our lab to perform such studies (see appendix for further details). The studies will be developed to understand the impact of Sph abnormal accumulation, and the other lipid species, on lysosomal function.

The results to be obtained on the above suggested studies in conjugation with the ones obtained during this dissertation work are expected to provide important information regarding how Sph affects membrane organization in different cell types and in different subcellular locations, providing a better understanding of the effect of Sph abnormal accumulation in cells of NPC patients. This knowledge might contribute to the identification of new therapeutic targets and the developments of new treatments for NPC patients.

References

1. Woodcock, J. Sphingosine and ceramide signalling in apoptosis. *IUBMB Life* **58,** 462–6 (2006).
2. Zhang, H., Buckley, N. E., Gibson, K. & Spiegel, S. Sphingosine stimulates cellular proliferation via a protein kinase C-independent pathway. *J. Biol. Chem.* **265,** 76–81 (1990).
3. Lloyd-Evans, E. *et al.* Niemann-Pick disease type C1 is a sphingosine storage disease that causes deregulation of lysosomal calcium. *Nat. Med.* **14,** 1247–1255 (2008).
4. Ahn, E. H. & Schroeder, J. J. Induction of apoptosis by sphingosine, sphinganine, and C(2)-ceramide in human colon cancer cells, but not by C(2)-dihydroceramide. *Anticancer Res.* **30,** 2881–4 (2010).
5. Pewzner-Jung, Y. *et al.* Sphingoid long chain bases prevent lung infection by Pseudomonas aeruginosa. *EMBO Mol. Med.* **6,** 1205–1214 (2014).
6. Tavakoli Tabazavareh, S. *et al.* Lack of Sphingosine Causes Susceptibility to Pulmonary Staphylococcus Aureus Infections in Cystic Fibrosis. *Cell. Physiol. Biochem.* **38,** 2094–2102 (2016).
7. Contreras, F. X., Sot, J., Alonso, A. & Goñi, F. M. Sphingosine increases the permeability of model and cell membranes. *Biophys. J.* **90,** 4085–4092 (2006).
8. Georgieva, R., Koumanov, K., Momchilova, A., Tessier, C. & Staneva, G. Effect of sphingosine on domain morphology in giant vesicles. *J. Colloid Interface Sci.* **350,** 502–510 (2010).
9. Hashimoto, N. *et al.* Cholesterol-dependent increases in glucosylceramide synthase activity in Niemann-Pick disease type C model cells: Abnormal trafficking of endogenously formed ceramide metabolites by inhibition of the enzyme. *Neuropharmacology* **110,** 458–469 (2016).
10. Furukawa, K., Ohmi, Y., Ohkawa, Y., Tajima, O. & Furukawa, K. in *Advances in neurobiology* **9,** 307–320 (2014).
11. Vanier, M. T. Niemann-Pick disease type C. *Orphanet J. Rare Dis.* **5,** 16 (2010).

APPENDIX

APPENDIX - Lysosomal purification from different cell lines

1. Introduction

The lysosome was discovered in the early 50´s by Christian De Duve[1]. Lysosomes are cytoplasmic organelles responsible to degrade and recycle cellular waste. While the extracellular material reach the lysosome mainly through endocytosis[2] and phagocytosis[3], the delivery of intracellular materials is mediated by autophagy[4,5]. In addition to cellular clearance, lysosomes are also now recognized by their involvement in multiple biological processes such as secretion[6], PM repair[7], cholesterol transport[8], nutrient sensing and gene regulation[9]. Due to its cellular function the lysosomes contain a variety of different hydrolytic enzymes, such as phosphatases, phospholipases, proteases and nucleases, in an acidic environment (pH 4.5-5 approximately), which can breakdown the macromolecules to their simplest subunits[10]. When alterations occur in lysosomal enzymatic activity, transporter proteins, membrane proteins or activator proteins, the accumulation of the material meant for lysosomal degradation occurs, as in the case of Niemann-Pick diseases types A, B and C, Gaucher disease and Tay-Sachs disease. The accumulation of different types of SLs in these diseases[10,11], cause irreversible cell dysfunction and damaging in multiple organs[12]. Duo to the severity of LSDs, lysosomal research assume an important role in trying to better understand the molecular mechanisms underlying lysosomal dysfunction and develop potential therapies for LSDs patients. The study of lysosomes in an isolated environment has been hampered due to difficulties in purifying these organelles. Density gradient centrifugation techniques[13,14] have been commonly used but the contamination with other organelles and the lack of structural function is related with the low success of these techniques. This is especially relevant in the case of LSDs where the abnormal accumulation of macromolecules, such as lipids, causes changes in the buoyant density of the lysosomes[15]. Magnetic separation methods for purifying lysosomes appeared as alternative promising techniques. Pioneering work in this field was performed by Winchester[16], Ioannou[17] and Krise[18] groups and recently improved by Lloyd-Evans group[15]. In this later version the magnetic separation of lysosomes from whole cells is performed with ferrofluid solution from Liquids Research Ltd. containing superparamagnetic nanoparticles conjugated to dextran and

provides, depending on the cell line, a greater yield of pure, functional lysosomes when compared to the previous methodologies[15]. This technique is now being implemented in our lab, in order to further characterize the impact of Sph on the biophysical properties of biological membranes, in this case lysosomal membranes purified from different cell lines.

2. Experimental procedures

2.1. Cell Culture

CHO-K1, SH-SY5Y and CHO-M12 cells were grown in DMEM Ham F-12 (Sigma-Aldrich, MO, USA) and HEK 293 cells were grown in DMEM (Sigma-Aldrich, MO, USA). The Medium was supplemented with 10% fetal bovine serum (Sigma-Aldrich, MO, USA), heat inactivated at 60°C for 1 hour, 1% L-glutamine (100x) (Life Technologies, CA, USA) and 1% pen-strep (Life Technologies, CA, USA). The cells were grown as monolayers at 37 °C with 5% CO_2 in a humidified incubator.

2.2. Lysosomal purification protocol

Lysosomal purification was performed as described by[15]. Briefly, the cells (2 x T75 flasks or 1 T175 flask at ap. 85% confluence) were treated with 10 or 20 mL of pulse medium (appropriate cell culture medium with 10% ferrofluid solution (Liquids Research Ltd, Gwynedd, UK), and 10 mM HEPES pH 7.2) for 24h. The pulse medium was then removed and the cells were washed two/three times with PBS 1x, before the addition of regular medium and a period of 24 h chase at 37 °C. After this period, the cells were washed twice with ice cold PBS and all the subsequent steps were performed on ice. The cells were re-suspended with 4 mL (1 T75 flask, double volume for a T175 flask) of hypotonic buffer A (15 mM KCL, 1.5 mM MgAc, 1 mM DTT, 10 mM HEPES, 1 to 3 µL of protease inhibitor cocktail (Sigma-Aldrich, MO, USA), make up with dH_2O to 50 mL), with the aid of a scraper. The cell suspension was then homogenized on ice using a tight dounce homogenizer for 30 strokes and the homogenate was passed through a 23 gauge needle eight times. After this step 1 mL (or 2 mL if using a T175 flask) of hypertonic buffer B solution (220 mM Hepes pH 7.2, 0.1 mM sucrose, 375 mM KCl, 22.5 mM MgAc, 1 mM DTT, 25 U/mL DnaseI (Life Technologies, CA, USA), make up with dH_2O to 5 mL) was added to

the cell suspension and mixed by inversion five times, followed by a 5 minutes incubation at 37 °C. The suspension was centrifuged at 1500 rpm for 10 minutes at 4 °C and the resulting supernatant was passed through the magnetic separation column (Miltenyi Biotec, Bergisch Gladbach, Germany) in the next step.

The LS column was placed onto the QuadroMACS magnetic separator (Miltenyi Biotec, Bergisch Gladbach, Germany) and the column was equilibrated with 1 mL of 0.5% bovine serum albumin (BSA) in PBS at room temperature. The supernatant from the previous centrifugation was passed through the column and the flow-through was collected in a sample tube. The column was then washed with 1 mL Dnase I solution (25 U prepared in PBS)) and left to stand for 10 minutes. After this, the column was washed twice with 1 mL PBS. The column was removed from the magnet and the lysosomes were eluted to a sample tube with 0.5 mL of PBS (supplemented with 0.1 mM sucrose) using the supplied plunger. This step was repeated in an attempt to increase the yield of lysosomes. The samples were then used in other experiments or frozen for the protein assay and western blots. Protein inhibitor cocktail (Sigma-Aldrich, MO, USA) was added to the samples to avoid protein degradation during storage at -20 °C.

2.3. Protein assay

Micro BCA protein assay kit (Life Technologies, CA, USA) was used to quantify the total protein in sample according to the manufacturer´s instructions. Samples were incubated in 96 well plate and absorbance (562 nm) was measured using an absorbance reader.

2.4. Western-blotting

A standard Western-blot protocol was used. Briefly, after quantifying the protein present in the lysosomal and the rest of the cell fractions, 5 µg protein (dilution in dH_2O) per sample was used for denaturation. For each 3 µL protein/water, 1 µL of sample buffer (4x; 10g Glycerol, 0.785g Tris-HCl, 0.004g Bromophenol Blue, 2g SDS, 2 mL β-mercaptoethanol in 25 mL total volume – make up with dH_2O) was used. The samples were then put in the oven at 60 °C for 1h. After, the samples were placed in the fridge while waiting for the gels.

The samples were fractionated by SDS-PAGE on a 10% gel along with the protein ladder (NZY colour Protein Marker II; NZYTech, Lisbon, Portugal) and transferred to a polyvinylidene difluoride (PVDF) (Bio-Rad, CA, USA) membrane using a transfer apparatus according to the manufacturer's protocols (Bio-Rad, CA, USA). After incubation with 5% nonfat milk (VWR, PA, USA) in 1x TBST (10x stock solution, pH 7.5: 60.55g Tris, 87.66g NaCl, 10 mL Tween20, make up to 1L with dH_2O) for 60 minutes at room temperature, the membrane was washed three times (10 minutes each) with 1x TBST and incubated with antibodies (dilution in 1% blocking solution) against β-actin (1:500; sc-47778, SantaCruz, KS, USA), calnexin (1:1000; Novus Biologicals, CO, USA); EEA1 (1:2500; NBP1-30914, Novus Biologicals), Rab7 (1:250; NBP1-87174, Novus Biologicals), FTCD (1:200; sc-271788, SantaCruz) and NPC2 (1:200; sc-33776, SantaCruz) at 4 °C for 16 h. Membranes were washed three times for 10 minutes with 1x TBST and incubated with a 1:5000 dilution of horseradish peroxidase-conjugated anti-mouse or anti-rabbit antibodies (SantaCruz) for 2 h. Blots were washed with 1x TBST three times and developed with the ECL system (Life Technologies, CA, USA) according to the manufacturer's protocols, and visualized with a ImageQuant LAS 500 imager (GE Healthcare, IL, USA).

3. Preliminary Results

The lysosomal purification protocol was performed for different cell lines: CHO-K1 cells, SH-SY5Y neuroblastoma cells, HEK 293 cells and CHO-M12 cells. Table 1 shows the lysosomal yield obtained for each cell line, which revealed to be quite low, especially considering that all the lysosomal purifications were from a T175 confluent flask or 2 T75 flasks. It was previously described that a single confluent T175 flask of CHO cells could yield up to 300-400 µg of lysosomal material[15], which was not the case in these preliminary experiments at least for the CHO-K1 cells. Details in the experimental procedures, e.g. homogenization technique, centrifugation speeds, are probably related with this low yield as discussed previously[15] and need to be re-adjusted.

Table 1 – Lysosomal purification from different cell lines.

Cell line	Lysosomal yield (µg)	Number of experiments
CHO-K1	101.7 ± 72.0	*n* = 3
HEK 293	128.7 ± 32.3	*n* = 3
SH-SY5Y	114.0 ± 91.9	*n* = 2
CHO-M12	277.0	*n* = 1

In addition to the low lysosomal yield, the lysosomal fractions were not pure and revealed to be contaminated with other cell organelles such as ER and LE (Fig. 1). Moreover, some of the antibodies used did not work (SantaCruz antibodies used to detect the lysosomal protein NPC2 and Formiminotransferase Cyclodeaminase (FTCD) from the Golgi compex) and alternative antibodies need to be tested.

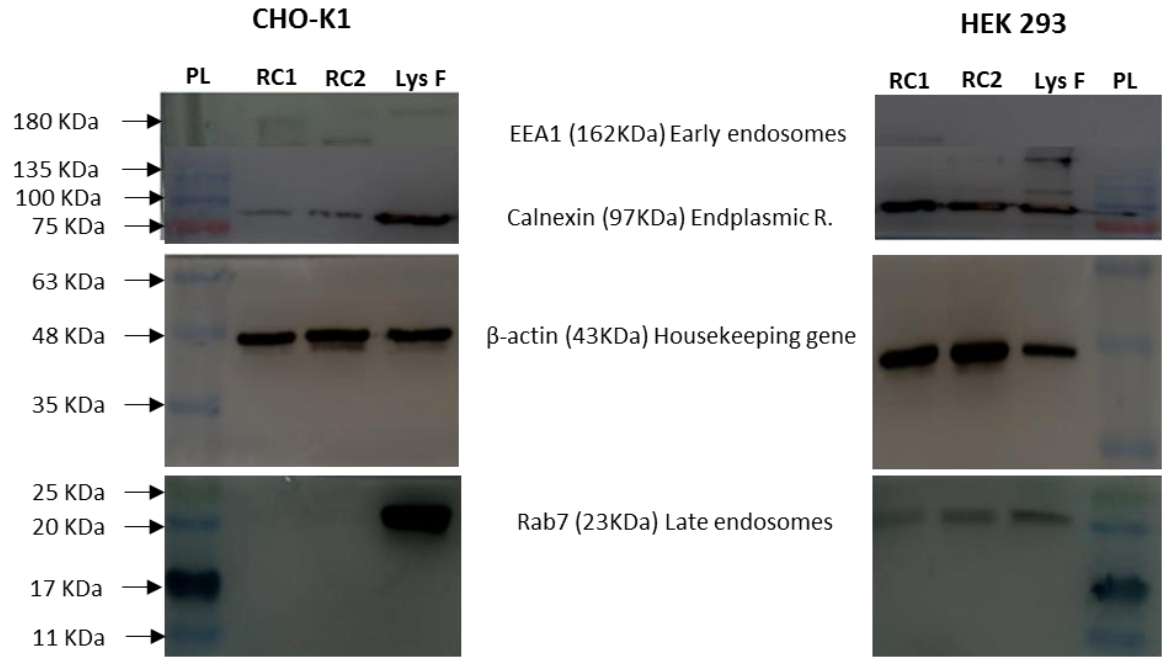

Figure 1 – Western blots performed for samples obtained from CHO-K1 and HEK 293 cells, after 24 h incubation with ferrofluid solution and 24h chase. Legend: PL – Protein ladder; RC1 – Rest of the cell (1st recovery); RC2 – Rest of the cell (2nd recovery); Lys F – Lysosomal fraction.

4. Conclusion

Lysosomal purification is in fact of great importance for the study of lysosomal function and the lysosome related cellular processes. Different methodologies can be applied, including diverse magnetic separation methods that differ in the final yield, lysosomal functionality, purity and toxicity[15]. Every methodology has their own nuances and different experimental parameters that need to be considered and carefully adjusted to obtain good results. Examples of this are the composition of the buffers (isotonic solutions), the homogenization techniques, and centrifugation speeds[15]. Other important aspects to consider are the choice of the most suitable superparamagnetic iron oxide nanoparticles (SPIONs), the maintenance of its magnetic properties and the selection of the cell type that better suit the purpose of our experiments[15].

5. References

1. de Duve, C. The lysosome turns fifty. *Nat. Cell Biol.* **7,** 847–849 (2005).
2. Luzio, J. P., Parkinson, M. D. J., Gray, S. R. & Bright, N. A. The delivery of endocytosed cargo to lysosomes. *Biochem. Soc. Trans.* **37,** 1019–1021 (2009).
3. Wong, C.-O. *et al.* Lysosomal Degradation Is Required for Sustained Phagocytosis of Bacteria by Macrophages. *Cell Host Microbe* **21,** 719–730.e6 (2017).
4. Eskelinen, E.-L. & Saftig, P. Autophagy: A lysosomal degradation pathway with a central role in health and disease. *Biochim. Biophys. Acta - Mol. Cell Res.* **1793,** 664–673 (2009).
5. Martini-Stoica, H., Xu, Y., Ballabio, A. & Zheng, H. The Autophagy-Lysosomal Pathway in Neurodegeneration: A TFEB Perspective. *Trends Neurosci.* **39,** 221–234 (2016).
6. Holt, O. J., Gallo, F. & Griffiths, G. M. Regulating Secretory Lysosomes. *J. Biochem.* **140,** 7–12 (2006).
7. Michelet, X. *et al.* Lysosome-Mediated Plasma Membrane Repair Is Dependent on the Small GTPase Arl8b and Determines Cell Death Type in *Mycobacterium tuberculosis* Infection. *J. Immunol.* **200,** 3160–3169 (2018).
8. Storch, J. & Cheruku, S. R. in *Lysosomes* 100–111 (Springer US, 2005). doi:10.1007/0-387-28957-7_9
9. Lim, C.-Y. & Zoncu, R. The lysosome as a command-and-control center for cellular metabolism. *J. Cell Biol.* **214,** 653–64 (2016).
10. Ferreira, C. R. & Gahl, W. A. Lysosomal storage diseases. *Transl. Sci. Rare Dis.* **2,** 1–71 (2017).
11. Vitner, E. B., Platt, F. M. & Futerman, A. H. Common and uncommon pathogenic cascades in lysosomal storage diseases. *J. Biol. Chem.* **285,** 20423–7 (2010).
12. Parkinson-Lawrence, E. J. *et al.* Lysosomal Storage Disease: Revealing Lysosomal Function and Physiology. *Physiology* **25,** 102–115 (2010).
13. Arborgh, B., Ericsson, J. L. E. & Claumann, H. Method for the isolation of iron-loaded lysosomes from rat liver. *FEBS Lett.* **32,** 190–194 (1973).
14. Graham, J. M. in *Current Protocols in Cell Biology* **Chapter 3,** Unit 3.6 (John Wiley & Sons, Inc., 2001).
15. Walker, M. W. & Lloyd–Evans, E. in *Methods in cell biology* **126,** 21–43 (2015).

16. Diettrich, O., Mills, K., Johnson, A. W., Hasilik, A. & Winchester, B. G. Application of magnetic chromatography to the isolation of lysosomes from fibroblasts of patients with lysosomal storage disorders. *FEBS Lett.* **441,** 369–72 (1998).
17. Chen, F. W., Gordon, R. E. & Ioannou, Y. A. NPC1 late endosomes contain elevated levels of non-esterified ('free') fatty acids and an abnormally glycosylated form of the NPC2 protein. *Biochem. J.* **390,** 549–561 (2005).
18. Duvvuri, M. & Krise, J. P. A Novel Assay Reveals That Weakly Basic Model Compounds Concentrate in Lysosomes to an Extent Greater Than pH-Partitioning Theory Would Predict. *Mol. Pharm.* **2,** 440–448 (2005).